Chemical Modulation of the Forkhead Box M1 Transcription Factor

By

Seyed Amirhossein Tabatabaei Dakhili

A thesis submitted in partial fulfillment of the requirements for the degree of

Doctor of Philosophy

in

Pharmaceutical Sciences

Faculty of Pharmacy and Pharmaceutical Sciences

University of Alberta

Abstract

Thousands of transcription factors control the process of gene expression and protein synthesis in the human body. These nuclear proteins are fundamental for healthy organ development, cellular function, immunity and body response to diseases and stress. Mutated, overexpressed, or dysregulated transcription factors are linked to cancer, neurological disorders, metabolic, and autoimmunity diseases. Forkhead Box M1 (FOXM1) is a transcription factor required for the normal progression of the cell cycle as well as tissue regeneration, homeostasis, and DNA repair. However, in many types of cancer, its expression is dysregulated. As the "master regulator of the cell cycle", its overexpression leads to tumorigenesis, angiogenesis, metastasis and poor patient prognosis. Accumulating evidence suggests that inhibition of FOXM1 as the Achilles heel of cancer could be the master key for the cancer-treatment lock. However, direct targeting of the FOXM1 transcription factor is a challenging task due to the lack of binding pocket and ligand-binding site.

In the past decade, several small molecules have been introduced with the ability to decrease the FOXM1 expression with a different and distinct mechanism. Most-recently it is found that compounds thiostrepton (previously found to inhibit FOXM1 indirectly through proteasome inhibition) and Forkhead Domain Inhibitor-6 (FDI-6) can directly bind to the FOXM1 DNA binding domain (DBD) and suppress its activity. However, the exact mechanism of binding of these agents to the FOXM1-DBD is not reported. Since the fundamental of designing inhibitors for any target is an extensive structural analysis of the target, we used a series of molecular dynamics (MD) simulations

to understand the mechanism of FOXM1-DBD/DNA recognition. Next, using different approaches, we identified a binding pocket on the DNA recognition helix of FOXM1-DBD.

Furthermore, using molecular modeling and docking techniques, we found a mutual binding mode for known FOXM1 inhibitors, thiostrepton, FDI-6, and troglitazone. We found that these compounds form a complex with the FOXM1-DBD mainly through a strong pi-sulfur interaction with His287 of FOXM1-DBD. Additionally, we reported that FDI-6 forms an additional strong halogen bonding with Arg297 by its 4-fluorophenyl ring.

To provide evidence regarding the existence of halogen bonding, we chemically modified the structure of FDI-6. Then, using protein immunoblot and EMSA of recombinant human FOXM1-DBD, we proved that only those derivatives carrying halogen atoms at positions 3 and 4 are active. To validate the hypothesis of pi-sulfur interaction, we used two different pathways, chemical and biological. First, we exchanged the sulfur atom in the structure of FDI-6 and confirmed that the sulfur atom is essential for its FOXM1 inhibitory activity. Next, using site-directed mutagenesis, we mutated the His287 of recombinant FOXM1-DBD to a simple and non-aromatic amino acid (alanine) and also to an aromatic amino acid (phenylalanine). Using EMSA, we confirmed that FDI-6 was unable to bind to the alanine mutated FOXM1-DBD, while its binding was unaffected by phenylalanine mutation. These results point to the probability that the theoretical binding site we identified using molecular modeling of the FOXM1-DBD is valid.

Based on the gained knowledge of binding sites as well as the structural requirements necessary for a small molecule to inhibit this oncogenic transcription factor, we designed a series of compounds based on the structure of thiazolidinediones (troglitazone) capable of suppressing the FOXM1 transcriptional program. Among them, compound TFI-10 was able to target and decrease the cellular level of FOXM1 without affecting FOXM1's closely related family members and key tumor suppressors, FOXO1, and FOXO3a.

We also showed that the currently known selective FOXO1 inhibitor, AS1842856, could also target FOXM1 and decrease its protein level as well as its target genes by a mechanism other than direct binding to the DBD. We demonstrated that FOXM1b could promote the expression of FOXO1 while the other FOXM1 isoform, FOXM1c, negatively regulates the level of FOXO1. We also presented using colony formation assay and gene silencing techniques that dual inhibition of FOXM1 and FOXO1 can dramatically decrease the ability of breast cancer cells to proliferate and form colonies.

Preface

A modified version of Chapter 2 of this thesis was published as Tabatabaei-Dakhili, S. A., Aguayo-Ortiz, R. A., Domínguez, L. & Velázquez-Martínez, C. (2018), "**Untying the knot of transcription factor druggability: Molecular modelling study of FOXM1 inhibitors**", *Journal of Molecular Graphics and Modelling*, *80*, 197–210. I was responsible for the data collection, analysis, and composition of the manuscript.

A modified version of Chapter 3 of this thesis was published as Tabatabaei Dakhili, S. A., Pérez, D. J., Gopal, K., Tabatabaei Dakhili, S. Y., Ussher, J. R., & Velázquez-Martínez, C. (2019), "**A structure-activity relationship study of Forkhead Domain Inhibitors (FDI): The importance of halogen binding interactions**." *Bioorganic Chemistry*, 93, 103269. I was responsible for concept formation, data collection, and analysis, as well as manuscript composition.

Chapter 4 of this manuscript is submitted as Tabatabaei Dakhili, S. A., Pérez, D. J., Gopal, K., Haque, M., Lai, R., Ussher, J. R., & Velázquez-Martínez, C." **Thiazolidinediones derivatives as FOXM1 suppressors.**". I designed and performed the experiments and wrote the manuscript.

Chapter 5 of this manuscript will be submitted as Tabatabaei Dakhili, S. A., Pérez, D. J., Gopal., Ussher, J. R., & Velázquez-Martínez, C." **FOXM1 inhibitors: The promising binding interaction of sulfur atom in drug molecules**" A part of this chapter was published (Conference abstract) as Tabatabaei Dakhili, S. A., Pérez, D. J., Gopal., Ussher, J. R., & Velázquez-Martínez, C. " **FOXM1 inhibitors: emergence of a neglected binding force.**" *Proceedings 22*, 58. I was responsible for concept formation, data collection, and analysis as well as manuscript composition.

Chapter 6 of this manuscript will be submitted as Tabatabaei Dakhili, S. A., Pérez, D. J., Gopal., Ussher, J. R., & Velázquez-Martínez, C.” **AS1842856 is a dual inhibitor of FOXO1 and FOXM1 transcription factors.**”. I was responsible for the experimental design as well as data collection and analysis.

To the memory of innocent hearts & souls lost in the tragedy of Flight PS752.

Acknowledgment

I would like to express my sincerest gratitude to my supervisor Dr. Carlos Velazques for his continuous support, patience, guidance, and encouragement throughout my research years at the University of Alberta. I also wish to thank my committee members, Dr. Ayman El-Kadi and Dr. Frank Wuest.

A very special thanks to Dr. David Perez for the assistance, valuable suggestions, and inspiration at all levels of my research project without whom this work would not have been possible. My warm appreciation also goes to Dr. Keshav Gopal and Dr. John Ussher for their motivating advice and helpful discussions.

I would also like to extend my appreciation to my past and present lab mates and colleagues, Dr. Rami Al-batran, Searra Giga, and Sean Larade, who made my time in the lab a memorable and pleasant experience.

I take this opportunity to thank my wonderful parents, my beloved sister, and brother, Samira, and Yasin, for their unconditional love, support, and patience throughout my studies in Canada and my entire life.

Finally, I would like to acknowledge the financial assistance provided by the University of Alberta through the following scholarships: Dr. Ronald Micetich Memorial Graduate Scholarship, Antoine Noujaim Graduate Scholarship, Dr. John Samuel Memorial Graduate Scholarship, and Dr. Ed Knaus Graduate Scholarship in Pharmaceutical Research.

Table of Contents

List of Figures

List of Tables

List of Schemes

List of Abbreviations

ACPYPE	Antechamber Python Parser Interface
AR	Androgen Receptor
ARS	Axenfeld-Rieger Syndrome
ATCC	American Type Culture Collection
BCP-ALL	B Cell Precursor Acute Lymphoblastic Leukaemia
bHLH-Zip	basic Helix-Loop-Helix Leucine Zipper
BLBC	Basal-Like Breast Carcinoma
BRCA2	Breast Cancer-Associated Gene-2
CETSA	Cellular Thermal Shift Assay
CHK2	Checkpoint Kinase-2
DBD	DNA Binding Domain
DIM	3, 3'-Diindolyl Methane
DMEM	Dulbecco's Modified Eagle's Medium
DMF	Dimethylformamide
DMSO	Dimethyl Sulfoxide
DTT	Dithiothreitol
DWM	Dandy-Walker Malformation
EDTA	Ethylenediaminetetraacetic Acid
EGFR	Epidermal Growth Factor Receptor
EMSA	Electrophoretic Mobility Shift Assay
ER	Estrogen Receptor
FBS	Foetal Bovine Serum

FDI	Forkhead Domain Inhibitor
FOXA	Forkhead Box A
FOXC	Forkhead Box O
FOXM	Forkhead Box M1
FOXO	Forkhead Box O
G6P	Glucose-6-Phosphatase
GST	Glutathione S-Transferase
HAT	Histone Acetyl Transferases
HDAC	Histone Deacetylase
HIF1α	Hypoxia Inducible Factor-1 Alpha
HTH	Helix-Turn-Helix
IC_{50}	Half Maximal Inhibitory Concentration
IKZF	Ikaros Family Zinc Finger Protein
IPTG	Isopropyl B-D-1-Thiogalactopyranoside
Kd	Dissociation Constant
Ki	Inhibitory Constant
LB	Luria Broth
LBD	Ligand Binding Domain
LINCS	Linear Constraint Solver
MD	Molecular Dynamics
MDM-2	Murine Double Minute-2
miRNA	micro Ribonucleic Acid
MMP	Matrix Metalloproteinase-1

MMPBSA	Molecular Mechanic Poisson Boltzmann Surface Area
mRNA	messenger Ribonucleic Acid
mTOR	mammalian Target of Rapamycin
MTT	3-(4,5-Dimethylthiazol-2-Yl)-2,5-Diphenyltetrazolium Bromide
NMR	Nuclear Magnetic Resonance
NPM	Nucleophosmin
NRD	Negative Regulatory Domain
NRFM	Negative Regulator of Forkhead Box M1
PAX	Paired Box
PDB	Protein Data Bank
PI3K	Phosphoinositide-3 Kinase
PKB	Protein Kinase B
PL	Placental Lactogen
PLK-1	Polo-Like Kinase-1
PPAR	Peroxisome Proliferator-Activated Receptor
Pre-mRNA	Precursor messenger Ribonucleic Acid
RCM-1	Robert Costa Memorial Drug-1
RMSD	Root Mean Square Deviation
RMSF	Root Mean Square Fluctuation
RNAi	Ribonucleic Acid interference
RPMI	Roswell Park Memorial Institute Medium;
rRNA	ribosomal Ribonucleic Acid
SDS-PAGE	Sodium Dodecyl Sulfate-Polyacrylamide Gel electrophoresis

SEM	Standard Error of The Mean
shRNA	short hairpin Ribonucleic Acid
siRNA	small interfering Ribonucleic Acid
SP1	Specificity Protein 1
SSD	Signal Sensing Domain
STAT3	Signal Transducer and Activator of Transcription-3
TAD	Trans-Activation Domain
TF	Transcription Factor
TFI	Thiazolidinedione Forkhead Inhibitor
TLC	Thin Layer Chromatography
TMS	Tetramehtylsilane
TRD	Trans-Repression Domain
TRD	Trans-Repression Domain
tRNA	transfer Ribonucleic Acid
USP21	Ubiquitin Specific Peptidase-21
vdW	van der Waals
XRCC1	X-Ray Repair Cross-Complementing Protein-1

Thesis layout

Chapter 1 provides background information on the process of gene expression, the role of transcription factors, the significance of inhibiting the transcription factor and strategies for inhibiting transcription factors in cancer treatment. Furthermore, it highlights the link between forkhead box superfamily, specially FOXM1 transcription factor in cancer development and implication of its inhibition and underlines some known FOXM1 inhibiting small molecules.

Chapter 2 presents the extensive and complete molecular dynamic simulation performed to understand the mechanism of FOXM1 DNA interaction. This section provides information on a potential binding pocket on the surface of the FOXM1-DBD and explains the mechanism of binding interaction of known FOXM1 inhibitors.

Chapters 3 and 4 provide experimental evidence of **chapter 1** hypothesis regarding the binding pocket of FOXM1-DBD. These chapters prove the accuracy of the theoretical prediction of the binding site and essential binding interactions highlighted in **chapter 1** using chemical modifications and biological assays.

Chapter 5 identifies a series of novel FOXM1 inhibitors based on the structure of thiazolidinediones. In this chapter, based on the structural requirement that we identified in **chapter 1**, 11 different derivatives of thiazolidinediones were synthesized and evaluated.

Chapter 6 describes that a previously known selective FOXO1 inhibitor could also inhibit the transcriptional activity of FOXM1. This chapter also underlines the significance of FOXM1/FOXO1 dual inhibition.

Chapter 7 is the conclusions and future directions.

Chapter 1

Introduction

1.1 Gene Expression and Transcription Factors

Thousands of human proteins have been identified with a variety of biological roles essential for normal body function (1). Gene expression is a highly regulated process responsible for the construction of these large and complex macromolecules. When a gene expresses, the information stored in the DNA gets converted into a functional protein or a non-coding RNA (tRNA, rRNA and, etc.) (2) (3). The process of gene expression starts by binding of one or more transcription factors (TF) to either enhancer region or silencer region of the DNA. These nuclear proteins target and bind to a sequence of DNA called TF binding motif to either inhibit or initiate the transcription of a gene depending on where they bind (enhancer or silencer region) (4).

Binding of TF to nucleosome is a competitive process. TFs may compete with other TFs, chromatin remodelers, and other DNA binder proteins for DNA binding (5). However, TF can never work independently (6); For TFs to start gene expression or repression, they require to form a multi-component complex with other proteins and TFs, including RNA polymerase. When TFs bind the genomic DNA, they may recruit activators or repressors and chromatin remodellers. These proteins bind to TF factors or DNA to intensify or lower the rate of transcription. (5)

When the transcriptional complex binds to the promoter region of the DNA, RNA polymerase II unwinds the DNA and makes an RNA copy of the coding region (7). In eukaryotes, the transcription of genomic DNA leads to the formation of precursor messenger RNA (pre-mRNA) (8). In a process called post-transcriptional modification, the pre-mRNA undergoes several different modifications before becoming

the mature and functional mRNA. This process may include Polyadenylation, 5'capping and RNA splicing (9).

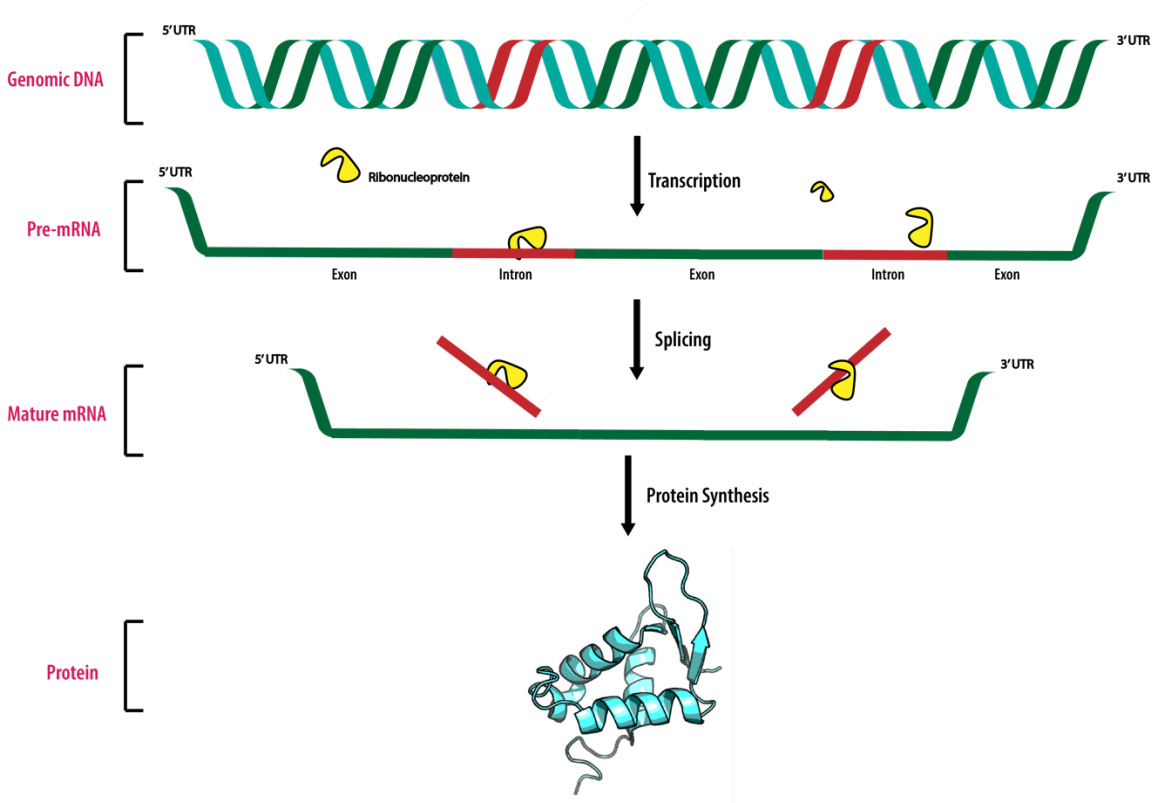

Figure 1-1. **The schematic representation of gene expression and RNA splicing**. Pre-mRNA undergoes post-transcriptional modification (including splicing) before mature mRNA gets translocated into the cytoplasm and serves as a template for protein translation.

Unlike capping and polyadenylation, where the modification protects the mRNA from degradation, splicing is a powerful tool for the manipulation of genetic information by the cell (10). In splicing, a complex known as spliceosome removes or retains the alternatively positioned introns (non-coding sequence) of pre-mRNA. This leads to the formation of different mRNA products, depending on which introns are retained or

detached by spliceosomes (11). Finally, the resulting mature mRNA in eukaryotes transports to the cytoplasm to serve as a template for protein synthesis by the ribosome in a process known as translation (12).

TFs, as the regulator of this process, have vital prominence in the highly regulated and complex process of gene expression. **Figure 1-1** shows the process of Gene expression in eukaryotes and highlights the RNA splicing.

1.2 TFs Structure and Classification

TFs have several domains: a DNA Binding Domain (DBD) responsible for recognition and binding to a specific sequence of DNA, one trans-activation domain (TAD) and Tran-repression domain (TRD), responsible for protein-protein interaction with other proteins including co-activator and co-repressors and a Signal Sensing Domain (SSD), which regulate DNA or protein binding in response to cellular signals (5). The DBD is a particular part of TFs, which makes them different from other proteins like non-specific DNA binders involves in gene regulation (13).

The unique feature of TFs is their ability to recognize a specific sequence of DNA (14). So far, around 1500 different TFs have been identified and classified in different families, typically based on the similarity of their DBDs (15,16). It means that TFs in which their DBDs have similar sequence homology belongs to the same family of TFs (17). Stegmaier and collogues classified the TF based on the homology of their DBD into five superclasses: Basic domains, zinc coordinating domain, helix-turn-helix (HTH), beta scaffold domain and others (those who does not fall into any class) (18).

1.3 Approaches in Targeting TFs

Mutation and overexpression of TFs have been related extensively to different diseases in the literature (19). 165 TFs are directly related to 277 different diseases (15) Including cancer, inflammatory disease, metabolic disorder, and heart abnormalities [reviewed in reference (19)]. So, pharmacological inhibition of TFs is becoming the primary therapeutic goal in the treatment of many diseases. in the literature, many attempts have been made using different approaches to target TFs. With the main emphasis on cancer, we briefly discuss the different TF targeting strategies reported in the literature using small molecules only. The inhibition of TF by oligonucleotides, miRNA, and CRISPR-CAS9 will not be discussed here.

1.3.1 Indirect Targeting of TFs

1.3.1.2 Inhibition of TF Expression

The regulation of many TFs is controlled by surface receptors and specific protein kinases. As a result, any modulation in their effect (including mutation) could result in the deregulation of the corresponding downstream TF.

Many agents are claimed in the literature to be the specific inhibitor of TFs, which in fact target the upstream molecules, receptors, or kinases. In other words, this strategy target and inhibit the TFs at the expression level.

A suitable example could be the oncogenic TF Forkhead Box M1 (FOXM1). Antidiabetic thiazolidinediones (troglitazone), mainly known to be the activator of Peroxisome proliferator-activated receptor (PPAR) gamma TF, can considerably suppress the level of FOXM1. Petrovic et al. reported that these compounds could inhibit the SP1, a TF known to promote FOXM1 expression (20).

Mammalian target of rapamycin (mTOR) complex is a member of the kinase family and serves as the key and central regulator of cellular growth, metabolism, and other vital cellular processes (21). In the literature, several studies are published on the effect of mTOR1 inhibition and substantial gene expression deregulation. These findings revealed that mTOR lay in the upstream of many physiologically essential TFs, including Signal transducer and activator of transcription 3 (STAT3), PPAR alpha, PPAR gamma, and hypoxia-inducible factor 1 alpha (HIF1α) (22).

For example, HIF1α is the master regulator of cellular response to the oxygen level. Under the hypoxic condition, the HIF1α regulates anaerobic regulation of metabolism, angiogenesis, and cell proliferation via regulation oxygen-independent pathways (23). HIF1α is known to be positively regulated by mTOR, and inhibition of mTOR suppressed the HIF1α activity (22,24).

1.3.1.3 Inhibition via Epigenetic DNA Modifiers

As we mentioned earlier, repressors, activators, different co-factors, and many other proteins and enzymes, including epigenetic DNA modifiers, can directly or indirectly bind and modulate the process of transcription.

Epigenetic modifiers act by adding, reading, or removing different functional groups like methyl and acetyl groups to either DNA or histones without altering the DNA sequence (25). As the backbone of the chromatin, DNA is tightly wrapped around histone protein: H2A, H2B, H3, and H4 (26). Histone modifiers classified into three classes, either they add a group: like histone acetyltransferases (HATs), read specific epigenetic groups on the DNA or histone-like ARID1A or remove a group like histone Deacetylase (HDACs) [reviewed in reference (27)].

The state of DNA packaging is known to have a significant effect on the rate of gene expression (28). For example, acetylation of histone by HATs increase the level of transcription and gene expression by opening the condensed chromatin while removing of an acetyl group from the lysine amino acid on the histone by HDACs which force the DNA to bind tighter around histones and turn off the gene expression (29,30). Hence, Modulation of HDAC or HAT function can lead to a significant increase in the expression of specific genes.

They can also indirectly affect TFs by modifying their protein modulators. HDAC5 and 6 deacetylate the heat shock proteins HSP70 and HSP90 to increase the stability of HIF1α. Inhibition of HDAC5 and 6 leads to over acetylation and hence, degradation of HIF1α (31,32).

1.3.1.4 Targeting via Protein Degradation

The protein level of TF as the critical regulator of gene expression is cautiously controlled by ubiquitination and proteasomal degradation as a part of post-translational modification (33). E3 ubiquitin ligase is a protein that upon binding to the specific protein substrate, drive ubiquitylation and protein degradation (34),

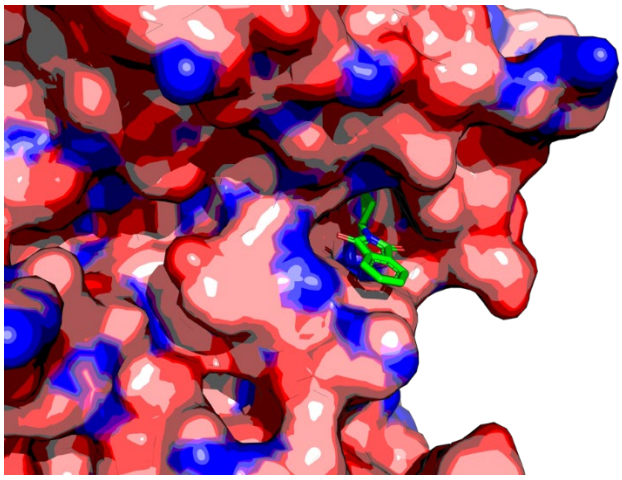

Figure 1-2. **Structure of thalidomide binding to the Ddb1-Crbn E3 ubiquitin ligase.** Upon binding, thalidomide promotes the ubiquitation and proteasomal degradation of IKZF1 and IKZF3 TFs.

A relevant example of this type of TF targeting is the inhibition of Ikaros family zinc finger protein (IKZF1 and IKZF3) TFs, the critical drivers of myeloma, which are commonly considered undruggable (35,36). Thalidomide is initially approved for morning sickness and later on withdrawn from the market due to its tragic teratogenicity. Studies suggested it could be repurposed as an effective treatment of myeloma by decreasing the level of IKZF1 and IKZF3(36) (37). It is found that it increases the binding of E3 ubiquitin ligase cereblon (CRBN) to IKZF1 and IKZF3 and thereby boosting their degradation (36). **Figure 1-2** is the solved structure of thalidomide in complex with DDB1-Crbn E3 ligase (PDB ID: 4CI1) (38).

1.3.1.5 Direct Targeting of DNA

Sequence-specific targeting DNA using a small molecule is another indirect approach to interfere with the binding of oncogenic TFs to their genomic DNA. A different class of drugs with diverse modes of DNA binding has been introduced and are currently in the

clinic. Among them are alkylating agents with the ability to covalently bind to the DNA helix or intercalate the DNA base pairs, etc.

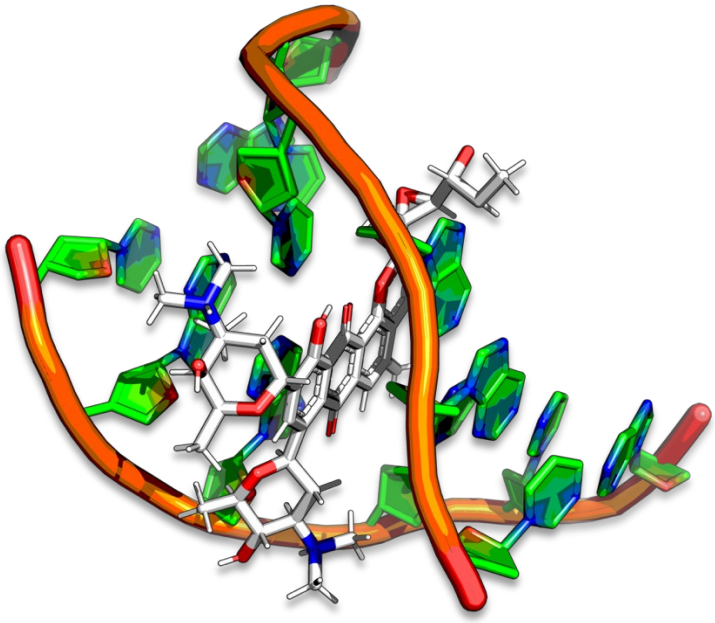

Figure 1-3. **The Solution structure of hedamycin in complex with DNA.** Hedamycin directly targets DNA through intercalation and modulate transcription.

The naturally occurring antibiotic, hedamycin, is a member of pluramycin alkylating drugs. It covalently binds and intercalate the DNA bases and alkylate the N7 atom of guanine residue (39). Please see **Figure 1-3** (PDB ID: 1JHI) (40).

Another well-known and currently widely used chemotherapeutic drug is cisplatin (41). It has been used in the clinic for the treatment of various cancer types, including lung (42), gastric (43), lymphoma (44), etc. Once cisplatin enters the cell and cytoplasm, the chlorine atoms are exchanged with a water molecule and make the resulting compound a potent electrophile which violently reacts with numerous electrophiles inside the cell including sulfhydryl group of proteins and nucleic acid [**Figure 1-4**. PDB ID:

5BNA (45)]. This process leads to intra and inter-strand crosslinking, which results in DNA bending, distortion and denaturation (46).

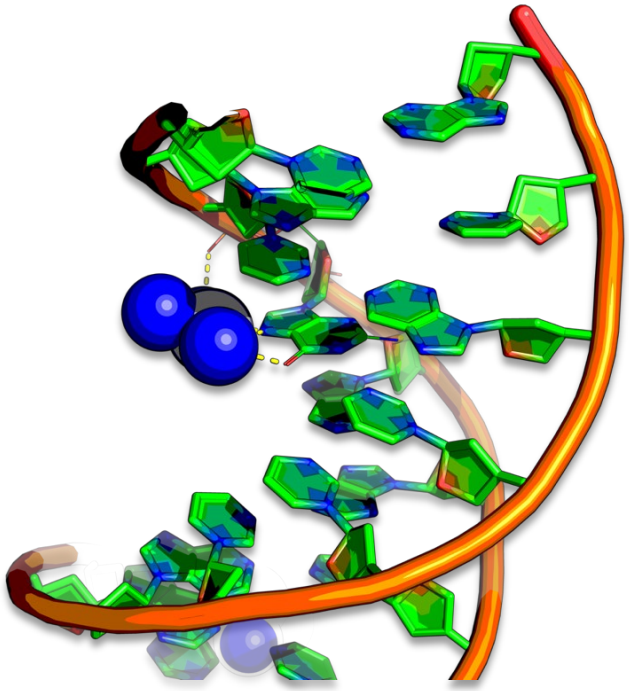

Figure 1-4. Solved structure of cisplatin in complex with B-DNA dodecamer. Cisplatin influences transcription by influencing DNA structure and damage.

1.3.2 Direct Targeting of TFs

Direct inhibition of TFs is a challenging task as they lack a well-defined binding site on their surface. Contrarily to what is explained in indirect inhibition, which could lead to activation, inactivation of deregulation of many off-target effects, direct inhibition would lead to a better and more precious therapeutic output (47).

1.3.2.1 Dimerization Interruption

As described earlier, TF may bind to many other proteins, including co-factors, co-activator, or repressors, and even other TFs to facilitate their binding to the genomic DNA.

Figure 1-5. **3D structure of dimerized MYC/MAX in complex with the DNA**. Cartoon representation of dimerized Myc (blue) and Max (purple) bound to their target DNA.

An example of this type of inhibition was observed with Myc TF. Myc is the transcription regulator of almost 15% of the whole genome, and researchers refer to them as "super-TFs" [(reviewed in reference (48)]. MYC is found to be essential in normal embryonic development and regulate cell growth and apoptosis. In cancer, the MYC regulation is disrupted, which leads to its over-amplification and tumor formation (48).

This oncogenic protein undergoes heterodimerization with its associate proteins MAX or MAD, to regulate or repress gene transcription. **Figure 1-5** shows the 3D structure of the MYC/MAX complex binding to the DNA (PDB ID: 4HG7) (49). Upon binding to MAX, it recruits different chromatin-modifying complexes and binds to the target gene promoter regions. (50)

Many attempts have been made with the purpose of inhibition of MYC/MAX dimerization. Yin et al. identified several small molecules capable of binding to the Helix-Loop-Helix Leucine Zipper (bLHL-Zip) domain of Myc and inhibit its dimerization with MAX (51). D'Agnando and colleagues introduced another class of Myc dimerization inhibitors. They synthesized a mimetic peptide capable of binding to the leucine zipper region of the MAX and hence interfere with the MYC/MAX complex DNA binding ability (52). In another approach, wang et al. discovered the unique properties of a natural product celastrol to disrupt the MYC-MAX dimer and abolish the DNA binding of the complex (53).

1.3.2.2 Inhibition of Protein/Protein interaction

A relevant example of this type of TF targeting is P53, which is also known as the "guardian of the genome" (54). As the name implies, it protects the genome from any unexpected mutation and DNA damage by sending the stop signal and terminating the cell cycle (55). It is well-known that more than 50% of all human cancer carries a mutation in their TF P53 (56). Upon DNA binding, P53 activates the formation of another factor called P21, which interacts with cell division protein kinase 2, an essential regulator of the S phase to stop the cell cycle (57). Murine double minute 2 (MDM2) a ubiquitin ligase that upon binding to the p53 promotes its degredation and subsequent translocation

(58). P53 regulates the expression of MDM2, were they form an autoregulatory loop to keep the cellular level of p53 low in the absence of stress (59). **Figure 1-6** represents the 3D structure of MDM2 in complex with the p53 TAD.

The level of MDM2 is overexpressed in majority of human sarcomas (60,61), which leads to excessive degradation of p53, where lack of this vital tumor suppressor TF leads to severe consequences.

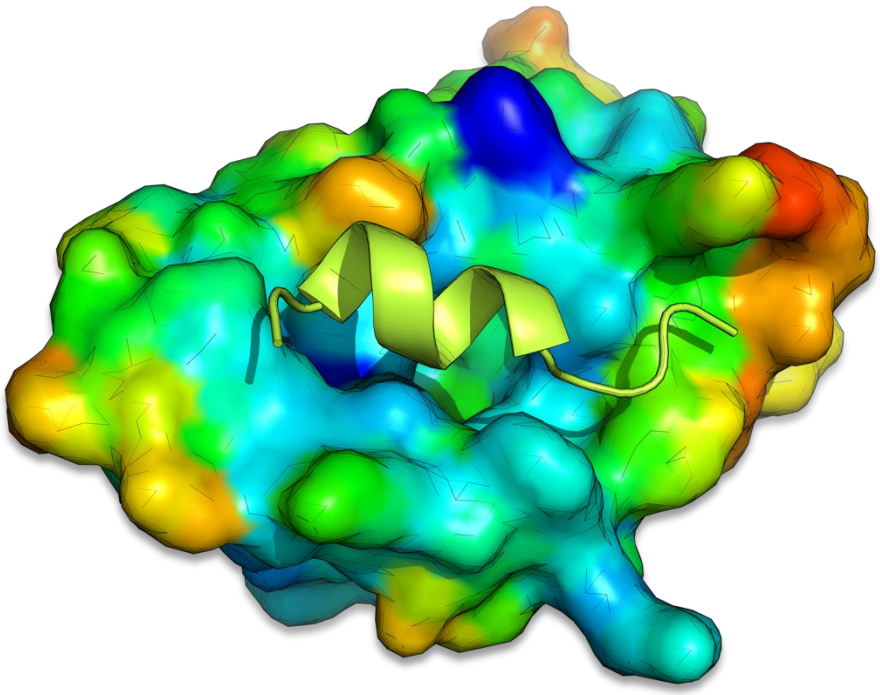

Figure 1-6. 3D rendered structure of MDM2 bound to the TAD of p53. MDM2 (green ribbon), a ubiquitin ligase, binds to the TAD of p53 and negatively regulates it.

Blocking the activity of MDM2 has the significance of elevating the level of one of the most crucial human protein suppressor proteins, p53. Vassilev et al., using high throughput screening of a large library of compounds, found several potent inhibitors of MDM2 (Nutlin1-3), which could block the binding of MDM2 and reactivate the p53 pathway (62). **Figure 1-7** portrayed the 3D structure of MDM-2 in complex with nutin-3

(PDB ID: 4HG7) (63). Most Recently, a nutlin derivatives (RG7112) currently in the clinical trial, was found to be effective in the upregulation and stabilization of p53 at the cellular level (64).

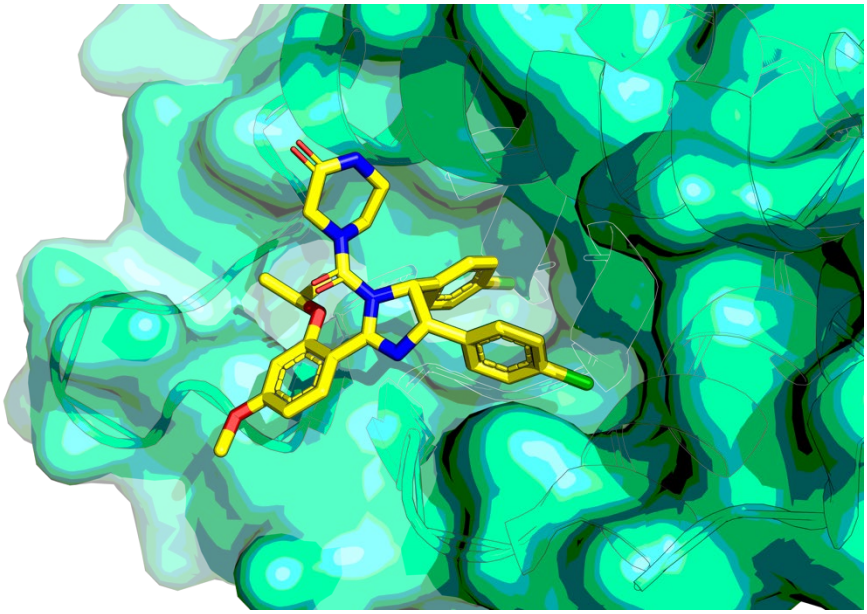

Figure 1-7. 3D structure of MDM2 in complex with nutlin-3. Cartoon representation of MDM2 inhibitor nutlin-3 (yellow sticks) in complex with MDM2. Nutlin-3 blocks the binding of MDM2 to p53 and inhibit its MDM2 mediated degradation.

These are just a few examples of numerous attempts using different approaches to target the MDM2-p53 complex.

1.3.2.4 Inhibition via Ligand-Binding Domain

Unlike many other TFs, nuclear hormone receptors superfamily possesses a highly conserved binding site where their natural ligand (hormones) binds and modulate gene expression (65). Due to the presence of a well-defined pocket in the ligand-binding

domain (LBD), the design and identification of small molecule inhibitors is a much easier task in comparison to other TFs.

Around 70% of all cases of breast cancer express the estrogen receptor (ER) (66). A different class of drugs has been introduced to inhibit the growth and cell proliferating signal of this receptor and hence stop the cancer progression. When the natural ligand of the ER (estrogen) binds to its LBD, recruits co-activators, and undergoes necessary conformational changes and receptor dimerization before binding to the ER element of DNA (67,68).

Tamoxifen is a drug that belongs to the selective ER modulators (SERMs) class of ER inhibitors (69). When the tamoxifen binds to the LBD, the resulting conformational changes block the binding of co-activators and instead recruit co-repressors resulting in the alteration of gene expression (70). **Figure 1-8** shows the crystal structure of tamoxifen in complex with the ER-alpha LBD (PDB ID: 2JF9) (71) Fulvestrant belongs to the selective ER degraders (SERDs) class. Upon binding to the LBD, it inhibits ER dimerization and accelerates its degradation (72).

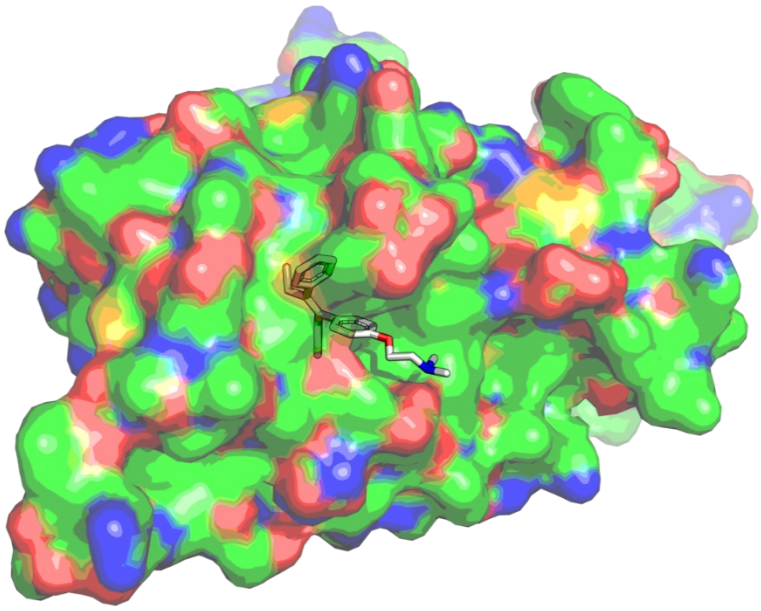

Figure 1-8. Crystal structure of tamoxifen in complex with the ER alpha LBD. The conformational changes induced by tamoxifen recruits co-repressors and modulate the target gene expression.

1.3.2. Inhibition via Binding to DBD

As mentioned previously, the lack of a well-defined binding pocket on the surface of TFs makes them extremely difficult to target directly. Hypothetically, a perfect inhibitor would be a small molecule with the ability to selectively bind to the DBD of the TF and prevents its binding to the target DNA. Efforts to target the DBD of TFs have been widely reported in the literature.

Androgen receptors (AR) belong to the family of the nuclear hormone receptor and are responsible for the expression of the genes for the development of the male phenotype (73). However, androgen has been found to play a critical role in the progression and occurrence of several types of prostate cancer (74). Currently, in the clinic, there are several antiandrogen drugs with the ability to compete with the

endogenous androgen hormone in the LBD. However, there are several reports published regarding cancer acquiring resistance to these antiandrogens (75,76). As a result, there was an emerging need to obtain a new strategy to inhibit these TFs.

In a major advance in 2014, Li et al., by employing computational modeling, identified a potential binding pocket on the surface of the AR DBD. Then, using *in silico* high-throughput screening of around 3000000 purchasable chemical compounds deposited in the zinc library, found a potent hit. They optimized the discovered hit and finally reported a compound capable of directly binding to the AR DBD, equipotent to the FDA approved antiandrogen enzalutamide (77).

In 2014, Huang and co-workers identified a potent inhibitor of STAT3 using computer-aided screening. The DBD binding agent ins3-54 was able to potently prevent the binding of STAT3 to DNA in a DNA binding activity assay as well as the luciferase reporter assay (78).

Paired box-2 (PAX2) is a member of the PAX family, which commonly reactivates in kidney and renal cell carcinoma (79). It is shown that the reduction in the level of PAX enhanced the apoptosis and improved the sensitivity of cells to the chemotherapeutic agents (80,81). Griemly and collogues used computer-aided virtual screening and the 3D structure of PAX2 to identify a lead compound that would disrupt the binding of PAX2 to its consensus DNA. Out of the initial 227 hits, using the luciferase reporter assay, five were found to be specific towards PAX2. Among them, compound EG1 was found to inhibit PAX2 selectively (79).

1.4 Forkhead box Superfamily

Forkhead boxes are diverse families of TFs essential for the regulation of cell growth, differentiation, DNA repair, angiogenesis, tumorigenesis, hemostasis, and longevity (82,83). The members of these TFs share a conserved winged-helix DBD containing 80-100 amino acids but possess discrete transactivation and repression domains (TAD & TRD) (84,85). Despite the resemblance in their DNA binding sequence and DBD, the variation in their other domains gives each member a unique function (86).

In humans, over 50 members of this family have been identified, and their sequence homology classified them into 19 different species (87). Some members of the FOX TFs family have been extensively connected to cancer. Among these, the involvement of FOXA, FOXC, FOXO, and FOXM in cancer development and tumorigenesis has been comprehensively studied (88).

1.4.1 Forkhead Box A

Frokhead box As (FOXAs) are an essential class of the forkhead family of TFs required for organogenesis, glucose metabolism, and hemostasis (89). Several members of this family have been recognized and found to be involved in cancer (FOXA1, FOXA2, FOXA3) (90–92). The elevated level of FOXA1 has been observed in breast invasive ductal carcinoma (IDC) (93). In a recent finding, FOXA1 was identified as a probable non-small cell lung carcinoma proto-oncogene. It has also been reported that FOXA1 gene silencing led to a decrease in cell invasion, proliferation and cell cycle arrest of lung carcinoma (94).

The other member of this group of TFs (FOXA2) has an opposing effect. The notable tumor-suppressing activity of FOXA2 has been recently explained in the literature (95). It has been also shown that loss of FOXA2 function promotes EMT and supports metastasis in liver cancer (96). **Figure 1-9** shows the 3D structure of FOXA2 in complex with its consensus DNA (PDB ID: 5X07) (97).

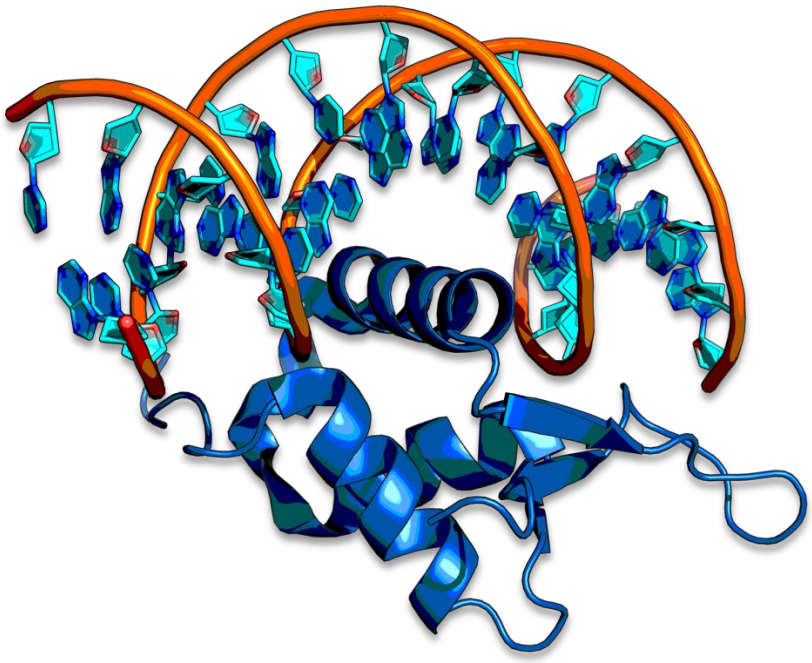

Figure 1-9. Crystal structure of FOXA2 DBD bound to its consensus DNA. Cartoon representation of FOXA2 DBD (blue) in complex with the major groove of its consensus DNA.

However, the role of FOXA3 has not yet fully understood. Some preliminary work was carried out in 2019 and linked FOXA3 overexpression to tumor invasion and metastasis. Nevertheless, the effect was the consequences of direct regulation of FOXA1 and FOXA2 by FOXA3(98).

1.4.2 Forkhead Box C

A growing body of literature has investigated the role of FOXCs in tumorigenesis. FOXC1 is a vital regulator of cerebral and ocular development, and its mutation has been linked to Axenfeld Reiger Syndrome (ARS) and Dandy-Walker Malformation (DWM) (99–101). Besides these, several studies highlighted the role of this developmental TF to tumorigenesis and metastasis in basal-like breast cancer (BLBC), Hepatocellular, and endometrial carcinoma (102–105).

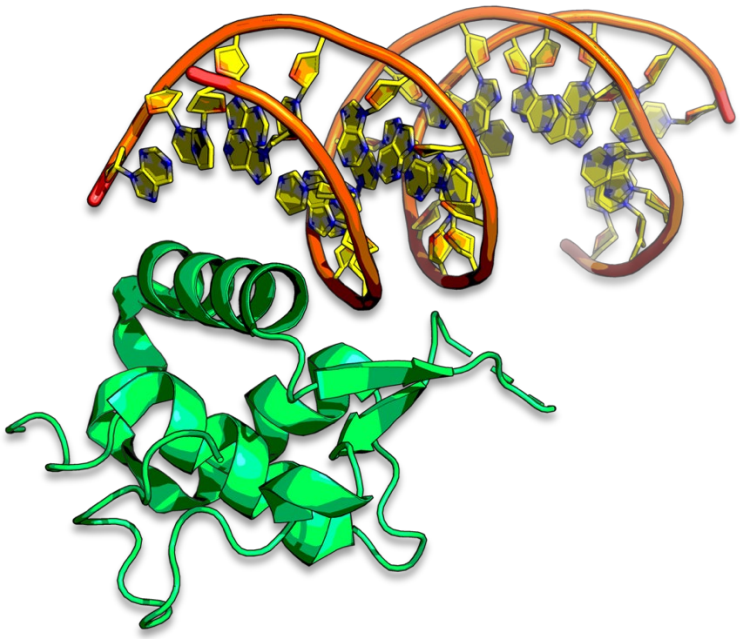

Figure 1-10. 3D structure of the FOXC2 DBD in complex with the DNA. Cartoon representation of FOXC2 DBD (green) bound to the DAF-16 binding element.

FOXC2 [**Figure 1-10** (PDB ID: 6AKP)] (106) is an essential regulator of blood vessel formation and development (107). The fundamental role of FOXC2 in cancer has also been investigated in the literature. It has been proposed that FOXC2 enhances the proliferation of glioblastoma cells by direct regulation of the epidermal growth factor

receptor (EGFR) (108). Moreover, FOXC2 is shown to promote colorectal cancer cell growth by negatively modulating the level of Cyclin D1 and p27 by activating other protein kinases like MAPK and AKT and inactivating the bonafide tumor suppressor, FOXO3a (109).

1.4.3 Forkhead Box O

The "O" subclass of Forkhead box TFs consists of 4 members (110). Despite their high degree of sequence homology, they show discrete function and tissue expression patterns (111). FOXO1, FOXO3, FOXO4, and FOXO6 all have 4 main domains. They use their highly conserved winged-helix DBD to tightly bind as a monomer to the DAF-16 family members binding element (5′-GTAAACAA-3′). These transcription factors could also target and bind to the Insulin Response Element (5′-(C/A)(A/C)AAA(C/T)AA-3') (112,113). They also possess a nuclear localization signal (NLS) and nuclear export sequence (NES) in charge of shuttling the protein between cytosol and nucleus and a C terminal TAD mainly in charge of protein interaction (110,114). 3D rendered crystal structure of FOXO1 is illustrated in **Figure 1-11**.

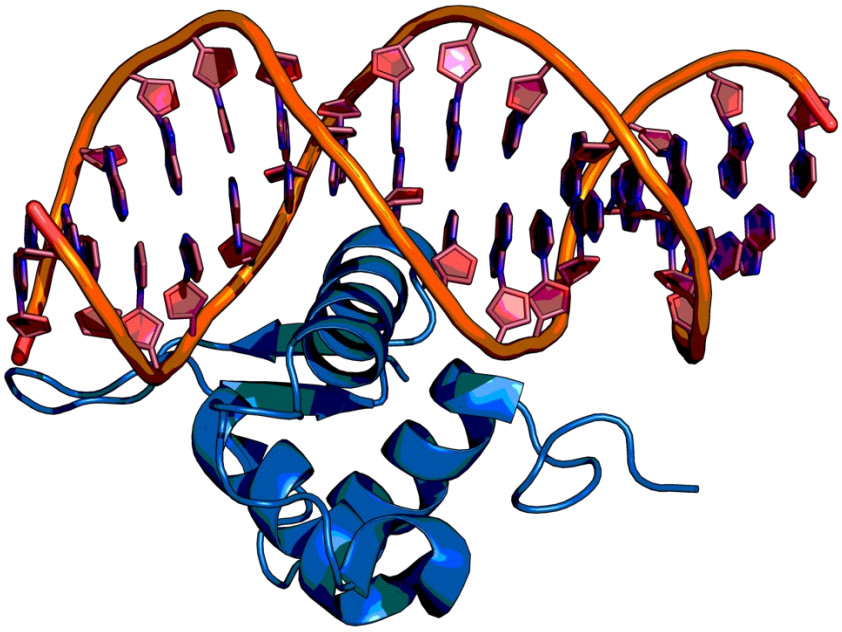

Figure 1-11. Crystal structure of FOXO1 DBD bound to DNA. Cartoon representation of FOXO1 DBD (blue) in complex with its consensus DNA recognition sequence (Orange).

Several post-translational modifications control the function of FOXO proteins. The highly conserved insulin–phosphatidylinositol 3-kinase–AKT/Protein kinase B (AKT/PKB) signaling pathway is the most well-studied regulator of FOXOs. AKT/PKB phosphorylates different sites on the FOXO proteins, one on the N-terminal domain and the other one on the NLS domain. The regulatory protein 14-3-3 recognizes and binds to these two sites and facilitates the shuttling of FOXOs to the cytosol (115–119). It's binding also hinders the DBD and functionally inactivates FOXOs (120).

FOXOs are known as “bona fide” tumor suppressors (121). The adult mice having triple FOXO knock out (FOXO1, FOXO3, and FOXO4) showed a significant increase in tumor formation (122). It has been shown that they interact with other proteins or TFs to

induce or suppress tumorigenesis. It was reported that FOXO3 is essential for p53 dependent apoptosis (123). More recent evidence suggested that loss of FOXO3 function increased MYC-driven lymphomagenesis (124).

The role of FOXO1 in carcinogenesis has been extensively studied. An interesting investigation showed that FOXO1 activation in osteosarcoma (which the FOXO1 express is extremely low) led to an increase in colony formation and cancer cell proliferation via modulation of WNT/ß-catenin pathway (125).

FOXO3, another member of this family, is commonly inactivated or mutated in cancer. Its inactivation by stimulation of the PI3K/AKT pathway is strongly linked to cancer initiation, invasion, and progression in different tumors (126,127). FOXO3 inactivation in transgenic adenocarcinoma resulted in the loss of cell cycle control and cancer progression (128).

Despite their confirmed role in tumor suppression, several studies claimed that FOXOs could support tumorigenesis (129). It is reported that mutation in FOXO1 in the residues that support the 14-3-3 binding leads to an increase in nuclear localization of active FOXO1. Surprisingly, these mutations in FOXO1 were associated with poor patient prognosis treated with chemotherapeutic drugs, and bring uncertainty toward FOXOs as genuine tumor suppressors (130). The overexpression of FOXO3 has also been linked to a decline in survival rate in patients suffering from acute Myeloid Leukemia (AML) (131).

Besides these, FOXO3 and FOXO1 have been found to support tumor metastasis. FOXO3 dependent regulation of matrix metalloproteinases 9 and 13 (MMP9 and MMP13) and FOXO1 medicated regulation of MMP1 has been strongly linked to metastasis (132,133).

There is still considerable uncertainty regarding the tumor supporting or suppressing function of FOXOs, and further investigation is required to shed light on these mysterious TFs.

1.4.4 Forkhead Box M

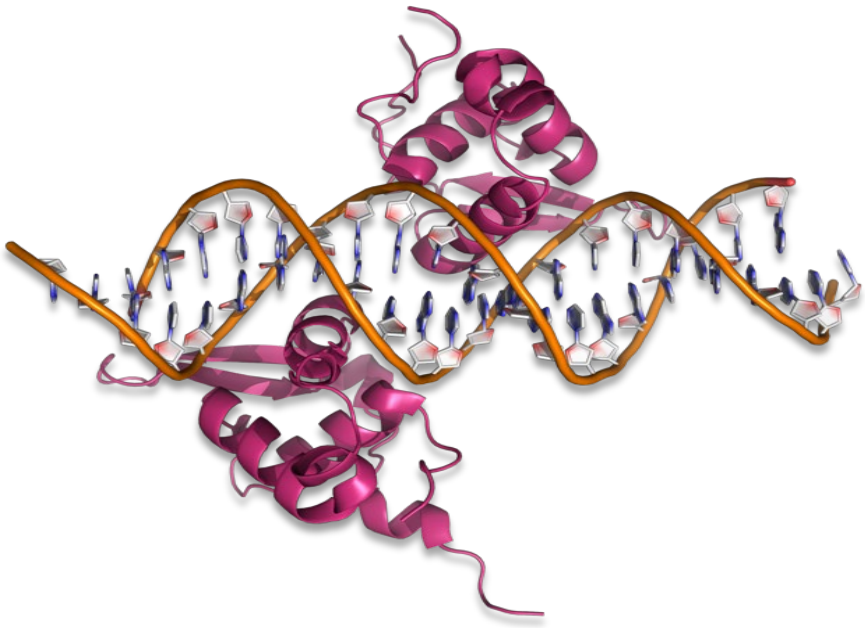

Figure 1-12. Structure of FOXM1 DBD in complex with DNA. Cartoon representation of winged-helix DBD of FOXM1 (red) bound to the major groove of its consensus DNA.

HNF-3, Trident, or FOXM1 [**Figure 1-12** (PDB ID: 3G73)] (134) is another critical and extensively investigated member of the forkhead box superfamily (135). To date, four different isoforms of FOXM1 has been identified. As shown in **Figure 1-13**, the FOXM1 gene carries ten exons on chromosome 12, where alternative splicing of exons A1 and A2 gives four different isoforms (136,137). The longest isoform being translated from the mRNA carrying all ten exons is FOXM1a and found to be transcriptionally inactive. The

disrupted TAD of FOXM1a with the fact that it only has a functional DBD might make it a negative transcriptional regulator (138).

On the other hand, FOXM1b possess none of exons A1 and A2 and regarded as the smallest member of FOXM1. FOXM1c only carries exon A1 and the most recently found FOXM1d has been identified to have exon A2 only (138,139). While all are capable of binding to the DAF-16 and IR element, FOXM1c can furthermore bind to the TATA box and activate additional genes (112,140).

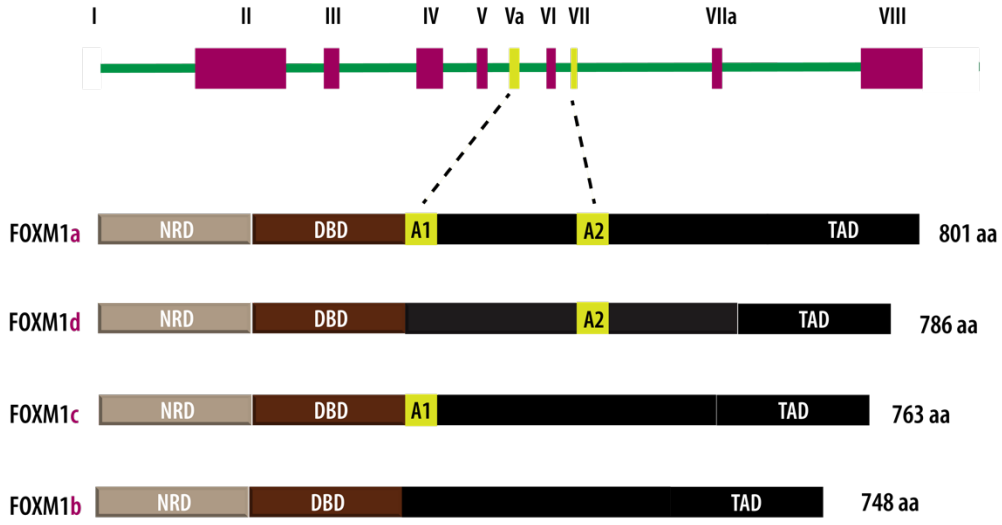

Figure 1-13. Graphical representation of four different FOXM1 isoforms. FOXM1 gene comprises of ten exons, of which exon VA and VIIa are splicing exons. The process of RNA splicing results in 4 different FOXM1 isoforms, FOXM1a, b, c, and d.

FOXM1 level can only be detected in actively proliferating cells while its level is null in quiescent cells (141). External and internal stimuli and transmembrane receptors like EGFR, estrogen, polo-like kinase 1 (PLK1), placental lactogen (PL) could boost the expression of FOXM1 which force the resting cell to re-enter the cell cycle (142–145). Re-expression of FOXM1 was also observed after tissue regeneration upon injury. Organs

with regenerative capacity like liver, lung, and pancreas; re-express FOXM1 during their tissue repair (146–148).

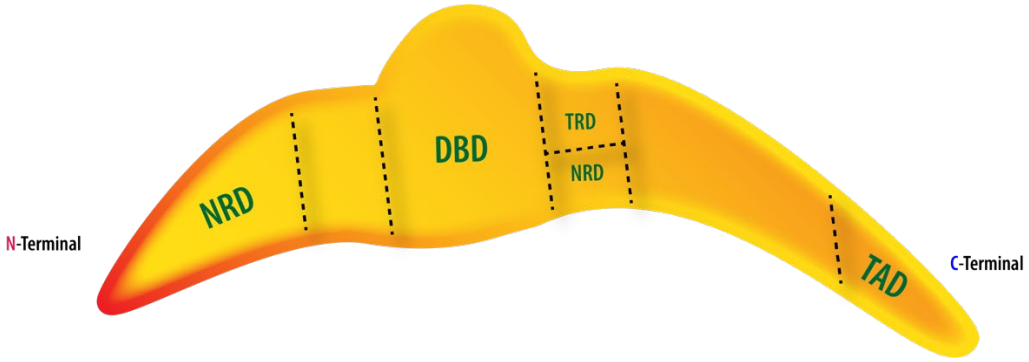

Figure 1-14. Schematic illustration of 5 functional domains of FOXM1. FOXM1 protein consists of several domains: a DBD, two NRD, one transactivation, and one transrepression domain.

As shown in **Figure 1-14**, FOXM1c has five functional domains (149). One highly conserved DBD in the middle (134,150), a robust acidic TAD at the c-terminal, two negative regulatory domain (NRD), one on the opposite side (N-terminal) and the other one in the middle and lastly one transrepression domain (TRD) near the DBD (151).

Antiproliferative and proliferative signals highly control the FOXM1 expression. In the presence of proliferative signals (149,152), FOXM1 induces cell cycle progression by promoting G1/S and G2/S transitions (141). The nuclear level of functional FOXM1 is highly regulated through an autorepression mechanism (151). The NRD of FOXM1 binds to the RXL/LXL motif on the FOXM's TAD and acts as an on/off switch (**Figure 1-15**) (153). Despite the high level of FOXM1 expression, it is shown that binding of cyclin E/CDK2 complex to the TAD and phosphorylation of FOXM1 is not sufficient for the full activation of FOXM1. However, the autorepression is relieved by binding and

phosphorylation of cyclin A/CDK during the G2 phase (153). Finally, in late mitosis, the E3 ubiquitin ligase $APCC^{cdh1}$ binds and promotes its degradation by proteasomes (154).

The expression of FOXM1 is induced during the growth phase (G1) and continues with the cell cycle during synthesis (S) and mitosis (M) phase (155). As an activating TF, FOXM1 binds to the promoter region of many target gene and regulate their expression. Other than that, FOXM1 is also capable of hypermethylation of DNA or recruiting co-repressor to modulate transcription of target genes (156).

FOXM1 can also bind to other proteins and promote the expression of target genes without directly binding to their promoter region. A report published by Zheng et al. suggested that the FOXM1 binds to ß-catenin and promotes its nuclear localization as well as its transcriptional activity (157). Another study proposed that FOXM1 binding to SMAD3 prevents its degradation by proteasome by blocking the E3 ubiquitin-binding and hence inhibiting SMAD3/SMAD4 dimerization (158).

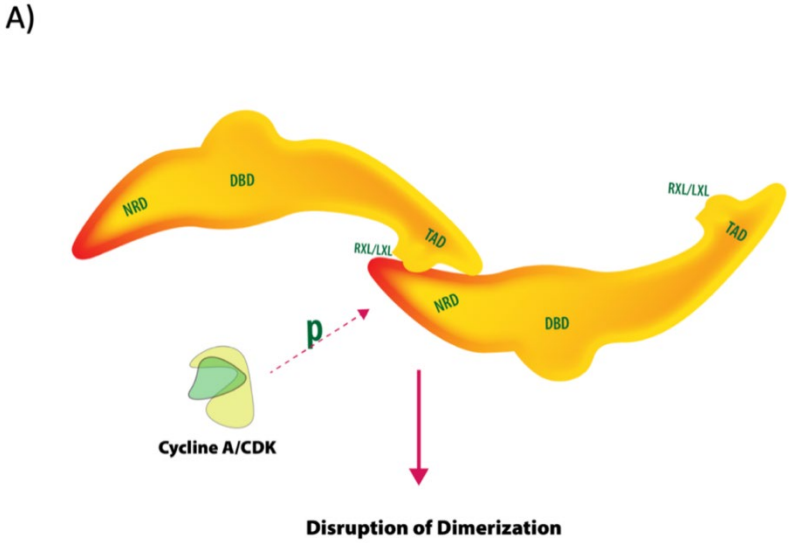

B)

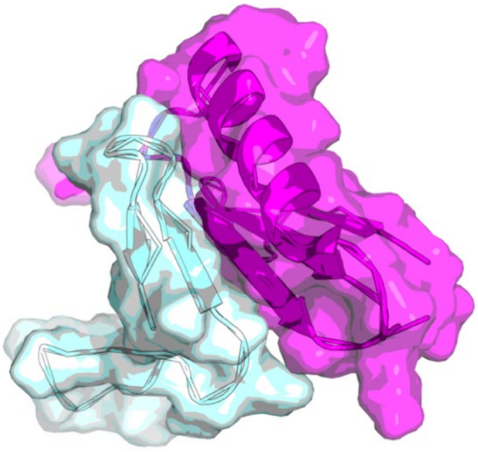

Figure 1-15. The mechanism of FOXM1 autorepression. A) the RXL/LXL domain on the TAD of FOXM1 binds to the NRD of FOXM1 and inactivates it. FOXM1 phosphorylation with Cyclin A/CDK complex relives the autorepression. B) The solution structure of the TAD of FOXM1 bound to the N-terminal repression domain (PDB ID: 6OSW) (159).

Besides its role in enhancing the cell cycle and hence cell proliferation, FOXM1 is found to be involved in DNA repair and DNA damage response. It was shown that the level of FOXM1 was substantially increased upon induction of DNA damage by IR and UV radiation. It was suggested that FOXM1 stabilization by phosphorylation of checkpoint kinase 2 (CHK2) enhanced FOXM1 dependent expression of DNA repair factor x-ray cross-complementing group 1 (XRCC1) and breast cancer-associated gene 2 (BRCA2) (160).

In the literature, many proteins (including USP21 (161), NPM (162), HSP70 (163)) are found to regulate the transcription of FOXM1. An excellent example of this was recently published by Arceci et al. (161). They found that ubiquitin carboxyl-terminal hydrolase 21 (USP21) binds to FOXM1 and decreases FOXM1 ubiquitination and hence

increases its activity and stabilization. In another study, Bhat et al. found that nucleophosmin (NPM), interact with FOXM1 and modulate its localization (162). Another chaperone family, HSP70, was reported by the same group and found to inhibit the FOXM1 DNA interaction by directly binding to FOXM1 (163).

Direct binding of TFs to the promoter region of FOXM1 has also been reported. The most significant example of this type of FOXM1 modulation is FOXM1 itself. FOXM1 binds to its own promoter and regulates its expression through a positive feedback loop (164). p53 is known to negatively regulate FOXM1 expression. The level of FOXM1 mRNA and protein level increased upon p53 knockdown, whereupon reinduction, FOXM1 level returned to normal (165).

In tumors, FOXM1 expression is dysregulated. Cancer cells highly rely on FOXM1 for their prompt growth, proliferation, and invasion. (141). Many TFs (c-MYC, Notch1, STAT3) and some vital tumor suppressors (p53, FOXO3a) are found to be responsible for FOXM1 regulation. Since many of these proteins are either overexpressed or mutated in many cancers, it is believed that they may also contribute to the FOXM1 upregulation in cancer [reviewed in reference (166)].

FOXM1 (mainly FOXM1b) (167) is found to be overexpressed in a vast majority of cancers including breast (168), ovarian (169), prostate (170), lung (171), melanoma (172), lymphoma (173,174), osteosarcoma (175), pancreas (176), kidney (177), colon (178) and etc. The direct involvement of FOXM1 in cancer tumorigenesis (179–182), aggressiveness (183,184), metastasis (178,185,186) and its relations with poor patient prognosis (182,187,188) has been widely reported in the literature. Many bodies of literature reported that inhibition of FOXM1 leads to a significant decrease in cancer cell proliferation, migration, angiogenesis and drug resistance [reviewed in reference (189)].

These findings raised the attention toward this oncogenic TF and made it an attractive target for cancer therapy.

1.4.4.1 FOXM1 Inhibition

Many attempts have been made to inhibit the FOXM1 transcriptional activity. Gusarova and colleagues (190) in 2007 introduced a cell-penetrating peptide based on the structure of previously known FOXM1 negative regulator $p19^{ARF}$ capable of inhibiting the FOXM1 as well as cell proliferation in cancer (191). The RNA interference (RNAi) was among the first methods to demonstrate the significance of the FOXM1 role in carcinogenesis. FOXM1 gene silencing and its subsequent mRNA neutralization in colorectal (192), lung (193) leukemia (194), and pancreatic (195) cancer was found to affect cell proliferation and decrease the xenograft tumor growth. Nevertheless, short interfering RNAs (siRNA) have their own limitations in terms of drug delivery and specificity.

In a major advance in 2006, a cell-based assay found the first known chemical inhibitor of FOXM1, siomycin A (196). Later on, they reported a structurally similar drug called thiostrepton, also capable of inhibiting FOXM1 activity (197).

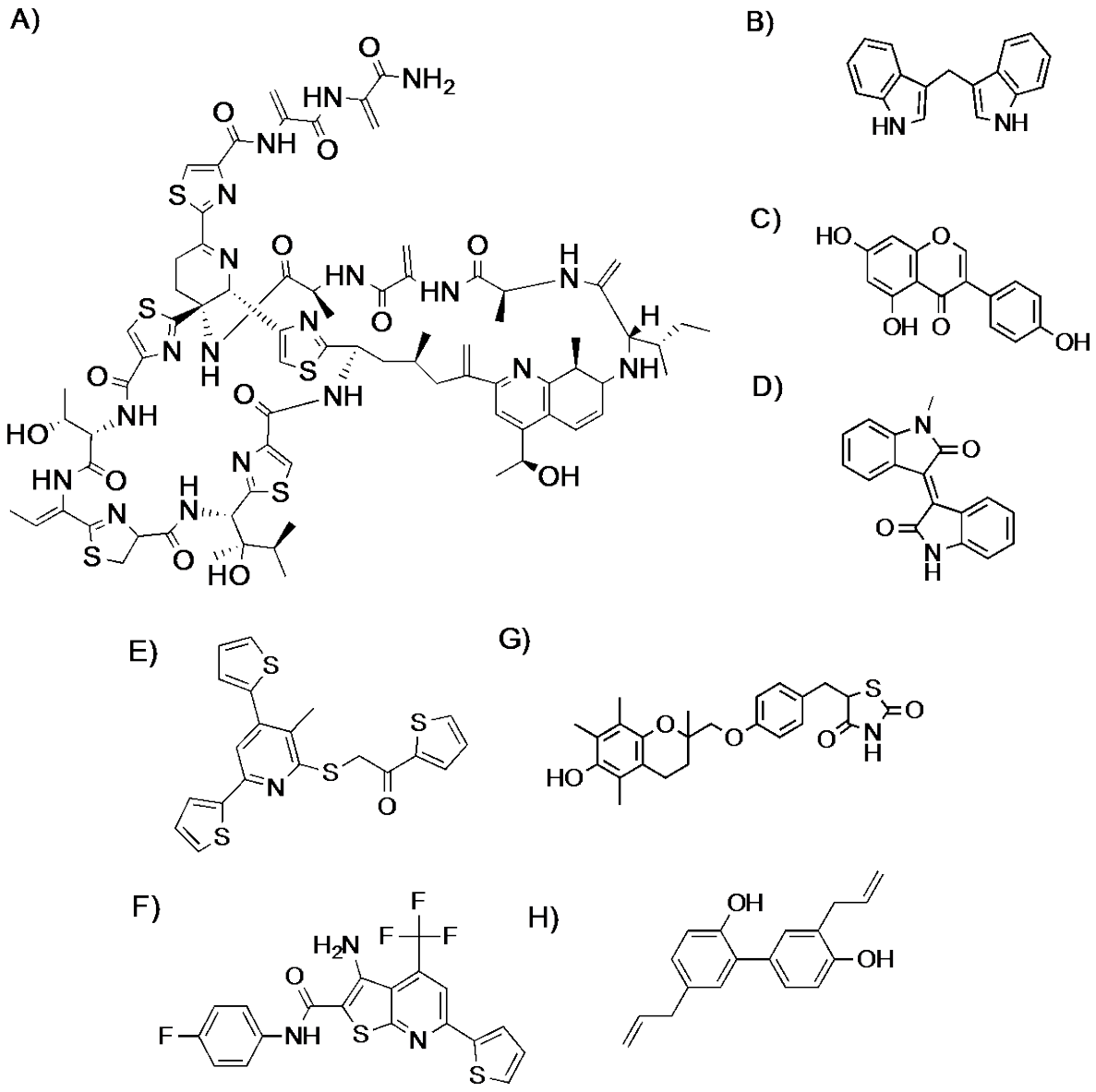

Figure 1-16. Chemical structure of known FOXM1 inhibitors. A) thiostrepton, B) 3,3'-diindolylmethane, C) genistein, D) natura-alpha, E) RCM-1, F) FDI-6, G) trgolitazone, H) honokiol.

Later on, another protease inhibitor like MG115, MG132, and bortezomib was also reported by the same group to negatively regulate the expression of FOXM1 and suggesting a mutual mechanism of action (197). It was hypothesized that the stabilization of FOXM1 negative regulators (p53, p2, MDM-2) by proteasome inhibitors is responsible

for the downregulation of FOXM1 by siomycin, thiostrepton, and other proteasome inhibitors (198). On the same subject, Hedge et al. using the EMSA found that thiostrepton can bind to FOXM1-DBD and disrupts its DNA binding (199). In 2015, Chen et al. reported an *in silico* investigation and used molecular modeling to predict the binding of thiostrepton to the FOXM1 and DNA (200). Later on, in 2019, Kongsema et al. using MD simulation suggested that thiostrepton can bind to the FOXM1 and it is a possible direct inhibitor (201). However, there is a continuous debate on the genuine thiostrepton inhibition mechanism and requires further investigation.

3,3'-diindolylmethane (DIM) was another reported small molecule capable of downregulating the level of FOXM1 in breast cancer cell lines (202). As previously discussed, specificity protein 1 (SP1) TF can bind to the FOXM1 promoter region and enhance its expression. Petrovic and colleagues in 2010 found that inhibition of SP1 by its inhibitor (mithramycine), resulted in significant downregulation of FOXM1. They suggested that PPARY agonist, troglitazone, and other glitazones negatively regulate the expression of FOXM1 by SP1 inhibition (203).

In 2011, two other small molecules (genistein (204) and natura-alpha (205)) were found to inhibit the transcriptional activity of FOXM1 in prostate cancer. In another investigation, Gormally et al. using fluorescence polarization assay, EMSA and mass spectroscopy found a series of compounds capable of directly binding to the FOXM1-DBD and suppressing its transcription by affecting the positive regulatory loop (206).

In 2017, Sun and co-workers identified a compound called Robert Costa memorial drug-1 (RCM-1) using high-throughput screening of around 50.000 molecules (207). This small molecule could inhibit the level of FOXM1 as well as inhibiting the FOXM1/ß-

catenin interaction and hence their nuclear localization. The compound RCM1 was able to decrease cell proliferation, tumor size, and enhanced the tumor apoptosis (208).

Recently, Halasi et al. reported a natural product, honokiol, which can suppress the transcriptional activity of FOXM1. Using EMSA and electron transfer difference nuclear magnetic resonance (NMR) spectroscopy, they suggested that Honokiol binds to FOXM1 and modulate its transcriptional program (209). **Figure 1-16** illustrates known FOXM1 inhibitors with a vast diversity of chemical scaffolds.

1.2 Research Aim

The central aim of this project is to elucidate the mechanism of action as well as the structural requirements of direct FOXM1 inhibitors. This information will significantly help to introduce a novel class of FOXM1 direct inhibitors to the field. In order to achieve the mentioned goals, six objectives were set:

1) To carry out an extensive molecular dynamics simulation using the solved crystal structure of FOXM1 DBD to capture the dynamics of FOXM1-DBD and DNA interaction.
2) To determine a probable small molecule binding site on the surface of FOXM1-DBD.
3) To find a mutual binding mode for current FOXM1 direct inhibitors using different small molecule docking protocols.
4) To validate the proposed binding site using chemical modifications and biological assays.
5) To demonstrate the structural requirement of a small molecule capable of targeting the DBD of FOXM1.

6) To design, synthesize, and evaluate novel FOXM1 inhibitors based on the obtained theoretical and experimental information.

Chapter 2

Untying the Knot of Transcription Factor Druggability: Molecular Modeling Study of FOXM1 Inhibitors

A version of this chapter has been published in:

J Mol Graph Model. 2018 Mar;80:197-210. doi: 10.1016/j.jmgm.2018.01.009

2.1 Introduction

Recent developments in the fields of cancer biology and genetics have significantly increased our understanding of how to validate new drug targets, including TFs, which have been considered "undruggable." Unlike enzymes, ion channels, and cell membrane receptors, TFs do not possess well-defined drug binding sites, and therefore, are challenging (but promising) drug targets (211,212).

The FOXM1 protein, also known as HNF3 or HFH-11, is one of several TFs in the pipeline of drug discovery research programs (212,213). From a structural point of view, there are three different protein isoforms identified in human cells, namely FOXM1a, FOXM1b, and FOXM1c. The FOXM1a isoform appears to be transcriptionally inactive, whereas FOXM1b and FOXM1c are described as "gene activators" (214).

The increasing interest in the FOXM1 TF is based on experimental observations associating the overexpression of this protein with practically all stages of cancer development, including cancer initiation, progression, metastasis, and chemoresistance (215). The FOXM1 protein is one of the main regulators of the cancer cell cycle (193,195), cancer-related angiogenesis (195), decreased rates of cancer cell apoptosis (216), and accelerated DNA damage repair (217). Consequently, FOXM1 overexpression correlates well with poor disease prognosis (218–220). In this regard, the *in vitro* inhibition of FOXM1's transcriptional activity is associated with decreased cell proliferation for different cancer cell types, including liver (221,222), prostate (223), brain (224), breast (216), lung (225), colon (192,226), pancreas (227), skin (228–230), cervix (231), ovary (232), mouth (233), blood (234), and nervous system (235).

Consequently, targeting the FOXM1 TF with small molecule drugs is an emerging and attractive area in medicinal chemistry.

There are several reports on small-molecule drugs with the ability to interfere with *in vitro's* FOXM1 transcriptional activity. From a mechanistic point of view, drugs targeting the transcriptional activity of the FOXM1 act either directly or indirectly. In this regard, indirect inhibitors target upstream proteins that promote FOXM1 expression, whereas direct inhibitors are supposed to dissociate the FOXM1-DNA protein complex by direct binding interactions (206). Examples of indirect FOXM1 inhibitors include proteasome inhibitors, which increase the levels of an endogenous negative regulator of FOXM1 (NRFM) (198). Thiostrepton is probably the most commonly used indirect FOXM1 inhibitor, although recent reports suggest that this potent thiazole antibiotic may also exert direct inhibition (236).

Another relevant group of drugs that are of interest to this investigation is the thiazolidinediones (troglitazone and pioglitazone), which are agonists of the PPARγ TF. Glitazones are established (and widely used) antidiabetic agents with potential anticancer properties (20). In a recent paper, Petrovic et al. reported a plausible mechanism of action by which thiazolidinediones (troglitazone, pioglitazone, and rosiglitazone) decrease the *in vitro* expression of FOXM1 indirectly via inhibition of SP1 TF, a known FOXM1 regulator. Nevertheless, the authors suggest that the activity of glitazones on the downregulation of FOXM1 seems to be PPARγ-independent.

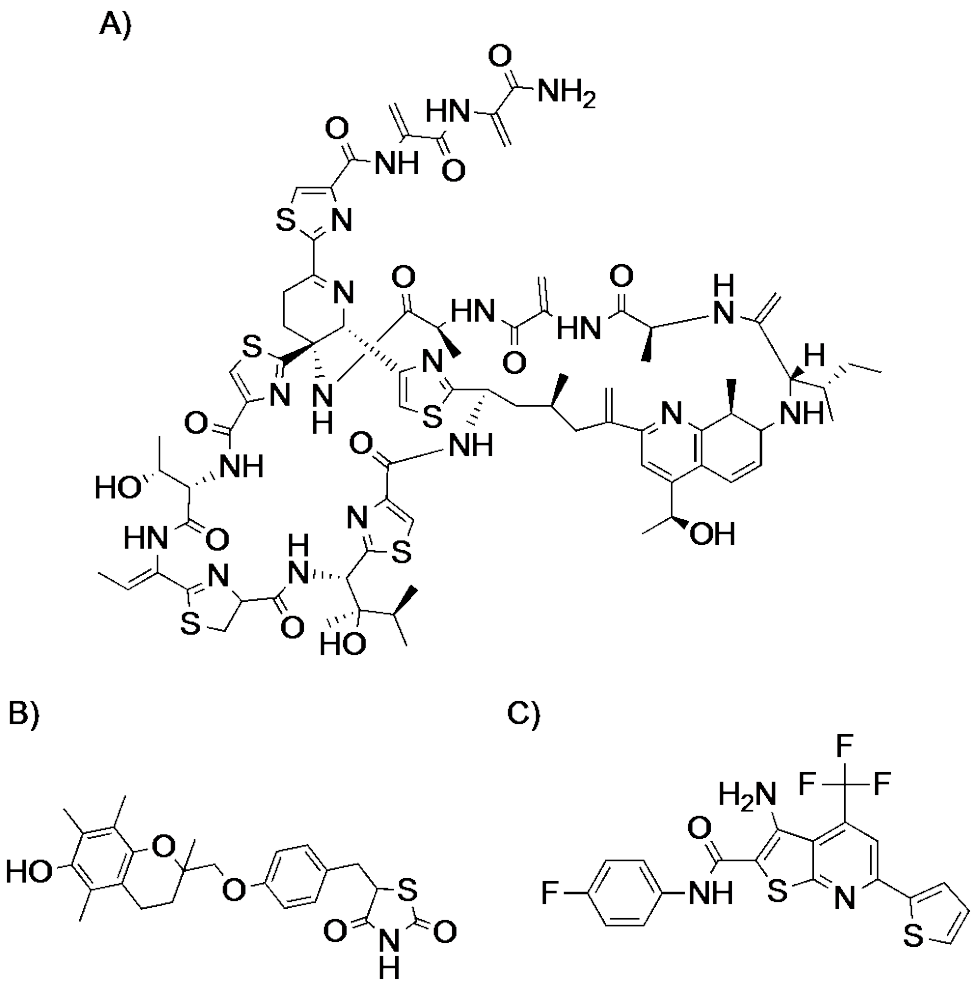

Figure 2-1. Chemical structures of the FOXM1 inhibitors. Thiostrpeoton (A), troglitazone (B) and FDI-6 (C) showing a wide variety of structural scaffolds.

Finally, Gormally et al. reported in 2014 a series of direct FOXM1 inhibitor known as "FDI", among which the drug FDI-6 was the most potent suppressor of the transcriptional activity of FOXM1 by direct dissociation of the FOXM1-DNA complex (237). This compound, along with thiostrepton and troglitazone (**Figure 2-1**), constitutes structurally-diverse compounds that seem to exert similar binding interactions within the FOXM1-DBD, which is the subject of this investigation. Based on a series of MD and docking studies, we hypothesize that different FOXM1 inhibitors may, in fact, share common features that allow them to interact with (and inhibit) the FOXM1-DBD.

Docking and MD simulation have become one of the most potent tools in predicting the binding site and binding interaction of the new scaffolds. Utilizing these techniques in drug discovery is rapidly increasing, and it is starting to produce tangible results (238–240). We propose that this interaction is primarily a pi-sulfur drug-protein interaction involving an electron-deficient sulfur atom in a heterocyclic ring of the drug molecule. Computer-based protocols designed to analyze the structure and dynamics of the FOXM1-DNA bimolecular complex generated valuable qualitative and semi-qualitative information supporting the assumption that structurally different FOXM1 inhibitors act by a common mechanism of action. This hypothesis might offer essential information to guide the design of new (improved) drugs targeting this protein. In summary, this study presents a series of MD simulations in which we present preliminary evidence to hypothesize on a pi-sulfur interaction as one of the main binding interactions driving the inhibitory profile of structurally different FOXM1 (direct) inhibitors.

2.2 Materials and Methods

2.2.1 Structure Preparation

The FOXM1-DBD crystal structure was obtained from the protein data bank (PDB) (PDB_ID: 3G73) with a resolution of 2.21 Å (134). First, we removed FOXM1's chain A and all water molecules using the protein wizard of Maestro (Schrodinger, L.; MacroModel versions 10.4 & 11.0, New York, USA, 2015). The structure was completed by adding the missing side chains and assigning the protonated groups at pH 7.0 (PROPKA) (241).

2.2.2 Molecular Docking

The ready-to-dock 3D format structures of drugs (except thiostrepton) were downloaded from the ZINC database (242). The 3D NMR structure of thiostrepton was obtained from the PDB (PDB_ID: 2L2W) (243). The Dockprep tool of UCSF Chimera v1.10.2 (244) was used to prepare the ligands in the framework of AMBER99SB force field. Autodock Vina (245) was used to perform the docking by "boxing" the binding site (coordinates) into a grid of 40 x 40 x 40 Å, with a spacing of 0.375 Å. All rotatable bonds (except those from amide bonds) were allowed to rotate freely, and 12 runs were carried out for each ligand, with exhaustiveness of 40.

2.2.3 Molecular Dynamics Simulations

2.2.3.1 FOXM1-DBD With and Without DNA

Two different MD simulations were performed for the FOXM1-DBD either with the corresponding DNA sequence or "DNA-free", both using the GROMACS 4.5.6 package (246). The first MD simulation showed amino acid residues in FOXM1 likely to interact with the DNA binding site, whereas the second MD simulation (DNA-free) provided a point of comparison with information to estimate the relative stability of the protein-DNA complex. This information was also used to predict potential binding sites. The simulation system was solvated in a cube-shaped box containing TIP3P water molecules, with 1 nm cushion in all directions. The system was neutralized, and enough NaCl was added to achieve a theoretical concentration (0.15 M). The FOXM1-DBD/DNA and FOXM1-DBD/DNA free system reached the total atom number slightly larger than 30,000 and 9,000, respectively. The whole system was energy minimized using the AMBER99SB-

ILDN force field, followed by heating (300 K) and equilibration (500 ps) using the Berendsen Thermostat.

We performed an additional equilibration (500 ps) using the isothermal-isobaric ensemble at 1 bar with the Parrinello-Rahman barostat. Finally, we performed a 50 ns production run for both FOXM1-DBD/DNA, and FOXM1-DBD/DNA free, using the periodic boundary condition. The bond lengths were set by using the LINear Constraint Solver (LINCS) algorithm. Then, we used the Lenard-Jones, the Coulomb (cut-off = 1.0 nm), and the particle mesh Ewald (PME) methods to compute the van der Waals (vdW) and electrostatic interactions. The unit cells were large enough were adjacent proteins were not imposing any short-range interactions. The trajectory frames were written to file every 2 picoseconds (ps). The root mean square deviation (RMSD), root mean square fluctuation (RMSF), and hydrogen bonding analysis were generated using GROMACS tools and plotted with GraphPad prism 6.07. All visualizations were carried out using the Discovery Studio Visualizer (Dassault Systèmes BIOVIA, 2015) and the Schrodinger's Pymol package (Molecular Graphics System, Version~1.8. (2015).

2.2.4 Binding Site Prediction

We used the Autoligand (247) module of Autodock Tools (248), and the Sitemap module of Maestro (Schrodinger, L. SiteMap version 3.7, N.Y., USA, 2015), to identify potential binding sites. Autoligand characterizes the binding sites using a grid-based energy evaluation, while Sitemap assigns numerical descriptors by a series of physical parameters such as hydrophobic/hydrophilic character and hydrogen bonding interactions.

2.2.5 FOXM1-ligand Complex

We performed a 20 ns MD simulation to examine the dynamic state and stability of FOXM1-ligand complexes. The ligand was parametrized using antechamber python parser interfacE (ACPYPE) (249), and charges were calculated using SQM with AM1-BC followed by an MD simulation, using the same methodology described above. The ligand positional RMSD, the backbone RMSD, and the number of hydrogen bonds observed for each ligand were calculated using Gromacs tools and plotted using GraphPad Prism 6.0.7.

2.2.6 Free Energy Calculation

Molecular Mechanic Poisson-Boltzmann Surface Area (MM-PBSA) has shown to be one of the most regularly used methods to compute the binding energies between small molecules and their target biomolecules because these calculations provide relevant information on the relative stability of the corresponding biomolecular complex. We calculated the binding free energy for each ligand using the g_mmpbsa Gromacs tool (250). This program uses the MM-PBSA to estimate the free energy interactions exerted by each ligand and calculates the molecular mechanics' potential energy, including electrostatic, vdW interactions, polar, and nonpolar solvation energies. In this regard, the formula for calculating the binding free energy of a protein with the ligand in the implicit solvent environment can be expressed as:

$$\Delta G_{binding} = G_{complex} - (G_{protein} + G_{ligand}) \quad \textbf{(Equation 1)}$$

The G_mmpbsa module of Gromacs uses a similar equation (**Equation 2**) to calculate the binding free energy; this script calculates each component in **Equation 1**, calculating the binding free energy as:

$G = E_{MM} + G_{solv} - TS$ (**Equation 2**)

Where: E_{int} = average of molecular mechanics potential; G_{solv} = solvation free energy and TS is the temperature and entropy, respectively (251). To calculate the binding free energy of each ligand, we only used the last 5 ns of each simulation (high number of frames per simulation).

2.3 Results and Discussion

2.3.1 The FOXM1/DNA interface

The identification of amino acid residues responsible for the binding interactions of FOXM1 at the DNA site was essential to establish potential drug binding sites used by different drug molecules. We labeled the secondary structure of the FOXM1-DBD using H1, H2, and H3 for helices, and S1 and S2 for the two β-strands. We also used the labels L1 and L2 for loops (**Figure 2-2**). The helix H3 (containing the main DNA recognition sites) was positioned perpendicular to the DNA major groove, to maximize the contact surface with the corresponding DNA binding site (H3). Upon performing both MD simulations and MM-PBSA calculations, we observed that the FOXM1-DBD interacts with DNA through direct hydrogen bonding, water-mediated hydrogen bonding, vdW interactions, and electrostatic bonds.

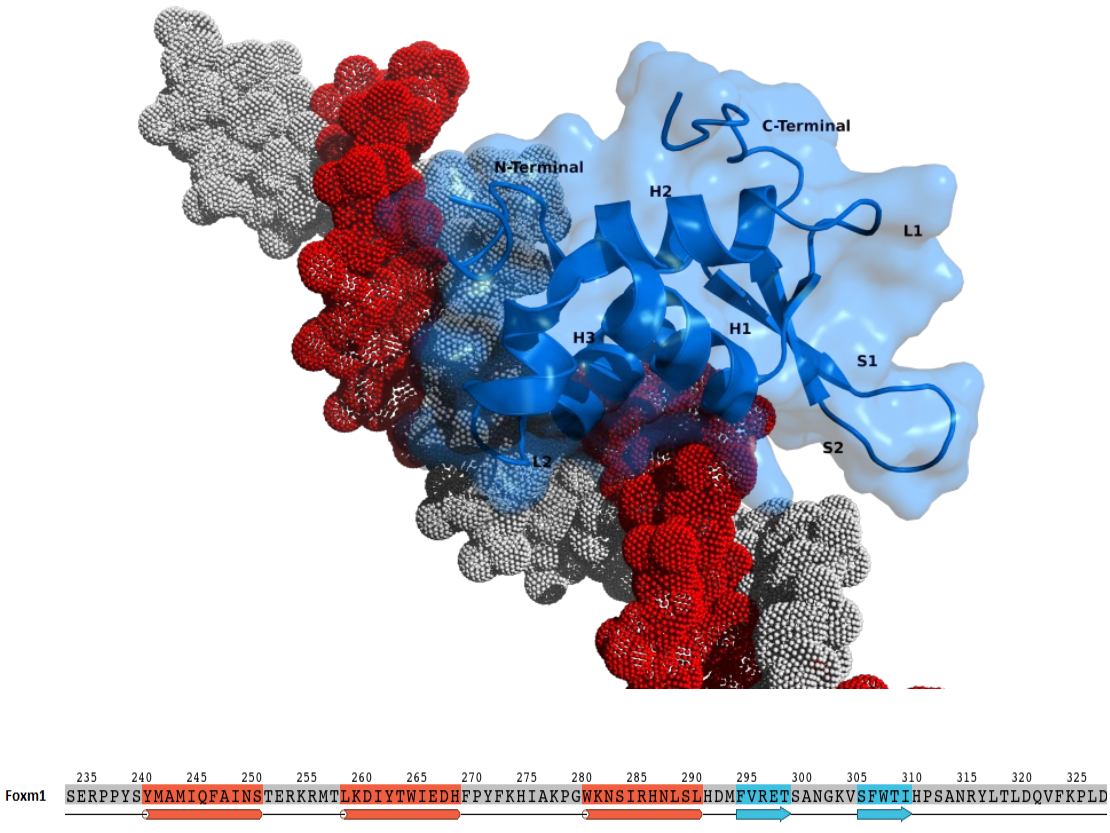

Figure 2-2. Cartoon representation of the FOXM1-DBD/DNA interface. The protein (blue ribbon and blue space) is shown on top of its DBD (dotted; red and gray). The secondary structure components of FOXM1-DBD were labeled as H1, H2, and H3 for helices; S1 and S2 for the two β-strands; and L1 and L2 for the loops. The H3 helix positioned perpendicularly into the DNA major groove.

Upon initial docking of H3 onto the corresponding DNA major groove, we observed a 15° torsion of the DNA backbone produced by several binding interactions between the L1, L2, and H1 chains. However, we also noticed that the H3 chain was mainly responsible for causing this torsion. The sum of all these interactions seemed to stabilize the FOXM1/DNA complex.

We performed a 50 ns simulation of the FOXM1-DNA complex, monitoring any protein residues interacting with DNA, by recording snapshots every one ns (**Figure 2-3**). When we analyzed the MD simulations and the MM-PBSA free energy calculations, we observed that the most significant interactions between the FOXM1 protein and DNA were hydrogen bond interactions. In this regard, generally, vdW forces contribute about two-thirds of all binding interactions, and about one-third involves hydrogen bonding (252).

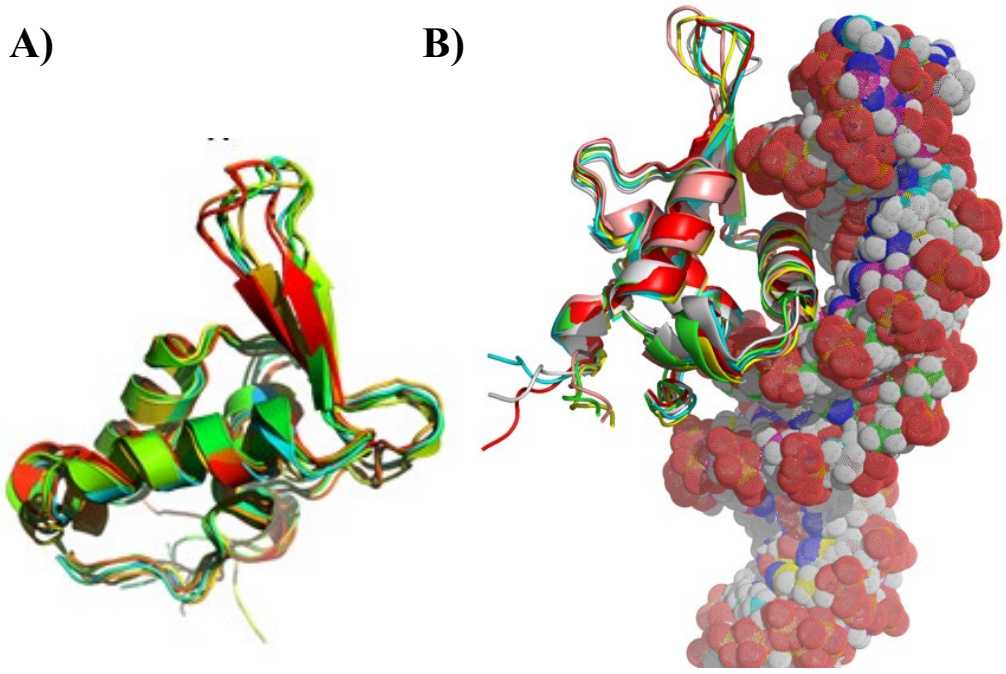

Figure 2-3. Snapshots of MD simulations performed for FOXM1-DBD and FOXM1-DBD/DNA. Six representative snapshots taken during two different 50 ns-long MD simulations of (**A**) the FOXM1-DBD; and (**B**) the FOXM1-DBD – DNA complex. Each time point is represented at different colors: time 0: red, 10 ns: yellow, 20 ns: gray, 30 ns: pink, 40 ns: green and 50 ns: cyan.

According to our calculations, the FOXM1 protein starts the binding recognition process onto DNA, mainly due to the interactions exerted by three amino acid residues present in H3, among which, His287 seemed to be the most important. In this regard, His287 appears to be exposed (available); this means that His287 is likely to "guide" FOXM1 toward the DNA recognition site (initial contact). Furthermore, unlike other nearby residues present in H3 (Asn83, Asn283, and Asn286), His287 formed four different and complementary hydrogen bonds with three DNA backbone residues, namely Thy9, Thy8, and Thy14. Comparatively speaking, Asn283 formed only two hydrogen bonds with Ade16, whereas Asn286 formed a hydrogen bond with Gua6 and an electrostatic interaction with Thy5.

During the MD simulation of the protein-DNA complex (compared to the protein alone), we observed significant fluctuations in amino acid residues present in the *N*-terminal loop, which participates in the FOXM1-DNA binding. In this regard, Tyr241, Arg236, and Ser240 were three residues found in the N-terminal loop that apparently played a critical role in complex stabilization. Tyr241 also formed an electrostatic salt bridge with the sugar-phosphate backbone of Ade13 and Thy14, whereas Arg236 formed three electrostatic interactions with Thy14. Finally, Asn240 is another residue located at the *N*-terminal loop region considered essential due to its suitable position. These observations suggest a possible (and potentially important) role of the *N*-terminal domain in the FOXM1-DNA complex interaction (**Figure 2-4**).

We observed that at least one amino acid residue from the S1 and S2 β-strands also contributed to the binding of FOXM1 to DNA. Arg297 (from S1) is positioned close to (and making contact with) Gua6 by forming hydrogen bonds and electrostatic interactions. Moreover, Gua6 was the target residue for Trp308 (from S2) by making a 2

Å hydrogen bond with the DNA phosphate backbone. Lys278 from L3 and Arg316 from the C-terminal loop also contributed to the overall stability of the protein-DNA complex by forming electrostatic interactions with Thy14, Ade15, Ade16, and Thy16.

A)

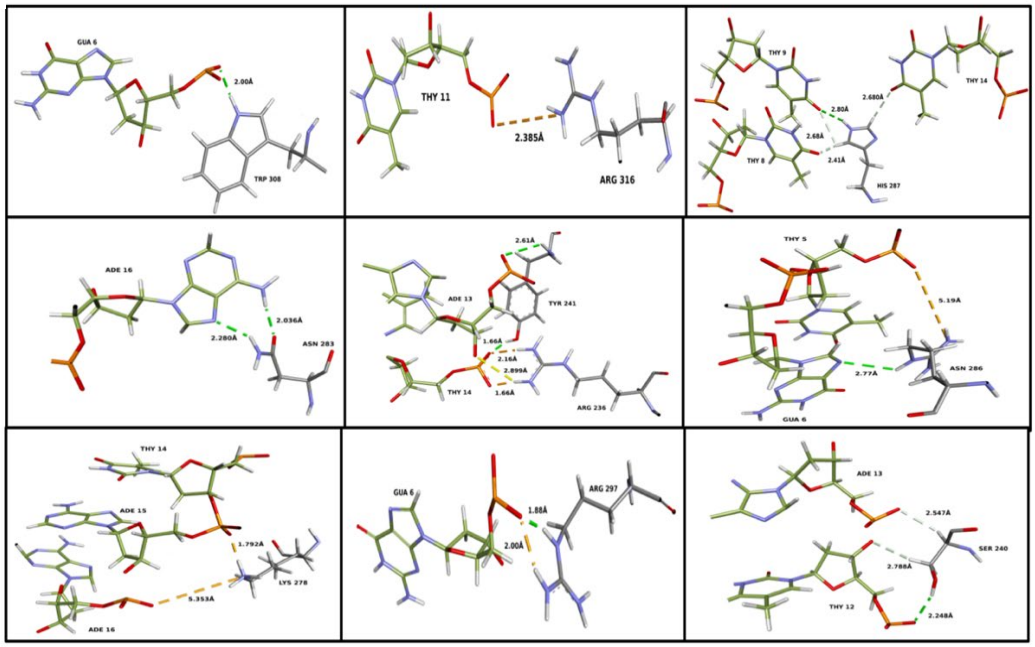

B)

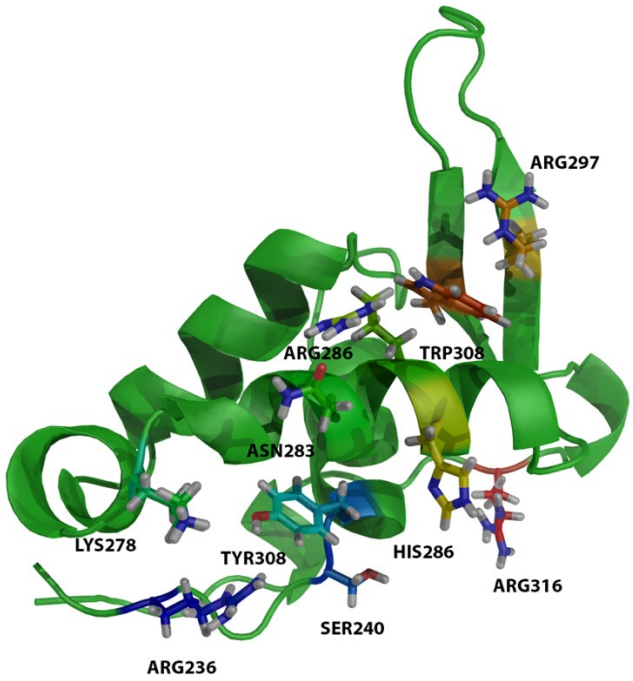

Figure 2-4. **FOXM1-DBD/DNA interacting residues.** A) Proposed amino acid residues responsible for the binding interaction exerted by FOXM1-DBD on DNA; the numbers represent bond lengths in Å. Green and white lines represent hydrogen bonding interactions; amber lines represent electrostatic interactions; B) location of amino acid residues of the FOXM1-DBD interacting with DNA.

2.3.2 The Role of Water Molecules at the FOXM1-DNA Interface

Water molecules are an essential component of any biological system. Previous studies have demonstrated that water molecules are involved in hydrogen bond networks that enhance binding interactions between proteins and either the phosphodiester backbone of DNA base pairs (253). In our particular case, data obtained from all the 50 snapshots recorded between the FOXM1 binding domain and its DNA recognition site, suggested that Gly280, Ser284, Asn288, Met242, and Tyr241 exert water-mediated binding interactions with the DNA backbone (**Figure 2-5**). Contrarily, amino acid residues

present in the N-terminal loop formed weak (non-permanent) water-mediated hydrogen bonds with some DNA base pairs (disregarded; not shown).

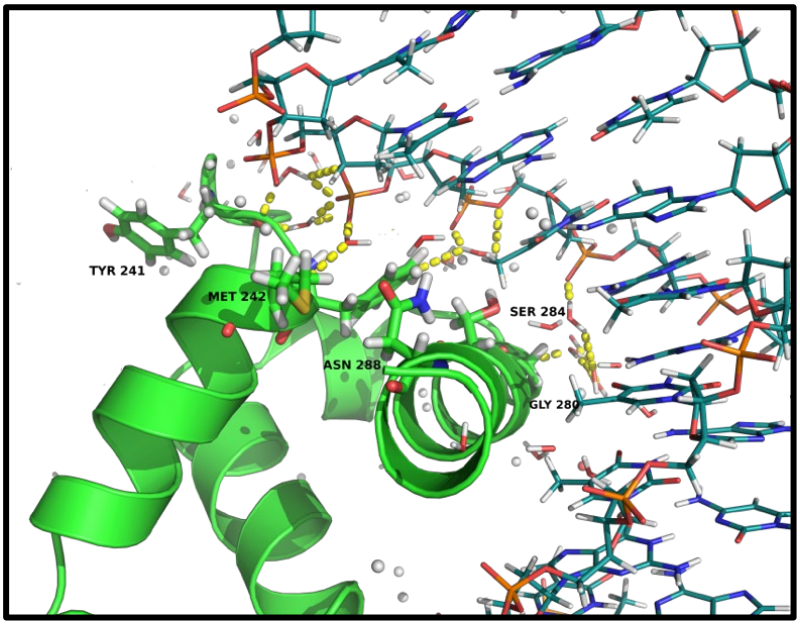

Figure 2-5. **Role of water molecules at the FOXM1-DBD/DNA interface**.Water-mediated hydrogen bonding interactions (yellow lines) at FOXM1-DBD – DNA interface. The FOXM1-DBD is shown in green; DNA is shown in dark cyan (stick) presentation. Most amino acid residues involved in water-mediated hydrogen bonding interactions (50 ns MD simulation) are labelled as follows: Tyr241, Met242, Asn288, Gly280, and Ser284.

2.3.3 Protein Interaction Analysis and β Factor profile

We calculated the backbone RMSF (**Figure 2-7-A**) and the RMSD (**Figure 2-7-B**) values for both the FOXM1-DNA complex and the FOXM1 DNA-free systems over a 50 ns time MD simulation. Both structures showed an acceptable degree of stability throughout the trajectory. However, we observed higher RMSD values in the FOXM1 DNA-free simulation due to significant fluctuation in the *N*-terminal loop, which was not seen in the

FOXM1-DNA complex simulations. A lower RMSD value for the FOXM1-DBD-N-terminal (N-terminal removed) in comparison to the FOXM1-DBD, confirmed this observation (**Figure 2-6**).

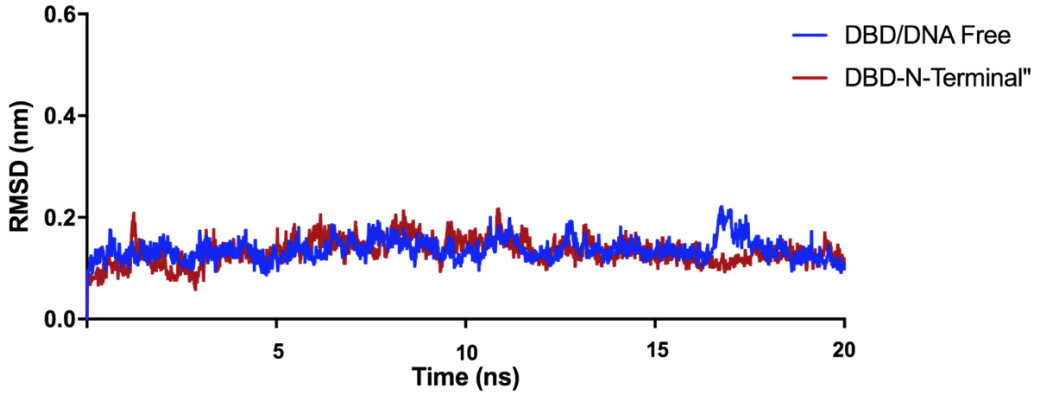

Figure 2-6. Effect of N-terminal on the FOXM1-DBD binding. Calculated backbone RMSD values for the FOXM1-DBD and FOXM1-DBD-N-Terminal" (N-terminal removed).

The superimposed RMSF plots from both structures revealed a significant contribution of vdW contacts between the FOXM1-DBD and DNA, among which, residues 240-310 in the H3 chain of the FOXM1-DBD showed the largest interactions with DNA. In this regard, we observed that the H3 chain was conveniently positioned inside the corresponding DNA major groove, and it may be responsible for the initial FOXM1-DNA contact. This observation is supported by the β factor profile, where the binding energy contribution of interacting residues were converted to β factor using the energy2bfac module of g_mmpbsa. **Figure 2-7-C** shows the contributions by H3 during the FOXM1-DNA interaction. A structure of the FOXM1-DBD–DNA complex (color-coded by β factors) is shown in **Figure 2-7-C.** The intensity of the red color and the width

of the loop (H3, S1, and S2) indicate different binding strengths as determined by the MD simulation.

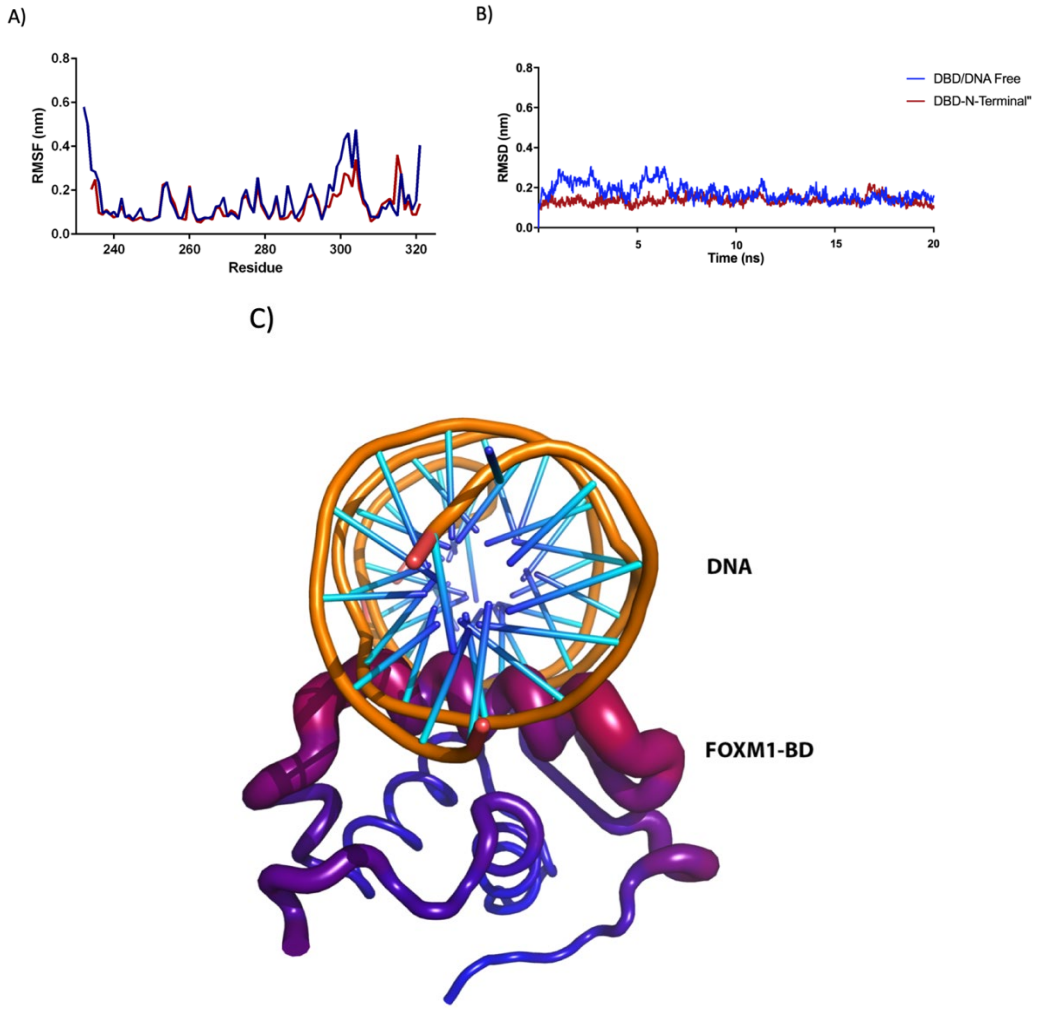

Figure 2-7. RMSF, backbone RMSD and sidechain RMSF of FOXM1-DBD and FOXM1-DBD/DNA.A) Superimposed RMSF plot of the FOXM1-DBD (blue color) and the FOXM1-DBD – DNA complex (red color) during a 50 ns MD simulation. B) RMSD of the FOXM1-DBD (blue) and the FOXM1-DBD – DNA complex (red) during a 50 ns MD simulation. C) structure of the FOXM1-DBD – DNA complex (intensity of red color and girth of the loop suggest higher binding contribution).

2.3.4 Prediction of the FOXM1-DBD/DNA Binding Site

This task was challenging to perform due to the absence of a clear hydrophobic pocket on the protein surface, and the lack of a co-crystallized structure of the FOXM1-DBD. Briefly, we used 30 snapshots from the MD simulations to study the FOXM1-DBD (vdW) surface. This procedure generated essential information defining a possible region containing all binding interactions described above, which at the same time, could potentially be used to dock small-molecule drugs. We employed the Autoligand module of Autodock to characterize the binding sites of all 30 snapshots of FOXM1-DBD using a grid-based energy evaluation; then, these results were validated with the Sitemap module of Maestro by analyzing both hydrophobic and hydrophilic features, as well as hydrogen bonding interactions. Finally, we chose the best possible binding site from selected sites based on (a) the contribution of individual amino acid residues involved in binding interactions with DNA; (b) amino acid type; (c) their hydrophobicity; and (d) solvent accessibility (**Figure 2-8**).

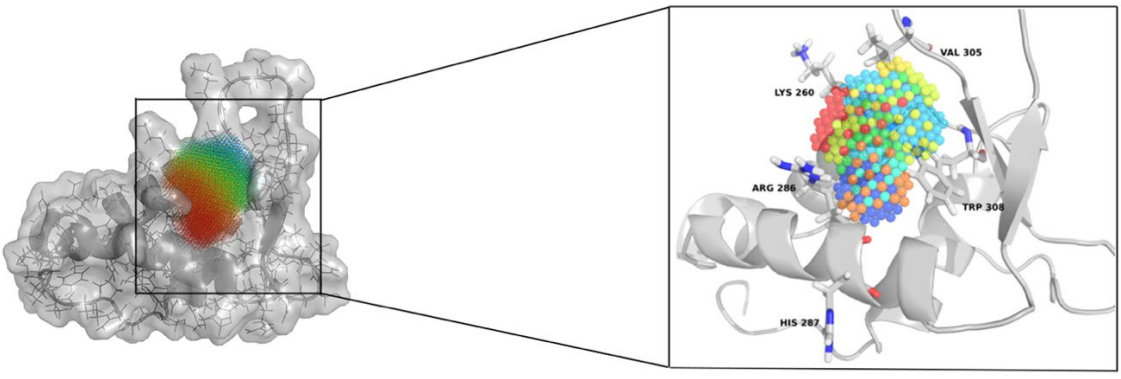

Figure 2-8. **The predicted drug-binding site at the interface of FOXM1-DBD and DNA.**The spheres are representing the hypothetical position of the predicted binding site. The zoomed-in FOXM1 structure is shown in gray color; the interacting residues

(Lys260, Arg286, His287, Trp308, and Val305) are shown in gray (stick presentation); the most favorable region for binding of small molecules is presented using a rainbow-colored group of spheres.

2.3.5 Prediction of the Binding Mode for Thiostrepton

Thiostrepton is an antibiotic derived from Streptomycetes, which exerts significant cell proliferation inhibition activity on breast cancer cells by exerting a combination of direct and indirect inhibition of FOXM1's transcriptional activity (254). Thiostrepton was the first drug reported to bind directly to FOXM1(236); however, to our knowledge, no reports are describing the co-crystallization of this drug on (or in) the FOXM1 protein, and consequently, we were interested in studying the binding interactions of this molecule with the FOXM1-DBD. We docked thiostrepton into the binding site calculated previously using a 20 ns MD simulation, to examine its stability as a complex with the protein. Nevertheless, due to the complex structure of thiostrepton, we carried out this protocol under special considerations; we prepared the drug as described by Bond et al. (255) with some small modifications (**Figure 2-9**). Briefly, we divided thiostrepton into three "building blocks (BB)" as follows: group 1 consisted of BBs 1, 4, 6 and 14 (all of them containing 1,3-thiazole rings); group 2 consisted of BBs 9, 10, 11, 12, 15 and 16

(amino acid-like groups); and group 3 including BBs 2, 3, 5, 8 and 13 (the rest of the groups).

Building block	Description
1	Thiazole-2-carbaldehyde
2	Threonine
3	Dehydrobutyrine
4	Thiazole-2-carbaldehyde
5	Thiostrepton fragment
6	Thiazole-2-carbaldehyde
7	Thiostrepton acid fragment
8	Quinaldic acid
9	Isoleucine
10	Alanine
11	Pyruvic acid
12	Alanine
13	Tetrahydro-pyridin-3-ylamine
14	Thiazole-2-carbaldehyde
15	Pyruvic acid
16	Pyruvic acid

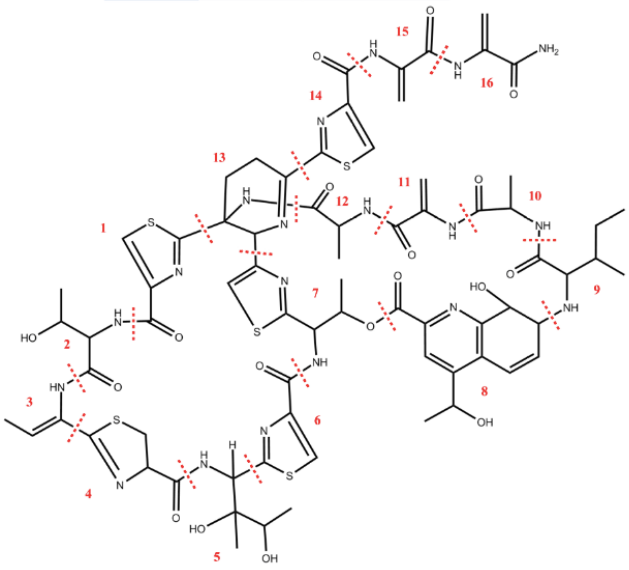

Figure 2-9. **Thiostrepton Building blocks.**The structure of the FOXM1 inhibitor Thiostrepton divided into smaller groups by adding red dotted lines to separate different building blocks (BB) or fragments, shown using red numbers on the structure; the table on the right lists each BB and the name of the corresponding BB.

As shown in **Figure 2-10-A**, the docking protocol showed several potential binding interactions between thiostrepton and FOXM1-DBD, including a significant

His287 – pi-sulfur interaction in BBs 6 and 7 (amber color), a pi-pi stacking, and a hydrogen bond (green color). Also, we observed hydrogen bonds between Ser290, Leu291, and Val296 with thiostrepton's BB 15 and 16 (green color). Finally, we observed another pi-sulfur interaction between Trp308 and BB 14. All these interactions are shown in **Figure 2-10-A**. The ligand positional RMSD calculations of the FOXM1-DBD – thiostrepton complex (**Figure 2-10-B**) suggest excellent stability during the 20 ns MD simulation. We also determined the RMSF values for both, the FOXM1-DBD alone (residues 231-321) and the FOXM1-DBD – thiostrepton complex (**Figure 2-10-C**), in which non-overlapping regions in the graph suggest binding interactions.

Comparatively, literature reports describe pi-sulfur interactions contribute around -11.03 KJ/mol to binding energies at about 3.8 Å distance. In this regard, pi-sulfur interactions involve an imidazole ring present in histidine residues and a positively charged sulfur atom in the drug. Individual contributions from different pi-sulfur interactions depend on the relative position of the sulfur atom concerning aromatic rings (256). These pi-sulfur interactions are strong electrostatic interactions (256) and play a significant role in protein folding and protein stability (257,258). In another study, Viguera et al. reported a significant contribution of a pi-sulfur interaction to the stability of alpha-helices (259). These observations agree with the pi-sulfur binding interactions

determined in our docking protocol between thiostrepton and the FOXM1-DBD, which provided stability to the protein structure.

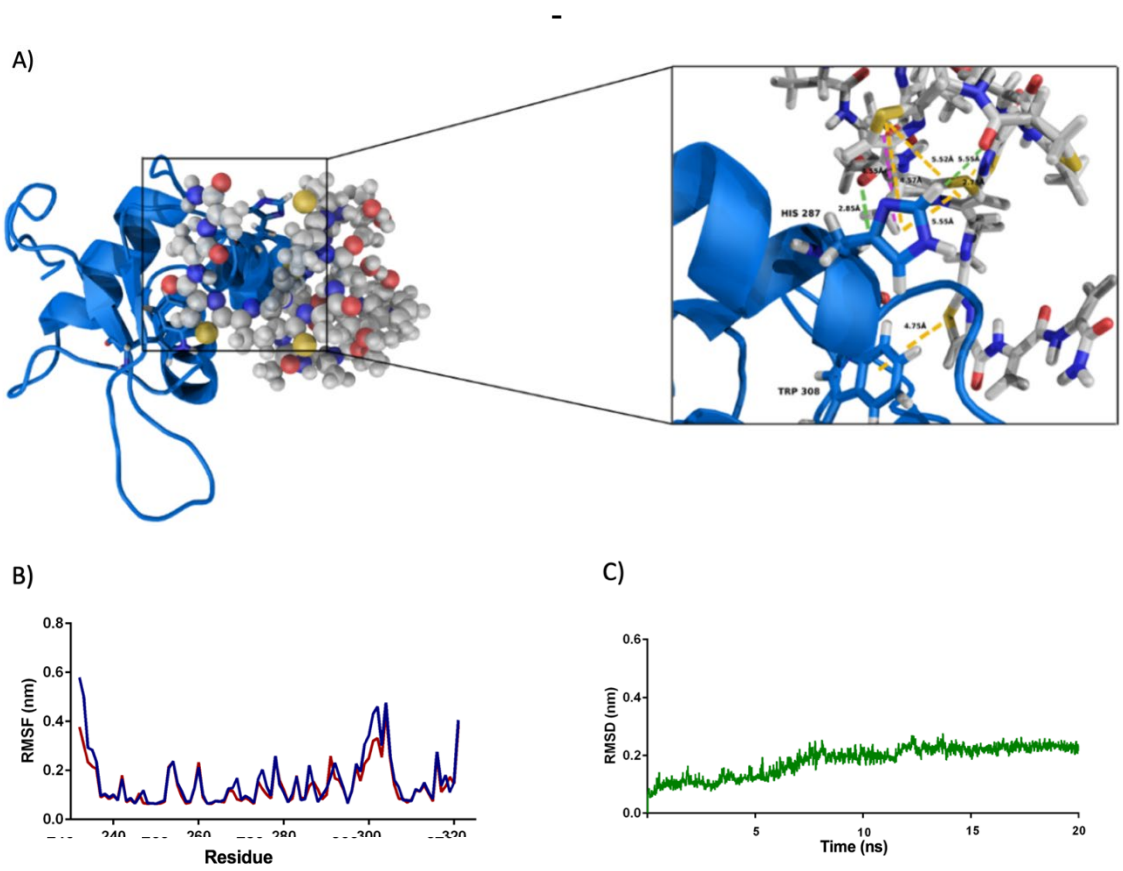

Figure 2-10. The proposed binding mode and its respective MD analysis for thiostrepton.A) The proposed structure of the FOXM1-DBD – thiostrepton complex showing a zoom-in region where thiostrepton (gray color, stick presentation) binds to FOXM1-DBD (marine color). The different binding interactions are shown using different colors: pi-sulfur (amber lines); pi-pi interactions (purple lines); hydrogen bonds (green lines). Each number indicates the corresponding bond distance (Å). B) Calculated RMSF values for the FOXM1-DBD (blue line) and the FOXM1-DBD – thiostrepton complex (red line). C) Calculated RMSD values for the FOXM1-DBD – thiostrepton complex.

In addition to intermolecular binding interactions, we also observed intramolecular bonds that contributed to the overall stability of the thiostrepton – FOXM1-DBD complex. In this regard, we determined intramolecular pi-sulfur interactions between thiostrepton's building blocks 1 and 7, and 7 and 6, producing a distinctive curved shape in the drug. Furthermore, intramolecular hydrogen bonds were important in stabilizing the thiostrepton specific conformation. The total binding energy calculated for thiostrepton was -121.5 ± 7.9 KJ/mol (**Table 2-1**). Please refer to the methodology section (MM-PBSA) for more details on binding free energy calculations.

Table 2-1. Binding energy calculated for thiostrepton, troglitazone, and FDI-6. The binding energy of ligands was calculated based on the total contribution of vdW , electrostatic, solvent accessible surface area (SASA) subtracted from the polar solvation energy.

Drug	Van der Waal energy (KJ/mol)	Electrostatic energy (KJ/mol)	Polar solvation energy (KJ/mol)	SASA energy (KJ/mol)	Binding energy (KJ/mol)
Thiostrepton	-152.1 ± 9.4	-2.3 ± 2.0	46.2 ± 3.5	-13.2 ± 0.4	-121.5 ± 7.9
Troglitazone	-125.06 ± 40.6	-9.8 ± 5.9	67.8±15.5	-13.0± 4.4	-80.5 ±4.30
FDI-6	-150.5 ± 13.1	5.4 ± 6.6	54.5 ± 23.8	-13.8 ± 0.8	-104.4 ± 25.8

Chen et al. reported a similar docking study using thiostrepton and the FOXM1 protein. The authors conducted an *in silico* screening protocol followed by an *in vitro* evaluation of lead molecules using ovarian cancer cell lines (200). Nevertheless, the authors report neither any potential binding site nor MD simulations. Besides, Chen et al. describe "neither the single-wing nor double wings showed any significant binding site that could accommodate thiostrepton." Also, authors only suggest "a large contact area

between thiostrepton and the FOXM1:dimer: DNA complex" involving residues Arg236, Pro 237, Ser 240 and Tyr 239. Our study went a couple of steps above and beyond the report by Chen et al. because we prepared the structure of thiostrepton, performed the MD simulation and the corresponding docking derived from these two steps. We think this comprehensive procedure may bring an alternative but more complete and accurate representation of a potential binding site in which thiostrepton might locate within the FOXM1-DNA.

2.3.6 Expanded Binding Mode for Thiostrepton

To evaluate the importance of a possible pi-sulfur interaction involving a His287 in the FOXM1-DBD, we "cleaved" the bond between the thiazole-2-carbaldehyde group and the tetrahydropyridine-3-yl amine, to cause additional flexibility in the molecule (**Figure 2-11**). The ligand positional RMSD values (**Figure 2-11-B**) suggested a stable system within the first eight ns of MD simulation. The initial RMSD fluctuations of the docked structure were probably caused by the thiazole rings, which underwent conformational changes when interacting with His287, as shown in **Figure 2-11-A**. Upon stabilization of the drug-protein complex, building blocks 1, 4, 6, and 7 surrounded the His287 residue via pi-sulfur interactions (amber lines in **Figure 2-11-A**). At the same time, Trp308 formed a complementary pi-sulfur interaction with a thiazole-2-carbaldehyde group in building block 14 of thiostrpeton (purple line). Finally, we observed additional pi-alkyl interactions between Leu289 and 259 and BB14, as well as Arg286 and BBs 14 and 7.

These three amino acids formed a relatively hydrophobic pocket in the FOXM1-DBD. Consequently, we think that the pi-sulfur interaction by the thiazole-2-carbaldehyde group is essential for thiostrepton's direct inhibition of FOXM1. To

complement the observations described above, we calculated the RMSF values of FOXM1-DBD, using residues 231 to 332. The blue line shows the RMSF values of the FOXM1-DBD (alone), and the red line represents the RMSF values of the FOXM1-DBD – thiostrepton complex (expanded). The regions where there is no line overlap suggest the residues involved in the binding interaction (**Figure 2-11-C**). We calculated a mean number of hydrogen bonds = 10 for the last five ns of the trajectory, but only four seemed to be involved in the protein-ligand interaction. The other hydrogen bonds participated in intramolecular interactions. As predicted, the higher number of hydrogen bonding interactions observed in the expanded protocol was likely due to the higher flexibility of the molecule.

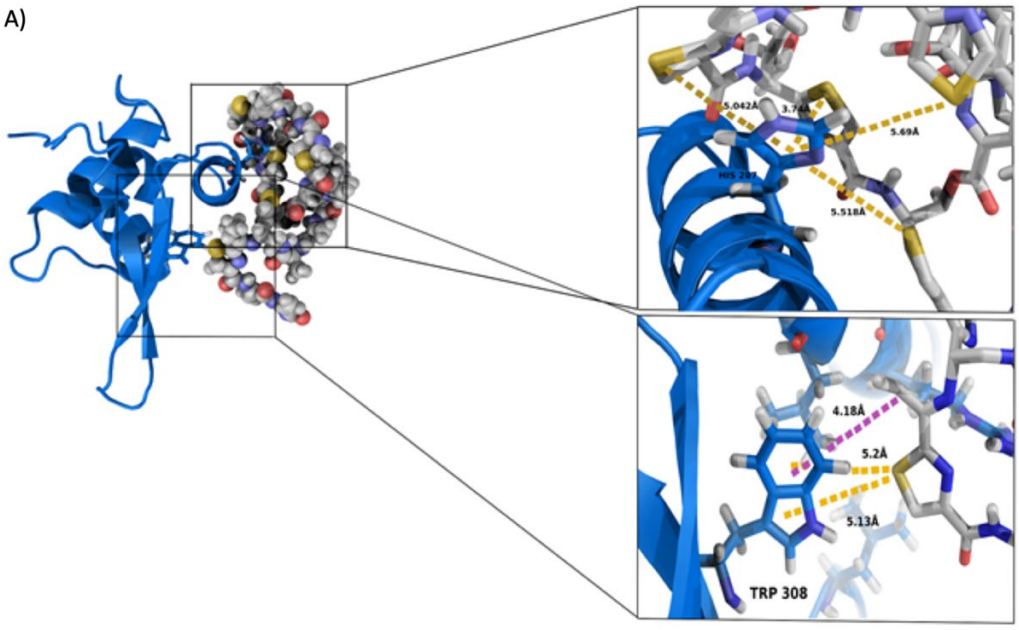

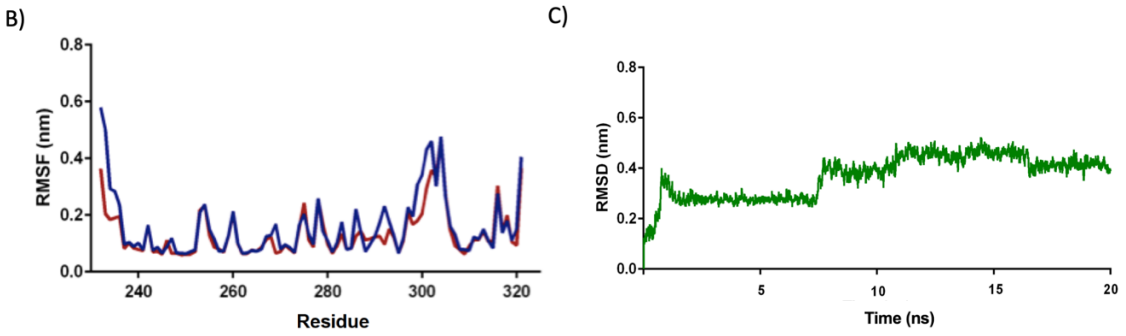

Figure 2-11. The proposed binding mode and its respective MD analysis for expanded thiostrepton.A) The proposed structure for the FOXM1-DBD (expanded) thiostrepton complex is showing zoom-in regions at the interface between the expanded thiostrepton (gray color, stick presentation) and the FOXM1-DBD (marine color, cartoon presentation). The theoretical pi-sulfur interactions (amber lines) and one pi-pi interaction (purple line) at the FOXM1-DBD (expanded) – thiostrepton interface are described with their respective distances (Å). B) Calculated RMSF values for the FOXM1-DBD (blue line) and the FOXM1-DBD (expanded) – thiostrepton (red line), showing interacting residues. C) Calculated RMSD values for the FOXM1-DBD (expanded) – thiostrepton complex (the complex shows an acceptable stability after the 8th ns of the MD simulation at about 0.4 nm.

2.3.7 Prediction of the Binding Mode for Troglitazone

We noted that troglitazone binds directly to FOXM1-DBD, similar to that of thiostrepton. Troglitazone adopted an orientation in which the thiazolidinedione ring exerts a pi-sulfur interaction with His287, at an angle of about 45° (amber line, **Figure 2-12**). Arg286 formed a hydrogen bond with the ketone group in the thiazolidinedione ring (shown in green), which is oriented in a hydrophobic pocket formed by Leu259 and 260 (purple

lines). The ligand positional RMSD plot calculated for troglitazone is presented in **Figure 2-12-B**, suggesting a relatively stable protein-drug complex during the 20 ns MD simulation. Complementary to the RMSD calculation, we also determined the RMSF for the FOXM1-DBD (residues 231 to 332). In this regard, the blue line describes RMSF values for the FOXM1-DBD (alone), and the red line displays RMSF values for the FOXM1-DBD – troglitazone complex (**Figure 2-12-C**).

As described for thiostrepton above, regions without an overlap, represent residues that are not involved in the drug-protein binding interactions. In this regard, we predict a drug-binding site including three different regions in FOXM1-DBD, namely 296-304, 315-320, and 274-277. The calculated binding affinity for troglitazone is around -80.5 ± 4.3 KJ/mol (**Table 2-1**). Based on these observations, we suggest that the binding mode for both drugs, troglitazone, and thiostrepton, involves a similar pi-sulfur interaction via a thiazolidinedione or 1,3-thiazole rings, respectively.

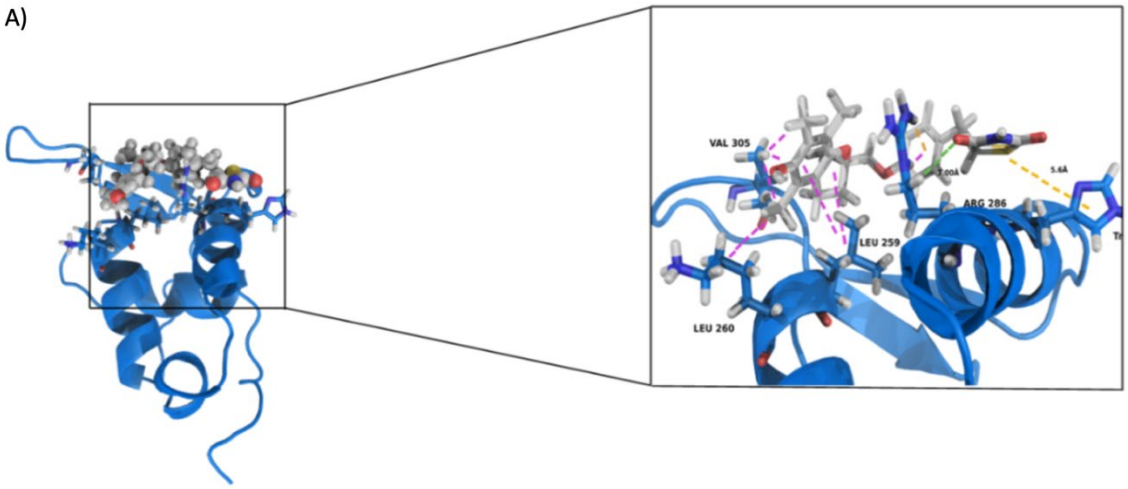

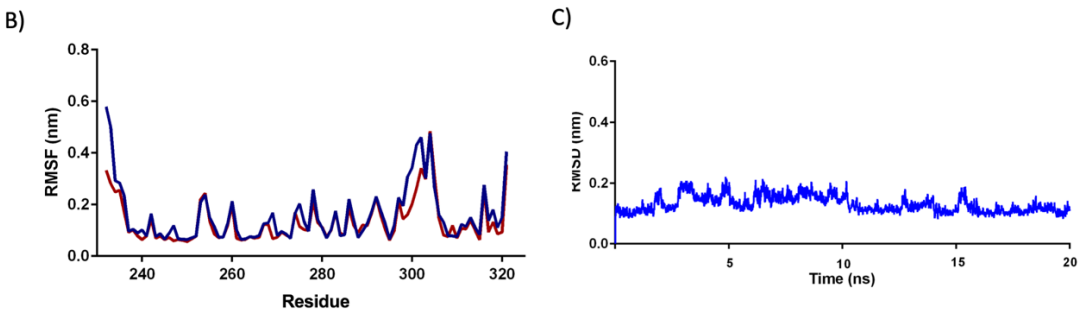

Figure 2-12. The proposed binding mode and its respective MD analysis for troglitazone.A) The proposed structure for the FOXM1-DBD – troglitazone complex showing a zoom-in region at the interface between the troglitazone (gray sticks) and the FOXM1-DBD (marine color). The primary binding amino acid residues involved in this model are Leu259, Leu260, Arg286, His287, and Val305; different interactions are shown using different colors: amber lines (pi-sulfur interactions), green lines (hydrogen bonds), and purple lines (pi- pi, pi-alkyl, and alkyl-alkyl interactions). B) Calculated RMSF values for the FOXM1-DB (blue line) and the FOXM1-DBD – troglitazone (red line); overlapping lines suggest interacting amino acid residues at the complex interface. C) Calculated ligand positional RMSD values for the FOXM1-DBD – troglitazone complex, which has acceptable stability during the MD simulation (at 0.2 nm).

2.3.8 Prediction of the Binding Mode for FDI-6

As we have already discussed, the pi-sulfur interaction between the positive sulfur and a His287 residue is likely responsible for the inhibitory binding interactions exerted by troglitazone (and probably other glitazones) and thiostrepton. To our surprise, we observed that this hypothesis is supported by additional computer-based MD simulations carried out with the drug FDI-6, another direct FOXM1 inhibitor reported recently (206).

Gormally et al. reported three new molecules (FDI-6 and FDI-10 and FDI-11) that interfere with, and inhibit, the transcriptional activity of FOXM1 by direct binding with the FOXM1-DBD. We suspected that the new FDI-series of molecules, and especially FDI-6 (the most potent), might exert similar binding interactions involving a pi-sulfur binding.

According to our calculations, FDI-6 exerts a very similar binding pattern to the FOXM1-DBD, compared to troglitazone and thiostrepton, via a potential pocket formed by the amino acid residues His287, Arg286, Asn283 (**Figure 2-13-A**). We also observed a significant contribution of a positively charged sulfur atom and His287. Nevertheless, as shown in **Figure 2-13-A**, the pi-sulfur interaction in FDI-6 took place via a thiophene ring, very similar to the one observed with troglitazone.

As in every computer-based predictive model, the validation of *in silico* observations is essential to support any hypothesis. Consequently, we are currently conducting a series of experiments aimed to confirm the theoretical binding interactions proposed in this investigation. In this regard, we are planning to tackle this issue by two different methods: (a) the biological evaluation of thiostrepton, troglitazone, and FDI-6 using a similar EMSA experiment to that reported by Gormally et al. (206), using the corresponding DNA region and the FOXM1 binding domain in which the His287 is replaced by a similar amino acid residue (i.e. arginine or lysine); and (b) the chemical synthesis of troglitazone derivatives in which we replace the electron-deficient sulfur atom by an isosteric group (i.e. a methylene group). **Table 2-2** outlines all the simulation parameters performed.

In both instances, we should observe a significant decrease in the binding affinity of the drugs. If our hypothesis is correct, the direct binding interactions exerted by known

(thiostrepton, troglitazone, and FDI-6) and new (troglitazone derivatives) should be significantly decreased. Nevertheless, this discussion goes well beyond the scope of this initial investigation, and we will, therefore, continue this interesting discussion for upcoming (follow up) publications.

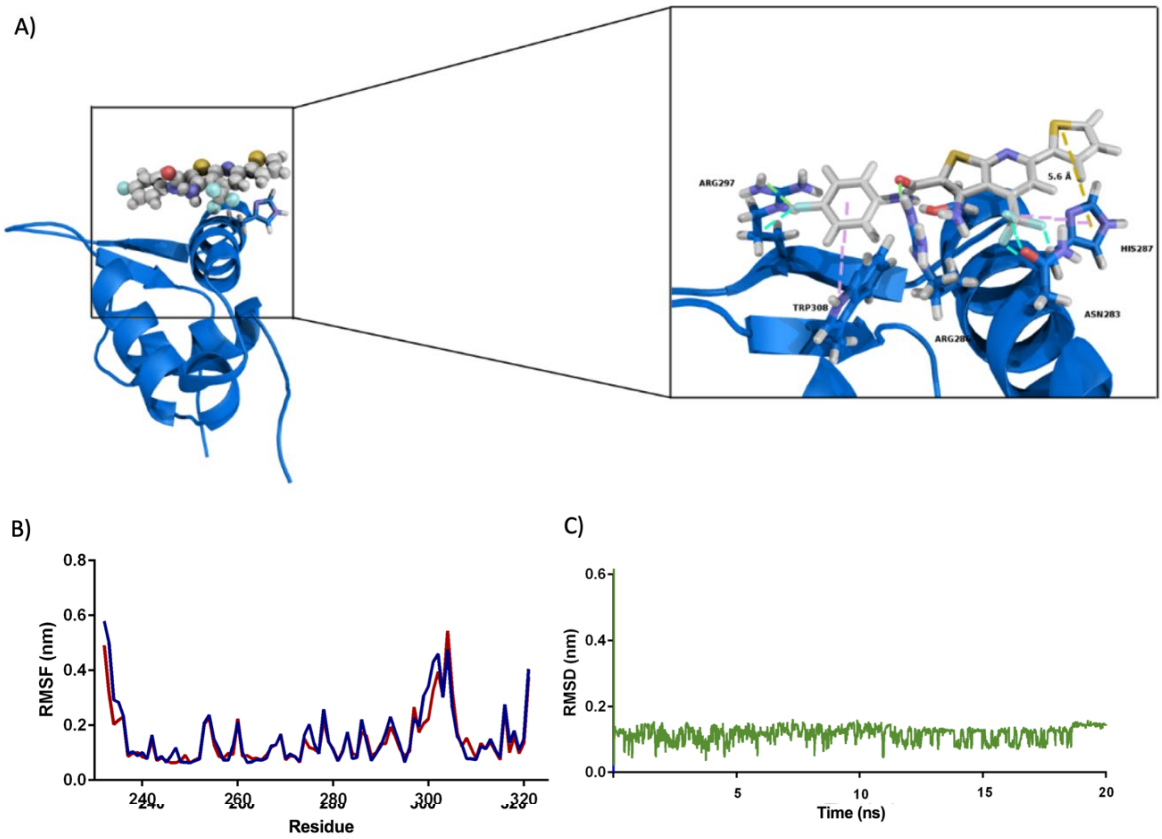

Figure 2-13. The proposed binding mode and its respective MD analysis for thiostrepton. A) The proposed structure for the FOXM1-DBD – FDI-6 complex, showing a zoom-in region at the interface between the drug (gray sticks), and the FOXM1-DBD (marine color). The main binding amino acid residues involved in this model are Arg297, Arg 283, Arg286, His287 and Trp208, and Asn283; different interactions are shown using different colors: amber lines (pi-sulfur interactions), green lines (hydrogen bonds), purple lines (pi- pi, pi-alkyl, and alkyl-alkyl interactions) and

Cyan lines (Halogen bonding). B) Calculated RMSF values for the FOXM1-DB (blue line) and the FOXM1-DBD – FDI-6 (red line); overlapping lines suggest interacting amino acid residues at the complex interface. C) Calculated ligand positional RMSD values for the FOXM1-DBD – FDI-6 complex, which has acceptable stability during the MD simulation (at 0.1 nm).

Table 2-2. The summary of the MD simulations performed. The number of atoms involved, the diameter of simulation box and the length of MD simulations performed for each system are described.

System	Number of water molecules + ions	Simulation box diameter (nm)	Simulation length (ns)
FOXM1-BDD/ DNA FREE	9232	7.813	50
FOXM-DBD/DNA COMPLEX	30508	4.646	50
FOXM1-DBD (no n-terminal)	7358	4.178	50
FOXM1-DBD/Thiostrepton	9903	4.804	20
FOXM1-DBD/Flexible-Thiostrepton	9903	4.804	20
FOXM1-DBD/Troglitazone	9948	4.804	20
FOXM1-DBD/FDI-6	9956	4.804	20

2.4 Summary and Conclusion

This report presents a preliminary computer-based approach to elucidate the potential binding mode exerted by troglitazone, thiostrepton, and FDI-molecules, three structurally different FOXM1 inhibitors that seem to exert a similar binding pattern within the FOXM1-DBD.

This investigation proposes a (potential) but common mechanism of the action exerted by known FOXM1 inhibitors via a potential “binding pocket” formed by several amino acid residues, among which, His287 seems to be one of the most important ones. If this computer-based model is correct, we submit that the design of future (novel)

generations of FOXM1 inhibitors may benefit from having a positively charged sulfur atom that interacts with His287, as described in this work. We also suggest that the proposed pi-sulfur interaction between the drug molecule and the FOXM1-DBD – DNA may be obtained via different groups such as an aromatic five-member ring (a thiophene ring – observed for troglitazone and FDI-6), a sulfoxide group (observed for FDI-11), or thiazole rings (as determined for thiostrepton).

It should be noted that, with this model, we do not rule out (yet) any other positively charged sulfur atom group present in other functional groups. In summary, we present preliminary evidence supporting the hypothesis that troglitazone, thiostrepton, and the FDI-series of molecules, despite having seemingly different structures, sizes, and conformations, they all seem to exert a standard binding mode that suggests a similar mechanism of action. This mechanism may constitute the basis for the design of new drugs for which a direct binding mechanism is required to inhibit the FOXM1-DNA interface.

Chapter 3

A Structure-Activity Relationship Study of Forkhead Domain Inhibitors (FDI): The Importance of Halogen Binding Interactions

A version of this chapter is published in:

BIOORG CHEM. 2019 Dec;93. https://doi.org/10.1016/j.bioorg.2019.103269

3.1 Introduction

The FOXM1 protein is an essential TF required for mitotic progression and cell division. Unlike normal cells, cancer cells (of practically any tissue origin) undergo changes leading to overexpression of FOXM1 and the abnormal activation of its transcriptional cascade (138,214,261). Hence, cancer cells sustain a rapid cell replication pattern. In addition to its role in cell proliferation, FOXM1 is also involved in cancer initiation (227,233), angiogenesis (262,263), and metastasis (185). **Figure 3-1** presents a schematic summary of the different roles played by FOXM1 in cancer initiation and cancer progression. The carcinogenic features associated with an overexpression of FOXM1 make this protein an emerging and promising drug target for cancer treatment (264,265).

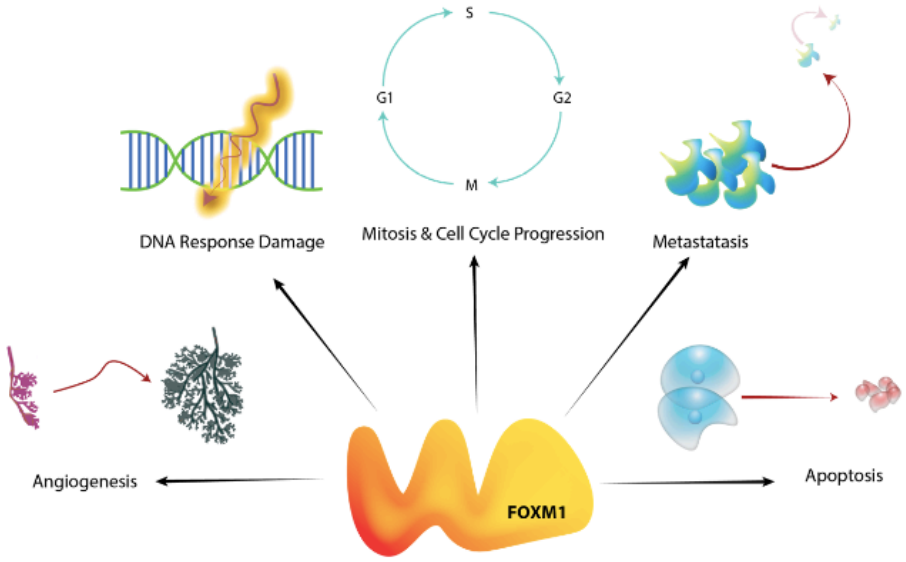

Figure 3-1. The role of FOXM1 in normal cells and cancer initiation and progression. FOXM1 is involved in the activation of different genes and the expression of proteins that control angiogenesis, DNA repair, metastasis, and apoptosis.

Similar to other FOX proteins, FOXM1 has a conserved DBD that is responsible for binding to the corresponding promoter regions (266). Hypothetically, any small molecule capable of binding to this winged-helix could inhibit the FOXM1/DNA complex. Nevertheless, TFs have been regarded as "challenging" or "inaccessible" using small molecules (267). This generalization was, at least in part, due to the large solvent-accessible area observed on the TF and the lack of well-defined binding pockets on the protein's hydrophobic surface (25,206). In this regard, Gormally et al. (206) reported a high-throughput screening technique to test more than 50,000 small-molecules, selecting those capable of inhibiting the binding interaction between FOXM1 and its DBD. Gormaly's group selected 16 different FDIs among which, the compound FDI-6 was the most potent.

We previously conducted and reported a detailed *in silico* study (210) to determine FOXM1-DBD/DNA binding interactions exerted by three structurally-different FOXM1 inhibitors, namely thiostrepton (199,268), troglitazone (20), and FDI-6 (206). In our previous study, we proposed a protein-drug-DNA binding model involving a sulfur-His287 interaction. Besides, we also proposed another essential drug binding interaction involving the fluorine atom at the 4-position of the phenyl ring present in FDI-6, and the Arg297 residue in FOXM1. To prove the importance of this halogen binding, in this complementary study we report (i) a structure-activity relationship (SAR) between the parent (lead) drug FDI-6, and ten derivatives possessing halogen (Cl, Br, I) atoms, as well as other substituents at the 4-fluorophenyl (H-, CH_3-, CF_3-) position. Furthermore, we also studied the effects of relocating the 4-fluorine atom to a 2- and 3-position (**Figure 3-2**).

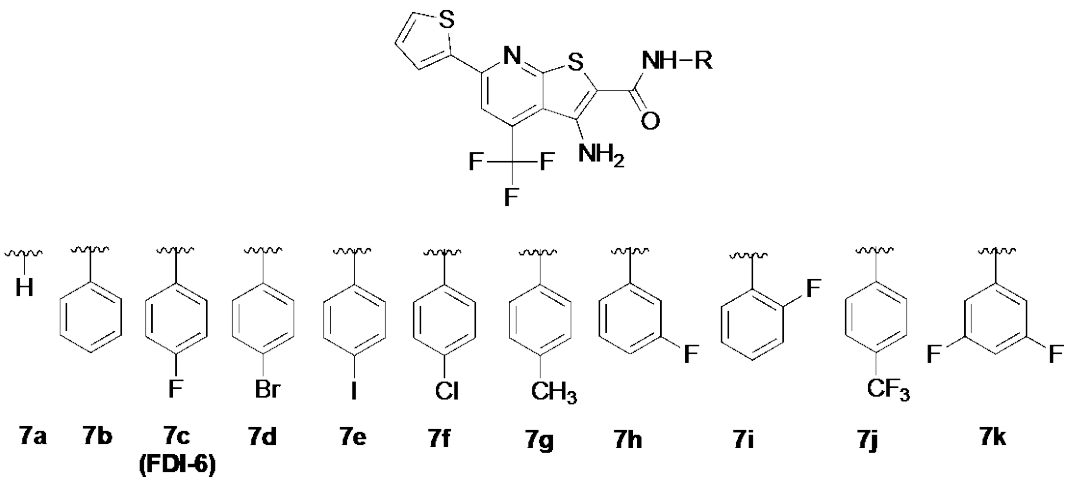

Figure 3-2. Compounds 7a-7k were prepared by replacing the 4-fluorophenyl group of FDI-6 (7c).

We report preliminary evidence validating the essential role of a halogen atom in FDI-6 derivatives, responsible for binding to an Arg297 residue. The results of our experiments validate the hypothesis of a 4-(halo) phenyl moiety as an essential structural feature in FDIs, as one of the required drug binding forces at the interface of the FOXM1 protein and its DBD.

3.2 Materials and Methods

3.2.1 General Information

All the reagents and solvents were purchased from Sigma-Aldrich and were used without further purification. All reactions were monitored by thin-layer chromatography (TLC) (RediSep® TLC plates) and visualized using UV light. Melting points were measured with an electrothermal melting point apparatus (Thermofisher, USA) and were uncorrected. ^{1}H-NMR and ^{13}C-NMR spectra were determined on a Bruker FT-600 MHz instrument (600 MHz and 150 MHz, respectively) using DMSO-d6 as the solvent and

Tetramethylsilane (TMS) as a reference. Chemical shifts (δ) and coupling constants (*J*) are expressed in parts per million and Hertz, respectively. Signal multiplicity is expressed as s (singlet), d (doublet), t (triplet), q (quartet), m (multiplet) and br (broad singlet). Elemental analyses were performed on a Carlo Erba EA1108 elemental analyzer, and the results are within ± 0.4% of the theoretical values. The synthesis of 6-(thiophen-2-yl)-2-thioxo-4-(trifluoromethyl)-1,2-dihydropyridine-3-carbonitrile (3) was carried out following the method reported (269), and confirmed by ^{1}H, ^{13}C, and ^{19}F NMR. 2-Chloroacetamide (6a) was purchased from Sigma Aldrich, whereas compounds 6b-6k were synthesized based on the protocols previously reported (270–272) and confirmed by ^{1}H NMR. FDI derivatives 7a-7c, and 7f, were confirmed by ^{1}H and ^{13}C spectra, both in agreement to those reported in the literature (269). See Appendices for NMR spectra. The microwave-assisted synthesis of derivatives 7a-7k was carried out using an Initiator Reactor (Biotage). All test compounds were purified by flash column chromatography using a Combi Flash EZ prep (Teledyne isco), using prepacked silica cartridges (RediSep Rf® Gold Resolution) and a gradient of hexane-ethyl acetate as mobile phase.

3.2.2 General Procedure for the Synthesis of Compounds 7a-7k

The corresponding chloroacetamide 6a-6k (1 eq.), compound 3 (1 eq.) was mixed with K_2CO_3 (1 eq.), and ethanol (5 mL) in a microwave reaction vessel. This mixture was stirred at 90 °C for 2 hours using a “high energy absorption” setting. The crude product was filtered-off, washed with water and fixed onto silica gel powder before running a solvent gradient flash column chromatography. Combined organic fractions were dried under vacuum and the corresponding final product was recrystallized from ethanol (when needed).

3-amino-N-(4-bromophenyl)-6-(thiophen-2-yl)-4-(trifluoromethyl)thieno[2,3-b]pyridine-2-carboxamide *(***7d***)*. 6d (65 mg, 0.22 mmol), 3 (63 mg, 0.22 mmol) and K_2CO_3 (30 mg, 0.22 mmol) in 5 mL of ethanol, yellow (flocculent) crystals, 90 % yield (100 mg, 0.2 mmol), mp: 225-227 °C; ^{1}H NMR (600 MHz, DMSO-d6) δ 9.78 (s, 1H), 8.33 (s, 1H), 8.25 (dd, J = 3.8, 1.1 Hz, 1H), 7.89 (dd, J = 5.0, 1.1 Hz, 1H), 7.75 – 7.68 (m, 2H), 7.56 – 7.51 (m, 2H), 7.32 (dd, J = 5.0, 3.7 Hz, 1H), 6.91 (s, 2H).13C NMR (151 MHz, DMSO) δ 164.49, 160.99, 152.15, 142.72, 132.16, 131.91, 131.55, 131.38, 129.49, 129.23, 125.93, 124.26, 124.12, 122.30, 120.49, 118.74, 112.86, 112.82. Anal. Calc. for (%) $C_{19}H_{11}BrF_3N_3OS_2$, C 45.79; H 2.23, N 8.43; S 12.87; found C 45.72, H 2.44, N 8.10, S 12.51.

3-amino-N-(4-iodophenyl)-6-(thiophen-2-yl)-4-(trifluoromethyl)thieno[2,3-b]pyridine-2-carboxamide *(***7e***)*. 6e (55 mg, 0.18 mmol), 3 (54 mg, 0.18 mmol) and K_2CO_3 (25 mg, 0.18 mmol) in 5 mL of ethanol, yellow (flocculent) crystals, 92% yield (90 mg, 0.19 mmol); mp: 226-228 °C;^{1}H NMR (600 MHz, DMSO-d6) δ 9.87 (s, 1H), 8.35 (s, 1H), 8.28 (dd, J = 3.8, 1.1 Hz, 1H), 7.91 (dd, J = 5.0, 1.1 Hz, 1H), 7.77 – 7.71 (m, 2H), 7.63 – 7.57 (m, 2H), 7.32 (dd, J = 5.0, 3.7 Hz, 1H), 6.85 (s, 2H). ^{13}C NMR (151 MHz, DMSO-d6) δ 164.09, 161.04, 152.78, 145.55, 142.54, 137.59, 132.47, 132.25, 131.67, 129.57, 129.54, 125.84, 124.12, 122.21, 118.27, 113.16, 113.12, 88.03. Anal. Calc. for (%) $C_{19}H_{11}F_3IN_3OS_2$, C 41.85, H 2.03, N 7.71, S 11.76; found C 41.31, H 2.10, N 7.45, S 11.69.

3-amino-N-(4-methylphenyl)-6-(thiophen-2-yl)-4-(trifluoromethyl)thieno[2,3-b]pyridine-2-carboxamide *(***7g***)*. 6g (40 mg, 0.2 mmol), 3 (60 mg, 0.2 mmol) and K_2CO_3 (30 mg, 0.18 mmol) in 5 mL of Ethanol, yellow (flocculent) crystals yellow powder, 90%

yield (80 mg, 0.18 mmol), mp: 233-235 °C;[1]H NMR (600 MHz, DMSO-d6) δ 9.69 (s, 1H), 8.31 (s, 1H), 8.23 (dd, J = 3.8, 1.1 Hz, 1H), 7.86 (dd, J = 5.0, 1.1 Hz, 1H), 7.58 – 7.53 (m, 2H), 7.28 (dd, J = 5.0, 3.8 Hz, 1H), 7.19 – 7.15 (m, 2H), 6.75 (s, 2H), 2.30 (s, 3H). ^{13}C NMR (151 MHz, DMSO-d6) δ 163.91, 160.95, 152.70, 145.33, 142.56, 136.31, 133.53, 132.46, 132.24, 131.64, 129.54, 129.38, 124.04, 122.21, 118.37, 113.15, 113.11, 101.61, 20.99. Anal. Calc. for (%) $C_{20}H_{14}F_3N_3OS_2$, C 55.42, H 3.26, N 9.69, S 14.79, found C 55.42, H 3.31, N 9.49, S 15.08

3-amino-N-(2-fluorophenyl)-6-(thiophen-2-yl)-4-(trifluoromethyl)thieno[2,3-b]pyridine-2-carboxamide (7h). 6h (45 mg, 0.23 mmol), 3 (65 mg, 0.23 mmol) and K_2CO_3 (30 mg, 0.23 mmol) in 5 mL of ethanol, yellow (flocculent) crystals yellow powder, 92% yield (90mg, 0.21 mmol), mp: 218-220 °C; ^{1}H NMR (600 MHz, DMSO-d6) δ 9.95 (s, 1H), 8.35 (s, 1H), 8.27 (dd, J = 3.8, 1.1 Hz, 1H), 7.90 (dd, J = 5.0, 1.1 Hz, 1H), 7.71 (ddd, J = 11.8, 2.6, 1.9 Hz, 1H), 7.57 (ddd, J = 8.2, 1.9, 0.9 Hz, 1H), 7.44 (td, J = 8.2, 6.9 Hz, 1H), 7.32 (dd, J = 5.0, 3.7 Hz, 1H), 6.99 (tdd, J = 8.5, 2.6, 0.9 Hz, 1H), 6.87 (s, 2H). ^{13}C NMR (151 MHz, DMSO): δ 164.21, 163.21, 161.61, 161.07, 152.91, 145.83, 142.50, 140.95, 132.53, 132.31, 131.72, 130.54, 130.48, 129.63, 129.55, 125.83, 124.02, 122.20, 118.18, 117.49, 117.48, 113.20, 113.16, 110.76, 110.62, 108.56, 108.39, Anal. Calc. for (%) $C_{19}H_{11}F_4N_3OS_2$, C 52.17, H 2.53, N 9.61, S 14.66 found C 51.80, H 2.63, N 9.28, S 14.88.

3-amino-N-(3-fluorophenyl)-6-(thiophen-2-yl)-4-(trifluoromethyl)thieno[2,3-b]pyridine-2-carboxamide (7i). 6i (45 mg, 0.23 mmol), 3 (65 mg, 0.23 mmol) and K_2CO_3 (30 mg, 0.23 mmol) in 5 mL of ethanol, yellow (flocculent) crystals, 95% yield (93mg, 0.22 mmol); mp: 248-250 °C;[1]H NMR (600 MHz, DMSO-d6) δ 9.73 (s, 1H), 8.32

(s, 1H), 8.24 (dd, J = 3.8, 1.1 Hz, 1H), 7.86 (dd, J = 5.0, 1.1 Hz, 1H), 7.51 (t, J = 7.8 Hz, 1H), 7.36 – 7.29 (m, 2H), 7.28 (dd, J = 5.0, 3.7 Hz, 1H), 7.27 – 7.20 (m, 1H), 6.76 (s, 2H). ^{13}C NMR (151 MHz, DMSO-d6) δ 164.08, 161.10, 157.77, 156.13, 152.87, 145.57, 142.53, 132.61, 132.39, 131.72, 129.64, 129.56, 128.47, 127.97, 127.92, 125.74, 125.66, 124.78, 124.00, 122.19, 118.29, 116.38, 116.25, 113.19, 113.15, 100.96. Anal. Calc. for (%) $C_{19}H_{11}F_4N_3OS_2$ C 52.17, H 2.53, N 9.61, S 14.66 found C 52.19, H 2.71, N 9.36, S 15.02.

3-amino-6-(thiophen-2-yl)-4-(trifluoromethyl)-N [4(trifluoromethyl)phenyl]thieno[2,3-b]pyridine-2-carboxamide (7j*).* 6j (55 mg, 0.22 mmol), 3 (65 mg, 0.22 mmol) and K_2CO_3 (30 mg, 0.22 mmol) in 5 mL of ethanol, yellow (flocculent) crystals, 95 % yield (100 mg, 0.21 mmol), mp: 183-185 °C; ^{1}H NMR (600 MHz, DMSO-d6) δ 10.05 (s, 1H), 8.30 (s, 1H), 8.23 (dd, J = 3.8, 1.1 Hz, 1H), 7.94 (d, J = 8.5 Hz, 2H), 7.86 (dd, J = 5.0, 1.1 Hz, 1H), 7.70 (d, J = 8.5 Hz, 2H), 7.27 (dd, J = 5.0, 3.7 Hz, 1H), 6.86 (s, 2H): ^{13}C NMR (151 MHz, DMSO-d6) δ 164.52, 161.14, 152.85, 142.54, 132.50, 132.28, 131.70, 129.60, 129.54, 127.62, 126.15, 126.13, 126.10, 125.82, 124.03, 122.22, 121.65, 121.63, 120.40, 118.22, 113.16, 113.12. Anal. Calc. for (%) $C_{20}H_{11}F_6N_3OS_2$ C 49.28, H 2.27, N 8.62, S 13.15 found C 49.09, H 2.30, N 8.33, S 12.93.

3-amino-N-(3,5-difluorophenyl)-6-(thiophen-2-yl)-4-(trifluoromethyl)thieno[2,3-b]pyridine-2-carboxamide (7k). 6k (50 mg, 0.23 mmol), 3 (65 mg, 0.23 mmol) and K_2CO_3 (35 mg, 0.23 mmol) in 5 mL of ethanol, red needle crystals, 95 % yield (100 mg, 0.22 mmol), mp: 208-210 °C; ^{1}H NMR (600 MHz, DMSO-d6) δ 10.02 (s, 1H), 8.30 (s, 1H), 8.23 (dd, J = 3.8, 1.1 Hz, 1H), 7.86 (dd, J = 5.0, 1.1 Hz, 1H), 7.54 – 7.46 (m, 2H), 7.27 (dd, J = 5.0, 3.7 Hz, 1H), 6.92 (t, J = 9.3 Hz, 1H), 6.86 (s, 2H). ^{13}C NMR (151 MHz,

DMSO-d6) δ 163.53, 163.43, 161.92, 161.82, 161.15, 153.15, 148.79, 146.32, 146.31, 132.64, 132.42, 132.03, 131.85, 129.92, 129.77, 129.57, 125.80, 123.99, 122.17, 118.02, 113.30, 113.26, 104.31, 104.27, 104.15, 104.11, 99.37, 99.20, 99.03. Anal. Calc. for (%) $C_{19}H_{10}F_5N_3OS_2$ C 50.11, H 2.21, N 9.23, S 14.08 found C 49.78, H 2.39, N 8.91, S 13.66.

3.2.3 General Procedure for the Synthesis of Compound 3

The titled compound was prepared by following a reported method with an overall yield of 64 % (**Scheme 3-1**). The identity of the product was confirmed by ^{1}H-, ^{13}C- and ^{19}F-NMR. Briefly, to a solution of 1 (1 eq., 2.2 g, 10 mmol) and DABCO (1.1 g, 10 mmol) in ethanol (20 mL) was added 2 (1 eq., 1.5 g, 15 mmol). The reaction mixture was refluxed and stirred for 5 hours until the reaction was completed (monitored by TLC). The resultant yellowish precipitate was filtered off, washed with water (3×10 mL), and used without any further purification.

Scheme 3-1. Synthesis rout of compound 3. Reagents and conditions: (a) DABCO, ethanol, reflux, 5 hours.

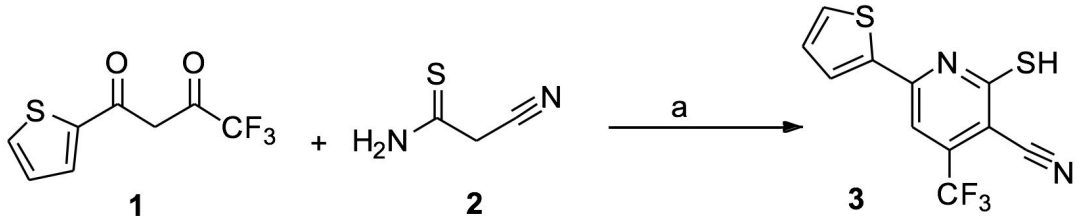

3.2.4 General Procedure for the Synthesis of Compounds 6a-6k

2-Chloroacetamide (6a) was purchased from Sigma Aldrich; the synthesis of the titled compounds was achieved by following reported methods (270–274), with an overall yield of 80% and confirmed by ^{1}H NMR (**Scheme 3-2**). Briefly, chloroacetylchloride (5) (1.4

eq.) was added dropwise to a solution of Et_3N (2 eq.) and the corresponding aniline (4b-4k) (1 eq.) in dry dichloromethane (20 mL). The reaction mixture was stirred for 5 hours at r.t. and monitored by TLC. Once completed (as judged by TLC), ethyl acetate (20 mL) was added to the reaction mixture, which yielded a precipitated in the form of white crystals, which were removed by filtration; the filtered solution was washed with water (3 × 20 mL) and dried with $MgSO_4$. Ethyl acetate was removed under reduced pressure, to yield a powder that was recrystallized from a mixture of hexane and ethyl acetate (90:10).

Scheme 3-2. Synthesis route of the amides 6b-6k. Reagents and conditions: (a) Et_3N, dry CH_2Cl_2, r.t., 5 hours.

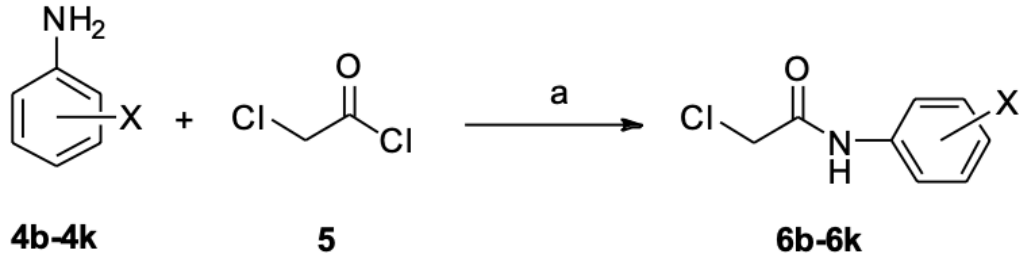

4b-4k **5** **6b-6k**

4b, 6b: X = H
4c, 4c: X = 4-F
4d, 6d: X = 4-Br
4e, 6e: X = 4-I
4f, 6f: X = 4-Cl
4g, 6g: X = 4-CH_3
4h, 6h: X= *3-F*
4i, 6i: X= *2-F*
4j, 6j: X = 4-CF_3
4k, 6k: X= *3,5-F*

3.2.5 Cell Culture

The MDA-MB-231 and MCF-7 cells were a generous gift from Dr. Frank Wuest (Cross Cancer Institute; Edmonton, Alberta, Canada). The cells were cultured in RPMI and DMEM media respectively, supplemented with 10% fetal bovine serum (FBS) in a 5% CO2 atmosphere at 37 °C.

3.2.6 Cell Proliferation Assay (MTT)

Cells were seeded in 96-well plates (approx. 4000 cells/well for MDA-MB-231 and approx. 5000 for MCF-7), then we added the test compounds at different concentrations, and we incubated all plates for 72 hours. We added 30 μL of 3-(4,5-Dimethylthiazol-2-Yl)-2,5-Diphenyltetrazolium Bromide (MTT) solution (3 mg/ml) and continued the incubation for three hours at 37 °C. The precipitated crystals were dissolved using DMSO, and the absorbance of the resulting solution was recorded at 570 nm using a Synergy H1-Hybrid Multi-Mode Reader (BioTek). We analyzed the data using GraphPad Prism. All experiments were carried out in triplicate.

3.2.7 Antibodies

FOXM1 mouse monoclonal antibody (mouse, sc-271746) was purchased from Santa Cruz Biotechnology and IRDye® 800CW goat anti-Mouse IgM was received from Li-Cor Biosciences.

3.2.8 Western Blot

After treatment with test compounds for 24 hours at different concentrations, the cells were trypsinized; the FOXM1 protein was isolated with RIPA lysis and extraction buffer (ThermoFisher) according to the manufacturer's protocol. The protein levels in the supernatant were measured using the Bradford assay. Then the protein (40 μg/lane) was loaded into a 4-20% SDS-PAGE (Sodium dodecyl sulfate polyacrylamide gel electrophoresis). After completion of the run, the protein was transferred from the gel to a nitrocellulose membrane (Thermofisher) and stained with REVERT (Li-Cor Biosciences) total protein stain. The membrane was then detected in the 700 nm channel

using an Odyssey scanner (LI-COR Biosciences). The REVERT was then reversed and the membrane was blocked with 10% fat-free milk in TBST for 1 hour. The membrane was incubated with the primary antibody (1:1000 dilution) at 4 °C overnight. Then, the membrane was washed three times with TBST, incubated with the corresponding Li-Cor secondary antibody, and incubated again at r.t. for 1 hour. The membrane was washed three times (15 minutes total) with TBST. The blots were visualized using Odyssey scanner (LI-COR Biosciences). The quantification was carried out for all proteins relative to total protein (REVERT) using ImageJ for each lane.

3.2.9 Recombinant Protein Production and Purification

We used the PEX-N-GST-FOXM1C-DBD plasmid (OriGene Technologies, USA) transformed into BL21(DE3) E. Coli cells; positive colonies were selected on luria broth (LB) agar plates with ampicillin (100 μg/mL). Then, these cells were grown in LB media with ampicillin (100 μg/ml) at 37 °C with orbital shaking at 220 rpm until reaching an optical density (OD600) of 0.8; protein expression was induced by adding 1 mM isopropyl β-D-1-thiogalactopyranoside (IPTG) for 6 hours at 37 °C. The Glutathione-S-Transferase (GST) protein and GST-FOXM1 protein from soluble fractions were purified using glutathione resin (GenScript, USA), following the manufacturer's instructions. Please see **A.2.1** GST-FOXM1-DBD (Wild type) for the representative gel image of purified recombinant GST-FOXM1-DBD.

3.2.10 Electrophoretic Mobility Shift Assay

All values of the titration (binding) curve of recombinant FOXM1-DBD with its target double-strand DNA oligo (Forward strand: 5′-/IRD700/-

AAACAAACAAACAATCAAACAAACAAACAATC-3′), were recorded using EMSA by the method previously reported by Gormally et al. (206). Briefly, double-stranded DNA (dsDNA) and an increasing concentration of the FOXM1 protein were incubated at r.t. for 30 minutes in a buffer solution containing 20 mM Tris (pH 7.5), 100 mM KCl, 1 mM ethylenediaminetetraacetic acid (EDTA), 0.1 mM dithiothreitol (DTT), and 10% glycerol, before running the samples on 6% native gel for 30 min at 120 V. The dissociation constant (Kd) of protein DNA complex was calculated using GraphPad Prism 6.2. The displacement EMSA experiments were carried out by incubating each test compound with the recombinant FOXM1-DBD protein, for 1.5 hours, at r.t., followed by a second incubation with DNA, for 20 minutes, before conducting the electrophoresis. The concentration of FOXM1-DBD and DNA in each reaction was 480 nM and 12.8 nM, respectively. The inhibitory constant (Ki) values were calculated for each compound (7a-7k) using **Equation 1** (275):

$$Ki = {[I]_{50}} \Big/ \left(\frac{([I]_{50})}{K_d} + {[P]_0}/{K_d} + 1\right) \qquad \textbf{Equation } (1)$$

Where: $[I]_{50}$ = IC_{50} of the inhibitor; $[L]_{50}$ = concentration of IR-labelled DNA at 50% inhibition; [P] = concentration of the FOXM1 protein; and Kd = dissociation constant calculated from the initial titration curve.

3.2.11 Molecular Modeling and Dynamics Simulations

The crystal structure of FOXM1-DBD was acquired from the PDB (PDB_ID: 3G73) (266). Using Pymol v.1.8 (276), we removed Chain A followed by a short minimization

using CHIMERA V 1.10.2 (277), the missing sidechains were added and the protonated group was equilibrated to the biological pH 7.0 using PROPKA (241).

All the 3D format structures were prepared for docking using the Dockprep tool of UCSF CHIMERA V1.10.2 in the framework of AMBER99SB force field. All the compounds were docked in a previously identified binding pocket (210), into a grid of 40 x 40 x 50 Å with a spacing of 0.375 Å using Autodock vina (245); 12 runs per docking were performed with the exhaustiveness of 40 for each ligand. Before performing the MD simulation on the Protein-ligand complexes, we performed a MD simulation on the FOXM1-DBD using GROMACS 4.5.6 package (278). We used the TIP3P water models to solvate the protein with 1 nm marginal cushion on each side. The box was then neutralized using NaCl, and the system was minimized using the AMBER99SB0ILDN force field. The system was heated to 300 K and equilibrated for 500 ps using the Berendsen thermostat. A 20 ns production run was performed using the periodic boundary condition. The Lenard-Jones, the Coulomb (Cut-off=1.0 nm), and the PME were used to calculate the vdW and electrostatic interactions. The FOXM1-DBD/Ligand complexes were performed using the same condition. The ACEPYPE (249) was used for ligand parameterization. The RMSD, RMSF and ligand positional RMSD were calculated using GROMACS tools. All the data were plotted using the GraphPad Prism 6.0.7. Discovery Studio Visualizer (279) and the Schrodinger's Pymol package were used as the visualization tools.

The free energy of interaction between each ligand and FOXM1-DBD was calculated using the g_mmpbsa Gromacs tool (250). Using the MM-PBSA, this program calculates the binding free energy based on the electrostatic and vdW interactions besides

polar and non-polar solvation energies. The G_mmpbsa module solves the following **Equations** (2) and (3) to calculate the binding energy of ligands:

$$\Delta G_{bidning} = G_{complex} - \left(G_{protein} + G_{ligand}\right) \quad \textbf{(Equation 2)}$$

where the $G_{complex}$ is the protein-ligand complex total free energy, $G_{protein}$ is the total free energy of protein and G_{ligand} is the total energy of ligand in solvent. The free energy of protein-ligand complex, isolated protein and isolated ligand (G) can be given by:

$G = E_{MM} + G_{solv} - TS$ **(Equation 2)**

where E_{MM} is the average of molecular mechanics potential in vacuum, TS is the Temprature and Entropy respectively and $G_{solvation}$ is the solvation free energy.

3.3 Results and Discussion

3.3.1 Design and Synthesis

To conduct a structure-activity relationship study on the role of the fluorine atom present in FDI-6, we synthesized ten derivatives possessing different functional groups at the 4-phenyl position of the lead molecule. We adapted the methods previously reported for the synthesis of FDI-6 (206,269) and prepared the FDI derivatives 7a-7k in an overall 80% yield by using a microwave-assisted synthesis. The proposed series of test molecules consisted of an FDI-6 derivative without the phenyl group, -H (7a), replacement of the –4-fluorophenyl by –Ph atom (7b), –Br (7d), –I (7e), –Cl (7f), $–CH_3$ (7g), a 3-fluorophenyl (7h), 2-fluorophenyl (7i), a 3,5- difluorophenyl group (7k) and a 4-CF_3 (7j) (**Scheme 3-3**).

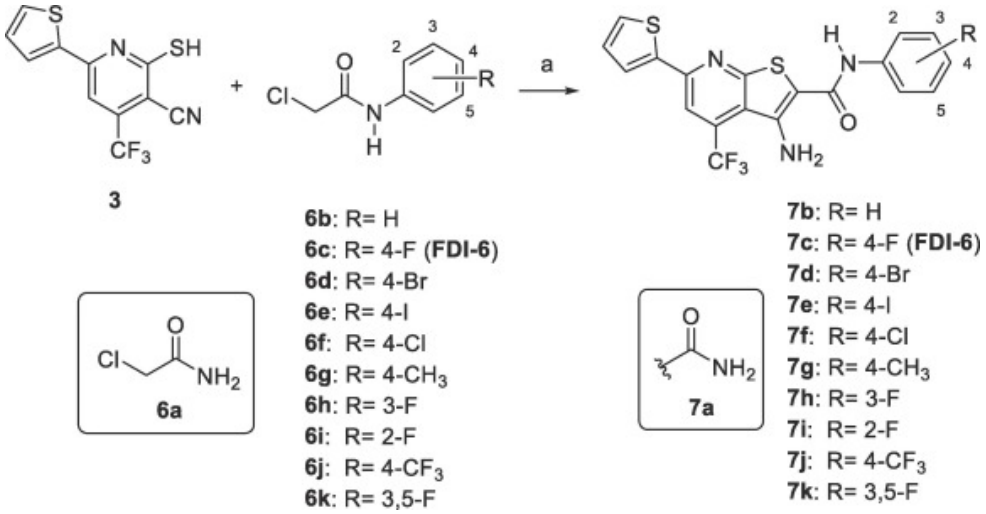

Scheme 3-3. Chemical synthesis of FDI-6 derivatives, 7a-7k. (a) Reagents and conditions: K_2CO_3, EtOH, 90 °C, μW, 2 hours.

3.3.2 Cell Proliferation Assay

First, we determined the effect of all FDI-derivatives on cell proliferation using two human breast cancer cell lines, namely the triple negative-breast cancer cell line MDA-MB-231 and the ER-positive cell line MCF-7, using the MTT assay.

Briefly, after a 72 hours incubation period of MDA-MB-231 and MCF-7 cells in the presence of different concentrations of the corresponding drug molecule, we observed that drug potency was significantly reduced in molecules without a 4-(halo)phenyl group (7a, 7b), as well as drugs in which the fluorine atom was moved from the 4-position (7c) to the 2-position (7i). We also observed an apparent lack of activity in the derivative possessing a 3,5-difluorophenyl group (7k). We also observed that replacement of the fluorine atom present in FDI-6 (7c), by a 4-bromo (7d), 4-iodo (7e), or 4-chloro (7f), resulted in increased potency (decreased cell proliferation) in both cell lines; however the MCF-7 shows relatively higher susceptibility towards all these compounds. Interestingly,

there was an apparent inverse correlation between the electronegativity of the halogen atom and the potency of the corresponding derivative, in which the lower the electronegativity of the halogen atom, the higher the potency (**Table 3-1**). These observations suggest that the 4-(halo) phenyl ring is essential for cancer cell proliferation inhibition *in vitro*.

Assuming that a methyl group could be a suitable bioisosteric replacement for big halogen atoms (280), we synthesized and screened compounds 7g [4-(CH_3) phenyl] and 7j [4-(CF_3) phenyl]. We observed an equipotent profile for both drugs compared to the analogs possessing a 4-(halo)phenyl group, including the lead drug FDI-6. Consequently, these observations strongly suggest that the 4-substituted phenyl ring in the FDI is essential to exert significant cell proliferation inhibition of these two breast cancer cells.

Table 3-1. IC_{50} values calculated for ten FDI inhibitors using the human breast cancer cell lines MDA-MB-231 and MCF-7. These values were calculated based on a 72 hours incubation period with the drug molecules; all values represent the mean ± Standard error of the mean (SEM) of three different experiments, each one in triplicate.

Compound	MDA-MB-231 IC_{50} (µM)	MCF-7 IC_{50} (µM)
7a	>50	>50
7b	>50	35.27 ± 6.03
7c (FDI-6)	31.1 ± 8.7	13.43 ± 1.82
7d	12.5 ± 4.4	3.04 ± 0.75
7e	9.8 ± 2.2	1.36 ± 0.39
7f	14.6 ± 4.2	2.90 ± 1.15
7g	24.8 ± 5.0	11.25 ± 2.9
7h	35.75 ± 6.3	23.35 ± 6.09
7i	>50	>50
7j	12.6 ± 1.6	10.53 ± 1.9
7k	>50	>50

We also investigated the effect of moving the fluorine atom from the 4- to 3-position (7h), and we observed a minor decrease in potency compared to FDI-6, which along with the observation that the 2-fluorophenyl compound was inactive (up to a maximum test drug concentration of 50 μM), we observed that the halogen-Arg297 interaction becomes weaker as the halogen is located farther apart from the initial 4-position. This statement is based on the assumption that the observed cell proliferation inhibition is, at least in part, FOXM1-dependent. Finally, we observed that the compound having a 3,5-difluorophenyl moiety (7k) was inactive, likely not because of weaker binding interactions, but because it was not soluble enough in the cell media employed in the MTT assay (we observed precipitation at increasingly higher concentrations). Nevertheless, we will need to carry out additional experiments using different pharmaceutical excipients (other than DMSO) to increase the water solubility of this (and all other molecules (s)).

3.3.3 FOXM1 Expression Level

Considering that FOXM1 modulates its own transcriptional expression(281), we determined the effect of the test drugs on the expression levels of this protein, by western blot analysis (whole-cell lysis), after a 24 hours incubation period with the corresponding drug molecules using triple negative-breast cancer cells (MDA-MB-231). We conducted this experiment assuming that a drug-dependent decrease in FOXM1 at the protein level could be due, at least in part, to a drug-induced dissociation of the nuclear FOXM1-DNA complex, which in turn would suggest transcriptional inhibition. We observed a drug-dependent decrease in FOXM1 protein in MDA-MB-231 breast cancer cells (**Figure 3-3**).

Based on a simple structure-activity relationship study, we can make a few preliminary statements describing the effect of substituting specific functional groups on protein expression in these cells. For example, compound 7a devoid of the 4-fluorophenyl group (present in the lead drug FDI-6) and compound 7b [4-(phenyl)], were practically inactive at 40 μM. As expected, the lead molecule FDI-6 [4-(fluoro) phenyl; 7c] significantly decreased the concentration of FOXM1. Interestingly, compounds possessing a 4-(bromo)phenyl (7d), 4-(iodo) phenyl (7e) and 4-(chloro) phenyl (7f) were equipotent to FDI-6 (non-significant differences between them) in this assay, and it correlates well with the cancer cell proliferation inhibition exerted on MDA-MB-231 cells described above.

Nevertheless, we observed that compound 7g [4-(methyl) phenyl] exerted a non-significant decrease in FOXM1 expression, despite its good cell proliferation inhibitory profile. This suggests that bioisosteric replacements with methyl group may not be a suitable approach to decrease the expression of FOXM1 in triple negative-breast cancer cells, despite their relatively significant effects on cell proliferation inhibition.

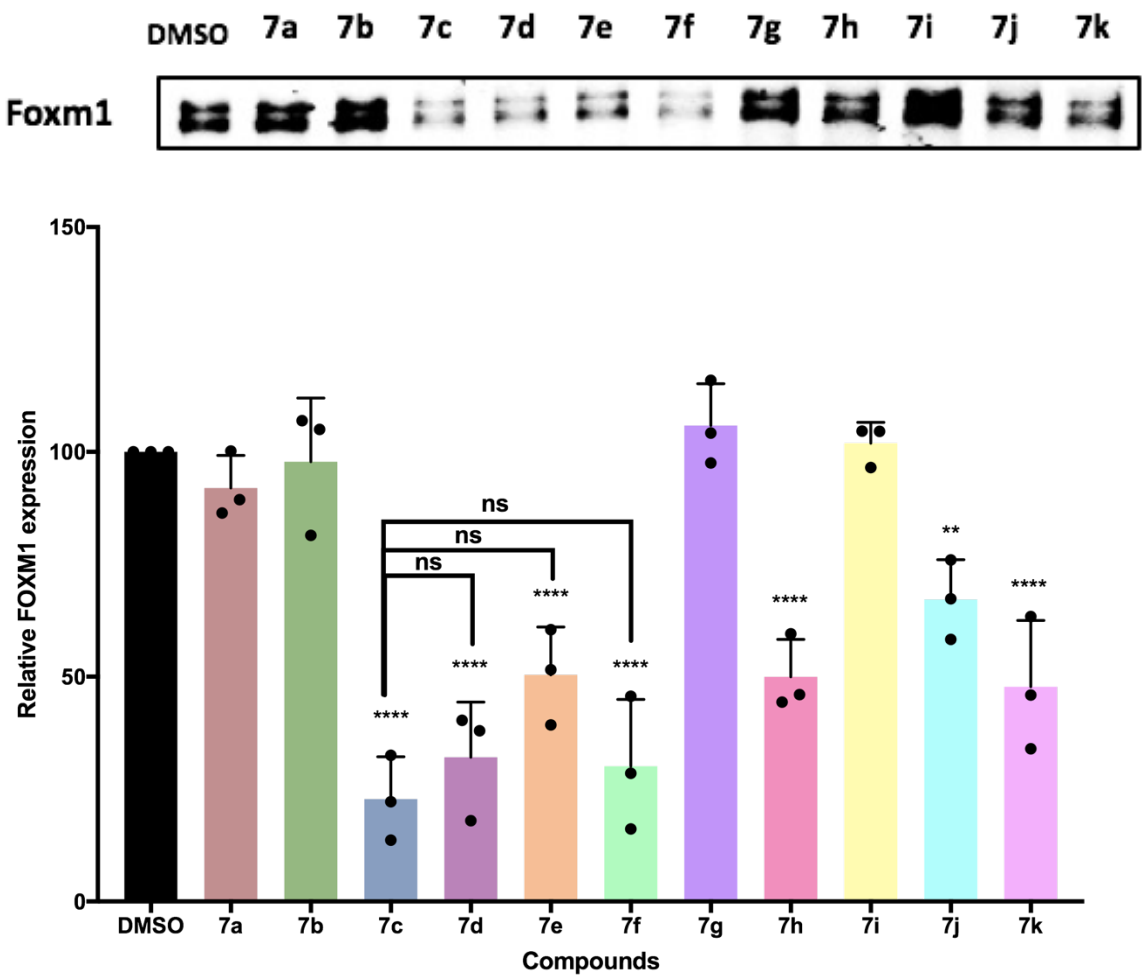

Figure 3-3. Expression levels of the FOXM1 protein and the concentration-dependent inhibitory effect produced by the lead drug (7c) and ten derivatives. Incubation time= 24 hours; cell line= triple negative-breast cancer (MDA-MB-231); drug concentration= 40 μM; bars represent the corresponding average values of three independent experiments ± SEM; one-way ANOVA was used to determine significance (* = $P \leq 0.05$, ** = $P \leq 0.01$, **** = $P \leq 0.0001$) compared to DMSO. (Detection of two bands is most likely due to the presence of different FOXM1 isoforms)

These results are in agreement with our hypothesis: the 4-(halo) phenyl moiety is essential to exert binding interactions resulting in inhibition of FOXM1's transcriptional

activity. Only the 4-(halo) phenyl derivatives significantly decreased FOXM1, suggesting effective binding interactions between the 4-(halo) phenyl group in FDI and Arg297 in the FOXM1 protein.

Extending the SAR study to other derivatives in the series, we observed that compound 7h [3-(fluoro) phenyl] was active at 40 μM, whereas compound 7i [2-(fluoro) phenyl] was inactive, which provides a "fine-tuning" of the hypothesis described above in the sense that, the farther apart from position 4-, the weaker the binding interaction. Finally, we observed that compound 7k (3,5-difluorophenyl) and 7j [4-(trifluoromethyl) phenyl] exerted a moderate decrease in FOXM1 levels, likely as the result of their lower solubility.

3.3.4 Electrophoretic Mobility Shift Assay

This cell-free assay was selected based on its ability to measure the concentration-dependent effect produced by drug molecules to prevent the formation of the FOXM1-DNA complex *in vitro*. This screening method was first reported by Gormally et al. as part of a high-throughput screening approach to find new FOXM1 inhibitors, in which the drug FDI-6 was identified as the most potent molecule. Based on their model, we incubated the recombinant FOXM1-DBD reported to bind to DNA, with the target DNA, in the presence of the corresponding FDI derivatives (1.5 hours incubation at 25º C) and then running the mixture on a native polyacrylamide gel. As shown in **Figure 3-4**, we observed that compounds 7a (devoid of the 4-(halo) phenyl group) and 7b (phenyl) were weak drugs (IC_{50} values = 128.2 and 121.7 μM respectively), whereas compounds 7c [4-(fluoro) phenyl], 7d [4-(bromo) phenyl], and 7e [4-(iodo) phenyl] were significantly more active (IC_{50} values around 40 μM). Compound 7f [4-(chloro) phenyl], the most active

molecule in this series (IC_{50} value = 27.2 μM), was about 2-fold more potent than the lead drug FDI-6. These observations provide one more piece of evidence confirming our initial hypothesis, in which we proposed the need for a 4-halo substituted phenyl ring in the FDI scaffold.

Compound 7g possessing a 4-methyl (-CH_3) bioisosteric replacement for fluorine, was much less active (IC_{50} = 228.9 μM) than 7c (FDI-6) and other halogen-containing derivatives. Nevertheless, we observed that a 4-(trifluoromethyl) phenyl group (7j) restored the activity (IC_{50} = 27.5 μM), further supporting the need for a halogen atom at the 4-phenyl position, essential to exert a binding interaction with Arg297 in FOXM1. Finally, moving the fluorine atom from 4-(7c) to 3- maintained the activity of compound 7h (IC_{50} = 42.6 μM), but when the halogen is farther away (position 2-) the potency decreased for compound 7i (IC_{50} = 69.6 μM).

A

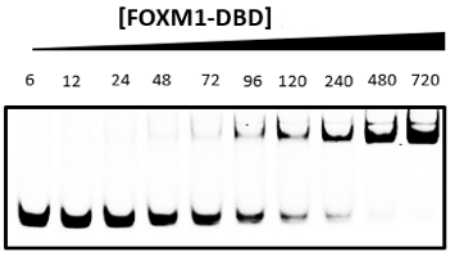
[FOXM1-DBD]
6 12 24 48 72 96 120 240 480 720

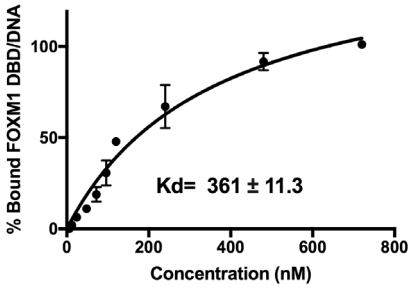
% Bound FOXM1 DBD/DNA
100
50
0
0 200 400 600 800
Concentration (nM)
Kd= 361 ± 11.3

B

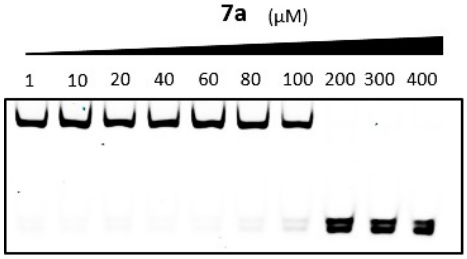
7a (μM)
1 10 20 40 60 80 100 200 300 400

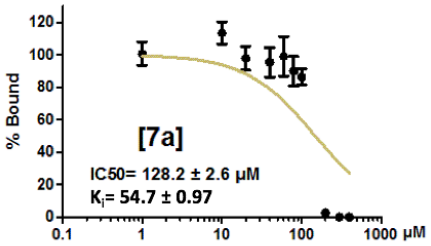
% Bound
120
100
80
60
40
20
0
[7a]
IC50= 128.2 ± 2.6 μM
Ki= 54.7 ± 0.97
0.1 1 10 100 1000 μM

C

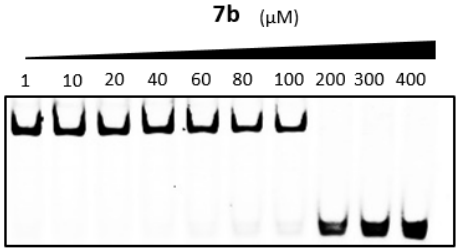
7b (μM)
1 10 20 40 60 80 100 200 300 400

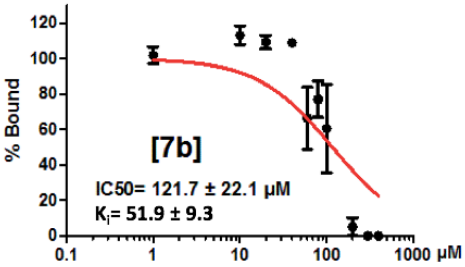
% Bound
120
100
80
60
40
20
0
[7b]
IC50= 121.7 ± 22.1 μM
Ki= 51.9 ± 9.3
0.1 1 10 100 1000 μM

D

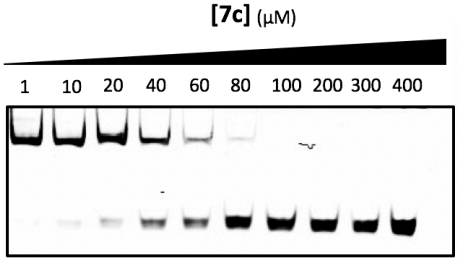
[7c] (μM)
1 10 20 40 60 80 100 200 300 400

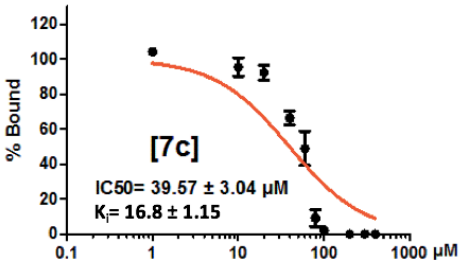
% Bound
120
100
80
60
40
20
0
[7c]
IC50= 39.57 ± 3.04 μM
Ki= 16.8 ± 1.15
0.1 1 10 100 1000 μM

E

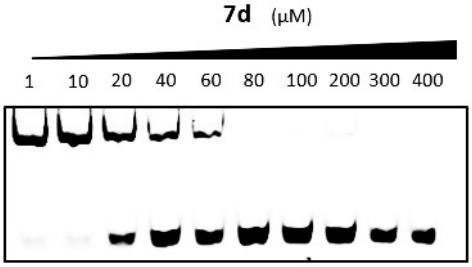
7d (μM)
1 10 20 40 60 80 100 200 300 400

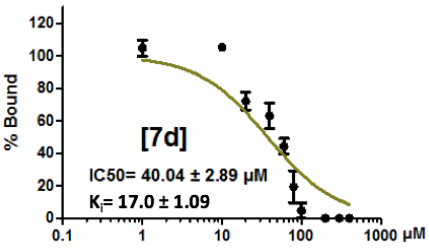
% Bound
120
100
80
60
40
20
0
[7d]
IC50= 40.04 ± 2.89 μM
Ki= 17.0 ± 1.09
0.1 1 10 100 1000 μM

F

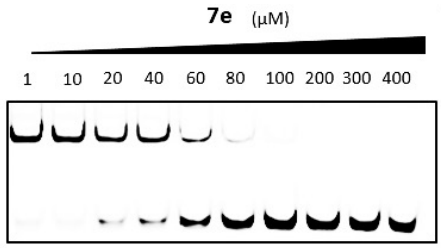
7e (μM)
1 10 20 40 60 80 100 200 300 400

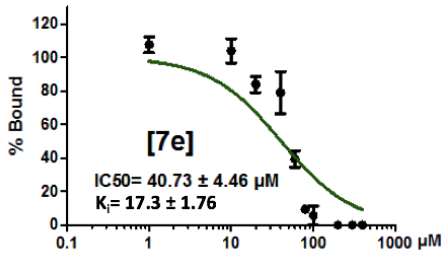
% Bound
[7e]
IC50= 40.73 ± 4.46 μM
Ki= 17.3 ± 1.76
0.1 1 10 100 1000 μM

G

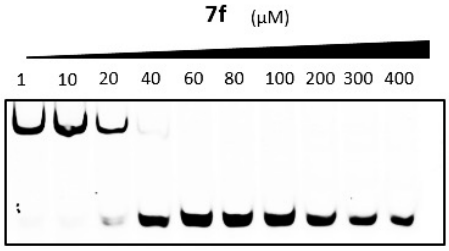
7f (μM)
1 10 20 40 60 80 100 200 300 400

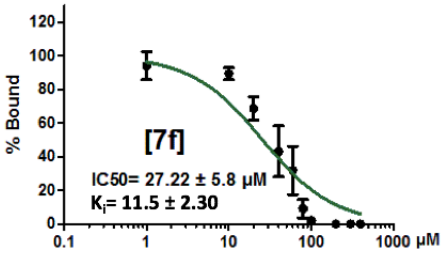
% Bound
[7f]
IC50= 27.22 ± 5.8 μM
Ki= 11.5 ± 2.30
0.1 1 10 100 1000 μM

H


7g (μM)
1 10 20 40 60 80 100 200 300 400

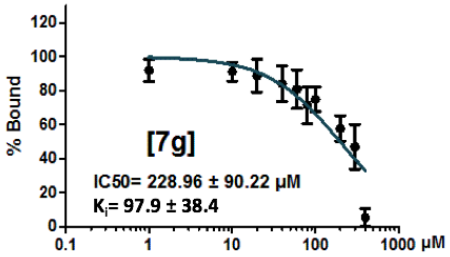
% Bound
[7g]
IC50= 228.96 ± 90.22 μM
Ki= 97.9 ± 38.4
0.1 1 10 100 1000 μM

I

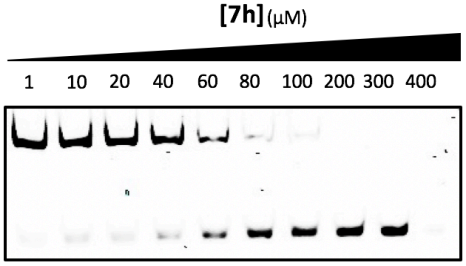
[7h] (μM)
1 10 20 40 60 80 100 200 300 400

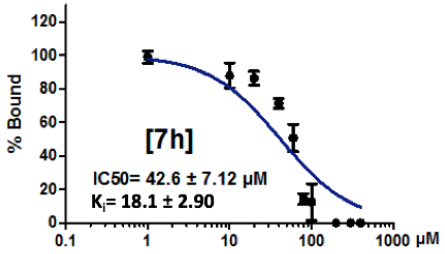
% Bound
[7h]
IC50= 42.6 ± 7.12 μM
Ki= 18.1 ± 2.90
0.1 1 10 100 1000 μM

J

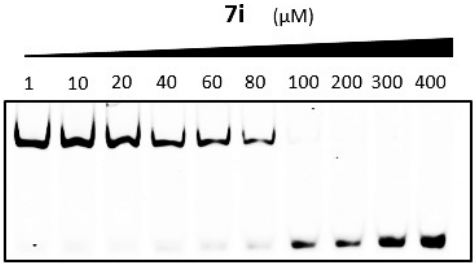
7i (μM)
1 10 20 40 60 80 100 200 300 400

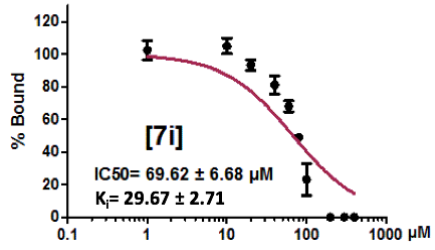
% Bound
[7i]
IC50= 69.62 ± 6.68 μM
Ki= 29.67 ± 2.71
0.1 1 10 100 1000 μM

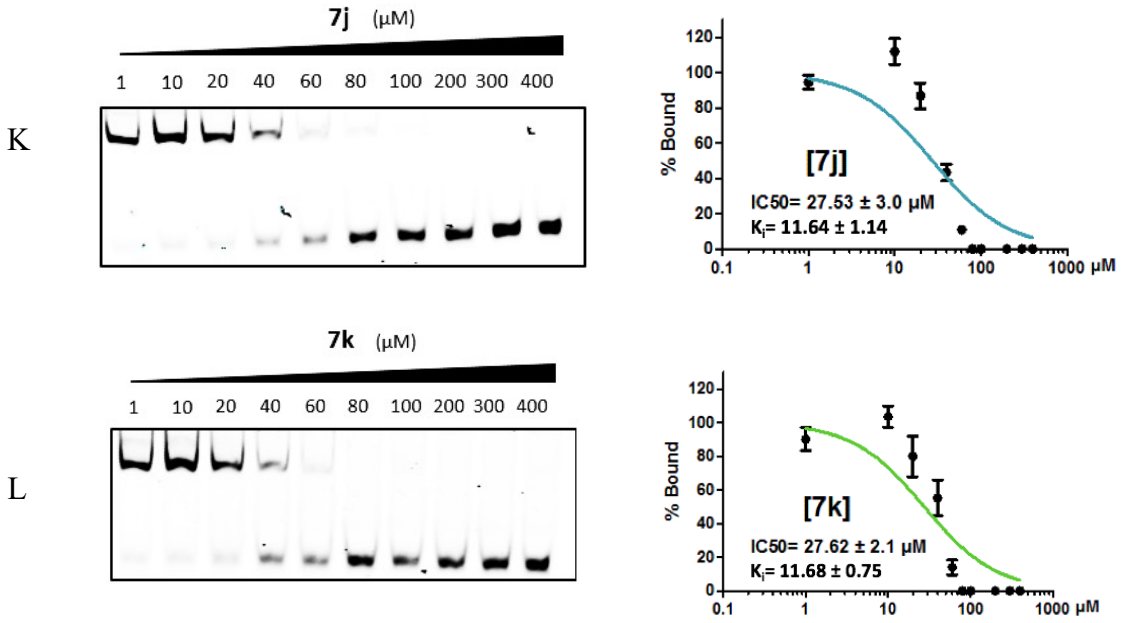

Figure 3-4. EMSA of FDI-6 derivatives showing the importance of halogen atoms in FOXM-DBD binding.A) Titration curve of FOXM1-DBD protein with the target DNA (5-/IRD700/-AAACAAACAAACAATCAAACAAACAAACAATC-3′); B to L) concentration-dependent effects of the drug molecules on the FOXM1-DNA complex presenting the calculated IC_{50} values, and their corresponding Ki's; all data are reported as average of three replicates (n = 3) and the error bars represent the SEM.

Finally, when we screened compounds 7k and 7j, possessing a 3,5-(difluoro) phenyl and [4-(trifluoromethyl) phenyl] moiety, we observed a good inhibitory profile of the FOXM1-DNA complex (IC_{50} = 27.6 and 27.5 μM respectively). It should be noted that in contrast to the results obtained in the protein immunoblot assay described previously, in which compound 7j and 7k showed a comparably weaker activity, in the cell-free EMSA the binding interactions exerted by this molecule may be more significant, considering that the soluble fraction of the drug is in direct contact with the FOXM1 protein, and apparently, it is good enough to exert inhibition of the

FOXM1/DNA complex. This observation should be considered when trying to extrapolate results from one assay to the other, and therefore to assess the complete profile of any given drug molecule as a TF "inhibitor", one must consider the results from several screening assays (e.g., EMSA). Moreover, to compare the activity of different inhibitors, the Ki values should be used as IC_{50} values can be altered by changing the protein concentration and hence be deceiving.

3.3.5 Molecular Modeling

To further support the experimental observations suggesting the need for a halogen atom at the 4-position of the phenyl moiety of FDI drugs, we carried out a series of complementary docking and MD simulations with compounds 7a, 7b, 7c, 7g, 7h, 7i, 7j and 7k comparing their binding profile with that of other molecules in the same series (**Table 3-2**). In this regard, we observed a direct relationship between the position of the halogen (fluorine) atom, and the total binding energy calculated for the corresponding drug molecule: 4-flouro (-25.2 kcal/mol), 3-flouro, -17.4 kcal/mol, and 2-flouro (-9.9 kcal/mol). With these results, we think it is reasonable to propose that the strength of the binding force between the drug molecule and the FOXM1 protein is determined, at least in part, by the relative position of the fluorine atom, in which 4-phenyl > 3-phenyl > 2-phenyl.

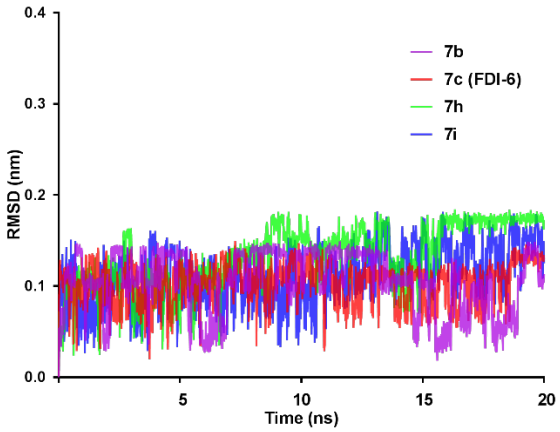

Figure 3-5. Ligand positional RMSD of compounds 7b, 7c, 7h, and 7i. The graph shows the stability of each compound over the entire MD simulations.

Compound **7c** (FDI-6) showed the strongest binding energy (-25.2 kcal/mol), with a low ligand RMSD, compared to compounds 7b (phenyl), 7h [3-(fluoro) phenyl], and 7i [2-(fluoro) phenyl] (**Figure 3-5)**. The low RMSD values observed for **7c**, along with the low vdW energy (-147.6 Kj/mol), suggests that the 4-(flouro) phenyl moiety increases the stability of a possible active conformation inside the binding pocket during the MD simulation.

Table 3-2. Free binding energies calculated for eight FDI derivatives. The total binding energies represent the sum of vdW, electrostatic, solvent accessible surface area (SASA), and polar solvation energy, during the last nanosecond of the corresponding MD simulation.

Compound	Van Der Waal Energy (kJ/mol)	Electrostatic Energy (kJ/mol)	Polar Solvation Energy A (kJ/mol)	SASA Energy (kJ/mol)	Binding Energy (kJ/mol)	Binding Energy (kcal/mol)
7a	-89.7 ± 5.3	-14.7 ± 3.7	55.9 ± 35.3	-9.09 ± 1.1	-57.6 ± 38.1	-13.7 ± 9.1
7b	-94.8 ± 16.9	-7.7 ± 5.5	40.6 ± 16.6	-11.5 ± 1.9	-73.4 ± 11.5	-17.5 ± 2.7
7c (FDI-6)	-147.6 ±16.2	-3.3 ± 2.9	59.0 ± 31.9	-13.7 ± 0.6	-105.6 ± 34.2	-25.2 ± 8.1
7g	-62.9 ± 41.6	0.5 ± 2.8	31.3 ± 31.6	-7.9 ± 5.1	-38.9 ± 44.7	-9.2 ± 10.6
7h	-122.4 ±12.0	-3.1 ± 3.3	55.7 ± 19.5	-12.9 ± 0.8	-72.9 ± 24.8	-17.4 ± 5.9
7i	-69.2 ± 34.6	-4.8 ± 4.8	41.0 ± 18.3	-8.6 ± 4.3	-41.7 ± 30.9	-9.9 ± 7.3
7j	-5.7 ± 25.5	-0.8 ± 3.9	-3.5 ± 31.5	-0.9 ± 2.8	-11.0 ± 15.3	-2.6 ± 3.6
7k	-96.2 ± 14.8	-7.6 ± 6.2	40.5 ± 17.0	-11.6 ± 1.5	-74.8 ± 10.0	-17.8 ± 2.3

As shown in **Table 3-2**, except for compound 7j, we could correlate the binding energies for all compounds with the screening assays described above. In other words, the unusually high theoretical binding energy (low binding force = -2.6 kcal/mol) calculated for 7j, would suggest a weak activity profile, but this was not the case. Compound 7j decreased cell proliferation in MDA-MB-231 cells, it significantly decreased the FOXM1 protein level of FOXM1, and it showed significant activity in the EMSA.

Finally, in **Figure 3-6** we present a graphical representation of the binding conformations observed for compounds 7c [4-(fluoro) phenyl] and 7h [3-(fluoro) phenyl] and their relative distance from Arg297 in which we observed practically the same binding interactions between the drug molecules and the Arg297.

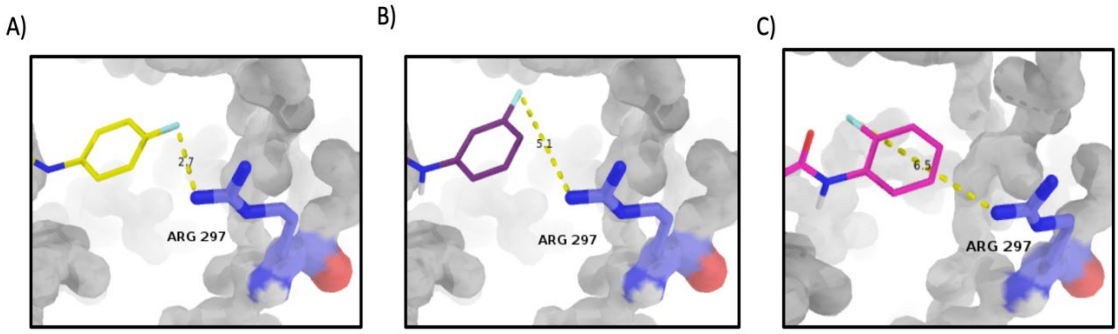

Figure 3-6. The graphical representation of the relative distance of the fluorine atom of 7c from Arg297. 7c, 2.7 Å (A), 7h, 5.1 Å (B) and 7i, 6.5 Å (C)

3.4 Summary and Conclusion

We present a series of *in vitro* and *in silico* experiments supporting the essential role of the 4-(halo) phenyl moiety present in FDI involving the Arg297 amino acid residue within the DBD of the FOXM1 protein. Despite a few minor differences in the relative potency of individual compounds, observed between different screening assays, we propose that (1) the halogen binding interaction is equipotent regardless of the halogen used (4-fluoro, 4-chloro, 4-bromo, or 4-iodo); (2) a bioisosteric replacement involving a 4-(methyl) phenyl group (7j) did not result in significant binding interactions or an improved activity profile. However, the use of a 4-(trifluoromethyl) phenyl moiety improved the potency of the lead molecule (FDI-6) by about two-fold (as shown in the EMSA), and it maintained the drug's cancer cell proliferation inhibitory profile in triple negative-breast cancer (MDA-MB-231) cells.

One major limitation associated with the current report is the fact that we are not considering the effects produced by the test drugs on other (potential) targets that would affect cell proliferation or FOXM1 protein expression. However, the EMSA assay is selective for direct FOXM1 inhibitors, and it effectively distinguishes between inactive and active drugs that bind to (and interfere with) the protein's DBD. In this regard, we used structurally unrelated molecules as negative controls (ranolazine and andrographolide), and we did not observe dissociation (at any drug concentration) of the protein-DNA complex (**Figure 3-7**)

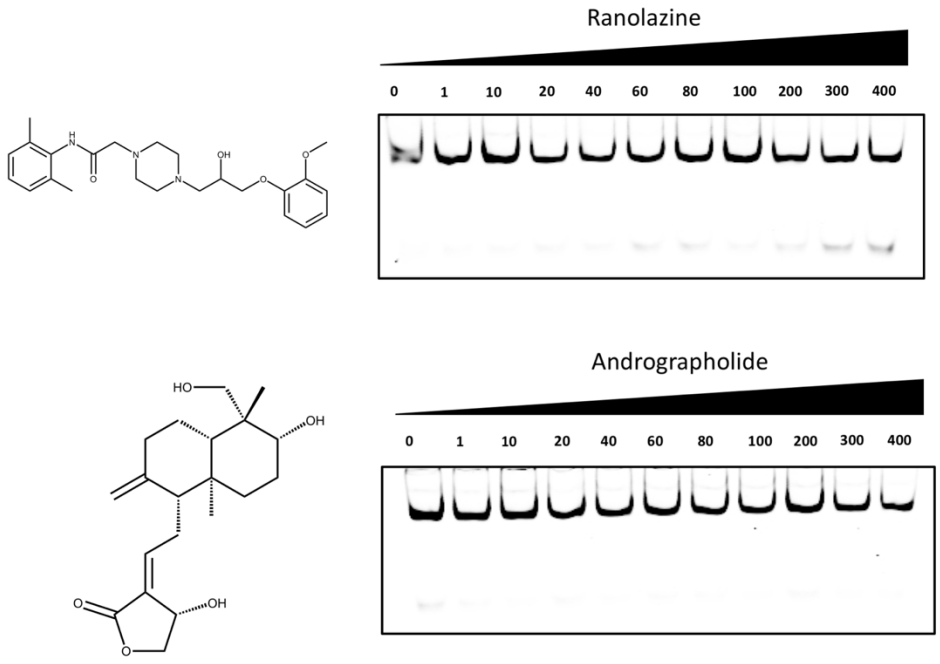

Figure 3-7. EMSA of structurally unrelated (negative control) drug molecules. Ranolazine and andrographolide were not able to dissociate the FOXM1-DBD/DNA complex.

In summary, we provide evidence validating the essential role of a 4-(halo) phenyl – Arg297 binding interaction as part of the overall mechanism of action exerted by FDI proposed by our group in a previous publication (210). In this report, we also propose a specific binding interaction to fine-tune the design of FOXM1 inhibitors based on the chemical scaffold of the lead FDI-6 molecule first described by Gormally et al. and we submit that this model could also be used in the design of other small-molecule drugs possessing a 4-(halo)phenyl moiety.

Chapter 4

FOXM1 Inhibitors: The Promising Binding Interaction of Sulfur Atom in Drug Molecules

4.1 Introduction

Several sulfur-containing compounds capable of inhibiting the oncogenic FOXM1 TF has been reported in the literature (20,197,237). In one of our publications (210), we identified the binding mechanism for these compounds (FDI-6, troglitazone, and thiostrepton) by implementing MD simulation and molecular modeling approaches. We proposed the presence of a binding site on the surface of FOXM1-DBD that these drugs can recognize and bind. In these theoretical observations, we mentioned that all these inhibitors have one thing in common, a sulfur atom; in thiazolidinedione ring of troglitazone, in thiazole rings of thiostrepton and in thiophene rings of FDI-6. We showed that based on our docking and MD simulations, the sulfur atom forms a pi-sulfur interaction with a histidine (His287) residue in the H3 helix of FOXM1-DBD. H3 helix was previously shown to be involved in DNA recognition (266). In the same investigation, we also showed that this histidine is the most projected residue in the H3 helix and mainly responsible for the first contact with the DNA. **Figure 4-1** shows a schematic position of His287 to the Sulfur atom in the structure of FOXM1 inhibitors.

The impact of pi-sulfur interaction on the stabilization of protein structure was first reported in early 1978 by Morgan and collogues (282). Later on, Reid and co-workers found that there is a favorable interaction between sulfur-bearing amino acids (cysteine and methionine) and the aromatic amino acids in the tertiary structure of proteins (283). After examining the structure of 36 proteins, they found that the average distance of the sulfur atom from the center of the aromatic ring is around 6 Å. They were first to notice that the occurrence of this type of interaction is more than what expected. Furthermore, Viguera et al. study on side-chain interaction between Phenylalanine and two sulfur-

bearing amino acids shows the importance of this type of interaction on the stability of alpha helix (259).

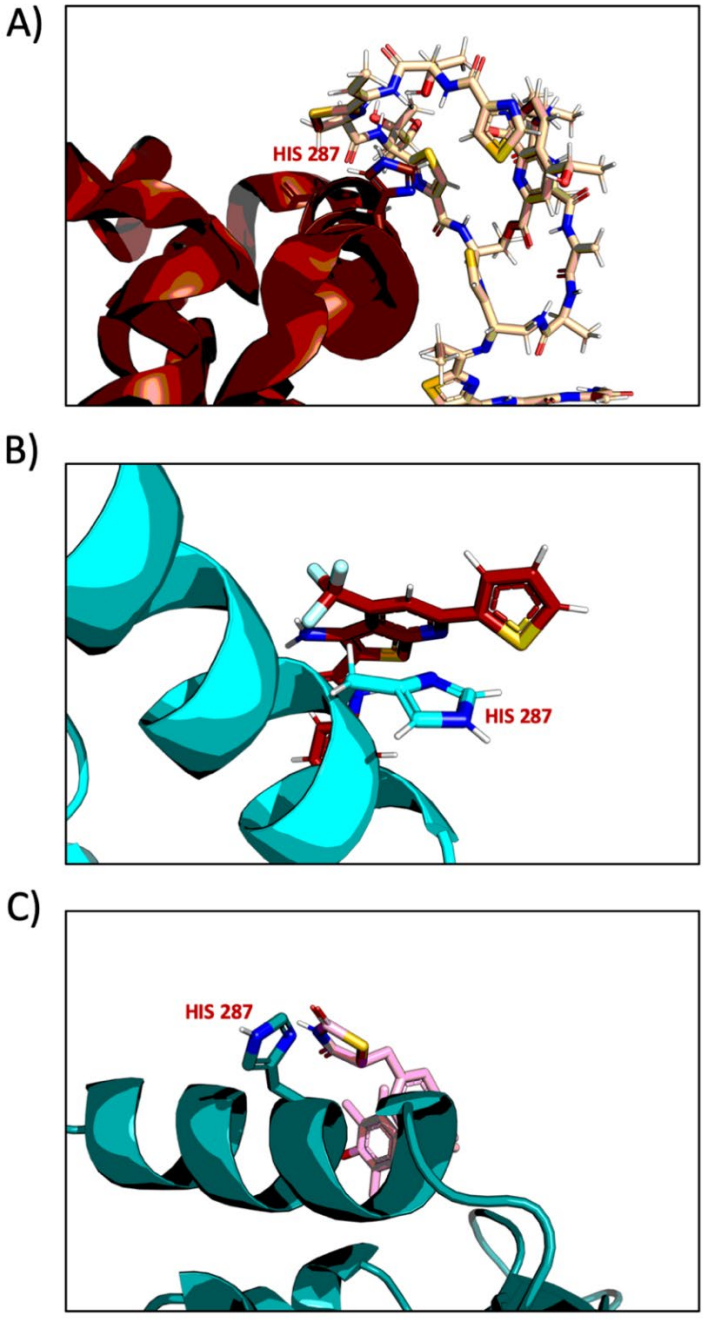

Figure 4-1. Binding mode sulphur bearing FOXM1 inhibitors at the interface of FOXM1-DBD. Thiostrepton (A), troglitazone (B) , and FDI-6 (C) are all binding with a pi-sulfur interaction to the imidazole ring of His287. Several quantum mechanical studies

have also carried out to calculate the energy of interaction between the sulfur atom and the aromatic ring. Cheney et al. used a cysteine-benzene model with the HF/3-21G level of theory to find the most favorable configuration. Following Reid et al. findings, they reported that the most favorable configuration reported was the one sulfur at 4.4 Å from the center of aromaticity with an angle of elevation of 56º (284).

In 2000, Zauhar et al. used extensive quantum mechanical studies on the Cambridge protein structure database of small compounds to study pi-aromatic interactions outside the protein models. In contraindication with the proteins where the optimal position for the sulfur atom is above the ring, they reported that the optimum pi-sulfur interaction happens when the lone pairs of sulfur are interacting directly with the ring hydrogens in the ring plane (285).

To the best of our knowledge, the significance of sulfur-pi interaction in small molecule binding interaction has not extensively studied in the literature. We carried out a series of experiments to validate our molecular modeling binding pocket hypothesis. We are also aiming to stress the importance of sulfur atom from a medicinal chemistry point of view.

4.2 Materials and Methods

4.2.1 General Information

All reagents and solvents were received from Sigma-Aldrich and used with no further purification. Redisep TLC plates were used to monitor the chemical reaction progression and completion. A Bruker FT-600 MHz instrument was used to record the ^{1}H and ^{13}C spectra. Signal multiplicity was reported using the followings: s (singlet), d (doublet), t (triplet), q (quartet), m (multiplet), and br (broad singlet). Biotage reactor was used to

perform the microwave-assisted synthesis. All graphical figures are made with Pymol (276).

4.2.2 Chemistry

4.2.2.2 General methods for the synthesis of the FDI-derivatives

Compounds 3b (286), 3c (286), 3d (287), 3e (288), and 3f (286) were prepared according to the reported methods. The corresponding FDI-intermediates (3b-f, 1 eq.) and 2-chloro-N-(4-fluorophenyl) acetamide (**4,** 1 eq.) were mixed with K_2CO_3 (2 eq.), and ethanol (5 mL) or dimethylformamide (DMF) (5 mL) in a microwave reaction vessel. This mixture was stirred at 90 °C for 2 hours using a "high energy absorption" setting. The crude product was filtered off, washed with water and fixed onto silica gel powder before running a solvent gradient (flash column chromatography). F1 (FDI-6) was prepared as previously reported (206,269). Combined organic fractions were dried under vacuum and the corresponding final products were recrystallized from ethanol (when needed).

3-amino-N-(4-fluorophenyl)-6-(furan-2-yl)-4-(trifluoromethyl)thieno[2,3-b]pyridine-2-carboxamide (F2). 3b (270 mg, 1 mmol), 4 (187 mg, 1 mmol), K_2CO_3 (277 mg, 2 mmol), in 5 mL of EtOH, yellow (flocculent) crystals, 70 % yield (0.7 mmol, 290 mg). ^{1}H NMR (600 MHz, DMSO) δ 9.84 (s, 1H), 8.05 (d, J = 33.2 Hz, 2H), 7.68 (dd, J = 9.0, 5.1 Hz, 2H), 7.55 (d, J = 3.4 Hz, 1H), 7.19 (t, J = 8.8 Hz, 2H), 6.98 – 6.49 (m, 3H). ^{13}C NMR (151 MHz, DMSO) δ 163.57, 160.88, 159.34, 157.74, 151.11, 148.22, 146.29, 144.91, 131.97, 131.75, 123.65, 123.60, 123.50, 121.68, 117.80, 115.16, 115.01, 113.14, 112.87, 112.12.

3-amino-N-(4-fluorophenyl)-6-(furan-2-yl)-4-(trifluoromethyl)furo[2,3-b]pyridine-2-carboxamide (F3*).* 3c (254 mg, 1 mmol), 4 (187 mg, 1 mmol), K_2CO_3 (277 mg, 2 mmol), in 5 mL of DMF yellow (flocculent) crystals, 5 % yield (8 mg, 0.02 mmol). ^{1}H NMR (600 MHz, DMSO) δ 10.39 (s, 1H), 8.04 – 7.94 (m, 2H), 7.86 (dd, J = 9.2, 5.1 Hz, 2H), 7.41 (d, J = 3.4 Hz, 1H), 7.19 (t, J = 8.9 Hz, 2H), 6.78 (d, J = 1.7 Hz, 1H), 5.79 (s, 2H). ^{13}C NMR (151 MHz, DMSO) δ 159.13, 159.09, 157.55, 151.37, 146.96, 146.16, 134.86, 134.85, 134.22, 132.03, 131.80, 126.95, 125.07, 123.26, 122.29, 122.24, 121.45, 115.23, 115.09, 113.15, 112.14, 110.62, 110.59, 108.04.

3-amino-N-(4-fluorophenyl)-6-(thiophen-2-yl)-4-(trifluoromethyl)furo[2,3-b]pyridine-2-carboxamide (F4). 3d (375 mg, 2 mmol), 4 (540 mg, 2 mmol), K_2CO_3 (330 mg, 24 mmol) in 5 mL of DMF, yellow (flocculent) crystals, 20 % yield (17 mg, 0.04 mmol). 1H NMR (600 MHz, DMSO) δ 10.37 (s, 1H), 8.29 (s, 1H), 8.22 (d, *J* = 2.7 Hz, 1H), 7.93 – 7.75 (m, 2H), 7.37 – 7.06 (m, 3H), 5.80 (s, 2H). ^{13}C NMR (151 MHz, DMSO) δ 159.16, 158.80, 157.53, 151.09, 142.48, 134.89, 134.34, 130.90, 129.16, 128.71, 126.75, 122.28, 122.23, 115.22, 115.08, 111.38, 107.86, 79.19, 78.97.

3-amino-N-(4-fluorophenyl)-6-methyl-4-(trifluoromethyl)thieno[2,3-b]pyridine-2-carboxamide (F5). 3e (202 mg, 1 mmol), 4 (187 mg, 1 mmol), K_2CO_3 (277 mg, 2 mmol), in 5 mL of EtOH, yellow (flocculent) crystals, 70 % yield (0.7 mmol, 258 mg). ^{1}H NMR (600 MHz, DMSO) δ 9.80 (s, 1H), 7.78 (s, 1H), 7.69 (dd, J = 9.2, 5.1 Hz, 2H), 7.19 (t, J = 8.9 Hz, 2H), 6.76 (s, 2H), 2.72 (s, 3H). ^{13}C NMR (151 MHz, DMSO) δ 163.71, 160.28, 160.20, 159.32, 157.73, 145.03, 144.95, 134.79, 131.34, 131.12, 130.90, 130.68, 125.49, 123.68, 123.53, 123.48, 121.86, 117.32, 117.13, 117.09, 115.15, 115.00, 99.91, 24.09.

3-amino-N-(4-fluorophenyl)-6-phenyl-4-(trifluoromethyl)thieno[2,3-b]pyridine-2-carboxamide (F6). 3f (264 mg, 1 mmol), 4 (187 mg, 1 mmol), K_2CO_3 (277 mg, 2 mmol),

in 5 mL of EtOH, yellow (flocculent) crystals, 70 % yield (0.7 mmol, 300 mg).^{1}H NMR (600 MHz, DMSO) δ 9.86 (s, 1H), 8.36 – 8.25 (m, 3H), 7.73 – 7.66 (m, 2H), 7.59 (d, J = 7.5 Hz, 3H), 7.21 (t, J = 8.9 Hz, 2H), 6.80 (s, 2H). ^{13}C NMR (151 MHz, DMSO) δ 163.60, 160.89, 159.39, 157.80, 156.65, 144.93, 136.38, 134.75, 130.69, 129.13, 127.42, 123.63, 123.57, 118.34, 115.20, 115.06, 113.81, 101.23.

4.2.3 Cell Culture

MDA-MB-231 triple-negative breast cancer cell line was grown in RPMI media supplemented with 10% FBS. The cells were grown at 37 °C in an incubator, maintaining 5% CO2 environment.

4.2.4 Antibodies

FOXM1 monoclonal antibody (mouse, sc-271746) and anti-mouse (sc-516102) secondary antibody was purchased from Santa Cruz Biotechnology.

4.2.5 Western Blot

3×10^5 MDA-MB-231 cells were seeded in 6 well plates and incubated overnight. The next day, compounds at different concentrations were added and incubated for 24 hours. Then, they washed twice with ice-cold PBS and extracted using the RIPA buffer (Thermofisher). Before loading 40 μg into a 10% SDS page gel, Bradford assay was employed to determine the protein concentration. After the completion of electrophoresis, the gel was transferred to a nitrocellulose membrane and incubated with milk for 45 minutes and the corresponding antibody overnight. The next day, the gel was washed twice with TBST and incubated with an appropriate secondary antibody for 45 minutes.

The blot was visualized using (Thermofisher) using ImageQuant™ LAS 4000 mini biomolecular imager (GE Healthcare Life Sciences) after the addition of chemiluminescence reagent (Thermofisher). All the band were quantified using ImageJ and plotted using Prism.

4.2.6 Site-Directed Mutagenesis

The PEX-N-GST-FOXM1C-DBD plasmid vector encoding wild-type FOXM1-DBD was purchased from (OriGene Technologies, USA). The mutants were generated using the Quick Change Multi Site-Directed Mutagenesis Kit (Agilent Technologies, USA) by the manufacturer's instructions. The following two primers were used;

His287: Ala mutagenesis

(Forward) 5'-gtgcagggaaaggttggcgcggatggagttcttc-3'

5'-gaagaactccatccgcgccaacctttccctgcac-3 (Reverse).

His287:Phe mutagenesis

(Forward) 5'-cgtgcagggaaaggttgaagcggatggagttcttcc-3'

5'-ggaagaactccatccgcttcaacctttccctgcacg-3' (Reverse).

All mutations were subsequently verified via DNA sequencing. (Please see Appendices-Section **A.3**)

4.2.7 Recombinant Protein Production and Purification

GST-FOXM1-DBD and corresponding mutated GST-FOXM1-DBD were prepared using a previously reported method. GST-FOXM1-DBD plasmid and mutated plasmids (OriGene technologies, USA) were transformed into BL21 (DE3) competent cells. Positive colonies on ampicillin containing LB agar were picked and grown in LB media

(100 μg/mL ampicillin) and incubated at 37 °C. After they reached the optical density of 0.8, 0.5 mM IPTG was added and re-incubated. After 6 hours, the cells were collected, centrifuged, and the cell pellet was extracted using B-PER (Thermofisher). The recombinant protein was purified using glutathione resin (GenScript, USA) according to the manufacturer's instructions. Please refer to section **A.2** of appendices for the representative gel image of purified proteins.

4.2.8 Electrophoretic Mobility Shift Assay

EMSA was performed as previously reported (237,260).

4.3 Results and Discussion

As previously mentioned, we predicted that troglitazone bind to the His287 of the H3 helix of FOXM1-DBD via a pi-sulfur interaction. The co-crystal structure of thiazolidinediones (troglitazone, rosiglitazone (289), and pioglitazone (290) is solved and available at the PDB. Upon analysis of the binding mode of these chemical entities, we observed that in all 3 complexes, the sulfur atom present in the thiazolidinedione ring forms a pi-sulfur interaction with a histidine residue in the ligand-binding pocket of PPAR gamma. We believe that there is a favorable interaction between electron-deficient sulfur present in the thiazolidinedione and the histidine ring.

4.3.1 Design and Synthesis

In our previous publication, we also showed that the FOXM1 inhibitor FDI-6 forms the same binding attraction with His287 with both its sulfur atoms, one in thiophene ring, and the other one incorporated in the ring (R1 position). To further validate our hypothesis on

the existence of pi-sulfur interaction at the interface of FOXM1-DBD, we also chemically modified this compound to replace its sulfur atom with its closely related element oxygen.

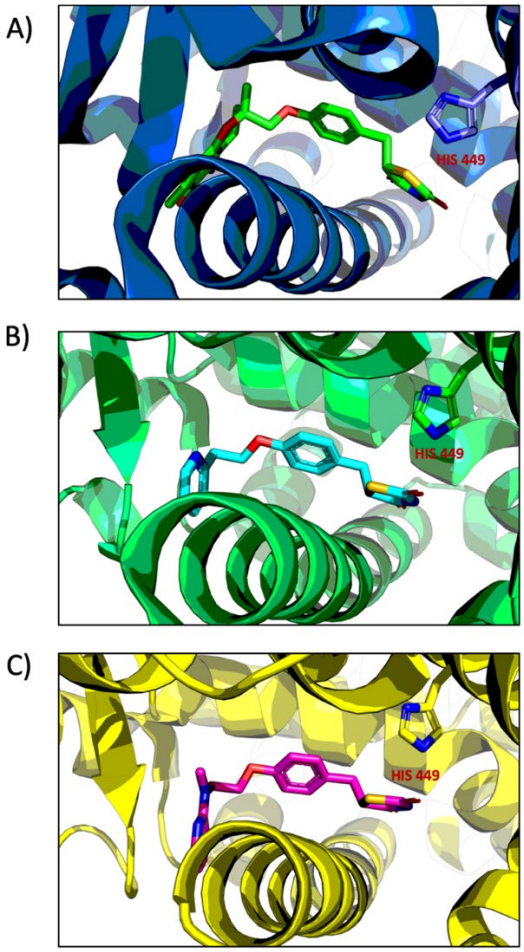

Figure 4-2. Crystal structure of thiazolidinediones in complex with PPAR gamma LBD. Troglitazone (A) (PDB ID: 6DGO), pioglitazone (B) (PDB ID: 5Y2O) and rosiglitazone (C) (PDB ID: 4EMA) all bind to His 449 via a pi-sulfur interaction.

Scheme 4-1. Synthetic route for the preparation of FDI derivatives (F1-F6).

Reagents and conditions: (a) K_2CO_3, ethanol/DMF, 90 °C, 2 hours.

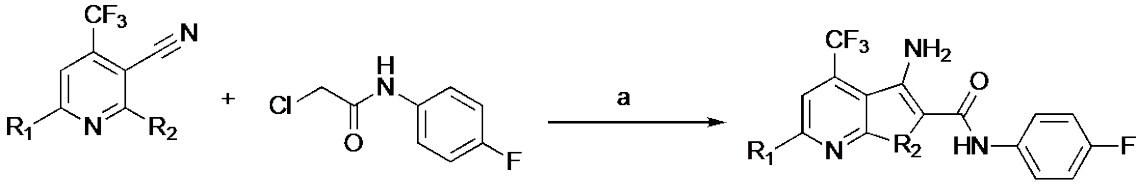

3b: R_1= SH, R_2= Furyl
3c: R_1= OH, R_2= Furyl
3d: R_1= OH, R_2= Thienyl
3e: R_1= SH, R_2= Methyl
3f: R_1= SH, R_2= Phenyl

F2: R_1= SH, R_2= Furyl
F3: R_1= OH, R_2= Furyl
F4: R_1= OH, R_2= Thienyl
F5: R_1= SH, R_2= Methyl
F6: R_1= SH, R_2= Phenyl

5 Different derivatives of FDI-6 (henceforth F1) were synthesized (**Scheme 4-1**). In compound F2 thiophene ring of F1 was replaced with Furan. Next, we replaced the other sulfur atom in the structure of F2 with oxygen (compound F3). Basically, in this compound, all sulfurs of F1 are replaced with oxygen. Next, oxygen in the R1 position is retained, but we reintroduced the thiophene ring into the R2 position. In F5, the thiophene ring was removed while it was replaced by phenyl in F5.

4.3.2 Determination of FOXM1 Expression

Next, we measured the ability of these compounds to suppress the transcriptional activity of FOXM1 in MDA-MB-231 using protein immunoblot. As shown in **Figure 4-3**, only compound F1 (FDI-6) were able to diminish the FOXM1 protein level. Between all the derivatives, only compound F6 was slightly active relative to the DMSO.

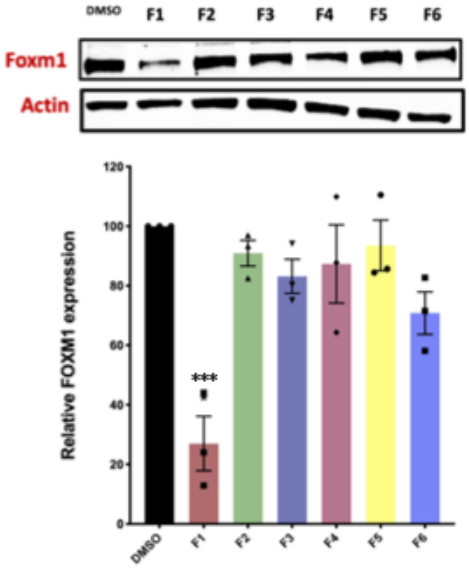

Figure 4-3. The FOXM1 expression level of compounds F1-F6 in MDA-MB-231 cell line. (24 hours incubation time, 40 μM). Bars represent the average value of three independent experiments. One-way ANOVA was used to determine the significance: ***: $P \leq 0.001$.

4.3.1 Electrophoretic Mobility Shift Assay

Furthermore, we employed EMSA assay and incubated these compounds in an increasing concentration with recombinant FOXM1-DBD to measure the ability of FOXM1-DBD to associate and bind with its consensus DNA.

Contrary to our expectation, Compound F1, which found to be inactive in protein immunoblot assay, shows stronger inhibition (Ki= 2.34 μM) in comparison to F1 (Ki= 16.8 μM). Compounds F3-F5 were inactive, and compound F6 was less active than F1 (Ki= 24.52), which is in complete agreement with the western blot data.

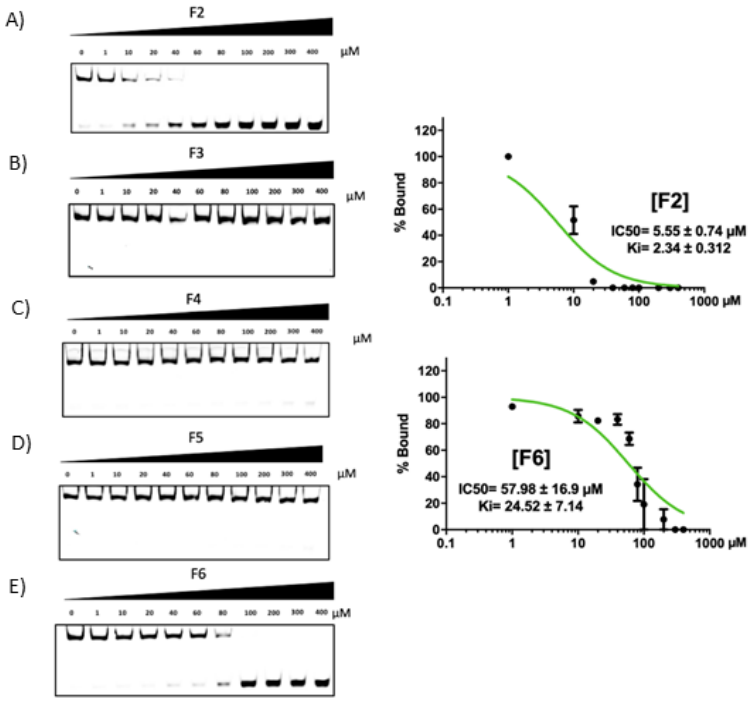

Figure 4-4. EMSA displacement experiment of compounds F2-F6. Compound F2 (A) in which the thiophene ring was replaced with furan was 7 times more potent (Ki: ~ 2.34 μM) than the parent compound F1 (previously reported Ki: ~16.8 μM). Compounds F3 (B), F4 (C), F5 (D) were inactive. The derivative in which the thiophene ring was replaced with phenyl ring was slightly active (Ki: ~24.52 μM), indicating the importance of aromaticity in that position.

Despite the lack of agreement between protein immunoblot and EMSA data for compound F2, these experiments demonstrate the sulfur is still essential for the activity of this compound. In terms of structure-activity relationship studies, the cell-free assay EMSA is more valuable since it shows the direct inhibition of compounds and does not have drug cell uptake and nuclear localization limitation. Then, since F2 is inactive, we can conclude that the sulfur atom in the thiazolidinedione ring is not critical and will not participate in pi-sulfur interaction. On the other hand, since F5 is inactive and F6 is active,

we can assume that aromaticity is playing a role in that position, possibly through a pi-pi interaction. However, the sulfur atom at position R1 is critical for activity. Notwithstanding the better activity of compound F1 in EMSA, when we replace sulfur at the R1 position in F2, the compound became entirely inactive.

As mentioned above, we hypothesized that all these compounds bind with their sulfur atom to a histidine residue (His287) in the H3 helix of FOXM1-DBD. To investigate the initial binding hypothesis from another angel, we employed site-directed mutagenesis technique to swap the His287. This will confirm if the predicted pi-sulfur atom is essential and also if only this interaction forms between any aromatic amino acid and not only the imidazole ring of histidine.

4.3.1 Site-directed Mutagenesis

As proposed, using the site-directed mutagenesis technique, first, we mutated the histidine to alanine, a simple non-aromatic amino acid (His287:Ala). Next, we measured the protein/DNA Kd value to investigate the effect of the mutation on the FOXM1 DNA recognition and binding ability. The Kd value calculated for His287:Ala mutation (444.6 nM) was found to be slightly higher than the wild type (361 nM).

Next, we performed the EMSA displacement experiment to examine if the FDI-6 is still able to bind to the FOXM1-DBD when the histidine and essentially aromaticity is absent. As anticipated, the Ki for F1 binding to the mutated FOXM-DBD (His287:Ala) was almost 4 fold higher than the FOXM1-DBD wild type.

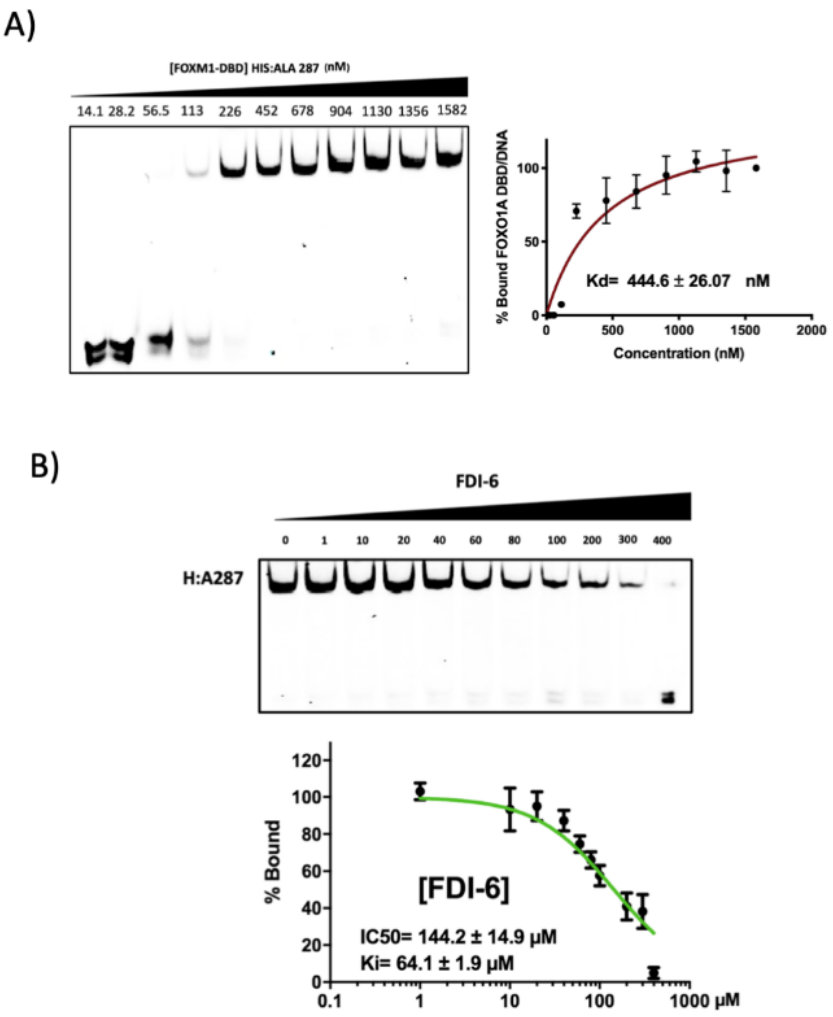

Figure 4-5. Dissociation constant of FOXM1-DBD (His287: Ala)/DNA and EMSA displacement experiment of FDI-6. A) The mutation of His287 to alanine increases the Kd value in comparison to the wild type. B) FDI-6 was unable to disrupt the binding of mutated FOXM1-DBD, proving the importance of histidine aromaticity.

In the next step, histidine residue was mutated to Phenylalanine (His287:Phe), an amino acid with a phenyl ring as a sidechain. The Kd calculated for the phenylalanine mutation was significantly lower (over two-fold) than the wild type FOXM1-DBD.

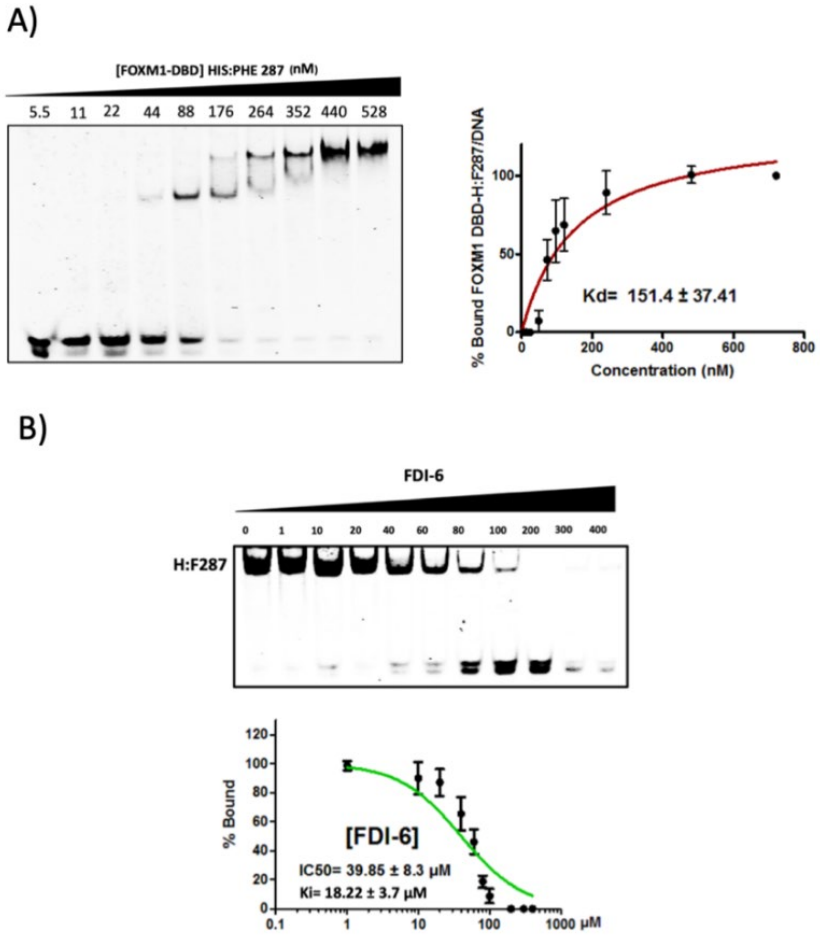

Figure 4-6. Dissociation constant of FOXM1-DBD (His287:Phe)/DNA as well as EMSA revealed the importance of pi-sulfur interaction. A) The mutation of His287 to phenylalanine decreased the Kd value in comparison to the wild type. B) FDI-6 was inhibited the binding of mutated FOXM1-DBD with the identical Ki as the wild type FOXM1-DBD.

Interestingly, compound F1 Ki was almost identical to the Ki value of F1 and FOXM1-DBD wild type, which indicates the importance of aromaticity at that specific position.

4.3 Summary and Conclusion

This paper has investigated the role of pi-sulfur interaction in small molecule inhibitors of FOXM1. We presented that FDI-6 inhibition and binding to the FOXM1-DBD depend on two factors, a sulfur atom in the thiazole ring of FDI and the presence of aromaticity in the His287 position, which confirms the existence of pi-sulfur interaction. These results further strengthen our previous theoretical discovery of the FOXM1-DBD binding pocket as well as the binding mode of FOXM1 inhibitors.

This work, as complementary to our previous publications, paves the way toward receptor-based drug design of FOXM1 inhibitors. With this confirmed binding pocket on the surface of FOXM1-DBD and with the implementation of pocket based drug design, novel inhibitors of FOXM1 can be introduced.

Chapter 5

Thiazolidinediones Derivatives as FOXM1 Suppressors

5.1 Introduction

The FOXM1 protein is a member of a large family of TFs that share a unique wing-helix DBD (291), and one of the proteins responsible for maintaining normal cell replication by promoting cell cycle progression (292). In healthy cells, FOXM1 is expressed during the S phase, and it induces the G1 phase and regulates cell cycle by expressing several G2/M related genes (155,293). However, cells finishing cell cycle, and those terminally differentiated have marginal expression levels of FOXM1 (164). FOXM1 undergoes multiple phosphorylation reactions by different kinases throughout the cell cycle, becoming transcriptionally active at the G2/M phase (294).

In contrast to its role in normal cell proliferation, FOXM1 is known to be extensively overexpressed as an essential regulator of tumorigenesis, causing genomic instability and uncontrolled cell division in a wide variety of human cell carcinomas including lung (188), oropharyngeal. (295), melanoma. (172), leukemia (194), pancreatic. (296), and breast tissue (265). FOXM1 overexpression is also linked to poor prognosis and chemotherapy resistance, which makes FOXM1 a useful biomarker and a promising drug target (169,176,231).

In one of our previous publications, we formulated a working hypothesis describing how the structurally different experimental FOXM1 inhibitors FDI-6, thiostrepton, and troglitazone can bind and disrupt the interaction between the FOXM1 protein and its DNA binding site (210). In this paper, we described the essential structural requirements needed to develop effective FOXM1 inhibitors based on a well-identified drug-binding pocket. In this regard, we highlighted two specific drug binding interactions involving (1) a pi-sulfur interaction between the aromatic imidazole ring present in

His287, and an electron-deficient sulfur atom present in each of the FOXM1 inhibitors; and (2) a halogen bonding interaction observed between the 4-fluorophenyl ring in the drug FDI-6 and the amino acid Arg297 in the protein. Based on these calculated binding interactions, we decided to test this hypothesis by measuring the ability of several thiazolidinedione derivatives to bind to, and inhibit, the *in vitro* transcriptional activity of the FOXM1 protein.

5.2 Materials and Methods

5.2.1 Cell Culture

The MDA-MB-231 cancer cell line was a gift from Dr. Frank Wuest (Cross Cancer Institute; Edmonton, Alberta, Canada). RPMI media was supplemented with 10% FBS in a 5% CO_2 atmosphere at 37 °C to grow and maintain the cells.

5.2.2 Antibodies

We used a FOXM1 monoclonal (mouse, sc-271746) antibody; SP1 monoclonal (mouse, sc-420) antibody; β-Actin monoclonal (mouse, sc-47778) antibody; anti-mouse (sc-516102) and anti-rabbit (sc-2030) secondary antibody from Santa Cruz Biotechnology.

5.2.3 Western Blot

$3x10^5$ cells were seeded in 6 well plates and treated with test compounds at different concentrations for 24 hours. Then, the cells were washed twice with ice-cold PBS before incubating and extracting with RIPA lysis and extraction buffer (Thermofisher) for 30 minutes. The protein levels were quantified using the Bradford assay before loading of 40μg of protein into a 10% SDS-PAGE (Sodium dodecyl sulfate polyacrylamide gel

electrophoresis). Upon completion of the run, the proteins were transferred from the gel to a nitrocellulose membrane (Thermofisher) and blocked with 10% fat-free milk in TBST for 45 minutes. The corresponding antibody was incubated with the membrane (1:1000 dilution) at 4 °C overnight. The next day, the membrane was washed with TBST before incubating the appropriate secondary antibody for 45 minutes at r.t. Then, The membrane was washed three times (15 minutes total) with TBST, and the conjugated protein bands were visualized by adding the Chemiluminescence reagent (Thermofisher) using ImageQuant™ LAS 4000 mini biomolecular imager (GE Healthcare Life Sciences). The quantification was carried out for all proteins relative to β-Actin using ImageJ.

5.2.4 Protein Expression and Purification

BL21 (DE3) competent cells were used to transform the PEX-N-GST FOXM1C-DBD, PEX-N-GST FOXO1-DBD, PEX-N-GST FOXO3-DBD plasmids (OriGene technologies, USA). Next, positive colonies on LB agar media supplemented with ampicillin (100 µg/mL) were selected and grown in LB media (100 µg/mL ampicillin) at 37 °C until they reached the optical density (OD600) of 0.8 and then 1 Mm IPTG was added. After 6 hours incubation at 37 °C, the supernatant layer was purified using glutathione resin (GenScript, USA) following the manufacturer's instructions.

5.2.5 Electrophoretic Mobility Shift Assay

For displacement experiments using EMSA, we followed the protocol as previously reported (206). Recombinant FOXM1-DBD, FOXO1-DBD and FOXO3-DBD were incubated with each compound for 1.5 hours at r.t. Then its target DNA oligo (Forward

strand: 5′-/IRD700/-AAACAAACAAACAATCAAACAAACAAACAATC-3′) was incubated with the mixture for 20 minutes in a buffer solution composed of 20 mM Tris (pH 7.5), 100 mM KCl, 1 mM EDTA, 0.1 mM DTT, and 10% glycerol. The mixture was then loaded on a non-denaturing 6% polyacrylamide gel for 30 min at 120 V. The Ki value was calculated based on the determined Kd value using the following formula **Equation 1**:

$$Ki = \frac{[I]}{(\frac{([I]_{50})}{K_d} + \frac{[P]_0}{K_d + 1})} \qquad \textbf{Equation } (1)$$

Where: [I]50 = IC50 of the inhibitor; [L]50 = concentration of IR-labelled DNA at 50% inhibition; [P] = concentration of the FOXM1 protein; and Kd= dissociation constant calculated from the titration curve. Protein concentration levels used in displacement assay for FOXM1-DBD, FOXO1-DBD, and FOXO3-DBD were 480, 530 and 265 nM, respectively.

5.2.6 Luciferase Reporter Assay

The 6x-FOXM1 firefly luciferase reporter and its corresponding backbone plasmid-pGL4.10 (i.e., empty reporter) were gifts from Drs. Carter J Barger and Adam R. Karpf. Briefly, MD-MB-231 cells were transiently transfected with equal amounts of the 6x-FOXM1 and empty luciferase reporter plasmids. Following 24 hours incubation, cells were treated with 40 μM of compounds for 12 hours. Cells were then washed with cold PBS and lysed with Reporter Lysis Buffer (Promega). Protein concentration was estimated, and equal amounts of total protein from each lysate was analyzed for firefly luciferase activity using the Luciferase Reporter Assay System (Promega). Assays were performed in triplicates.

5.2.7 Quantitative Real-Time PCR (qPCR)

The RNeasy Mini Kit (Qiagen, Valencia, CA) was used to isolate total RNA from cell lines. Trace DNA was removed on column through DNA digestion with DNAse I (Invitrogen, Carlsbad, CA). 1 μg of total RNA was used to prepare cDNA with the High-Capacity cDNA Reverse Transcription Kit (Invitrogen, Carlsbad, CA). qPCR reactions were prepared in 96-well plates (Invitrogen, Carlsbad, CA) with the PowerUp™ SYBR™ Green Master Mix (Invitrogen, Carlsbad, CA) according to the manufacturer's protocol. The Mastercycler® ep Realplex system (Eppendorf, Hamburg, Germany) was used for cycling and detecting amplification. Primers for all genes have been validated in prior studies and were purchased from Invitrogen. Sequences of the primers used in this study include:

Gene	Forward Strand	Reverse Strand
FOXM1	5-CGTCGGCCACTGATTCTCAAA-3	5-GGCAGGGGATCTCTTAGGTTC-3
CDC25B	5-CCTCCGAATCTTCTGATGCAG-3	5-GCGTCTGATGGCAAACTGC-3
CCNB1	5-GTAATGTTGTAGAGTTGGTGTCC-3	5-CATGGTGCACTTTCCTCCTT-3
GAPDH	5-GGTCTCCTCTGACTTCAACAGCG-3	5-ACCACCCTGTTGCTGTAGCCAA-3

qPCR cycling was setup as denaturation at 95°C for 10 minutes, followed by 40 cycles at 95°C for 15 seconds, annealing and subsequent extension at 60°C for 1 minute. The relative gene expression was determined using the ΔΔ-CT method. For each treatment group, target gene expression was normalized to *GAPDH* expression followed by normalization of target gene expression to the control treatment.

5.2.8 Molecular Modeling

The crystal structure of FOXM1C-DBD was retrieved from PDB (PDB_ID: 3G73) (266). Chimera v 1.10.12 (277), was used to prepare the structure followed by the charge assignment of protonated groups to pH 7 using PROPKA (241). Small molecule structures were prepared using the Dock-prep tool of Chimera and docked as previously reported. Pymol (276), and Discovery Studio Visualizer 32 (279) were used to visualize and make the figures.

5.2.9 Chemistry

5.2.9.1 General Information

Reagents and solvents were received from Sigma-Aldrich and were used with no further purification. Chemical reactions were monitored using RediSep TLC plates. The melting point of the chemicals were measured using an electrothermal melting point apparatus (Thermofisher). ^{1}H, ^{13}C, and ^{19}F NMR spectra were obtained on a Bruker FT-600 MHz instrument (600 MHz, 150 MHz, and 565 MHz, respectively). TMS was used as the reference. Coupling constants (*J*) are expressed a Hertz while chemical shifts (δ) are expressed in parts per million. Signal multiplicity was reported as s (singlet), d (doublet), t (triplet), q (quartet), m (multiplet) and br (broad singlet). The microwave-assisted synthesis was carried out using an Initiator Reactor (Biotage).

5.2.9.2 General Procedure for the Synthesis of Compounds TFI-1int - TFI-11int

We adapted the methods previously reported, to prepare compounds TFI-1int - TFI-11int by using microwave-assisted synthesis (297–300). The corresponding benzylbromide (1 eq.), the hydroxybenzaldehyde (1 eq.) and K_2CO_3 (1 eq.) were mixed in EtOH (5 ml) and

heated in a microwave reactor vessel to 90 °C for 12 hours. Upon completion of the reaction (monitored by TLC), the final product precipitated as white solid crystals (insoluble in EtOH), which were filtered off and washed with hot water (5 mL) and hexane (3 mL) to yield the intermediate (in a 95% purity as judged by ^{1}H and ^{13}C NMR), in an overall yield of 80 %. The previously reported compounds TFI-1int, TFI-3int, and TFI-10int, were confirmed by ^{1}H and ^{13}C NMR which were in agreement with the reported data (301).

3-nitro-4-[(4-nitrophenyl) methoxy] benzaldehyde (TFI-4int). 4-Hydroxy-3-nitrobenzaldehyde. (100 mg, 0.598 mmol), 4-nitrobenzyl bromide (129 mg, 0.598 mmol) and K_2CO_3 (83 mg, 0.598 mmol), white crystals, yield 80 %. ^{1}H NMR (600 MHz, DMSO) δ 9.96 (s, 1H), 8.49 (d, *J* = 2.1 Hz, 1H), 8.33 – 8.27 (m, 2H), 8.24 – 8.19 (m, 1H), 7.77 – 7.72 (m, 2H), 7.66 (d, *J* = 8.7 Hz, 1H), 5.62 (s, 2H). ^{13}C NMR (151 MHz, DMSO) δ 190.49, 154.85, 147.30, 143.14, 139.56, 135.05, 133.33, 130.58, 129.25, 128.15, 126.74, 124.37, 123.87, 123.81, 116.03, 69.90.

Methyl 4-[(4-formyl-2-nitrophenoxy) methyl] benzoate (TFI-5int). 4-Hydroxy-3-nitrobenzaldehyde (100 mg, 0.598 mmol), methyl 4-(bromomethyl) benzoate (137 mg, 0.598 mmol), K_2CO_3 (83 mg, 0.598 mmol), white crystals, yield 80 %. ^{1}H NMR (600 MHz, DMSO) δ 9.95 (s, 1H), 8.47 (d, *J* = 2.0 Hz, 1H), 8.20 (dd, *J* = 8.7, 2.1 Hz, 1H), 8.01 (d, *J* = 8.3 Hz, 2H), 7.63 (dd, *J* = 20.2, 8.6 Hz, 3H), 5.54 (s, 2H), 3.86 (s, 3H). ^{13}C NMR (151 MHz, DMSO) δ 190.47, 165.93, 154.99, 140.83, 139.59, 134.97, 129.47, 129.40, 129.12, 127.37, 126.67, 116.03, 70.42, 52.21.

4-methoxy-3-[(4-nitrophenyl) methoxy] benzaldehyde (TFI-6int). 3-Hydroxy-4-methoxybenzaldehyde (100mg, 0.66 mmol), 4-nitrobenzyl bromide (143 mg, 0.66 mmol)

and K_2CO_3 (90 mg, 0.66 mmol), white crystals, 80% yield. ^{1}H NMR (600 MHz, DMSO) δ 9.83 (s, 1H), 8.28 (d, *J* = 8.7 Hz, 2H), 7.73 (d, *J* = 8.8 Hz, 2H), 7.61 (dd, *J* = 8.2, 1.9 Hz, 1H), 7.48 (d, *J* = 1.9 Hz, 1H), 7.24 (d, *J* = 8.3 Hz, 1H), 5.35 (s, 2H), 3.91 (s, 3H). ^{13}C NMR (151 MHz, DMSO) δ 191.30, 154.51, 147.76, 147.08, 144.65, 129.58, 128.27, 126.89, 123.66, 111.73, 111.18, 68.69, 56.09.

4-methoxy-3-{[4-(trifluoromethyl)phenyl]methoxy}benzaldehyde (TFI7-int). 3-Hydroxy-4-methoxybenzaldehyde (100mg, 0.66 mmol), 4-(trifluoromethyl)benzyl bromide (158 mg, 0.66), K_2CO_3 (90 mg, 0.66 mmol), white crystals, 90%. ^{1}H NMR (600 MHz, DMSO) δ 9.83 (s, 1H), 7.78 (d, *J* = 8.0 Hz, 2H), 7.69 (d, *J* = 8.0 Hz, 2H), 7.60 (dd, *J* = 8.2, 1.9 Hz, 1H), 7.49 (d, *J* = 1.9 Hz, 1H), 7.22 (d, *J* = 8.3 Hz, 1H), 5.29 (s, 2H), 3.90 (s, 2H). ^{13}C NMR (151 MHz, DMSO) δ 191.31, 154.51, 147.90, 141.61, 129.59, 128.74, 128.53, 128.32, 128.09, 127.90, 126.94, 126.75, 125.41, 125.39, 125.36, 125.34, 125.14, 123.34, 121.54, 111.66, 111.09, 68.96, 56.04, 55.80, 39.52. ^{19}F NMR (565 MHz, DMSO) δ -60.96.

Methyl 4-[(3-formyl-2-methoxyphenyl)methoxy]benzoate (TFI8-int). 3-Hydroxy-4-methoxybenzaldehyde (100mg, 0.66 mmol), methyl 4-(bromomethyl) benzoate (152 mg, 0.66 mmol), K_2CO_3 (90 mg, 0.66 mmol), white crystal, 80%. (TFI-8int). ^{1}H NMR (600 MHz, DMSO) δ 9.82 (d, *J* = 1.1 Hz, 1H), 7.99 (d, *J* = 8.4 Hz, 2H), 7.59 (dd, *J* = 11.0, 4.9 Hz, 1H), 7.47 (d, *J* = 1.9 Hz, 1H), 7.22 (d, *J* = 8.3 Hz, 1H), 5.28 (s, 2H), 3.90 (s, 3H), 3.86 (s, 3H). ^{13}C NMR (151 MHz, DMSO) δ 191.31, 166.01, 154.52, 147.93, 142.26, 129.57, 129.36, 129.32, 129.08, 127.59, 127.57, 126.71, 111.66, 111.16, 69.20, 60.76, 56.05, 52.17, 39.52. ^{13}C NMR (151 MHz, DMSO) δ 191.31, 166.01, 154.52, 147.93,

142.26, 129.57, 129.36, 129.32, 129.08, 127.59, 127.57, 126.71, 111.66, 111.16, 69.20, 60.76, 56.05, 52.17.

3-methoxy-4-[(4-nitrophenyl)methoxy]benzaldehyde (TFI-9int). 4-Hydroxy-3-methoxybenzaldehyde (100 mg, 0.65 mmol), 4-nitrobenzyl bromide (142 mg, 0.65 mmol), K_2CO_3 (90 mg, 0.65 mmol), white crystals, 80%. ^{1}H NMR (600 MHz, DMSO) δ 9.85 (s, 1H), 8.28 (d, *J* = 8.8 Hz, 2H), 7.73 (d, *J* = 8.8 Hz, 2H), 7.55 (dd, *J* = 8.2, 1.9 Hz, 1H), 7.45 (d, *J* = 1.8 Hz, 1H), 7.25 (d, *J* = 8.3 Hz, 1H), 5.40 (s, 2H), 3.87 (s, 3H). ^{13}C NMR (151 MHz, DMSO) δ 191.43, 152.64, 149.44, 147.15, 144.25, 130.17, 128.39, 125.75, 123.70, 112.84, 109.94, 68.76, 55.69, 39.52.

Methyl 4-[(4-formyl-2-methoxyphenyl)methoxy]benzoate (TFI-11int). 4-Hydroxy-3-methoxybenzaldehyde (100 mg, 0.65 mmol), methyl 4-(bromomethyl) benzoate (150 mg, 0.65 mmol), K_2CO_3 (90 mg, 0.65 mmol). ^{1}H NMR (600 MHz, DMSO) δ 9.84 (s, 1H), 7.99 (d, *J* = 8.2 Hz, 2H), 7.60 (d, *J* = 8.1 Hz, 2H), 7.54 (dd, *J* = 8.2, 1.9 Hz, 1H), 7.43 (d, *J* = 1.8 Hz, 1H), 7.24 (d, *J* = 8.3 Hz, 1H), 5.32 (s, 2H), 3.85 (s, 6H). ^{13}C NMR (151 MHz, DMSO) δ 191.43, 166.00, 152.89, 149.44, 141.89, 130.04, 129.41, 129.21, 127.73, 127.71, 125.81, 112.78, 109.87, 69.32, 55.66, 52.19.

5.2.9.3 General Procedure for the Synthesis of Compounds TFI-1 - TFI-11

We adapted the methods previously reported, to use a microwave-assisted synthesis protocol. The corresponding intermediate (1 eq.), thiazolidinedione (3 eq.), piperidine (cat.), AcOH (cat.), and EtOH (5 mL) were mixed in a microwave reactor vessel and irradiated under microwave for 3 hours at 90 °C. Once completed, the reaction was allowed to cool down to r.t. yielding a pale yellowish precipitates that were filtered off and then washed with cold EtOH (10 mL) and water (10 mL) to afford the desired

products with an overall yields of around 60 %. The previously reported compound 2a was confirmed by ^{1}H and ^{13}C NMR, both in agreement with the reported data. All derivatives were found to be the *Z* isomer according to the previously reported methine proton chemical shift (302).

(5Z)-5-({4-[(4-nitrophenyl) methoxy] phenyl}methylidene)-1,3-thiazolidine-2,4-dione (TFI-1). Thiazolidinedione (67mg, 0.57 mmol), TFI-1int (50 mg, 0.19 mmol), piperidine (cat.) and AcOH (cat.), pale yellowish crystals, 60 % yield, m.p. 251-253 °C ^{1}H NMR (600 MHz, DMSO) δ 12.52 (s, 1H), 8.42 – 8.03 (m, 2H), 8.32 – 8.23 (m, 3H), 7.78 – 7.71 (m, 2H), 7.62 – 7.54 (m, 2H), 7.22 – 7.17 (m, 2H), 5.37 (s, 2H). ^{13}C NMR (151 MHz, DMSO) δ 168.02, 167.56, 159.58, 147.12, 144.45, 132.12, 131.60, 128.37, 126.11, 123.69, 120.84, 115.76, 68.27. [M-H]-: *m/z* calc. 355.0 found 355.1 *m/z* (100%).

(5*Z*)-5-[(4-{[4-(trifluoromethyl) phenoxy] methyl}phenyl)methylidene]-1,3-thiazolidine-2,4-dione (TFI-2). Thiazolidinedione (63mg, 0.54 mmol), TFI-2int (50 mg, 0.18 mmol), piperidine (cat.) and AcOH (cat.), pale yellowish crystals, 60 % yield, m.p. 202-203 °C. ^{1}H NMR (600 MHz, DMSO) δ 12.53 (s, 1H), 7.77 (d, J = 8.2 Hz, 2H), 7.75 (s, 1H), 7.68 (d, J = 8.1 Hz, 2H), 7.58 (d, J = 8.8 Hz, 2H), 7.20 (t, J = 10.3 Hz, 2H), 5.32 (s, 2H). ^{13}C NMR (151 MHz, DMSO) δ 167.97, 167.49, 159.72, 141.44, 132.11, 131.65, 128.56, 128.35, 128.13, 125.97, 125.43, 125.40, 120.69, 115.74, 68.54, 56.02. ^{19}F NMR (565 MHz, DMSO) δ -60.96. [M-H]-: *m/z* calc. 378.0 found 378.2 *m/z* (100%).

Methyl 4-({4-[(*Z*)-(2,4-dioxo-1,3-thiazolidin-5-ylidene) methyl] phenyl}methoxy)benzoate (TFI-3). Thiazolidinedione (64mg, 0.55 mmol), TFI-3int (50 mg, 18.5 mmol), piperidine (cat.) and AcOH (cat.). (TFI-3), pale yellowish crystals, 60 % yield, m.p. 220-222 °C. ^{1}H NMR (600 MHz, DMSO) δ 12.53 (br, 1H), 7.99 (d, J = 8.4

Hz, 2H), 7.74 (s, 1H), 7.59 (dd, J = 20.4, 8.6 Hz, 4H), 7.18 (d, J = 8.9 Hz, 2H), 5.30 (s, 2H), 3.86 (s, 3H). 13C NMR (151 MHz, DMSO) δ 167.97, 167.49, 165.98, 165.47, 159.79, 142.07, 141.99, 132.09, 131.67, 129.39, 129.35, 129.13, 127.62, 127.61, 125.92, 120.64, 115.74, 68.78, 60.77, 52.18. [M-H]-: *m/z* calc. 368.1 found 368.1 m/z (100%).

(5Z)-5-({3-nitro-4-[(4-nitrophenyl) methoxy] phenyl}methylidene)-1,3-thiazolidine-2,4-dione (TFI-4). Thiazolidinedione (59.73 mg, 0.51 mmol), TF-4int (50 mg, 0.17 mmol), piperidine (cat.) and AcOH (cat.), pale yellowish crystals, 60 % yield, m.p. 242-243 °C. ^{1}H NMR (600 MHz, DMSO) δ 12.67 (s, 1H), 8.33 – 8.27 (m, 2H), 8.21 (d, *J* = 2.2 Hz, 1H), 7.87 (dt, *J* = 14.6, 7.3 Hz, 1H), 7.81 (s, 1H), 7.76 – 7.71 (m, 2H), 7.59 (t, *J* = 9.4 Hz, 1H), 5.57 (s, 2H). ^{13}C NMR (151 MHz, DMSO) δ 190.49, 154.85, 147.30, 143.14, 139.56, 135.05, 129.25, 128.15, 126.74, 123.81, 116.03, 69.90. [M-H]-: *m/z* calc. 400.0 found 400.3 *m/z* (100%).

Methyl 4-({4-[(*Z*)-(2,4-dioxo-1,3-thiazolidin-5-ylidene) methyl]-2 nitrophenyl}methoxy) benzoate (TFI-5). Thiazolidinedione (56.2 mg, 0.51 mmol), TF-5int (50 mg, 0.16 mmol), piperidine (cat.) and AcOH (cat.), pale yellowish crystals, 60 % yield, m.p. 225-227 °C. ^{1}H NMR (600 MHz, DMSO). ^{1}H NMR (600 MHz, DMSO) δ 12.68 (s, 1H), 8.19 (d, *J* = 2.2 Hz, 1H), 8.03 – 7.98 (m, 2H), 7.85 (dd, *J* = 9.1, 2.3 Hz, 1H), 7.81 (s, 1H), 7.59 (t, *J* = 8.5 Hz, 3H), 5.49 (s, 2H), 3.86 (s, 3H). ^{13}C NMR (151 MHz, DMSO) δ 167.49, 167.22, 165.94, 151.74, 141.03, 139.64, 135.18, 129.46, 129.35, 127.33, 126.87, 126.04, 123.93, 116.39, 70.17, 52.21. [M-H]-: *m/z* calc. 413.0 found 413.2 *m/z* (100%).

(5*Z*)-5-({2-methoxy-3-[(4-nitrophenoxy) methyl] phenyl}methylidene)-1,3-thiazolidine-2,4-dione (TFI-6). Thiazolidinedione (61 mg, 0.52 mmol), TF-6int (50 mg, 0.17 mmol), piperidine (cat.) and AcOH (cat.), pale yellowish crystals, 60 % yield, m.p.

200-202 °C. ^{1}H NMR (600 MHz, DMSO). ^{1}H NMR (600 MHz, DMSO) δ 12.49 (s, 1H), 8.27 (d, *J* = 8.8 Hz, 2H), 7.75 – 7.67 (m, 3H), 7.25 – 7.20 (m, 2H), 7.20 – 7.16 (m, 1H), 5.33 (s, 2H), 3.87 (s, 3H). ^{13}C NMR (151 MHz, DMSO) δ 167.95, 167.37, 151.15, 147.39, 147.08, 144.70, 131.89, 128.28, 125.60, 124.56, 123.67, 120.73, 115.10, 112.56, 68.78, 55.88. [M-H]-: m/z calc. 385.1 found 385.3 m/z (100%).

(5*Z*)-5-[(4-hydroxy-3-{[4-(trifluoromethyl) phenoxy] methyl}phenyl)methylidene]-1,3-thiazolidine-2,4-dione (TFI-7). Thiazolidinedione (56.2 mg, 0.48 mmol), TFI-7int (50 mg, 0.16 mmol), piperidine (cat.) and AcOH (cat.). ^{1}H NMR (600 MHz, DMSO). ^{1}H NMR (600 MHz, DMSO) δ 12.50 (s, 1H), 7.77 (d, *J* = 8.2 Hz, 2H), 7.72 – 7.65 (m, 3H), 7.21 (dd, *J* = 11.5, 2.0 Hz, 2H), 7.16 (d, *J* = 8.3 Hz, 1H), 5.27 (s, 2H), 3.86 (s, 3H). ^{13}C NMR (151 MHz, DMSO) δ 167.95, 167.39, 151.15, 147.53, 141.63, 131.94, 128.76, 128.55, 128.34, 128.13, 128.06, 126.94, 125.60, 125.42, 125.40, 125.37, 125.35, 125.14, 124.47, 123.33, 121.53, 120.68, 114.99, 112.50, 69.04, 55.83. ^{19}F NMR (565 MHz, DMSO) δ -60.96. [M-H]-: m/z calc. 385.1 found 385.3 m/z (100%).

Methyl 4-({5-[(*Z*)-(2,4-dioxo-1,3-thiazolidin-5-ylidene) methyl]-2-methoxyphenyl} methoxy) benzoate. (TFI-8). Thiazolidinedione (53 mg, 0.45 mmol), TFI-8-int (50 mg, 0.15 mmol), piperidine (cat.) and AcOH (cat.), pale yellowish crystals, 60 % yield, m.p. 233-236 °C. ^{1}H NMR (600 MHz, DMSO). ^{1}H NMR (600 MHz, DMSO) δ 12.50 (s, 1H), 7.99 (d, *J* = 8.4 Hz, 2H), 7.69 (s, 1H), 7.60 (d, *J* = 8.5 Hz, 2H), 7.21 (dd, *J* = 4.3, 2.4 Hz, 2H), 7.17 (d, *J* = 9.0 Hz, 1H), 5.26 (s, 2H), 3.86 (d, *J* = 3.8 Hz, 6H). ^{13}C NMR (151 MHz, DMSO) δ 167.98, 167.41, 166.01, 165.50, 151.17, 147.58, 142.30, 142.22, 131.93, 129.38, 129.36, 129.34, 129.08, 127.59, 127.57, 127.55, 125.58, 124.49, 120.67, 115.00, 112.50, 69.28, 60.76, 55.84, 52.16. [M-H]-: m/z calc. 398.1 found 398.2 m/z (100%).

(5*Z*)-5-({3-methoxy-4-[(4-nitrophenoxy) methyl] phenyl} methylidene)-1,3-thiazolidine-2,4-dione (TFI-9). Thiazolidinedione (60 mg, 0.52 mmol), TFI-9int (50 mg, 0.17 mmol), piperidine (cat.) and AcOH (cat.), pale yellowish crystals, 65 % yield, m.p. 205-208 °C. ^{1}H NMR (600 MHz, DMSO) δ 12.53 (br., 1H), 8.29 – 8.25 (m, 2H), 7.75 (s, 1H), 7.73 – 7.70 (m, 2H), 7.25 (d, *J* = 2.0 Hz, 1H), 7.17 (dt, *J* = 8.4, 5.1 Hz, 2H), 5.36 (s, 3H). ^{13}C NMR (151 MHz, DMSO) δ 168.43, 167.92, 149.72, 149.68, 147.58, 144.98, 132.42, 128.81, 126.91, 124.15, 123.86, 114.24, 114.17, 69.14, 56.18. [M-H]-: m/z calc. 385.1 found 385.1 m/z (100%).

(5*Z*)-5-[(3-methoxy-4-{[4-(trifluoromethyl) phenoxy] methyl} phenyl) methylidene]-1,3-thiazolidine-2,4-dione (TFI-10). Thiazolidinedione (56 mg, 0.48 mmol), TFI-10int (50 mg, 0.16 mmol), piperidine (cat.) and AcOH (cat.), pale yellowish crystals, 65 % yield, m.p. 201-213 °C. ^{1}H NMR (600 MHz, DMSO) δ 12.51 (s, 1H), 7.78 (d, *J* = 8.0 Hz, 2H), 7.74 (s, 1H), 7.67 (d, *J* = 8.1 Hz, 2H), 7.24 (s, 1H), 7.18 (dd, *J* = 22.6, 8.5 Hz, 2H), 5.30 (s, 2H), 3.84 (s, 3H). ^{13}C NMR (151 MHz, DMSO) δ 167.97, 167.43, 149.39, 149.24, 141.49, 132.03, 128.77, 128.56, 128.35, 128.15, 126.93, 126.30, 125.45, 125.43, 125.40, 125.38, 125.13, 123.46, 123.32, 120.89, 113.67, 68.95, 55.68, 39.52. ^{19}F NMR (565 MHz, DMSO) δ -60.95. [M-H]-: m/z calc. 408.1 found 408.3 m/z (100%).

Methyl4-({4-[(*Z*)-(2,4-dioxo-1,3-thiazolidin-5-ylidene) methyl]-2 methoxyphenyl} methoxy) benzoate (TFI-11). Thiazolidinedione (56 mg, 0.48 mmol), TFI-11int (50 mg, 0.16 mmol), piperidine (cat.) and AcOH (cat.), yellowish crystals, 60% yield, m.p. 212-214 °C. ^{1}H NMR (600 MHz, DMSO) δ 12.53 (s, 1H), 7.99 (d, *J* = 8.4 Hz, 2H), 7.75 (s, 1H), 7.59 (d, *J* = 8.5 Hz, 2H), 7.24 (d, *J* = 2.0 Hz, 1H), 7.16 (dt, *J* = 8.6, 5.3 Hz, 2H), 5.28 (s, 2H), 3.86 (s, 3H), 3.84 (s, 3H).^{13}C NMR (151 MHz, DMSO) δ 191.42, 167.97, 167.42, 166.00, 149.47, 149.25, 142.13, 132.04, 129.38, 129.13, 127.71, 127.66, 126.26, 125.80,

123.45, 120.85, 113.70, 113.65, 112.78, 109.86, 69.30, 69.21, 55.68, 55.65, 52.18. [M-H]-: m/z calc. 398.1 found 398.2 m/z (100%).

5.2.9.3 General Procedure for the Synthesis of Compounds P11 and TFI-10-RHO

TFI-intermediate (1 eq.), rhodanine (1.2 eq.), piperidine (cat.), AcOH (cat.), and EtOH (5 mL) were mixed in a microwave reactor vessel and irradiated under microwave for 3 hours at 90 °C. For the synthesis of compound P11 we adapted the methodology previously reported for the synthesis of the phosphine-meleimide (303) and TFI-10-inter (confirmed by ^{1}H and ^{13}C NMR and both in agreement with the previously reported data). The reaction of phosphine-meleimide (1 eq.) and TFI-10-inter (1 eq.) under Wittig conditions (MeOH, 1 hour microwave irradiation, 90 °C) yielded compound P11.

(5Z)-5-[(3-methoxy-4-{[4-(trifluoromethyl)phenyl]methoxy}phenyl)methylidene]-2-sulfanylidene-1,3-thiazolidin-4-one (TFI-10-Rho). Rhodanine (60 mg, 0.45 mmol), 11a-int (160 mg, 0.375 mmol), piperidine (cat.) and AcOH (cat.), pale yellowish crystals, 65 % yield (64 mg, 0.18 mmol). ^{1}H NMR (600 MHz, DMSO) δ 13.77 (s, 1H), 7.78 (d, *J* = 8.1 Hz, 2H), 7.67 (d, *J* = 8.0 Hz, 2H), 7.61 (s, 1H), 7.25 – 7.14 (m, 3H), 5.31 (s, 2H), 3.85 (s, 3H). ^{13}C NMR (151 MHz, DMSO) δ 195.51, 169.43, 149.81, 149.33, 141.41, 132.09, 128.79, 128.58, 128.37, 128.16, 126.92, 126.23, 125.45, 125.43, 125.40, 125.38, 125.12, 124.33, 123.31, 122.76, 113.82, 113.74, 68.98, 55.70.

(3Z)-3-[(3-methoxy-4-{[4-(trifluoromethyl) phenyl]methoxy} phenyl)methylidene] pyrrolidine-2,5-dione (P11). Phosphine intermediate (180 mg, 0.5 mmol), TFI-10 Intermediate (195 mg, 0.5 mmol) in MeOH (5 mL), off-white powder, 70% yield (135 mg, 0.35 mmol). ^{1}H NMR (600 MHz, DMSO) δ 11.39 (s, 1H), 7.78 (d, *J* = 8.1 Hz, 2H), 7.66 (d, *J* = 8.0 Hz, 2H), 7.33 (t, *J* = 2.3 Hz, 1H), 7.24 – 7.12 (m, 2H), 7.10 (d, *J* = 8.5 Hz, 1H), 5.29 (s, 2H), 3.85 (s, 3H).

5.3 Results and Discussion

The former anti-diabetic drug troglitazone is an activator of the PPARγ, a ligand-activated TF that controls glucose and lipid metabolism. The anti-diabetic mechanism of action exerted by thiazolidinediones does not appear to be directly correlated to their inhibitory effect on FOXM1. However, Petrovic et al. (20), reported an interesting study in which they report an *indirect* mechanism by which thiazolidinediones (including troglitazone and pioglitazone) significantly decrease the expression of FOXM1, namely the inhibition of the SP1 protein, which is one of the many upstream activators of FOXM1 expression reported in the literature (304). In addition to the indirect mechanism of action exerted by thiazolidinediones on the expression of FOXM1, we hypothesize that the sulfur-containing ring in these molecules will bind directly to the FOXM1-DBD, disrupting the protein-DNA complex and causing transcriptional inhibition.

5.3.1 Chemistry and Design

To further investigate this hypothesis, we generated computer-based docking protocols and synthesized in the lab, eleven compounds (thiazolidinedione forkhead inhibitor (TFI)) possessing either the thiazolidinedione backbone or a benzyloxybenzenering, using the Knoevenagel condensation reaction. **Scheme 5-1** shows the synthetic procedure and a list of all derivatives (TFI-1 – TFI-11).

Scheme 5-1. Synthesis route and list of prepared thiazolidinedione derivatives.Reagents and conditions: (a) K_2CO_3, DMF/ethanol, 120° C, 18 hours; (b) 2,4-thiazolidinedione, ethanol, 120° C, 3 hours.

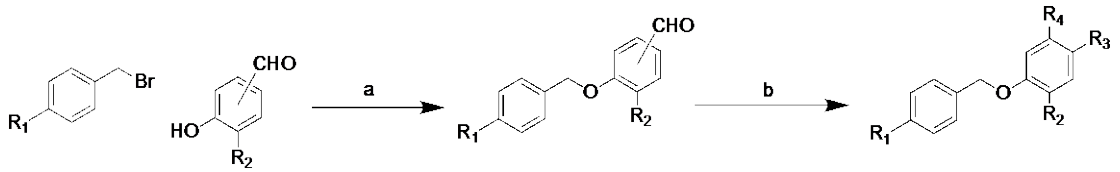

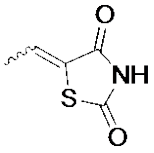

***CH-TZD=**

Compound	R1	R2	R3	R4
TFI 1	$-NO_2$	-H	-CH-TZD*	-H
TFI 2	$-CF_3$	-H	-CH-TZD	-H
TFI 3	$-COOCH_3$	-H	-CH-TZD	-H
TFI 4	$-NO_2$	$-NO_2$	-CH-TZD	-H
TFI 5	$-COOCH_3$	$-NO_2$	-CH-TZD	-H
TFI 6	$-NO_2$	$-OCH_3$	-H	-CH-TZD
TFI 7	$-CF_3$	$-OCH_3$	-H	-CH-TZD
TFI 8	$-COOCH_3$	$-OCH_3$	-H	-CH-TZD
TFI 9	$-NO_2$	$-OCH_3$	-CH-TZD	-H
TFI 10	$-CF_3$	$-OCH_3$	-CH-TZD	-H
TFI 11	$-COOCH_3$	$-OCH_3$	-CH-TZD	-H

Based on our computer-based approach, for the position R1, we chose the nitro group ($-NO_2$), trifluoromethyl ($-CF_3$), and a methyloxycarbonyl ($-CO_2CH_3$) ester group; for the R2 position, we observed the highest binding affinity for the methoxy ($-OCH_3$) and nitro groups. To complement the structure-activity relationship study, we investigated the effects produced by positional isomers by moving the position of the thiazolidinedione ring with respect to the benzyloxy benzene group either to the *para* or *ortho* position on the activity of the derivatives.

5.3.2 FOXM1 Protein Level Measurement

We measured the protein expression of FOXM1 in breast cancer cells after a 48-hours incubation period in the presence of increasing concentrations of the test compounds by western-blot analysis (**Figure 5-1**), using troglitazone, FDI-6, and thiostrepton as reference (positive) controls. In this regard, compounds TFI-1, TFI-2, TFI-6, and TFI-10

significantly reduced (more than 90%) the total expression of FOXM1 protein in breast cancer cells, while the other seven derivatives (TFI-1,3,4,5,7,8,9 and 11) showed only modest activity, compared to the reference compounds.

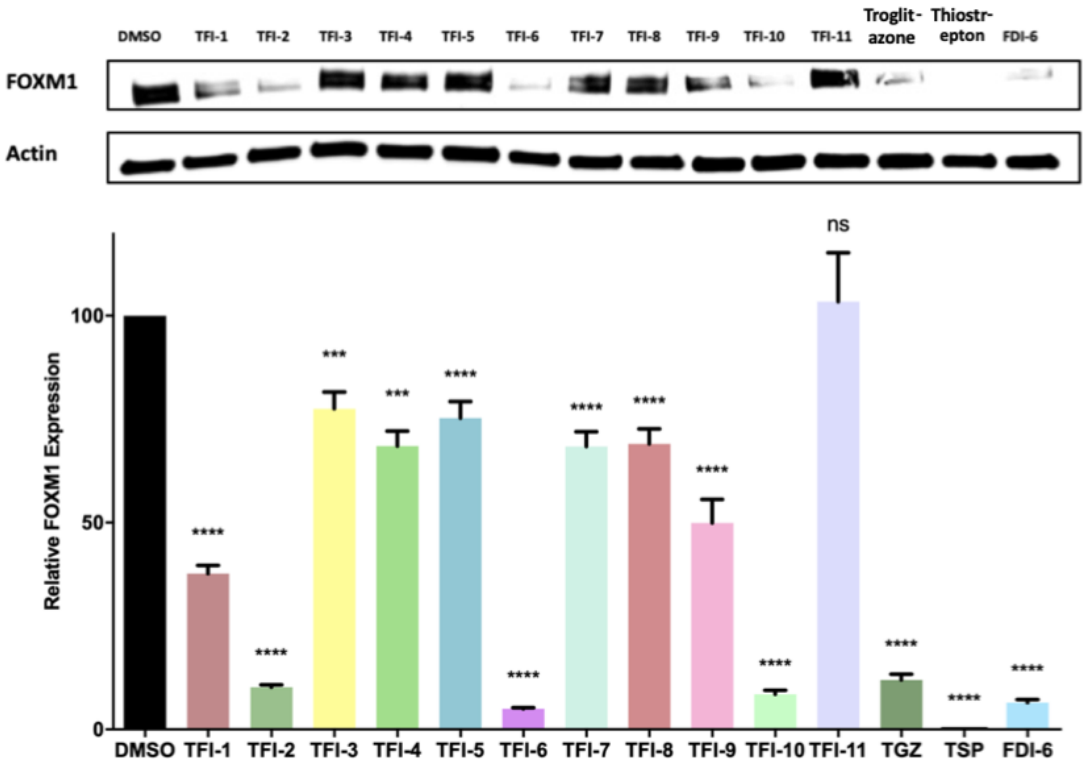

Figure 5-1. Western blot analysis of FDI Derivatives.FOXM1 protein levels of the test compounds (40 μM; 48 hours, MDA-MB-231 cell line). The p values were calculated with one-way ANOVA: *: $P \leq 0.05$; **: $P \leq 0.01$; ***: $P \leq 0.001$; ****:$P \leq 0.0001$.

5.3.3 Electrophoretic Mobility Shift Assay-FOXM1-DBD

It is well known in the literature that some FOXM1 inhibitors exert their mechanism of action by either indirect inhibition of upstream FOXM1 activator proteins and/or inhibition of the proteasome (which is a negative regulator of FOXM1). Consequently, to study the mechanism of action exerted by the troglitazone derivatives, we selected

compound TFI-10 to study if this molecule is capable of producing the dissociation of the protein-DBD using the cell-free EMSA to see if these compounds (including troglitazone) are whether direct or indirect FOXM1 inhibitors.

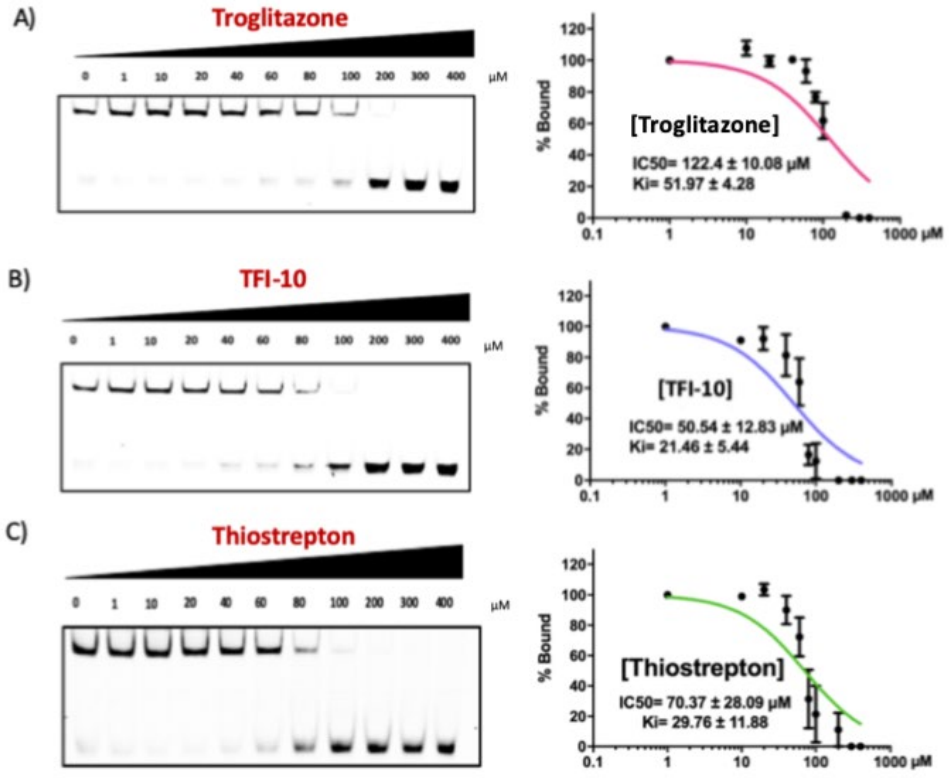

Figure 5-2. EMSA displacement experiment of troglitazone, TFI-10, and thiostrepton. EMSA displacement assay showing the Ki value for troglitazone (A), TFI-10 (B) and thiostrepton (C). TFI-10 was found to be almost twice as potent as troglitazone in displacing the FOXM1-DBD from its consensus DNA.

Incubation of recombinant FOXM1-DBD and its consensus DNA with the drug revealed troglitazone, TFI-10, and thiostrepton (as previously reported (236) could disrupt the binding of FOXM1 and DNA. As shown in **Figure 5-2 A-C,** troglitazone, thiostrepton, and TFI-10 inhibited the protein-DNA complex with Ki ~ 51.97, 29.87, and

21.46 µM, respectively, which gives an extra advantage to our compound (TFI-10) with a better DNA binding inhibition.

5.3.4 Luciferase reporter Assay

The observed increase in binding exerted by compound TFI-10 suggests a better inhibitory profile, and therefore, to evaluate this hypothesis we measured the ability of compound TFI-10 to inhibit the transcriptional activity of FOXM1 in triple-negative breast cancer cells determined by the use of a firefly luciferase reporter assay possessing the corresponding FOXM1 DNA binding sites.

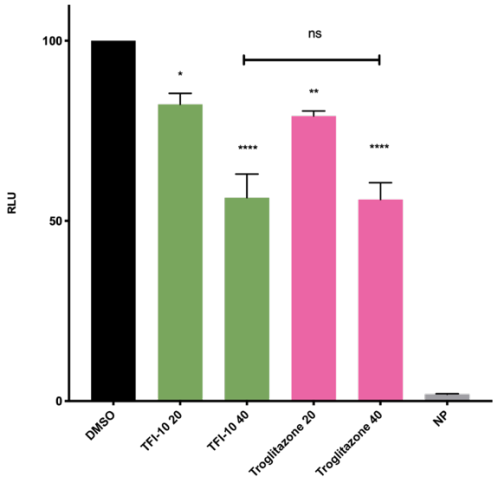

Figure 5-3. Luciferase level decreased after treatment with TFI-10 and troglitazone. Luciferase plasmid bearing FOXM1 promoter was transfected into MDA-MB-231 cells, and the relative level of luciferase activity was measured 24 hours after treatment with 20 and 40 µM of TFI-10 and troglitazone. All data indicate three replicates. The p values were calculated with one-way ANOVA: *: $P \leq 0.05$; **: $P \leq 0.01$; ***: $P \leq 0.001$; ****:$P \leq 0.0001$.

The relative decrease in FOXM1 transcriptional activity after incubation of cells in the presence of the drug molecules (**Figure 5-3**) resembled the pattern that we previously observed in the immunoblot experiment (**Figure 5-1**). As expected, both compounds (TFI-10 and troglitazone) showed significant activity in both 20 and 40 µM.

5.3.5 mRNA level analysis

To confirm the results obtained in both the western blot and luciferase assays described above, we measured the mRNA levels of not only the target protein FOXM1, but also some of its downstream target proteins such as *CCNB1* and *CDC25B*. CCNB1 and CDC25B proteins are essential regulators of cell cycle progression; CCNB1 promotes the entry of cell cycle from G2 to M phase, and CDC25 protein dephosphorylate the cyclin-dependent kinase, which allows the cell to enter M phase (305). In consistency with our previous protein immunoblot and EMSA experiments, TFI-10 decreased the mRNA levels of the target genes to a greater extent than that produced by troglitazone **(Figure 5-4)**.

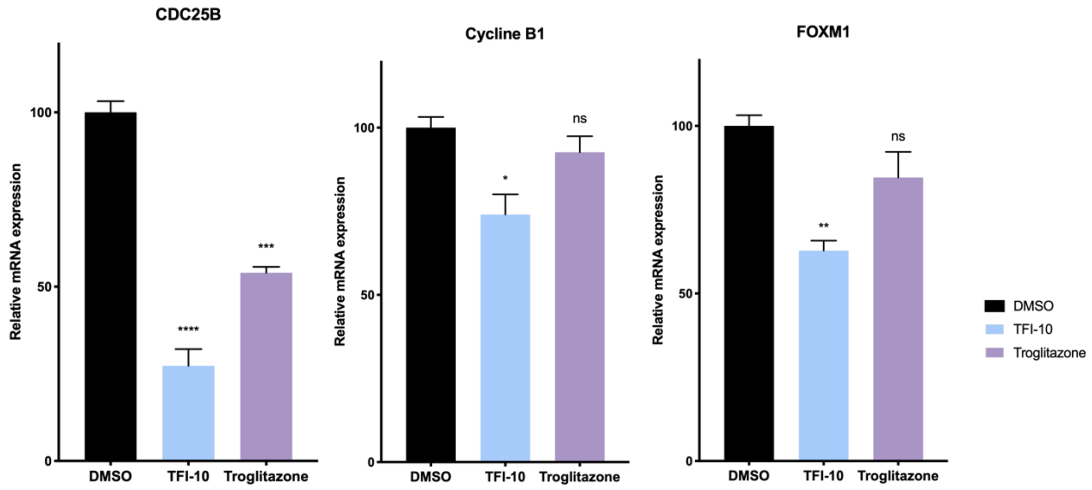

Figure 5-4. qPCR analysis of the mRNA level of human FOXM1 and its downstream targets, including *CDC25B and CCNB1*. TFI-10 was able to significantly decrease the

mRNA level of all targeted genes at 20 µM after 24 hours of treatment, but troglitazone was incapable of decreasing the level of human *Cyclin B1*; The p values were calculated with one-way ANOVA: *: $P \leq 0.05$; **: $P \leq 0.01$; ***: $P \leq 0.001$.

5.3.6 SP1 Expression level Determination

In this regard, a previous report by Petrovic et al. (20) showed that the drug-induced decrease in the expression of FOXM1 exerted by thiazolidinediones takes place, mainly through the inhibition of the TF SP1. Nevertheless, as we showed in **Figure 5-5**, we observed a significant decrease in the expression levels of SP1 exerted by with the parent molecule troglitazone; however, this effect is not observed when we incubate the breast cancer cells with compound TFI-10, suggesting that TFI-10 inhibits the expression of FOXM1 by a different mechanism and therefore, it may be reasonable to assume that our test molecule exerts a different mechanism of action, that is different than that observed for the original thiazolidinedione (parent) compound.

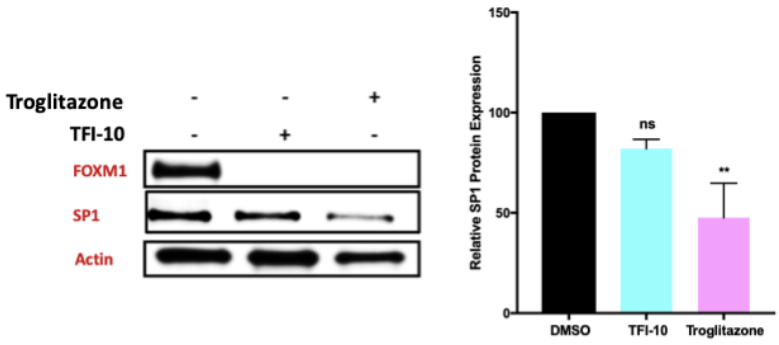

Figure 5-5. Western blot protein level analysis of TFs SP1 and FOXM1. Troglitazone and TFI-10 were significantly decreased the level of FOXM1 at 80 µM after 24 hours of treatment, whereas the level of SP1 was only diminished by troglitazone. The asterisks

above the bars represents statistically significant changes calculated using one-way ANOVA:**, $P \leq 0.01$.

5.3.7 Electrophoretic Mobility Shift Assay-FOXO1-DBD and FOXO3a-DBD

As we stated earlier, all members of forkhead box TFs have a conserved winged-helix DBD. Because of their high sequence similarity of their DBD, we hypothesized that the identified FOXM1 inhibitors might non-selectively target other FOXO families, especially those with confirmed tumor suppression activity. To test this hypothesis, we made recombinant FOXO1-DBD and FOXO3-DBD and employed EMSA to test if these drugs can also interrupt mentioned TB binding to their consensus DNA.

It's previously shown that FOXOs and FOXM1 TFs target the same consensus DNA sequence. This site has previously shown to be conserved in ERα (216), Cyclin B1 (155), HSP70 (140), and c-fos (140) genes. As shown in **Figure 5-6-A**, FOXO1 binds 1.5 times weaker to their consensus DNA (Kd ~ 508.7 nM) in comparison to the FOXM1 (Kd= ~361 nM). Set side by side, FOXO3a forms a tighter complex than FOXO1 and FOXM1, having a Kd value of about 119.8 nM (**Figure 5-6-B**). Next, we tested the ability of the drugs (TFI-10, troglitazone, and thiostrepton) to disrupt the DNA using EMSA. As illustrated in **Figure 5-6-A1**, thiostrepton was unable to inhibit the binding of FOXO1 to its target DNA while it inhibited the FOXO3 complex formation (**Figure 5-6-B1**). Nevertheless, according to the representing EMSA gel images in **Figure 5-6-A and B**, troglitazone inhibited the binding of both TFs. However, FOXO1 binding was more affected (**Figure 5-6-A2** and **Figure 5-6-B2**). Surprisingly, TFI-10 was unable to disrupt

the complex formation of both FOXOs and DNA at any concentration. According to these results, we can cautiously conclude that TFI-10 could selectively target FOXM1 without influencing FOXO1 and, FOXO3a (**Figure 5-6-A3** and **Figure 5-6-B3**).

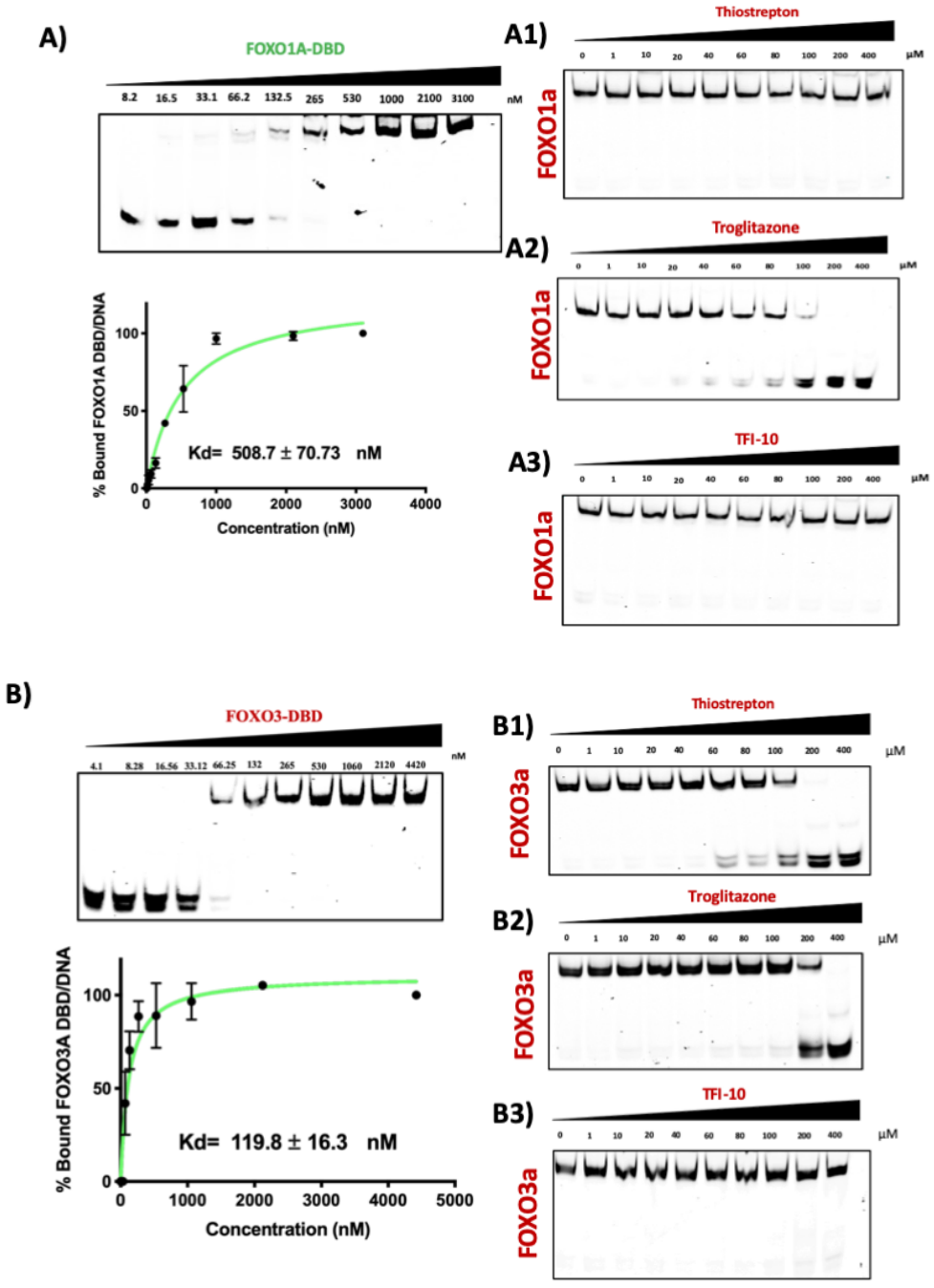

Figure 5-6. Determination of Kd for FOXO1/DNA and FOXO3a/DNA followed by EMSA displacement experiment for thiostrepton, troglitazone, and TFI-10. A) Determination of the Kd value of FOXO1 and its consensus DNA. A1-3) Displacement experiment for thiostrepton, troglitazone, and TFI-10; only troglitazone was able to inhibit FOXO3a/DNA complex formation. B) Determination of the Kd value of FOXO1 and its consensus DNA. B1-3) TFI-10 was unable to inhibit the FOXO3a/DNA at any concentration.

5.3.8 Molecular Modeling

To provide a fine-tuned justification for the observed biological profile shown by compound TFI-10, we conducted a computer-based molecular modeling study based on a previously reported protocol described by our group, in which we proposed a drug-binding pocket at the interface of the FOXM1-DBD. As shown in **Figure 5-7-A**, we observed a significant pi - sulfur binding interaction between the thiazolidinedione ring present in TFI-10 and the His287 residue, in agreement with our previous report. In this regard, the introduction of a methoxy group to TFI-10 contributed to its increased binding affinity by exerting two hydrogen-bonding interactions with the Arg289 residue.

Furthermore, we observed an additional binding interaction involving the trifluoromethyl moiety and the Trp308 and Arg297 residues, providing additional evidence to support our previously reported drug binding site. The role of a halogen binding is not only relevant and significant for the thiazolidinediones reported in this research, but also for structurally different FOXM1 inhibitors such as the FDI-6 molecule

reported by Gormally et al. (206). The superimposed structure of TFI-10 and troglitazone is shown in **Figure 5-7-B**.

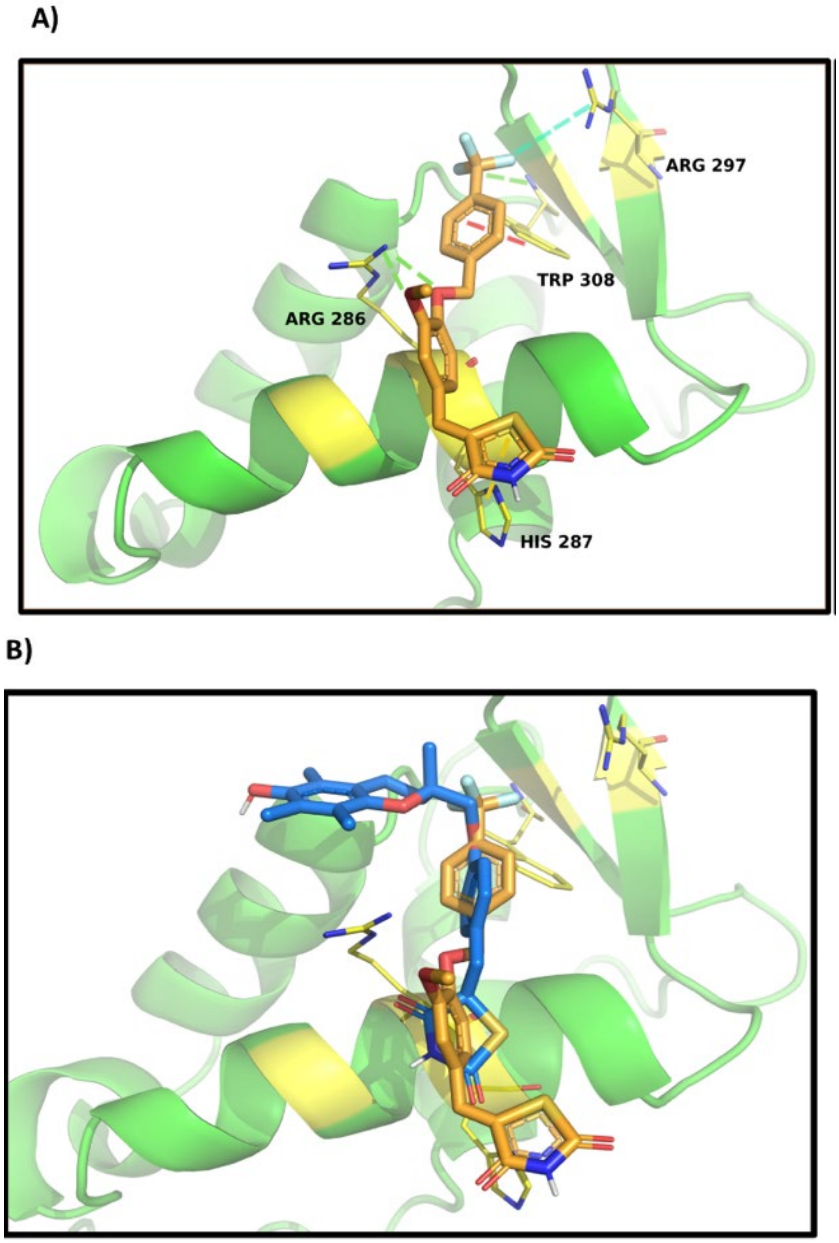

Figure 5-7. Binding mode of TFI-10 and troglitazone.A) The schematic 3D presentation of TFI-10 binding to the FOXM1-DBD. Amber line indicates pi-sulfur, green lines show hydrogen bonds, cyan represents halogen bonding, and the red line

shows pi-pi stacking interactions. B) Superimposed structure of TFI-10 and troglitazone at the FOXM1-DBD/DNA interface.

5.3.10 Sulfur Effect

Scheme 5-2. Synthetic route for the preparation of TFI-10 derivatives. A) P11, B) TFI-10-RHO: Reagents and conditions: (a) acetone, reflux, 1 hour; (b) ethanol, 120° C, 3 hours; (C) K_2CO_3, ethanol, 120° C, 18 hours; (D) MeOH, , 90 °C, 1 hour.

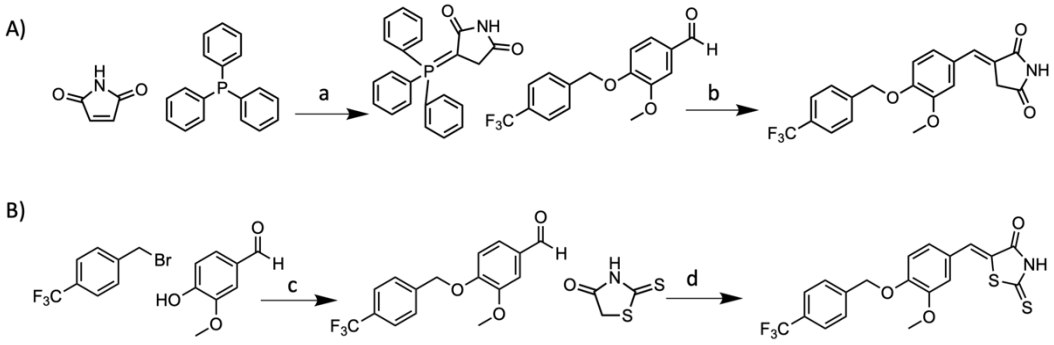

5.3.10.1 Chemistry

As previously reported (210,306) and as suggested by molecular modeling mentioned above, the sulfur atom is a vital and essential part of TFI-10 activity. To prove the importance of sulfur atom, we chemically altered TFI-10. We synthesized two different derivatives of TFI-10, where the thiazolidinedione was replaced with succinimide (P11) or rhodanine (TFI-10-RHO) rings (**Scheme 5-2**). In compound P11, the sulfur atom was replaced by a carbon atom, while in compound TFI-10-RHO, an extra sulfur atom was introduced.

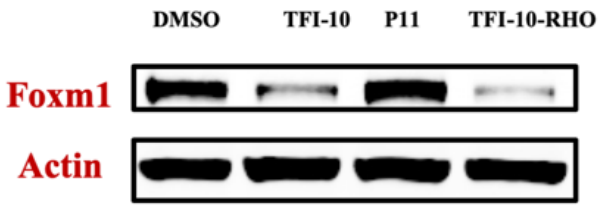

Figure 5-8. Non-sulfur bearing derivative (P11) was unable to decrease the FOXM1 protein level in MDA-MB-231. FOXM1 protein level of TFI-10, P11, and TFI-10-RHO after 24 hours. Treatment (40 μM) in the MDA-MB-231 cell line. Compound P11 in which sulfur was replaced with a carbon of thiazolidinedione ring was unable to decrease the FOXM1 protein level pointing toward the undeniable role of the sulfur atom

As we were expecting and shown in **Figure 5-8**, compound P11 was unable to decrease the FOXM1 protein level in MDA-MB-231, a breast cancer cell line where the FOXM1 is upregulated. However, the compound having one extra sulfur in its ring (TFI-10-RHO) was slightly more active than the parent molecule TFI-10.

We also employed the previously reported EMSA assay to investigate the ability of these new derivatives to dissociate the FOXM1-DBD/DNA interaction (**Figure 5-9**). In agreement with the protein immunoblot results, compound P11 was unable to bind to FOXM1-DBD, while compound TFI-10-RHO was significantly better Ki (7.35 μM) in compare to TFI-10 (Ki= 21.46 μM). These finding clearly shows that there is a strong relationship between the presence of sulfur atom and FOXM1 inhibitory capacity of these molecules further strengthening our previous finding regarding the importance of sulfur atom.

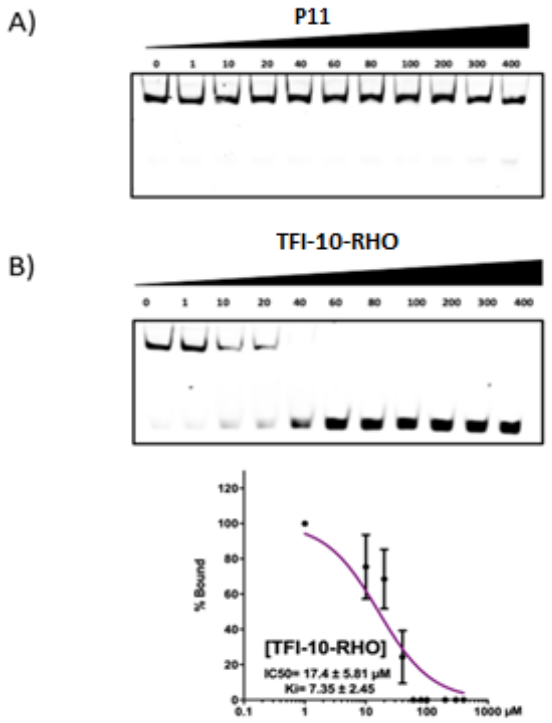

Figure 5-9. EMSA displacement experiment of compound P11 and TFI-10-RHO. Compound P11 (A) was unable to inhibit the binding of FOXM1 to its consensus DNA. Compound TFI-10-RHO (B) having rhodanine ring was almost three times more potent than TFI-10 (Ki: 7.35 µM).

5.4 Summary and Conclusion

In summary, this research article describes a new approach to modify the thiazolidinedione scaffold to produce derivatives that retain the desirable FOXM1 inhibitory profile, via an SP1-independent mechanism, which paves the way for the design of novel drug molecules with a good chance of exerting anticancer effects on triple-negative breast cancer cells. We demonstrate direct binding inhibition of the protein-DNA complex, and to some extent, a considerable transcriptional inhibition of

the FOXM1 protein, resulting in inhibition of downstream target proteins and a significant decrease in cancer cell colony formation *in vitro*. We also showed that TFI-10 could only target FOXM1-DBD but not the other closely related tumor suppressors (FOXO3a and FOXO1). However, EMSA only represents the binding of these drugs to the DBD, while drugs can bind and alter TF in numerous other ways. Finally, using chemical alteration, we proved that the role of the sulfur atom in FOXM1 inhibition is undeniable.

In conclusion, we submit a new approach to change the anticancer mechanism of action exerted by the thiazolidinedione scaffold, producing potent FOXM1 inhibition that is independent of the SP1 transcription pathway that was previously correlated to this group of molecules. These results could be valuable for designing selective FOXM1 inhibitors in the near future.

Chapter 6

AS1842856 is a Dual Inhibitor of FOXO1 and FOXM1 Transcription Factors

6.1 Introduction

Forkhead Box Os (FOXOs) are a family of TFs characterized by a distinct and DBD (89). These Transcription factors are all bind to the same sequence of DNA (Daf-16 Protein-binding element (DBE: 5′-TTGTTTAC-3′) and engage in numerous physiological process including cellular proliferation, apoptosis, cell cycle regulation, and cancer (110,112,113). Currently, four discrete types of FOXO family with different tissue-specific expression has been identified: FOXO1 (FKHR), FOXO3 (FKHRL1), FOXO4 (AFX) and FOXO6 (85,307). In particular, FOXO1 has been linked by many bodies of literature to diabetes mellitus as well as cancer.

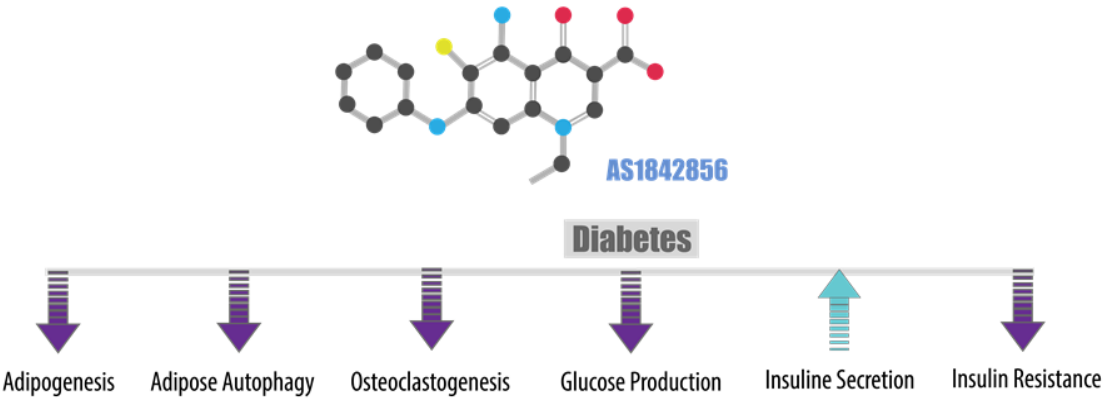

Figure 6-1. Promising effects of AS1842856 in diabetes In diabtetes, it presented to decrease adipogenesis (308), adipocyte autophagy (309), osteoclastogneesis (Indirectly linked to diabetes) (310), glucose production (311), and diminish insulin resistance (308).

FOXO1 expression is higher in insulin-responsive tissues like pancreas, liver, and adipose (312). Phosphoinositide 3-kinases (PI3K) gets activated by insulin in response to the high level of blood glucose level. Subsequent phosphorylation of AKT by PI3K leads

to FOXO1 phosphorylation by AKT and suppression of its transcriptional activity (115). FOXO1 is known to bind to the insulin response unit (IRU) within the promoter region of the Glucose 6-phosphatase (G6P), the enzyme that catalyzes the conversion of glucose-6-phosphate to glucose. The phosphorylation and subsequent deactivation of FOXO1 negatively regulate this process and inhibits G6P dependent gluconeogenesis and glycogenolysis (313). It has been shown that inhibition of FOXO1 leads to a decrease in the level of insulin and an increase in glucose tolerance (311).

On the other hand, FOXO1 induced glucose intolerance and promoted obesity and insulin resistance when overexpressed in the hypothalamus and pancreas (314). FOXO1 has also been linked to many metabolic pathways like skeletal muscle, adipose tissue differentiation, and lipid metabolism. [reviewed in reference (315)].

However, its role in cancer is controversial, and both its oncogenic and tumor-suppressive functions have been reported. *In vivo* knockout studies of FOXO1 resulted in mouse embryo lethality by interfering with angiogenesis; nevertheless, in cancer, the only aggregate loss of FOXO1/FOXO3/FOXO4 led to tumorigenesis (92).

Today, researchers are becoming more interested in understanding the role of FOXO1 in tumorigenesis to capture its controversial behavior. FOXOs are known to be the bonafide tumor suppressors (121).

Contrarily, it is found that inhibition of FOXO1 (both genetic and pharmacological) in B-cell precursor acute lymphoblastic leukemia (BCP-ALL) was antileukemic. (316). In another study, overexpression of FOXO1 was found to promote the proliferation and colony formation ability of AML1-ETO (AE) modeled leukemia

cells (317). Besides this, MMP1 as a metastasis facilitation factor is tightly regulated by FOXO1 (133).

AS1842856 was the first known selective inhibitor of FOXO1 with no significant effect on the level of other FOXOs, i.e., FOXO3 and FOXO4. This drug was able to reduce the FOXO1 mediated glucogenesis resulting in decreased plasma glucose levels. This finding suggested that FOXO1 inhibitors can serve as a new class of drugs for treating type 2 diabetes (311). Furthermore, AS1842856 was also able to decrease the FOXO1 mediated adipogenesis, which makes it very beneficial for those suffering from obesity as well as type 2 diabetes (308). **Figure 6-1** outlines the different effects of AS1842856 observed in diabetes.

Based on the high sequence homology in the structure of FOXOs and the oncogenic TF FOXM1, we hypothesized that AS1842856 could also target FOXM1. To test this hypothesis, we designed series of experiments to test the inhibitory effect of AS1842856 in two breast cancer cell lines (MDA-MB-231 and MCF-7), which has been previously shown to express both FOXM1 and FOXO1.

6.2 Materials and Methods

6.2.1 Reagents and Chemicals

AS1842856 was received from Sigma Aldrich and used without any purification. FDI-6 was synthesized and purified as previously reported (260).

6.2.2 Cell Culture

MDA-MB-231 and MCF-7 cells were maintained in RPMI, and DMEM media supplemented with 10% FBS in a 5% CO2 atmosphere at 37 °C, respectively.

6.2.3 Antibodies

The FOXM1 monoclonal (mouse, sc-271746) antibody; SP1 monoclonal (mouse, sc-420) antibody; beta-actin monoclonal (mouse, sc-47778), p53 monoclonal (mouse, -sc-126), CDC25B polyclonal (rabbit, sc-326), CCNB1 monoclonal (mouse, sc-7393), GAPDH monoclonal (mouse, sc-32233) were obtained from Santa Cruz Biotechnology. FOXO1 monoclonal (rabbit, 2880), P-FOXO1 Ser256 monoclonal (rabbit, 9461), AKT monoclonal (rabbit, 9272) and P-AKT Ser473 (rabbit, 9271) were received from Cell Signaling Technology.

6.2.4 Western Blot

MDA-MB-231 and MCF7 cells were seeded in 6 well plates ($3x10^5$) and either transfected or treated with different concentrations of drugs. The cells were washed with ice-cold PBS, and RIPA lysis and extraction buffer (ThermoFisher) containing the appropriate concentration of protease and phosphatase inhibitors were added. The cells were incubated for 30 minutes, and the protein was extracted according to the manufacturer's protocol. An equal amount of protein (30 µg) was loaded into a 4-12% Mini-PROTEAN® precast gel (Bio-Rad). Upon completion of the electrophoresis, the separated proteins were transferred from the gel to a nitrocellulose membrane and blocked with 10% fat-free milk in TBST for 1 hour. Then, the membrane was incubated with the

corresponding primary antibody overnight on a rocking platform. The next day, the membrane was washed with TBST for 15 minutes in total, before incubation with the corresponding secondary antibody for 1 hour. Next, the membrane was washed 3 times with TBST, and the protein of the interest was visualized by adding the Chemiluminescence reagent (ThermoFisher). The quantification was carried out using ImageJ software relative to either β-Actin or GAPDH.

6.2.5 Protein Expression and Purification

Recombinant FOXM1-DBD was prepared as previously reported. FOXO1-DBD recombinant protein was prepared by transforming the PEX-N-GST FOXO1-DBD plasmid (OriGene technologies, USA) into the BL21 (DE3) competent cells. Positive colonies were selected on LB agar media (ampicillin 100ug/mL) and inoculated into LB media containing the appropriate concentration of ampicillin at 37 °C until they reached the optical density of 0.6. Next, 1 mM IPTG was added. After 3 hours of incubation in an incubator shaker at 37 °C, the protein was extracted using B-PER™ Bacterial Cell Lysis (Thermofisher) and purified using glutathione resin (GeneScript, USA).

6.2.6 Plasmids and Short interfering RNAs

siRNA for FOXM1 and FOXO1 were purchased from Dharmacon (Lafayette, CO, USA). pCW57.1-FOXM1c and PCF257.1-FOXM1b were gifts from Adam Karpf (Addgene plasmids #68810 and #68811) (318). PGL4.10 was employed as the empty vector, as well as the backbone for the FOXM1 luciferase reporter vector containing the FOXM1 consensus sequence (319).

6.2.7 Lentiviral Based Transduction

The Lentiviral transduction was performed according to the method reported by Haque et al. protocol (320).

6.2.8 Cell Proliferation Assay (MTT)

The MTT experiment was performed as previously reported.

6.2.9 Electrophoretic Mobility Shift Assay

The Kd values were obtained by titrating the recombinant FOXO1-DBD and FOXM1-DBD with their consensus DNA oligo (12.8 nM) (Forward strand: 5′-/IRD700/-AAACAAACAAACAATCAAACAAACAAACAATC-3′) using EMSA as previously reported (260) . The concentration of FOXO1-DBD and FOXM1-DBD for displacement experiment was 265 nM and 480 nM, respectively.

6.2.10 Colony Formation Assay

MDA-MB-231 and MCF-7 cells were either treated with drugs or transfected with corresponding siRNAs. Treated drugs were harvested after 24 hours, while the cells were incubated with siRNA for 48 hours. Next, cells were trypsinized, resuspended and 750 cells were seeded into 10 cm Petri-dishes. After ten days, cells were washed with PBS and fixed using methanol. After 20 minutes, colonies were stained with 5 mL of 90% Crystal Violet solution for 30 minutes. Then, the dishes were rinsed three times with tap water and air-dried. The colonies were counted using ImageJ software, and the values were plotted using Prism.

6.2.10 Luciferase Assay

The empty reporter plasmid-PGL4.10 and the 6X-FOXM1 firefly reporter were gifts from Drs. Carter J Barger and Adam R. Karpf. MDA-MB-231 cells were transfected with Jetprime transfection reagents following manufacturer's protocol with an equal amount of 6x-FXOM1 and empty backbone plasmids. The cells were treated with 40 μM of drugs, and after 24 hours, cells were harvested using Reporter lysis Buffer (Promega). An equal amount of protein was analyzed for each sample following the manufacturer's protocol (Promega).

6.3 Results and Discussion

6.2.10 Protein Immunoblot and Gene Silencing

FDI-6, a non-proteasome inhibitor (unlike thiostrepton), and a known inhibitor of FOXM1 were chosen as a positive control for these experiments (206). FOXM1, FOXO1, and FOXM1 and FOXO1 double siRNA knockdown were performed on MDA-MB-23 for complete downstream target analysis. As shown in **Figure 6-2**, both FDI-6 and AS1842856 were able to decrease the protein level of FOXM1 at 40 μM significantly; however, AS1842856 at 20 μM showed no apparent inhibition compared to the vehicle control (DMSO). Surprisingly FDI-6, which is known to bind to the FOXM1-DBD, was also able to decrease the level of FOXO1 considerably. Besides that, the level of phosphorylated FOXO1 at Ser256 was also measured. It is well known that FOXO1 phosphorylation at this position is essential for its DNA binding ability and gene targeting (321). Intriguingly, the level of phosphorylated FOXO1 was not decreased by any of the tested drugs, and it is only reduced when the FOXO1 gene is silenced.

The level of SP1 TF (304), which is a known regulator of FOXM1 was also assessed; none of our drugs were able to affect the level of SP1. However, the level of SP1 was diminished when both FOXO1 and FOXM1 genes were silenced which requires further investigation.

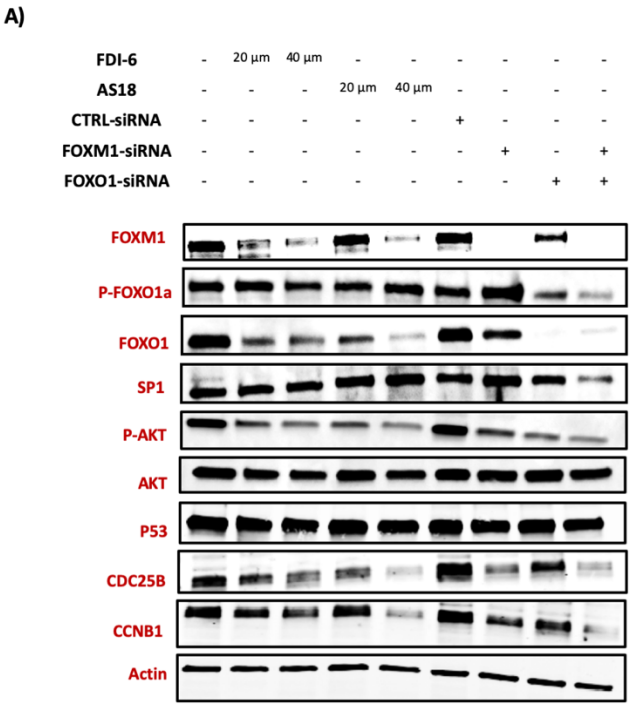

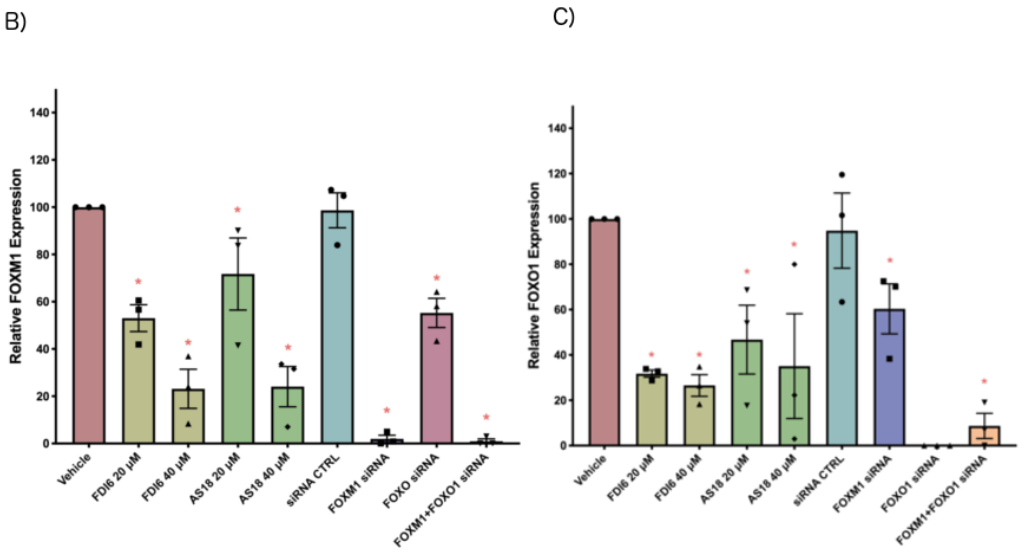

Figure 6-2. AS1842856 and FDI-6 decreased the FOXM1 and FOXO1 protein levels in MDA-MB-231. Protein expression level analysis of FOXO1, FOXM1 and their upstream and downstream regulators and targets after treatment with AS1842856 and FDI-6 or gene silencing of FOXM1 or FOXO1 (A). The cells are either knocked-down with appropriate siRNA or treated with test compounds at 20, and 40 μM for 24 hours. B) quantified relative FOXM1 expression of (A), C) quantification of relative FOXO1 expression of (A). Bars represent the average value of three independent experiments. The asterisks represent the significance calculated using one-way ANOVA: *: $P < 0.05$.

To confirm that the AS1842856 can also decrease the downstream targets of FOXM1, we also measured the protein level of CDC25B and CCNB1. As expected, the FOXO1 inhibitor could effectively decrease the protein level of these cyclins, which are known to be directly regulated by FOXM1.

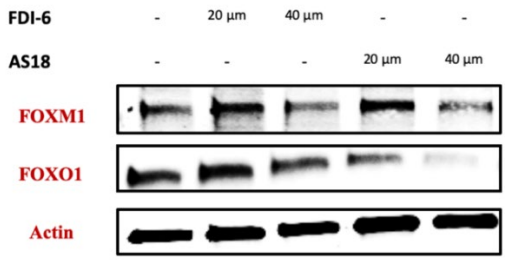

Figure 6-3. Effect of AS1842856 and FDI-6 of the protein level of FOXO1, FOXM1 in MCF-7 breast cancer cell line. AS1842856 decreased the expression level of both FOXM1 and FOXO1 in an ER positive breast cancer cell line.

The inhibition effect of AS1842856 on the other breast cancer cell line (MCF-7) was also measured, and the same results were obtained. AS1842856 was able to reduce the transcription level of FOXM1 in the ER-positive cell line (MCF-7). (**Figure 6-3**). The interesting and essential point revealed, was that the level of FOXM1 and FOXO1 did not notably decrease when the FOXO1 and FOXM1 gene were silenced, respectively.

6.2.10 Effect of FOXM1b and FOXM1c Overexpression on FOXO1

To understand the correlation between these two TFs, FOXM1b and FOXM1c were overexpressed in HEK293T cells. It is apparent from **Figure 6-4-A** that when we overexpressed the FOXM1b isoform, the level of FOXO1 and FOXM1 downstream target surge in the same order. On the other hand, overexpression of FOXM1c decreased the level of endogenous FOXO1. It does not fit into the context of this manuscript to state whether the FOXM1 isoform dependent regulation of FOXO1 is by direct or indirect regulation mechanism or not. However, what is apparent is that the determination of FOXM1 isoform-specific inhibition by FOXM1 inhibitors is essential. These results can also explain why the FOXM1 and FOXO1 levels upon gene silencing of FOXO1 and

FOXM1, were not notably decreased. With these findings, we can cautiously conclude that the effect of these drugs on the level of FOXM1 and FOXO1 are independent.

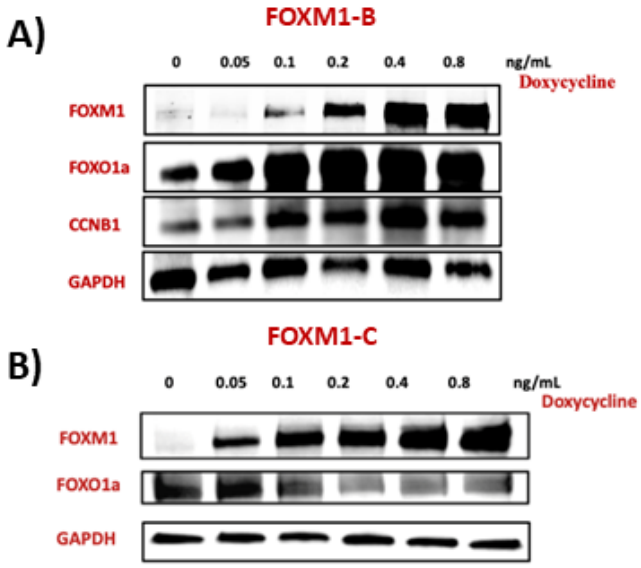

Figure 6-4. Western blot analysis of doxycycline-inducible (TET-ON) overexpression of FOXM1b and FOXM1c. A) Overexpression of FOXM1b enhanced the expression of FOXO1 as well as FOXM1's downstream target, CCNB1. B) FOXM1c overexpression decreased the level of endogenous FOXO1.

6.2.10 Luciferase Reporter Assay

Next, we measured the effect of these drugs on the transcription level of FOXM1 from another angel using Luciferase assay. As **Figure 6-5** suggests, both drugs could effectively decrease the level of luciferase in a dose-dependent manner, which directly reflects the level of available and transcriptionally active FOXM1.

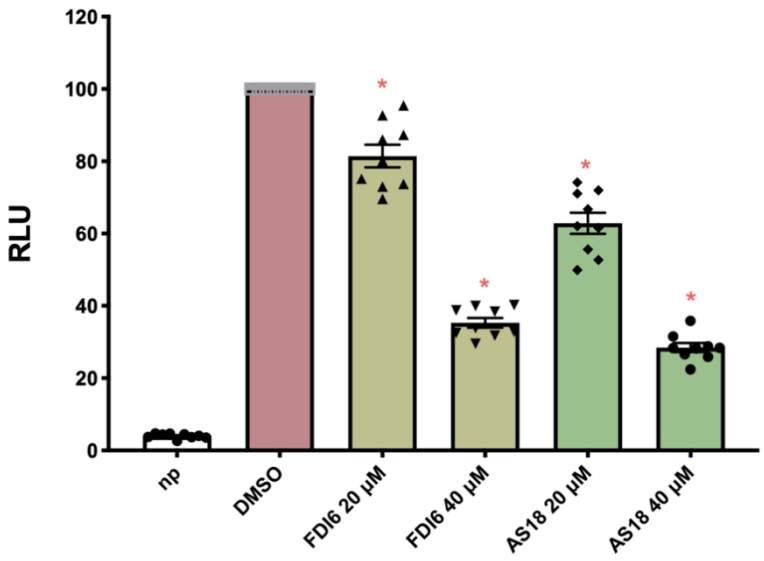

Figure 6-5. Dose dependent reduction in the level of luciferase by AS1842856 and FDI-6. The relative level of luciferase activity showed dose-dependent effect of AS1842856 and FDI-6 on the functional FOXM1 level after 24 hours of incubation. Bars represent the average value of three independent experiments. One-way ANOVA was used to determine the significance: *: $P < 0.05$.

6.2.10 Electrophoretic Mobility Shift Assay: FOXM1-DBD and FOXO1-DBD

Previously, Gormaly et al. showed that the FDI-6 could disrupt the binding of FOXM1 and its target gene using the EMSA (206). We also showed in our previous publication that FDI-6 and some other derivatives of it could directly bind to FOXM1 and prevent the binding of FOXM1 to its consensus DNA target. However, Nagashima et al. found using the mass spectrometric affinity that AS1842856 could only bind to the none Ser256 phosphorylated form of the FOXO1 (311).

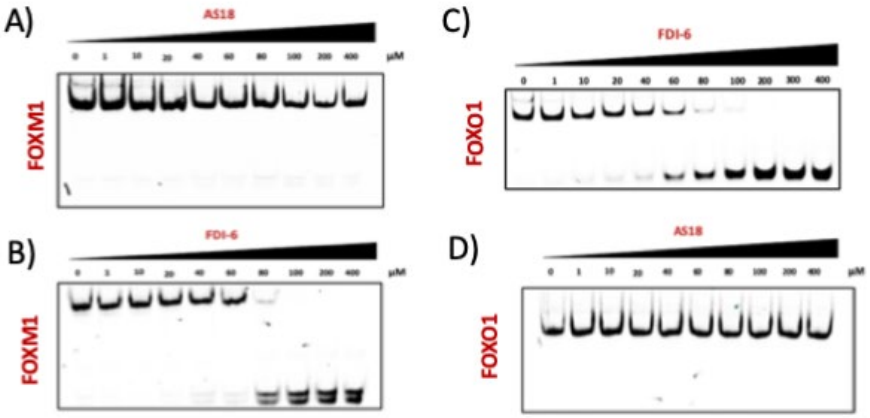

Figure 6-6. EMSA displacement experiment with recombinant FOXM1-DBD and FOXO1-DBD. A and D) AS1842856 was unable to dissociate the binding of FOXM1 and FOXO1 to its consensus DNA at any concentration, indicating that binding of this compound possibly does not alter the DNA binding ability of FOXM1 and FOXO1. B and C) FDI-6 targets both FOXM1-DBD (as previously reported) and FOXO1-DBD and inhibit their DNA binding.

To test if binding of AS1842856 to the FOXO1 disrupts the ability of FOXO1 protein binding, we performed the EMSA displacement experiment with the recombinant FOXO1-DBD protein. **Figure 6-6-D** shows that AS1842856 was unable to disrupt the binding of FOXO1 and DNA. On the other hand, FDI-6 **(Figure 6-6-C)** inhibited the binding of FOXO1 to its consensus DNA with an identical Ki value reported for FDI-6/FOXM1-DBD (260).

Next, we prepared recombinant human GST-FOXM1-DBD and performed the same displacement experiment discussed above. As illustrated in **Figure 6-6-A and B** only FDI-6 was able to prevent the FOXM1/DNA binding, and AS1842856 had no

affinity for the FOXM1-DBD similar to the effect we observed between the AS1842856 and FOXO1-DBD

These data suggest that these two drugs are inhibiting FOXM1 and FOXO1 with a different and distinct mechanism, i.e. FDI-6, by directly binding to these two-TFs DBD and AS1842856 probably binding to the other part of the protein, either altering the protein structure or phosphorylation state.

It is established that the FOXM1 is the Achilles hill of most cancers (322). The level of FOXM1 is highly increased in many cancers (188,318,323), its level is directly correlated to the chemotherapy resistance (169) and inversely linked to the patient prognosis. It is now a well-known fact that inhibition of this TF could be a new strategy for chemotherapy. This indicates that finding the novel mechanism of action of AS1842856 and FDI-6 as dual inhibitors of FOXM1 and FOXO1 could serve as a promising approach in cancer treatment.

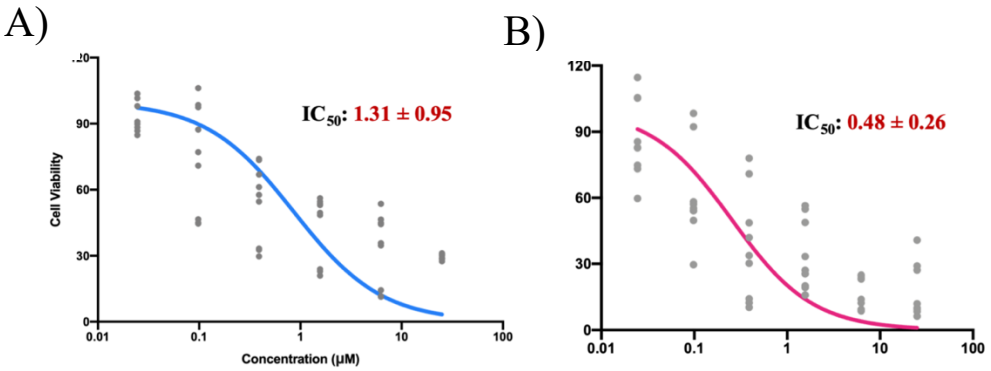

Figure 6-7. The effect of AS184256 on the cell viability of MCF-7 and MDA-MB-231 breast cancer cells as evaluated by MTT assay. As1842856 significantly decrease the number of viable cells with an IC50 of 1.31 and 0.48 μM in MCF-7 (A) and MDA-MB-231 (B), respectively, after 72 hours incubation time.

6.2.11 Cell Proliferation Assay (MTT)

Figure 6-7 shows the cell proliferation assay performed using AS1842856 in both MDA-MB-231 and MCF-7 cells. The IC50 value recorded for AS1842856 were 0.48 and 1.31 μM in MDA-MB-231 and MCF-7, respectively. AS1842856 was found to be more potent in terms of inhibiting the cancer cell proliferation in contrast to the FDI-6, where the IC50 values measured for this drug were 31.1 and 13.43 μM in MDA-MB-231 and MCF-7, respectively and as previously reported (260).

6.2.10 Colony Formation Assay

With the promising effects of AS1842856 on the tested breast cancer cell lines and its low IC50 values, we decided to measure the effect of our drugs as well as the gene knockdown on the colony production ability of breast cancer cells. **Figure 6-8** shows the number of colonies after either vehicle, drug treatment, or gene silencing.

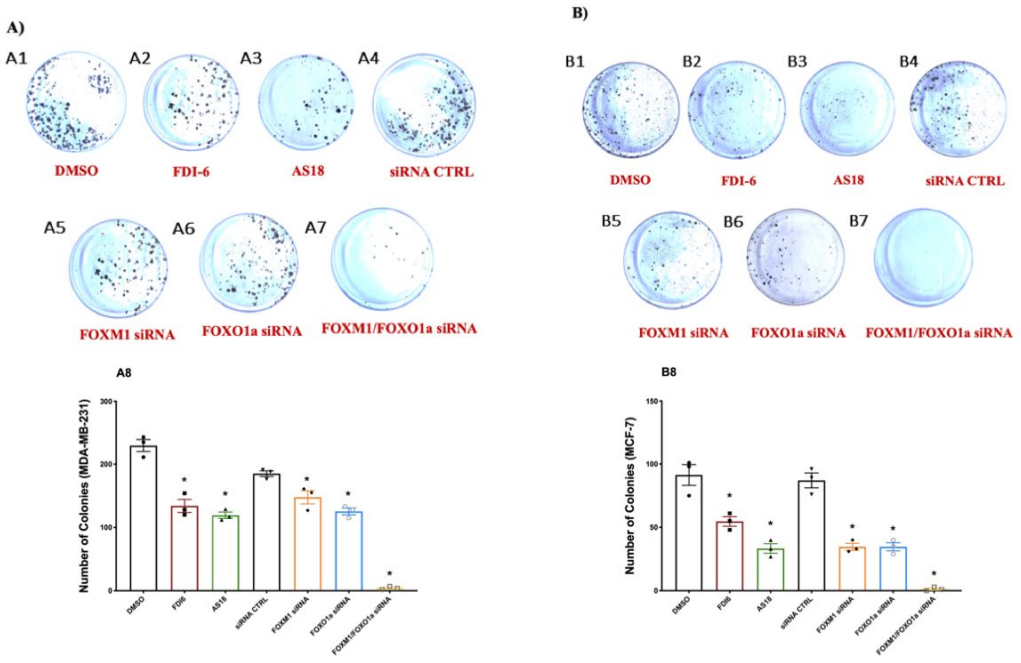

Figure 6-8. No colonies were able to grow after dual knockdown of FOXM1 and FOXO1 genes in the colony forming assay. 24 hours after incubation with AS1842856 or FDI-6 and 48 hours after transfection with FOXO1, FOXM1, or both, cells were collected and 750 cells allowed to grow for 10 days. In both cell lines (MDA-MB-231 (A) and MCF-7 (B)), AS1842856 treated cells colonies (A3 and B3) were less than colonies produced by FDI-6 treated cells (A2 and B2). No colonies were able to grow after dual knockdown of FOXM1 and FOXO1 in both MDA-MB-231 and MCF-7 (A7 and B7). The asterisk represents the significance calculated using one-way ANOVA: *: $P < 0.05$.

As shown in **Figure 6-8-A8** and **B8,** the cells formed significantly less colonies in both AS1842856 and FDI-6 treated cells and FOXM1 and FOXO1 knockdown groups in both cell lines. However, in MCF-7 cell line, the colonies produced by AS1842856

were fewer than those by the FDI-6. The surprising and unexpected observation was the inability of both cell lines to produce a significant number of colonies when both FOXM1 and FOXO1 genes were silenced.

In contrast to our observations, Guan et al. found that the activation of FOXO1 considerably diminished the ability of the osteosarcoma cells to form colonies and proliferate (125). In another study, FOXO1 silencing increased the colony producing capacity as well as the proliferation of gastric carcinoma cells (324). However, in our experiments, no significant effect in colony numbers after the FOXO1 knockdown was observed. The interesting finding was that almost no colonies were able to grow after 10 days by the cells where both FOXO1 and FOXM1 genes were silenced. This gives extra support to the claim that the dual inhibition of these two essential TFs can be clinically beneficial.

6.4 Summary and Conclusion

Pharmacological inhibitors are generally more popular choices than gene silencing methods like siRNA or short hairpin RNA (shRNA) as they are easier to use and the transfection steps can be skipped. Gene silencing can produce fewer off-target effects, but the effect may take days to be seen. Conversely, the effect of pharmacological inhibitors is usually achieved faster. At the same time, the *in vivo* siRNA delivery is a more challenging task compared to a pharmacological inhibitor, making the former a better and more preferred choice.

AS1842856 as the first reported pharmacological inhibitor of FOXO1 is being widely used in many research areas including diabetes and cancer, where inhibition of

FOXO1 is required. Based on the observed off-target effect of AS1842856 and its FOXM1 inhibitory activity, caution must be taken when describing the anti-proliferative or anti-tumor activity of AS1842856.

Besides, we demonstrated that the cells having dual knockdown of FOXO1 and FOXM1 are incapable of proliferation and colony formation. Not only AS1842856, but dual inhibition of FOXO1 and FOXM1 requires further attention and could serve as a novel target for chemotherapy.

Chapter 7

Conclusions and Future Directions

7.1 Conclusions

This thesis describes the general inhibition mechanism exerted by FOXM1 inhibitors and the structural requirements necessary for small molecules to inhibit and modulate this oncogenic TF. Furthermore, it introduces a novel class of FOXM1 inhibitors, namely the TFIs, which selectively target the FOXM1 and not its closely related FOXO tumor suppressor's proteins.

In this thesis, initially, we performed an extensive MD simulation to study the relationship between FOXM1 and its DBD that yields the FOXM1-DBD/DNA complex. Two different MD simulations were performed; one with the DNA complex and one with the isolated FOXM1-DBD. The FOXM1-DBD/DNA complex MD simulation revealed valuable information regarding the stability and the key amino acids required for DNA recognition. Amongst the amino acids required for DNA binding, we found that His287 is responsible for initial DNA recognition and binding. On the other hand, we used isolated FOXM1-DBD to identify a plausible binding pocket on the surface of FOXM1-DBD. After identification of the binding pocket, we used small-molecule docking protocols and reported a mutual binding mode for known FOXM1-DBD direct inhibitors (thiostrepton and FDI-6) as well as troglitazone. After careful analysis of the binding modes of these compounds, we found that they all have a sulfur atom bound to the His287 residue of FOXM1-DBD via a pi-sulfur interaction. Additionally, we proposed that FDI-6 forms a complex with FOXM1-DBD using a halogen bond with its 4-fluoro phenyl group.

To provide evidence of these observations, we designed several chemical and biological experiments to validate these findings. Initially, we introduced several changes

to the structure of FDI-6 to confirm if the halogen bonding is necessary for its FOXM1-DBD binding. After the determination of the cellular level of FOXM1 as well as cell-free EMSA assay in the presence of these drugs, we confirmed that any halogen at the para or meta position of the phenyl ring of FDI-6 is required for its inhibitory activity.

To validate the existence of pi-sulfur interaction, we replaced the sulfur atom in the structure of FDI-6 with its closely related atom, oxygen. We also investigated the effect of thiophene ring removal or replacement with a phenyl group in the structure of FDI-6. Furthermore, to evaluate the relevance of the aromatic character of His287, we employed the site-directed mutagenesis technique and mutated the His287 residue to a non-aromatic (alanine) and an aromatic (phenylalanine) amino acid. The results indicated that the presence of pi-electron cloud and aromaticity is vital for the binding of FDI-6, and inhibition of these molecules is in fact, sulfur-dependent.

With the lesson learned from the theoretical and experimental investigation of FOXM1 inhibitors and their binding site, we designed and synthesized a series of compounds bearing the backbone of thiazolidinediones (TFI series). At least 3 derivatives were considered active in the protein immunoblot analysis of cellular FOXM1. Among them, we picked compound TFI-10 for further analysis. Compound TFI-10 was able to decrease the mRNA level of *FOXM1*, and its downstream targets *CDC25B* and *CCNB1* to a greater extent than troglitazone. Furthermore, it was shown than TFI-10 is ~1.5 times more potent than the parent compound troglitazone in inhibiting the FOXM1/DNA complex formation in the EMSA assay. Besides, using the recombinant human FOXO1-DBD and FOXO3a-DBD and employing EMSA, we presented the finding that TFI-10, unlike thiostrepton and troglitazone, is incapable of interrupting the protein/DNA

complex formation of these important tumor suppressor proteins. Based on these results, we cautiously concluded that TFI-10 could be considered a selective FOXM1 inhibitor.

Finally, we report that the known FOXO1 “selective” inhibitor, AS1842856 is not in fact selective and can additionally target FOXM1. Gene silencing of FOXM1 and FOXO1 revealed that AS1842856 could also target and decrease the transcription level of FOXM1. Besides, the already known FOXM1-DBD direct inhibitor, FDI-6, exhibited dual inhibition of FOXO1 and FOXM1. We also showed that FOXM1b can promote the expression of FOXO1, and we suspect that FOXM1c can also repress the expression of FOXO1, but further investigations are required. EMSA revealed that unlike FDI-6, the binding of AS1842856 doesn’t affect FOXM1 and FOXO1 binding to their consensus DNA. FDI-6 on the other hand, inhibited the binding of FOXO1-DBD with similar fashion as previously reported for the FOXM1-DBD. These findings, besides the EMSA displacement assay of FDI-6 and AS1842856, indicated that these drugs inhibit the FOXO1 and FOXM1 TFs with a discrete mechanism. FDI-6 directly binds to the DBD while AS1842856 (as suggested by the group who reported the compound) possibly binds to the non-phosphorylated (active) form of FOXO1. We also highlighted that the dual knockdown of FOXM1 and FOXO1 stopped the growth and proliferation of two breast cancer cells and could be beneficial for cancer treatment.

Overall the finding of this thesis comprehensively presents the mechanism of direct FOXM1 inhibition as well as the structural requirements to design a potent FOXM1 inhibitor. We also introduced a novel class of FOXM1 inhibitors based on the structure of troglitazone and introduced compound TFI-10, to be known as the very first selective inhibitor of FOXM1.

7.2 Limitations of this Research

One major limitation of the current study was that we performed the EMSA with just the DBD of the proteins involved, FOXOs and FOXM1. This is particularly important because the use of full length proteins might produce different folding and conformation than the smaller DBD. Production of the full length proteins and their subsequent site directed mutagenesis is a promising but extremely difficult task to perform and not in the scope of this initial investigation.

Another limitation of our EMSA was the use of a very short fragment of DNA. In reality, the DNA is a very long macromolecule which is highly organized and tightly condensed in the nucleus of cells. A possible option to overcome this issue is the use of chromatin immunoprecipitation assay to investigate the interactions of DNA and the corresponding proteins *in vitro*.

Throughout this research, we did not consider the presence of possible metabolites of the tested compounds. This is an important point to consider since the effect observed for the *in vitro* experiments could, at least in part, be due to the presence of the metabolites. An example is the somewhat confusing results observed for compound F2 (see chapter 4) which was active in EMSA but inactive in western blot. This could represent an example of metabolism-based drug inactivation of compound F2. These metabolites could be identified (if present) using techniques such as LC-MS and NMR.

The other limitation of this study was the absence of *in vivo* data. Determination of the actual potency of a novel class of FOXM1 inhibitors might be impossible without performing the animal studies. Small molecules with even a small modification might have different and distinct absorption, distribution, metabolism, excretion and activity

patterns. This is particularly important since a compound which is active *in vitro* might be completely inactive *in vivo* or vice-versa.

7.3 Future Directions

7.3.1 Selective FOXM1 Targeting

As mentioned previously, other family members of the Forkhead box have a high level of sequence similarity in their conserved DBD. This is particularly important when designing a small molecule based on the structure of FOXM1-DBD, which could lead to unwanted off-target effects. Currently, crystal structures of FOXO1, FOXO3, and FOXO4 DBD is available in PDB . with the employment of MD simulations and other molecular modeling techniques; we can theoretically predict if these drugs are selective for FOXM1 or not. Next, designing and testing the effect of small molecules on the inhibition of these TFs is an essential step. EMSA, Chromatin immunoprecipitation and luciferase assay may be employed to test if any compound can modulate the effect of these important tumor suppressors.

7.3.2 Targeting FOXM1 TAD

Recently the NMR structure of FOXM1-TAD in complex with the FOXM1-NRD has been determined. This is predominantly important because our preliminary investigation revealed that there is a well-defined binding pocket capable of housing small molecules on the surface of TAD. As previously mentioned, TAD is one of the most crucial domains of FOXM1, required for protein-protein interaction with many co-factors and proteins. Any drug molecule capable of binding to the TAD could disrupt its structure and potentially switch off the protein function. MD simulation and molecular modeling can

be employed to define and study the binding pocket on the surface of TAD. Several cell-free experiments, including cellular thermal shift assay (CETSA) and EMSA, can be employed to confirm the binding of small molecules to the FOXM1 TAD.

As mentioned earlier in this thesis, Forkhead box family members possess a conserved DBD, but other domains have lower sequence similarity, which accounts for their distinct function. Inhibition of FOXM1 using this approach could at least, theoretically eliminate the off-target effects.

7.3.3 FOXM1 Isoform-Specific and FOXO1/FOXM1 Dual Inhibition

In chapter 6, we presented using colony formation assay that the dual knockdown of FOXO1 and FOXM1 almost made the cell incapable of forming colonies. Dual inhibition of FOXM1 and FOXO1 could be clinically relevant, and further *in vitro* and *in vivo* investigations are required to confirm their significance. In the same chapter, we found that FOXM1b and FOXM1c has a distinct effect on the level of FOXO1. However, we did not measure the effect of FOXM1 isoforms on the level of other FOXOs. Besides, we were unable to elucidate the mechanism of enhancement of FOXO1 expression by FOXM1b. Unrevealing, the mechanism of regulation of FOXM1 with other FOXOs, is not only crucial in better understanding of the tumor growth and proliferation but in designing a better and more selective inhibitor of FOXM1.

Bibliography

1. Berg JM, Tymoczko JL SL. Protein Structure and Function. In: Biochemistry. New York; 2002. p. Chapter 3.
2. Guo J. Transcription: the epicenter of gene expression. J Zhejiang Univ Sci B . 2014 May;15(5):409–11. Available from: https://www.ncbi.nlm.nih.gov/pubmed/24793758
3. Gokhale S, Nyayanit D, Gadgil C. A systems view of the protein expression process. Syst Synth Biol . 2011/10/19. 2011 Dec;5(3–4):139–50. Available from: https://www.ncbi.nlm.nih.gov/pubmed/23205157
4. Kolovos P, Knoch TA, Grosveld FG, Cook PR, Papantonis A. Enhancers and silencers: an integrated and simple model for their function. Epigenetics Chromatin . 2012;5(1):1. Available from: https://doi.org/10.1186/1756-8935-5-1
5. Wu J, Brown M. Chapter 2 - Epigenetics and Epigenomics. In: Hoffman R, Benz EJ, Silberstein LE, Heslop HE, Weitz JI, Anastasi J, et al., editors. Elsevier; 2018. p. 17–24. Available from: http://www.sciencedirect.com/science/article/pii/B9780323357623000020
6. Davidson EH, Peter IS. Chapter 1 - The Genome in Development. In: Davidson EH, Peter ISBT-GCP, editors. Oxford: Academic Press; 2015. p. 1–40. Available from: http://www.sciencedirect.com/science/article/pii/B9780124047297000010
7. Griffiths AJF, Miller JH, Suzuki DT et al. An Introduction to Genetic Analysis. 7th ed. New York; 2000.
8. Lee Y, Rio DC. Mechanisms and Regulation of Alternative Pre-mRNA Splicing. Annu Rev Biochem . 2015 Jun 2;84(1):291–323. Available from: https://doi.org/10.1146/annurev-biochem-060614-034316
9. Bhagavan N V, Ha C-E. Chapter 24 - Regulation of Gene Expression. In: Bhagavan N V, Ha C-EBT-E of MB (Second E, editors. San Diego: Academic Press; 2015. p. 447–64. Available from: http://www.sciencedirect.com/science/article/pii/B9780124166875000245
10. Wu J. Post-Transcriptional Gene Regulation : RNA Processing in Eukaryotes . Weinheim, GERMANY: John Wiley & Sons, Incorporated; 2013. Available from: http://ebookcentral.proquest.com/lib/ualberta/detail.action?docID=1180946
11. Will CL, Lührmann R. Spliceosome Structure and Function. Cold Spring Harb Perspect Biol . 2011;3(7). Available from: http://cshperspectives.cshlp.org/content/3/7/a003707.abstract
12. Cooper. GM. Translation of mRNA. In: The Cell: A Molecular Approach. Sunderland; 2000.
13. Agback P, Baumann H, Knapp S, Ladenstein R, Härd T. Architecture of nonspecific protein–DNA interactions in the Sso7d–DNA complex. Nat Struct Biol . 1998;5(7):579–84. Available from: https://doi.org/10.1038/836
14. Lambert SA, Jolma A, Campitelli LF, Das PK, Yin Y, Albu M, et al. The Human Transcription Factors. Cell. 2018 Feb;172(4):650–65.
15. Vaquerizas JM, Kummerfeld SK, Teichmann SA, Luscombe NM. A census of human transcription factors: function, expression and evolution. Nat Rev Genet . 2009;10(4):252–63. Available from: https://doi.org/10.1038/nrg2538
16. Wingender E, Schoeps T, Haubrock M, Dönitz J. TFClass: a classification of human transcription factors and their rodent orthologs. Nucleic Acids Res . 2014/10/31. 2015 Jan;43:D97–102. Available from: https://www.ncbi.nlm.nih.gov/pubmed/25361979

17. Wingender E, Schoeps T, Dönitz J. TFClass: an expandable hierarchical classification of human transcription factors. Nucleic Acids Res . 2012/11/24. 2013 Jan;41:D165–70. Available from: https://www.ncbi.nlm.nih.gov/pubmed/23180794
18. Stegmaier P, Kel AE, Wingender E. Systematic DNA-binding domain classification of transcription factors. Genome Inform. 2004;15(2):276–86.
19. Lee TI, Young RA. Transcriptional regulation and its misregulation in disease. Cell . 2013 Mar 14;152(6):1237–51. Available from: https://www.ncbi.nlm.nih.gov/pubmed/23498934
20. Petrovic V, Costa RH, Lau LF, Raychaudhuri P, Tyner AL. Negative regulation of the oncogenic transcription factor FoxM1 by thiazolidinediones and mithramycin. 2010;9(12):1008–16.
21. Saxton RA, Sabatini DM. mTOR Signaling in Growth, Metabolism, and Disease. Cell . 2017 Mar 9;168(6):960–76. Available from: https://www.ncbi.nlm.nih.gov/pubmed/28283069
22. Laplante M, Sabatini DM. Regulation of mTORC1 and its impact on gene expression at a glance. J Cell Sci . 2013/05/02. 2013 Apr 15;126(Pt 8):1713–9. Available from: https://www.ncbi.nlm.nih.gov/pubmed/23641065
23. Agani F, Jiang B-H. Oxygen-independent regulation of HIF-1: novel involvement of PI3K/AKT/mTOR pathway in cancer. Curr Cancer Drug Targets. 2013 Mar;13(3):245–51.
24. Kauffman EC, Lang M, Rais-Bahrami S, Gupta GN, Wei D, Yang Y, et al. Preclinical efficacy of dual mTORC1/2 inhibitor AZD8055 in renal cell carcinoma harboring a TFE3 gene fusion. BMC Cancer . 2019;19(1):917. Available from: https://doi.org/10.1186/s12885-019-6096-0
25. Redmond AM, Carroll JS. Defining and targeting transcription factors in cancer. Genome Biol. 2009;10(7):311.
26. Mariño-Ramírez L, Kann MG, Shoemaker BA, Landsman D. Histone structure and nucleosome stability. Expert Rev Proteomics . 2005 Oct;2(5):719–29. Available from: https://www.ncbi.nlm.nih.gov/pubmed/16209651
27. Lambert M, Jambon S, Depauw S, David-Cordonnier M-H. Targeting Transcription Factors for Cancer Treatment. Molecules . 2018 Jun 19;23(6):1479. Available from: https://www.ncbi.nlm.nih.gov/pubmed/29921764
28. Dong X, Weng Z. The correlation between histone modifications and gene expression. Epigenomics . 2013 Apr;5(2):113–6. Available from: https://www.ncbi.nlm.nih.gov/pubmed/23566087
29. Ellenbroek B, Youn J. Chapter 5 - Environment Challenges and the Brain. In: Ellenbroek B, Youn JBT-G-EI in P, editors. San Diego: Academic Press; 2016. p. 107–39. Available from: http://www.sciencedirect.com/science/article/pii/B9780128016572000057
30. Chen HP, Zhao YT, Zhao TC. Histone deacetylases and mechanisms of regulation of gene expression. Crit Rev Oncog . 2015;20(1–2):35–47. Available from: https://www.ncbi.nlm.nih.gov/pubmed/25746103
31. Yoo Y-G, Kong G, Lee M-O. Metastasis-associated protein 1 enhances stability of hypoxia-inducible factor-1alpha protein by recruiting histone deacetylase 1. EMBO J. 2006 Mar;25(6):1231–41.
32. Chen S, Yin C, Lao T, Liang D, He D, Wang C, et al. AMPK-HDAC5 pathway

facilitates nuclear accumulation of HIF-1alpha and functional activation of HIF-1 by deacetylating Hsp70 in the cytosol. Cell Cycle. 2015 Aug;14(15):2520–36.
33. Desterro JM, Rodriguez MS, Hay RT. Regulation of transcription factors by protein degradation. Cell Mol Life Sci. 2000 Aug;57(8–9):1207–19.
34. Tomar D, Singh R. Chapter 20 - TRIM13, Novel Tumor Suppressor: Regulator of Autophagy and Cell Death. In: Hayat MA, editor. Autophagy: Cancer, Other Pathologies, Inflammation, Immunity, Infection, and Aging . Amsterdam: Academic Press; 2014. p. 293–304. Available from: http://www.sciencedirect.com/science/article/pii/B9780124055308000200
35. Zhou N, Gutierrez-Uzquiza A, Zheng XY, Chang R, Vogl DT, Garfall AL, et al. RUNX proteins desensitize multiple myeloma to lenalidomide via protecting IKZFs from degradation. Leukemia . 2019;33(8):2006–21. Available from: https://doi.org/10.1038/s41375-019-0403-2
36. Krönke J, Udeshi ND, Narla A, Grauman P, Hurst SN, McConkey M, et al. Lenalidomide causes selective degradation of IKZF1 and IKZF3 in multiple myeloma cells. Science . 2013/11/29. 2014 Jan 17;343(6168):301–5. Available from: https://www.ncbi.nlm.nih.gov/pubmed/24292625
37. Palumbo A, Facon T, Sonneveld P, Bladè J, Offidani M, Gay F, et al. Thalidomide for treatment of multiple myeloma: 10 years later. Blood . 2008 Apr 15;111(8):3968–77. Available from: https://doi.org/10.1182/blood-2007-10-117457
38. Fischer ES, Bohm K, Lydeard JR, Yang H, Stadler MB, Cavadini S, et al. Structure of the DDB1-CRBN E3 ubiquitin ligase in complex with thalidomide. Nature. 2014 Aug;512(7512):49–53.
39. Hamilton PL, Arya DP. Natural product DNA major groove binders. Nat Prod Rep. 2012;29(2):134–43.
40. Owen EA, Burley GA, Carver JA, Wickham G, Keniry MA. Structural investigation of the hedamycin:d(ACCGGT)2 complex by NMR and restrained molecular dynamics. Biochem Biophys Res Commun. 2002 Feb;290(5):1602–8.
41. Rosenberg B, VanCamp L, Trosko JE, Mansour VH. Platinum compounds: a new class of potent antitumour agents. Nature. 1969 Apr;222(5191):385–6.
42. Aisner J, Abrams J. Cisplatin for small-cell lung cancer. Semin Oncol. 1989 Aug;16(4 Suppl 6):2–9.
43. Kim RH, Lee YW, Lee DC, Kim NH, Choi JS, Joo SK, et al. Advanced gastric carcinoma chemotherapy with cisplatin, mitomycin C, BCNU, and 5-fluorouracil in combination. Korean J Intern Med . 1987 Jan;2(1):48–51. Available from: https://www.ncbi.nlm.nih.gov/pubmed/3154817
44. Velasquez WS, Cabanillas F, Salvador P, McLaughlin P, Fridrik M, Tucker S, et al. Effective salvage therapy for lymphoma with cisplatin in combination with high-dose Ara-C and dexamethasone (DHAP). Blood. 1988 Jan;71(1):117–22.
45. Wing RM, Pjura P, Drew HR, Dickerson RE. The primary mode of binding of cisplatin to a B-DNA dodecamer: C-G-C-G-A-A-T-T-C-G-C-G. EMBO J . 1984 May;3(5):1201–6. Available from: https://www.ncbi.nlm.nih.gov/pubmed/6539674
46. Dasari S, Tchounwou PB. Cisplatin in cancer therapy: molecular mechanisms of action. Eur J Pharmacol . 2014/07/21. 2014 Oct 5;740:364–78. Available from: https://www.ncbi.nlm.nih.gov/pubmed/25058905

47. Yap JL, Chauhan J, Jung K-Y, Chen L, Prochownik E V, Fletcher S. Small-molecule inhibitors of dimeric transcription factors: Antagonism of protein–protein and protein–DNA interactions. Medchemcomm . 2012;3(5):541–51. Available from: http://dx.doi.org/10.1039/C2MD00289B
48. Chen H, Liu H, Qing G. Targeting oncogenic Myc as a strategy for cancer treatment. Signal Transduct Target Ther . 2018;3(1):5. Available from: https://doi.org/10.1038/s41392-018-0008-7
49. Nair SK, Burley SK. X-ray structures of Myc-Max and Mad-Max recognizing DNA. Molecular bases of regulation by proto-oncogenic transcription factors. Cell. 2003 Jan;112(2):193–205.
50. Grandori C, Cowley SM, James LP, Eisenman RN. The Myc/Max/Mad network and the transcriptional control of cell behavior. Annu Rev Cell Dev Biol. 2000;16:653–99.
51. Yin X, Giap C, Lazo JS, Prochownik E V. Low molecular weight inhibitors of Myc-Max interaction and function. Oncogene. 2003 Sep;22(40):6151–9.
52. D'Agnano I, Valentini A, Gatti G, Chersi A, Felsani A. Oligopeptides impairing the Myc-Max heterodimerization inhibit lung cancer cell proliferation by reducing Myc transcriptional activity. J Cell Physiol. 2007 Jan;210(1):72–80.
53. Wang H, Teriete P, Hu A, Raveendra-Panickar D, Pendelton K, Lazo JS, et al. Direct inhibition of c-Myc-Max heterodimers by celastrol and celastrol-inspired triterpenoids. Oncotarget. 2015 Oct;6(32):32380–95.
54. Lane DP. Cancer. p53, guardian of the genome. Vol. 358, Nature. England; 1992. p. 15–6.
55. Yeo CQX, Alexander I, Lin Z, Lim S, Aning OA, Kumar R, et al. p53 Maintains Genomic Stability by Preventing Interference between Transcription and Replication. Cell Rep . 2016;15(1):132–46. Available from: http://www.sciencedirect.com/science/article/pii/S2211124716302522
56. Ozaki T, Nakagawara A. Role of p53 in Cell Death and Human Cancers. Cancers (Basel) . 2011 Mar 3;3(1):994–1013. Available from: https://www.ncbi.nlm.nih.gov/pubmed/24212651
57. Elbendary AA, Cirisano FD, Evans ACJ, Davis PL, Iglehart JD, Marks JR, et al. Relationship between p21 expression and mutation of the p53 tumor suppressor gene in normal and malignant ovarian epithelial cells. Clin Cancer Res. 1996 Sep;2(9):1571–5.
58. Momand J, Zambetti GP, Olson DC, George D, Levine AJ. The mdm-2 oncogene product forms a complex with the p53 protein and inhibits p53-mediated transactivation. Cell. 1992 Jun;69(7):1237–45.
59. Picksley SM, Lane DP. What the papers say: The p53-mdm2 autoregulatory feedback loop: A paradigm for the regulation of growth control by p53? BioEssays . 1993 Oct 1;15(10):689–90. Available from: https://doi.org/10.1002/bies.950151008
60. Tortora G, Caputo R, Damiano V, Bianco R, Chen J, Agrawal S, et al. A novel MDM2 anti-sense oligonucleotide has anti-tumor activity and potentiates cytotoxic drugs acting by different mechanisms in human colon cancer. Int J Cancer . 2000 Dec 1;88(5):804–9. Available from: https://doi.org/10.1002/1097-0215(20001201)88:5%3C804::AID-IJC19%3E3.0.CO
61. Dembla V, Somaiah N, Barata P, Hess K, Fu S, Janku F, et al. Prevalence of

MDM2 amplification and coalterations in 523 advanced cancer patients in the MD Anderson phase 1 clinic. Oncotarget . 2018 Sep 4;9(69):33232–43. Available from: https://www.ncbi.nlm.nih.gov/pubmed/30237864
62. Vassilev LT, Vu BT, Graves B, Carvajal D, Podlaski F, Filipovic Z, et al. In vivo activation of the p53 pathway by small-molecule antagonists of MDM2. Science. 2004 Feb;303(5659):844–8.
63. Anil B, Riedinger C, Endicott JA, Noble MEM. The structure of an MDM2-Nutlin-3a complex solved by the use of a validated MDM2 surface-entropy reduction mutant. Acta Crystallogr D Biol Crystallogr. 2013 Aug;69(Pt 8):1358–66.
64. Ray-Coquard I, Blay J-Y, Italiano A, Cesne A Le, Penel N, Zhi J, et al. Effect of the MDM2 antagonist RG7112 on the P53 pathway in patients with MDM2-amplified, well-differentiated or dedifferentiated liposarcoma: an exploratory proof-of-mechanism study. Lancet Oncol . 2012;13(11):1133–40. Available from: http://www.sciencedirect.com/science/article/pii/S1470204512704746
65. Kumar R, Thompson EB. The structure of the nuclear hormone receptors. Steroids . 1999;64(5):310–9. Available from: http://www.sciencedirect.com/science/article/pii/S0039128X99000148
66. Masood S. Estrogen and progesterone receptors in cytology: a comprehensive review. Diagn Cytopathol. 1992;8(5):475–91.
67. Beekman JM, Allan GF, Tsai SY, Tsai MJ, O'Malley BW. Transcriptional activation by the estrogen receptor requires a conformational change in the ligand binding domain. Mol Endocrinol. 1993 Oct;7(10):1266–74.
68. Klinge CM. Estrogen receptor interaction with co-activators and co-repressors. Steroids. 2000 May;65(5):227–51.
69. Dutertre M, Smith CL. Molecular mechanisms of selective estrogen receptor modulator (SERM) action. J Pharmacol Exp Ther. 2000 Nov;295(2):431–7.
70. Shiau AK, Barstad D, Loria PM, Cheng L, Kushner PJ, Agard DA, et al. The structural basis of estrogen receptor/coactivator recognition and the antagonism of this interaction by tamoxifen. Cell. 1998 Dec;95(7):927–37.
71. Heldring N, Pawson T, McDonnell D, Treuter E, Gustafsson J-A, Pike ACW. Structural insights into corepressor recognition by antagonist-bound estrogen receptors. J Biol Chem. 2007 Apr;282(14):10449–55.
72. Carlson RW. The history and mechanism of action of fulvestrant. Clin Breast Cancer. 2005 Apr;6 Suppl 1:S5-8.
73. Chang C, Lee SO, Wang R-S, Yeh S, Chang T-M. Androgen receptor (AR) physiological roles in male and female reproductive systems: lessons learned from AR-knockout mice lacking AR in selective cells. Biol Reprod . 2013 Jul 25;89(1):21. Available from: https://www.ncbi.nlm.nih.gov/pubmed/23782840
74. Heinlein CA, Chang C. Androgen receptor in prostate cancer. Endocr Rev. 2004 Apr;25(2):276–308.
75. Bohl CE, Gao W, Miller DD, Bell CE, Dalton JT. Structural basis for antagonism and resistance of bicalutamide in prostate cancer. Proc Natl Acad Sci U S A. 2005 Apr;102(17):6201–6.
76. Balbas MD, Evans MJ, Hosfield DJ, Wongvipat J, Arora VK, Watson PA, et al. Overcoming mutation-based resistance to antiandrogens with rational drug design. Elife. 2013 Apr;2:e00499.
77. Li H, Ban F, Dalal K, Leblanc E, Frewin K, Ma D, et al. Discovery of Small-

Molecule Inhibitors Selectively Targeting the DNA-Binding Domain of the Human Androgen Receptor. J Med Chem . 2014 Aug 14;57(15):6458–67. Available from: https://doi.org/10.1021/jm500802j
78. Huang W, Dong Z, Wang F, Peng H, Liu J-Y, Zhang J-T. A Small Molecule Compound Targeting STAT3 DNA-Binding Domain Inhibits Cancer Cell Proliferation, Migration, and Invasion. ACS Chem Biol . 2014 May 16;9(5):1188–96. Available from: https://doi.org/10.1021/cb500071v
79. Grimley E, Liao C, Ranghini EJ, Nikolovska-Coleska Z, Dressler GR. Inhibition of Pax2 Transcription Activation with a Small Molecule that Targets the DNA Binding Domain. ACS Chem Biol . 2017/01/24. 2017 Mar 17;12(3):724–34. Available from: https://www.ncbi.nlm.nih.gov/pubmed/28094913
80. Hueber P-A, Iglesias D, Chu LL, Eccles M, Goodyer P. In vivo validation of PAX2 as a target for renal cancer therapy. Cancer Lett . 2008;265(1):148–55. Available from: http://www.sciencedirect.com/science/article/pii/S0304383508001043
81. Hueber P-A, Waters P, Clark P, Eccles M, Goodyer P. PAX2 inactivation enhances cisplatin-induced apoptosis in renal carcinoma cells. Kidney Int. 2006 Apr;69(7):1139–45.
82. Lam EW-F, Brosens JJ, Gomes AR, Koo C-Y. Forkhead box proteins: tuning forks for transcriptional harmony. Nat Rev Cancer . 2013 Jun 24;13:482. Available from: https://doi.org/10.1038/nrc3539
83. Martins R, Lithgow GJ, Link W. Long live FOXO: unraveling the role of FOXO proteins in aging and longevity. Aging Cell . 2015/12/08. 2016 Apr;15(2):196–207. Available from: https://www.ncbi.nlm.nih.gov/pubmed/26643314
84. Nakagawa S, Gisselbrecht SS, Rogers JM, Hartl DL, Bulyk ML. DNA-binding specificity changes in the evolution of forkhead transcription factors. Proc Natl Acad Sci U S A . 2013/07/08. 2013 Jul 23;110(30):12349–54. Available from: https://www.ncbi.nlm.nih.gov/pubmed/23836653
85. Kaestner KH, Knöchel W, Martínez DE. Unified nomenclature for the winged helix/forkhead transcription factors. Genes Dev . 2000;14(2):142–6. Available from: http://genesdev.cshlp.org/content/14/2/142.short
86. Laissue P. The forkhead-box family of transcription factors: key molecular players in colorectal cancer pathogenesis. Mol Cancer . 2019 Jan 8;18(1):5. Available from: https://www.ncbi.nlm.nih.gov/pubmed/30621735
87. Jackson BC, Carpenter C, Nebert DW, Vasiliou V. Update of human and mouse forkhead box (FOX) gene families. Hum Genomics . 2010 Jun;4(5):345–52. Available from: https://www.ncbi.nlm.nih.gov/pubmed/20650821
88. Zhang W, Duan N, Song T, Li Z, Zhang C, Chen X. The Emerging Roles of Forkhead Box (FOX) Proteins in Osteosarcoma. J Cancer . 2017 Jun 3;8(9):1619–28. Available from: https://www.ncbi.nlm.nih.gov/pubmed/28775781
89. Friedman JR, Kaestner KH. The Foxa family of transcription factors in development and metabolism. Cell Mol Life Sci C . 2006;63(19):2317–28. Available from: https://doi.org/10.1007/s00018-006-6095-6
90. Hu Q, Luo Z, Xu T, Zhang J-Y, Zhu Y, Chen W-X, et al. FOXA1: a promising prognostic marker in breast cancer. Asian Pac J Cancer Prev. 2014;15(1):11–6.
91. Wang B, Liu G, Ding L, Zhao J, Lu Y. FOXA2 promotes the proliferation, migration and invasion, and epithelial mesenchymal transition in colon cancer. Exp Ther Med . 2018/05/11. 2018 Jul;16(1):133–40. Available from:

https://www.ncbi.nlm.nih.gov/pubmed/29896233
92. Garon G, Bergeron F, Brousseau C, Robert NM, Tremblay JJ. FOXA3 Is Expressed in Multiple Cell Lineages in the Mouse Testis and Regulates Pdgfra Expression in Leydig Cells. Endocrinology . 2017 Apr 3;158(6):1886–97. Available from: https://doi.org/10.1210/en.2016-1736
93. Wolf I, Bose S, Williamson EA, Miller CW, Koeffler HP. FOXA1 expression and activities in breast cancer. Cancer Res . 2005 May 1;65(9 Supplement):17 LP – 17. Available from: http://cancerres.aacrjournals.org/content/65/9_Supplement/17.1.abstract
94. Li J, Zhang S, Zhu L, Ma S. Role of transcription factor FOXA1 in non-small cell lung cancer. Mol Med Rep. 2018;17(1):509–21.
95. Vorvis C, Hatziapostolou M, Mahurkar-Joshi S, Koutsioumpa M, Williams J, Donahue TR, et al. Transcriptomic and CRISPR/Cas9 technologies reveal FOXA2 as a tumor suppressor gene in pancreatic cancer. Am J Physiol Liver Physiol . 2016 May 5;310(11):G1124–37. Available from: https://doi.org/10.1152/ajpgi.00035.2016
96. Wang J, Zhu C-P, Hu P-F, Qian H, Ning B-F, Zhang Q, et al. FOXA2 suppresses the metastasis of hepatocellular carcinoma partially through matrix metalloproteinase-9 inhibition. Carcinogenesis . 2014;35(11):2576–83. Available from: https://doi.org/10.1093/carcin/bgu180
97. Li J, Dantas Machado AC, Guo M, Sagendorf JM, Zhou Z, Jiang L, et al. Structure of the Forkhead Domain of FOXA2 Bound to a Complete DNA Consensus Site. Biochemistry. 2017 Jul;56(29):3745–53.
98. Chen B, Yu J, Lu L, Dong F, Zhou F, Tao X, et al. Upregulated forkhead-box A3 elevates the expression of forkhead-box A1 and forkhead-box A2 to promote metastasis in esophageal cancer. Oncol Lett . 2019/02/26. 2019 May;17(5):4351–60. Available from: https://www.ncbi.nlm.nih.gov/pubmed/30944629
99. Smith RS, Zabaleta A, Kume T, Savinova O V, Kidson SH, Martin JE, et al. Haploinsufficiency of the transcription factors FOXC1 and FOXC2 results in aberrant ocular development. Hum Mol Genet. 2000 Apr;9(7):1021–32.
100. Tümer Z, Bach-Holm D. Axenfeld-Rieger syndrome and spectrum of PITX2 and FOXC1 mutations. Eur J Hum Genet . 2009/06/10. 2009 Dec;17(12):1527–39. Available from: https://www.ncbi.nlm.nih.gov/pubmed/19513095
101. Aldinger KA, Lehmann OJ, Hudgins L, Chizhikov V V, Bassuk AG, Ades LC, et al. FOXC1 is required for normal cerebellar development and is a major contributor to chromosome 6p25.3 Dandy-Walker malformation. Nat Genet. 2009 Sep;41(9):1037–42.
102. Han B, Qu Y, Jin Y, Yu Y, Deng N, Wawrowsky K, et al. FOXC1 Activates Smoothened-Independent Hedgehog Signaling in Basal-like Breast Cancer. Cell Rep. 2015 Nov;13(5):1046–58.
103. Xia L, Huang W, Tian D, Zhu H, Qi X, Chen Z, et al. Overexpression of forkhead box C1 promotes tumor metastasis and indicates poor prognosis in hepatocellular carcinoma. Hepatology. 2013 Feb;57(2):610–24.
104. Huang W, Chen Z, Zhang L, Tian D, Wang D, Fan D, et al. Interleukin-8 Induces Expression of FOXC1 to Promote Transactivation of CXCR1 and CCL2 in Hepatocellular Carcinoma Cell Lines and Formation of Metastases in Mice. Gastroenterology. 2015 Oct;149(4):1053-67.e14.

105. Chung TKH, Lau TS, Cheung TH, Yim SF, Lo KWK, Siu NSS, et al. Dysregulation of microRNA-204 mediates migration and invasion of endometrial cancer by regulating FOXC1. Int J cancer. 2012 Mar;130(5):1036–45.
106. Chen X, Wei H, Li J, Liang X, Dai S, Jiang L, et al. Structural basis for DNA recognition by FOXC2. Nucleic Acids Res. 2019 Apr;47(7):3752–64.
107. Norrmén C, Ivanov KI, Cheng J, Zangger N, Delorenzi M, Jaquet M, et al. FOXC2 controls formation and maturation of lymphatic collecting vessels through cooperation with NFATc1. J Cell Biol . 2009/04/27. 2009 May 4;185(3):439–57. Available from: https://www.ncbi.nlm.nih.gov/pubmed/19398761
108. Li W, Fu X, Liu R, Wu C, Bai J, Xu Y, et al. FOXC2 often overexpressed in glioblastoma enhances proliferation and invasion in glioblastoma cells. Oncol Res. 2013;21(2):111–20.
109. Cui Y-M, Jiang D, Zhang S-H, Wu P, Ye Y-P, Chen C-M, et al. FOXC2 promotes colorectal cancer proliferation through inhibition of FOXO3a and activation of MAPK and AKT signaling pathways. Cancer Lett. 2014 Oct;353(1):87–94.
110. Obsil T, Obsilova V. Structure/function relationships underlying regulation of FOXO transcription factors. Oncogene . 2008;27(16):2263–75. Available from: https://doi.org/10.1038/onc.2008.20
111. Tissenbaum HA. Chapter One - DAF-16: FOXO in the Context of C. elegans. In: Ghaffari SBT-CT in DB, editor. Forkhead FOXO Transcription Factors in Development and Disease . Academic Press; 2018. p. 1–21. Available from: http://www.sciencedirect.com/science/article/pii/S0070215317300698
112. Brent MM, Anand R, Marmorstein R. Structural basis for DNA recognition by FoxO1 and its regulation by posttranslational modification. Structure . 2008 Sep 10;16(9):1407–16. Available from: https://www.ncbi.nlm.nih.gov/pubmed/18786403
113. Furuyama T, Nakazawa T, Nakano I, Mori N. Identification of the differential distribution patterns of mRNAs and consensus binding sequences for mouse DAF-16 homologues. Biochem J. 2000 Jul;349(Pt 2):629–34.
114. Van Der Heide LP, Hoekman MFM, Smidt MP. The ins and outs of FoxO shuttling: mechanisms of FoxO translocation and transcriptional regulation. Biochem J. 2004 Jun;380(Pt 2):297–309.
115. Brunet A, Bonni A, Zigmond MJ, Lin MZ, Juo P, Hu LS, et al. Akt promotes cell survival by phosphorylating and inhibiting a Forkhead transcription factor. Cell. 1999 Mar;96(6):857–68.
116. Zhao X, Gan L, Pan H, Kan D, Majeski M, Adam SA, et al. Multiple elements regulate nuclear/cytoplasmic shuttling of FOXO1: characterization of phosphorylation- and 14-3-3-dependent and -independent mechanisms. Biochem J. 2004 Mar;378(Pt 3):839–49.
117. Obsil T, Ghirlando R, Anderson DE, Hickman AB, Dyda F. Two 14-3-3 binding motifs are required for stable association of Forkhead transcription factor FOXO4 with 14-3-3 proteins and inhibition of DNA binding. Biochemistry. 2003 Dec;42(51):15264–72.
118. Rena G, Guo S, Cichy SC, Unterman TG, Cohen P. Phosphorylation of the transcription factor forkhead family member FKHR by protein kinase B. J Biol Chem. 1999 Jun;274(24):17179–83.
119. Tang ED, Nunez G, Barr FG, Guan KL. Negative regulation of the forkhead

transcription factor FKHR by Akt. J Biol Chem. 1999 Jun;274(24):16741–6.
120. Silhan J, Vacha P, Strnadova P, Vecer J, Herman P, Sulc M, et al. 14-3-3 protein masks the DNA binding interface of forkhead transcription factor FOXO4. J Biol Chem . 2009/05/05. 2009 Jul 17;284(29):19349–60. Available from: https://www.ncbi.nlm.nih.gov/pubmed/19416966
121. Monsalve M, Olmos Y. The complex biology of FOXO. Curr Drug Targets. 2011 Aug;12(9):1322–50.
122. Paik J-H, Kollipara R, Chu G, Ji H, Xiao Y, Ding Z, et al. FoxOs are lineage-restricted redundant tumor suppressors and regulate endothelial cell homeostasis. Cell. 2007 Jan;128(2):309–23.
123. Renault VM, Thekkat PU, Hoang KL, White JL, Brady CA, Kenzelmann Broz D, et al. The pro-longevity gene FoxO3 is a direct target of the p53 tumor suppressor. Oncogene . 2011/03/21. 2011 Jul 21;30(29):3207–21. Available from: https://www.ncbi.nlm.nih.gov/pubmed/21423206
124. Vandenberg CJ, Motoyama N, Cory S. FoxO3 suppresses Myc-driven lymphomagenesis. Cell Death Dis . 2016;7(1):e2046–e2046. Available from: https://doi.org/10.1038/cddis.2015.396
125. Guan H, Tan P, Xie L, Mi B, Fang Z, Li J, et al. FOXO1 inhibits osteosarcoma oncogenesis via Wnt/β-catenin pathway suppression. Oncogenesis . 2015;4(9):e166–e166. Available from: https://doi.org/10.1038/oncsis.2015.25
126. Yan F, Liao R, Farhan M, Wang T, Chen J, Wang Z, et al. Elucidating the role of the FoxO3a transcription factor in the IGF-1-induced migration and invasion of uveal melanoma cancer cells. Biomed Pharmacother . 2016;84:1538–50. Available from: http://www.sciencedirect.com/science/article/pii/S0753332216314731
127. Santo EE, Stroeken P, Sluis P V, Koster J, Versteeg R, Westerhout EM. FOXO3a Is a Major Target of Inactivation by PI3K/AKT Signaling in Aggressive Neuroblastoma. Cancer Res . 2013 Apr 1;73(7):2189 LP – 2198. Available from: http://cancerres.aacrjournals.org/content/73/7/2189.abstract
128. Shukla S, Bhaskaran N, Maclennan GT, Gupta S. Deregulation of FoxO3a accelerates prostate cancer progression in TRAMP mice. Prostate. 2013 Oct;73(14):1507–17.
129. Qian Z, Ren L, Wu D, Yang X, Zhou Z, Nie Q, et al. Overexpression of FoxO3a is associated with glioblastoma progression and predicts poor patient prognosis. Int J Cancer . 2017 Jun 15;140(12):2792–804. Available from: https://doi.org/10.1002/ijc.30690
130. Trinh DL, Scott DW, Morin RD, Mendez-Lago M, An J, Jones SJM, et al. Analysis of FOXO1 mutations in diffuse large B-cell lymphoma. Blood . 2013/03/04. 2013 May 2;121(18):3666–74. Available from: https://www.ncbi.nlm.nih.gov/pubmed/23460611
131. Santamaria CM, Chillon MC, Garcia-Sanz R, Perez C, Caballero MD, Ramos F, et al. High FOXO3a expression is associated with a poorer prognosis in AML with normal cytogenetics. Leuk Res. 2009 Dec;33(12):1706–9.
132. Storz P, Doppler H, Copland JA, Simpson KJ, Toker A. FOXO3a promotes tumor cell invasion through the induction of matrix metalloproteinases. Mol Cell Biol. 2009 Sep;29(18):4906–17.
133. Feng X, Wu Z, Wu Y, Hankey W, Prior TW, Li L, et al. Cdc25A Regulates Matrix Metalloprotease 1 through Foxo1 and Mediates Metastasis of Breast Cancer Cells.

Mol Cell Biol . 2011 Aug 15;31(16):3457 LP – 3471. Available from: http://mcb.asm.org/content/31/16/3457.abstract
134. Littler DR, Alvarez-Fernández M, Stein A, Hibbert RG, Heidebrecht T, Aloy P, et al. Structure of the FoxM1 DNA-recognition domain bound to a promoter sequence. Nucleic Acids Res. 2010;38(13):4527–38.
135. Clark KL, Halay ED, Lai E, Burley SK. Co-crystal structure of the HNF-3/fork head DNA-recognition motif resembles histone H5. Nature . 1993;364(6436):412–20. Available from: https://doi.org/10.1038/364412a0
136. Yao K, Sha M, Lu Z, Wong GG. Molecular Analysis of a Novel Winged Helix Protein , WIN EXPRESSION PATTERN , DNA BINDING PROPERTY , AND ALTERNATIVE SPLICING WITHIN. 1997;272(32):19827–36.
137. Zhang X, Zhang L, Du Y, Zheng H, Zhang P, Sun Y, et al. A novel FOXM1 isoform, FOXM1D, promotes epithelial-mesenchymal transition and metastasis through ROCKs activation in colorectal cancer. Oncogene. 2017 Feb;36(6):807–19.
138. Ye H, Kelly TF, Samadani U, Lim L, Rubio S, Overdier DG, et al. Hepatocyte nuclear factor 3/fork head homolog 11 is expressed in proliferating epithelial and mesenchymal cells of embryonic and adult tissues. Mol Cell Biol . 1997;17(3):1626–41. Available from: https://mcb.asm.org/content/mcb/17/3/1626.full.pdf
139. Zhang X, Zhang L, Du Y, Zheng H, Zhang P, Sun Y, et al. A novel FOXM1 isoform, FOXM1D, promotes epithelial-mesenchymal transition and metastasis through ROCKs activation in colorectal cancer. Oncogene. 2017;36(6):807–19.
140. Wierstra I, Alves J. FOXM1c transactivates the human c-myc promoter directly via the two TATA boxes P1 and P2. FEBS J. 2006 Oct;273(20):4645–67.
141. Laoukili J, Stahl M, Medema RH. FoxM1: at the crossroads of ageing and cancer. Biochim Biophys Acta. 2007 Jan;1775(1):92–102.
142. Krupczak-Hollis K, Wang X, Dennewitz MB, Costa RH. Growth hormone stimulates proliferation of old-aged regenerating liver through forkhead box m1b. Hepatology. 2003 Dec;38(6):1552–62.
143. Karadedou CT. Regulation of the FOXM1 transcription factor by the estrogen receptor a at the protein level, in breast cancer. Hippokratia . 2006;10(3):128–32. Available from: https://www.scopus.com/inward/record.uri?eid=2-s2.0-33750218109&partnerID=40&md5=00df5740dd98b1f14759800179ca9e76
144. Dibb M, Han N, Choudhury J, Hayes S, Valentine H, West C, et al. The FOXM1-PLK1 axis is commonly upregulated in oesophageal adenocarcinoma. Br J Cancer . 2012;107(10):1766–75. Available from: https://doi.org/10.1038/bjc.2012.424
145. Zhang H, Zhang J, Pope CF, Crawford LA, Vasavada RC, Jagasia SM, et al. Gestational diabetes mellitus resulting from impaired β-cell compensation in the absence of FoxM1, a novel downstream effector of placental lactogen. Diabetes . 2010;59(1):143–52. Available from: https://www.scopus.com/inward/record.uri?eid=2-s2.0-77449086017&doi=10.2337%2Fdb09-0050&partnerID=40&md5=02e1f587cb5b709fbb22766235dc1f77
146. Ackermann Misfeldt A, Costa RH, Gannon M. β-Cell Proliferation, but Not Neogenesis, Following 60% Partial Pancreatectomy Is Impaired in the Absence of FoxM1. Diabetes . 2008 Nov 1;57(11):3069 LP – 3077. Available from:

http://diabetes.diabetesjournals.org/content/57/11/3069.abstract
147. Gieling RG, Elsharkawy AM, Caamaño JH, Cowie DE, Wright MC, Ebrahimkhani MR, et al. The c-Rel subunit of nuclear factor-κB regulates murine liver inflammation, wound-healing, and hepatocyte proliferation. Hepatology . 2010 Mar 1;51(3):922–31. Available from: https://doi.org/10.1002/hep.23385
148. Wang XH, Kiyokawa H, Dennewitz MB, Costa RH. The Forkhead Box m1b transcription factor is essential for hepatocyte DNA replication and mitosis during mouse liver regeneration. Proc Natl Acad Sci U S A . 2002;99(26):16881–6. Available from: https://www.ncbi.nlm.nih.gov/pmc/articles/PMC139238/pdf/pq2602016881.pdf
149. Wierstra, Inken; Alves J. FOXM1, a typical proliferation-associated transcription factor . Vol. 388, Biological Chemistry. 2007. p. 1257. Available from: https://www.degruyter.com/view/j/bchm.2007.388.issue-12/bc.2007.159/bc.2007.159.xml
150. Korver W, Roose J, Clevers H. The winged-helix transcription factor Trident is expressed in cycling cells. Nucleic Acids Res . 1997;25(9):1715–9. Available from: https://www.scopus.com/inward/record.uri?eid=2-s2.0-0030786320&doi=10.1093%2Fnar%2F25.9.1715&partnerID=40&md5=658054588e8f16dcc9a8494d04dc377b
151. Wierstra Inken, Jürgen A. Despite its strong transactivation domain, transcription factor FOXM1c is kept almost inactive by two different inhibitory domains . Vol. 387, Biological Chemistry. 2006. p. 963. Available from: https://www.degruyter.com/view/j/bchm.2006.387.issue-7/bc.2006.120/bc.2006.120.xml
152. Wang Z, Ahmad A, Li Y, Banerjee S, Kong D, Sarkar FH. Forkhead box M1 transcription factor: A novel target for cancer therapy. Cancer Treat Rev . 2010;36(2):151–6. Available from: http://www.sciencedirect.com/science/article/pii/S0305737209001807
153. Laoukili J, Alvarez M, Meijer LAT, Stahl M, Mohammed S, Kleij L, et al. Activation of FoxM1 during G2 requires cyclin A/Cdk-dependent relief of autorepression by the FoxM1 N-terminal domain. Mol Cell Biol . 2008/02/19. 2008 May;28(9):3076–87. Available from: https://www.ncbi.nlm.nih.gov/pubmed/18285455
154. Park HJ, Costa RH, Lau LF, Tyner AL, Raychaudhuri P. Anaphase-promoting complex/cyclosome-CDH1-mediated proteolysis of the forkhead box M1 transcription factor is critical for regulated entry into S phase. Mol Cell Biol . 2008/06/23. 2008 Sep;28(17):5162–71. Available from: https://www.ncbi.nlm.nih.gov/pubmed/18573889
155. Leung TWC, Lin SSW, Tsang ACC, Tong CSW, Ching JCY, Leung WY, et al. Over-expression of FoxM1 stimulates cyclin B1 expression. FEBS Lett. 2001;507(1):59–66.
156. Teh MT, Gemenetzidis E, Patel D, Tariq R, Nadir A, Bahta AW, et al. Foxm1 induces a global methylation signature that mimics the cancer epigenome in head and neck squamous cell carcinoma. PLoS One. 2012;7(3):1–9.
157. Zhang N, Wei P, Gong A, Chiu W-T, Lee H-T, Colman H, et al. FoxM1 promotes beta-catenin nuclear localization and controls Wnt target-gene expression and glioma tumorigenesis. Cancer Cell. 2011 Oct;20(4):427–42.

158. Xue J, Lin X, Chiu W-T, Chen Y-H, Yu G, Liu M, et al. Sustained activation of SMAD3/SMAD4 by FOXM1 promotes TGF-beta-dependent cancer metastasis. J Clin Invest. 2014 Feb;124(2):564–79.
159. Marceau AH, Brison CM, Nerli S, Arsenault HE, McShan AC, Chen E, et al. An order-to-disorder structural switch activates the FoxM1 transcription factor. Elife. 2019 May;8.
160. Tan Y, Raychaudhuri P, Costa RH. Chk2 mediates stabilization of the FoxM1 transcription factor to stimulate expression of DNA repair genes. Mol Cell Biol. 2007;27(3):1007–16.
161. Arceci A, Bonacci T, Wang X, Stewart K, Damrauer JS, Hoadley KA, et al. FOXM1 Deubiquitination by USP21 Regulates Cell Cycle Progression and Paclitaxel Sensitivity in Basal-like Breast Cancer. Cell Rep. 2019 Mar;26(11):3076-3086.e6.
162. Bhat UG, Jagadeeswaran R, Halasi M, Gartel AL. Nucleophosmin interacts with FOXM1 and modulates the level and localization of FOXM1 in human cancer cells. J Biol Chem. 2011 Dec;286(48):41425–33.
163. Halasi M, Váraljai R, Benevolenskaya E, Gartel AL. A Novel Function of Molecular Chaperone HSP70: SUPPRESSION OF ONCOGENIC FOXM1 AFTER PROTEOTOXIC STRESS. J Biol Chem . 2015/11/11. 2016 Jan 1;291(1):142–8. Available from: https://www.ncbi.nlm.nih.gov/pubmed/26559972
164. Halasi M, Gartel AL. A novel mode of FoxM1 regulation: Positive auto-regulatory loop. Cell Cycle. 2009;8(12):1966–7.
165. Pandit B, Halasi M, Gartel AL. p53 negatively regulates expression of FoxM1. Vol. 8, Cell cycle (Georgetown, Tex.). United States; 2009. p. 3425–7.
166. Wierstra I. Chapter Three - The Transcription Factor FOXM1 (Forkhead box M1): Proliferation-Specific Expression, Transcription Factor Function, Target Genes, Mouse Models, and Normal Biological Roles**The present chapter is Part I of a two-part review on the transcri. In: Tew KD, Fisher PBBT-A in CR, editors. Academic Press; 2013. p. 97–398. Available from: http://www.sciencedirect.com/science/article/pii/B9780124071735000042
167. Lam AKY, Ngan AWL, Leung M-H, Kwok DCT, Liu VWS, Chan DW, et al. FOXM1b, which is present at elevated levels in cancer cells, has a greater transforming potential than FOXM1c. Front Oncol . 2013;3(January):11. Available from: http://www.pubmedcentral.nih.gov/articlerender.fcgi?artid=3560383&tool=pmcentrez&rendertype=abstract
168. Wonsey DR, Follettie MT. Loss of the forkhead transcription factor FoxM1 causes centrosome amplification and mitotic catastrophe. Cancer Res. 2005;65(12):5181–9.
169. Tassi RA, Todeschini P, Siegel ER, Calza S, Cappella P, Ardighieri L, et al. FOXM1 expression is significantly associated with chemotherapy resistance and adverse prognosis in non-serous epithelial ovarian cancer patients. Vol. 36, Journal of Experimental & Clinical Cancer Research : CR. London; 2017.
170. Liu Y, Liu Y, Yuan B, Yin L, Peng Y, Yu X, et al. FOXM1 promotes the progression of prostate cancer by regulating PSA gene transcription. Oncotarget. 2017 Mar;8(10):17027–37.

171. Zhang Y, Qiao W-B, Shan L. Expression and functional characterization of FOXM1 in non-small cell lung cancer. Onco Targets Ther . 2018 Jun 11;11:3385–93. Available from: https://www.ncbi.nlm.nih.gov/pubmed/29928129
172. Miyashita A, Fukushima S, Nakahara S, Yamashita J, Tokuzumi A, Aoi J, et al. Investigation of FOXM1 as a Potential New Target for Melanoma. PLoS One . 2015 Dec 7;10(12):e0144241. Available from: https://doi.org/10.1371/journal.pone.0144241
173. Uddin S, Hussain AR, Ahmed M, Siddiqui K, Al-Dayel F, Bavi P, et al. Overexpression of FoxM1 offers a promising therapeutic target in diffuse large B-cell lymphoma. Haematologica. 2012 Jul;97(7):1092–100.
174. Buchner M, Park E, Geng H, Klemm L, Flach J, Passegué E, et al. Identification of FOXM1 as a therapeutic target in B-cell lineage acute lymphoblastic leukaemia. Nat Commun . 2015;6(1):6471. Available from: https://doi.org/10.1038/ncomms7471
175. Wang L, Liu Y, Yu G. Avasimibe inhibits tumor growth by targeting FoxM1-AKR1C1 in osteosarcoma. Onco Targets Ther . 2019 Jan 24;12:815–23. Available from: https://www.ncbi.nlm.nih.gov/pubmed/30774369
176. Xia J-T, Wang H, Liang L-J, Peng B-G, Wu Z-F, Chen L-Z, et al. Overexpression of FOXM1 Is Associated With Poor Prognosis and Clinicopathologic Stage of Pancreatic Ductal Adenocarcinoma. Pancreas . 2012;41(4). Available from: https://journals.lww.com/pancreasjournal/Fulltext/2012/05000/Overexpression_of_FOXM1_Is_Associated_With_Poor.20.aspx
177. Kocarslan S, Guldur M, Ekinci T, Ciftci H, Ozardali H. Comparison of clinicopathological parameters with FoxM1 expression in renal cell carcinoma. J Cancer Res Ther . 2014 Oct 1;10(4):1076–81. Available from: http://www.cancerjournal.net/article.asp?issn=0973-1482
178. Yang K, Jiang B, Lu Y, Shu Q, Zhai P, Zhi Q, et al. FOXM1 promotes the growth and metastasis of colorectal cancer via activation of beta-catenin signaling pathway. Cancer Manag Res. 2019;11:3779–90.
179. DW C, SYM Y, PM C, KM Y, VWS L, ANY C, et al. Over-expression of FOXM1 transcription factor is associated with cervical cancer progression and pathogenesis. J Pathol . 215(3):245–52. Available from: https://onlinelibrary.wiley.com/doi/abs/10.1002/path.2355
180. Liu M, Dai B, Kang S-H, Ban K, Huang F-J, Lang FF, et al. FoxM1B Is Overexpressed in Human Glioblastomas and Critically Regulates the Tumorigenicity of Glioma Cells. Cancer Res . 2006;66(7):3593–602. Available from: http://cancerres.aacrjournals.org/content/66/7/3593.full.pdf+html
181. Hui MKC, Chan KW, Luk JM, Lee NP, Chung Y, Cheung LCM, et al. Cytoplasmic forkhead box M1 (FoxM1) in esophageal squamous cell carcinoma significantly correlates with pathological disease stage. World J Surg. 2012;36(1):90–7.
182. Jiang L-Z, Wang P, Deng B, Huang C, Tang W-X, Lu H-Y, et al. Overexpression of Forkhead Box M1 transcription factor and nuclear factor–κB in laryngeal squamous cell carcinoma: a potential indicator for poor prognosis. Hum Pathol . 2011;42(8):1185–93. Available from: http://www.sciencedirect.com/science/article/pii/S004681771000434X
183. Chan DW, Hui WWY, Wang JJ, Yung MMH, Hui LMN, Qin Y, et al. DLX1 acts as a crucial target of FOXM1 to promote ovarian cancer aggressiveness by

enhancing TGF-β/SMAD4 signaling. Oncogene . 2017;36(10):1404–16. Available from: https://doi.org/10.1038/onc.2016.307
184. Pratheeshkumar P, Divya SP, Parvathareddy SK, Alhoshani NM, Al-Badawi IA, Tulbah A, et al. FoxM1 and β-catenin predicts aggressiveness in Middle Eastern ovarian cancer and their co-targeting impairs the growth of ovarian cancer cells. Oncotarget . 2017 Dec 16;9(3):3590–604. Available from: https://www.ncbi.nlm.nih.gov/pubmed/29423068
185. Fei B, He X, Ma Jie, Zhang M, Chai R. FoxM1 is associated with metastasis in colorectal cancer through induction of the epithelial-mesenchymal transition. Oncol Lett. 2017;14:6553–61.
186. Jiang L, Wang P, Chen H. Overexpression of FOXM1 is associated with metastases of nasopharyngeal carcinoma. Ups J Med Sci . 2014 Nov 1;119(4):324–32. Available from: https://doi.org/10.3109/03009734.2014.960053
187. Yu J, Deshmukh H, Payton JE, Dunham C, Scheithauer BW, Tihan T, et al. Array-Based Comparative Genomic Hybridization Identifies CDK4 and FOXM1 Alterations as Independent Predictors of Survival in Malignant Peripheral Nerve Sheath Tumor. Clin Cancer Res . 2011 Apr 1;17(7):1924 LP – 1934. Available from: http://clincancerres.aacrjournals.org/content/17/7/1924.abstract
188. Yang DK, Son CH, Lee SK, Choi PJ, Lee KE, Roh MS. Forkhead box M1 expression in pulmonary squamous cell carcinoma: correlation with clinicopathologic features and its prognostic significance. Hum Pathol . 2009;40(4):464–70. Available from: http://www.sciencedirect.com/science/article/pii/S0046817708004498
189. Liao G-B, Li X-Z, Zeng S, Liu C, Yang S-M, Yang L, et al. Regulation of the master regulator FOXM1 in cancer. Cell Commun Signal . 2018;16(1):57. Available from: https://doi.org/10.1186/s12964-018-0266-6
190. Gusarova GA, Wang I-C, Major ML, Kalinichenko V V, Ackerson T, Petrovic V, et al. A cell-penetrating ARF peptide inhibitor of FoxM1 in mouse hepatocellular carcinoma treatment. J Clin Invest. 2007 Jan;117(1):99–111.
191. Kalinichenko V V, Major ML, Wang X, Petrovic V, Kuechle J, Yoder HM, et al. Foxm1b transcription factor is essential for development of hepatocellular carcinomas and is negatively regulated by the p19ARF tumor suppressor. Genes Dev. 2004 Apr;18(7):830–50.
192. Yoshida Y, Wang IC, Yoder HM, Davidson NO, Costa RH. The Forkhead Box M1 transcription factor contributes to the development and growth of mouse colorectal cancer. Gastroenterology. 2007;132(4):1420–31.
193. Kim IM, Ackerson T, Ramakrishna S, Tretiakova M, Wang IC, Kalin T V, et al. The Forkhead Box m1 transcription factor stimulates the proliferation of tumor cells during development of lung cancer. Cancer Res . 2006/02/21. 2006;66(4):2153–61. Available from: http://www.ncbi.nlm.nih.gov/pubmed/16489016
194. Nakamura S, Hirano I, Okinaka K, Takemura T, Yokota D, Ono T, et al. The FOXM1 transcriptional factor promotes the proliferation of leukemia cells through modulation of cell cycle progression in acute myeloid leukemia. Carcinogenesis. 2010;31(11):2012–21.
195. Wang Z, Banerjee S, Kong D, Li Y, Sarkar FH. Down-regulation of Forkhead Box M1 transcription factor leads to the inhibition of invasion and angiogenesis of

pancreatic cancer cells. Cancer Res. 2007;67(17):8293–300.
196. Radhakrishnan SK, Bhat UG, Hughes DE, Wang I-C, Costa RH, Gartel AL. Identification of a Chemical Inhibitor of the Oncogenic Transcription Factor Forkhead Box M1. Cancer Res . 2006 Oct 1;66(19):9731 LP – 9735. Available from: http://cancerres.aacrjournals.org/content/66/19/9731.abstract
197. Bhat UG, Halasi M, Gartel AL. Thiazole antibiotics target FoxM1 and induce apoptosis in human cancer cells. PLoS One . 2009/05/18. 2009;4(5):e5592–e5592. Available from: https://www.ncbi.nlm.nih.gov/pubmed/19440351
198. Gartel AL. A new target for proteasome inhibitors: FoxM1. Expert Opin Investig Drugs. 2010;19(2):235–42.
199. Hegde NS, Sanders DA, Rodriguez R, Balasubramanian S. The transcription factor FOXM1 is a cellular target of the natural product thiostrepton. Nat Chem . 2011;3(9):725–31. Available from: https://www.ncbi.nlm.nih.gov/pubmed/21860463
200. Chen Y, Ruben EA, Rajadas J, Teng NNH. Bioorganic & Medicinal Chemistry In silico investigation of FOXM1 binding and novel inhibitors in epithelial ovarian cancer. Bioorg Med Chem . 2015;23(15):4576–82. Available from: http://dx.doi.org/10.1016/j.bmc.2015.06.002
201. Kongsema M, Wongkhieo S, Khongkow M, Lam EW-F, Boonnoy P, Vongsangnak W, et al. Molecular mechanism of Forkhead box M1 inhibition by thiostrepton in breast cancer cells. Oncol Rep. 2019 Sep;42(3):953–62.
202. Ahmad A, Ali S, Wang Z, Ali AS, Sethi S, Sakr WA, et al. 3,3'-Diindolylmethane enhances taxotere-induced growth inhibition of breast cancer cells through downregulation of FoxM1. Int J cancer. 2011 Oct;129(7):1781–91.
203. Petrovic V, Costa RH, Lau LF, Raychaudhuri P, Tyner AL. Negative regulation of the oncogenic transcription factor FoxM1 by thiazolidinediones and mithramycin. Cancer Biol Ther . 2010 Jun 6;9(12):1008–16. Available from: http://www.ncbi.nlm.nih.gov/pmc/articles/PMC3005150/
204. Tian T, Li J, Li B, Wang Y, Li M, Ma D, et al. Genistein exhibits anti-cancer effects via down-regulating FoxM1 in H446 small-cell lung cancer cells. Tumour Biol. 2014 May;35(5):4137–45.
205. Li Y, Ligr M, McCarron JP, Daniels G, Zhang D, Zhao X, et al. Natura-alpha targets forkhead box m1 and inhibits androgen-dependent and -independent prostate cancer growth and invasion. Clin Cancer Res. 2011 Jul;17(13):4414–24.
206. Gormally M V, Dexheimer TS, Marsico G, Sanders DA, Michael S, Jadhav A, et al. Suppression of the FOXM1 transcriptional programme via novel small molecule inhibition. 2014;
207. Sun L, Ren X, Wang I-C, Pradhan A, Zhang Y, Flood HM, et al. The FOXM1 inhibitor RCM-1 suppresses goblet cell metaplasia and prevents IL-13 and STAT6 signaling in allergen-exposed mice. Sci Signal. 2017 Apr;10(475).
208. Shukla S, Milewski D, Pradhan A, Rama N, Rice K, Le T, et al. The FOXM1 inhibitor RCM-1 decreases carcinogenesis and nuclear β-catenin. Mol Cancer Ther . 2019 Jan 1;molcanther.0709.2018. Available from: http://mct.aacrjournals.org/content/early/2019/04/30/1535-7163.MCT-18-0709.abstract
209. Halasi M, Hitchinson B, Shah BN, Váraljai R, Khan I, Benevolenskaya E V, et al. Honokiol is a FOXM1 antagonist. Cell Death Dis . 2018;9(2):84. Available from:

https://doi.org/10.1038/s41419-017-0156-7
210. Tabatabaei-Dakhili SA, Aguayo-Ortiz R, Domínguez L, Velázquez-Martínez CA. Untying the knot of transcription factor druggability: Molecular modeling study of FOXM1 inhibitors. J Mol Graph Model . 2018 Mar 1 [cited 2018 Mar 29];80:197–210. Available from: https://www.sciencedirect.com/science/article/pii/S1093326317305831?via%3Dihub
211. Mapp AK, Pricer R, Sturlis S. Targeting transcription is no longer a quixotic quest. Nat Chem Biol . 2015 Dec 17 [cited 2019 Oct 10];11(12):891–4. Available from: http://www.nature.com/articles/nchembio.1962
212. Yan C, Higgins PJ. Drugging the Undruggable: Transcription Therapy for Cancer. Biochim Biophys Acta . 2013;1835(1):76–85. Available from: http://www.ncbi.nlm.nih.gov/pmc/articles/PMC3529832/
213. Xu XS, Miao RC, Wan Y, Zhang LQ, Qu K, Liu C. FoxM1 as a novel therapeutic target for cancer drug therapy. Asian Pacific J Cancer Prev. 2015/02/03. 2015;16(1):23–9.
214. Yao KM, Sha M, Lu ZJ, Wong GG. DNA binding property, and alternative splicing within the DNA binding domain. J Biol Chem. 1997;272:19827–36.
215. Chiu WT, Huang YF, Tsai HY, Chen CC, Chang CH, Huang SC, et al. FOXM1 confers to epithelial-mesenchymal transition, stemness and chemoresistance in epithelial ovarian carcinoma cells. Oncotarget . 2015;6(4):2349–65. Available from: https://www.ncbi.nlm.nih.gov/pmc/articles/PMC4385856/pdf/oncotarget-06-2349.pdf
216. Madureira PA, Varshochi R, Constantinidou D, Francis RE, Coombes RC, Yao KM, et al. The forkhead box M1 protein regulates the transcription of the estrogen receptor alpha in breast cancer cells. J Biol Chem . 2006;281(35):25167–76. Available from: http://www.jbc.org/content/281/35/25167.full.pdf
217. Tan YJ, Raychaudhuri P, Costa RH. Chk2 mediates stabilization of the FoxM1 transcription factor to stimulate expression of DNA repair genes. Mol Cell Biol . 2007;27(3):1007–16. Available from: https://www.ncbi.nlm.nih.gov/pmc/articles/PMC1800696/pdf/1068-06.pdf
218. Wang YQ, Zhou XR, Xu MD, Weng WW, Zhang QY, Yang YS, et al. OTUB1-catalyzed deubiquitination of FOXM1 facilitates tumor progression and predicts a poor prognosis in ovarian cancer. Oncotarget. 2016;7(24):36681–97.
219. Wen N, Wang Y, Wen L, Zhao SH, Ai ZH, Wang Y, et al. Overexpression of FOXM1 predicts poor prognosis and promotes cancer cell proliferation, migration and invasion in epithelial ovarian cancer. J Transl Med. 2014;12:134.
220. Xu N, Jia DS, Chen WF, Wang H, Liu FL, Ge HY, et al. FoxM1 Is Associated with Poor Prognosis of Non-Small Cell Lung Cancer Patients through Promoting Tumor Metastasis. PLoS One. 2013;8(3):e59412.
221. Kalinina OA, Kalinin SA, Polack EW, Mikaelian I, Panda S, Costa RH, et al. Sustained hepatic expression of FoxM1B in transgenic mice has minimal effects on hepatocellular carcinoma development but increases cell proliferation rates in preneoplastic and early neoplastic lesions. Oncogene. 2003;22(40):6266–76.
222. Okabe H, Satoh S, Kato T, Kitahara O, Yanagawa R, Yamaoka Y, et al. Genome-wide analysis of gene expression in human hepatocellular carcinomas using cDNA microarray: Identification of genes involved in viral carcinogenesis and tumor

progression. Cancer Res. 2001;61(5):2129–37.
223. Kalin T V, Wang IC, Ackerson TJ, Major ML, Detrisac CJ, Kalinichenko V V, et al. Increased levels of the FoxM1 transcription factor accelerate development and progression of prostate carcinomas in both TRAMP and LADY transgenic mice. Cancer Res. 2006;66(3):1712–20.
224. Liu MG, Dai BB, Kang SH, Ban KC, Huang FJ, Lang FF, et al. FoxM1B is overexpressed in human glioblastomas and critically regulates the tumorigenicity of glioma cells. Cancer Res. 2006;66(7):3593–602.
225. Kim I, Ackerson T, Ramakrishna S, Tretiakova M, Wang I, Kalin T V, et al. The Forkhead Box m1 Transcription Factor Stimulates the Proliferation of Tumor Cells during Development of Lung Cancer The Forkhead Box m1 Transcription Factor Stimulates the Proliferation of Tumor Cells during Development of Lung Cancer. 2006;(21):2153–61.
226. Uddin S, Ahmed M, Hussain A, Abubaker J, Al-Sanea N, AbdulJabbar A, et al. Genome-wide expression analysis of middle eastern colorectal cancer reveals FOXM1 as a novel target for cancer therapy. Am J Pathol. 2011;178(2):537–47.
227. Wang ZW, Banerjee S, Kong D, Li YW, Sarkar FH. Down-regulation of Forkhead Box M1 transcription factor leads to the inhibition of invasion and angiogenesis of pancreatic cancer cells. Cancer Res. 2007;67(17):8293–300.
228. Teh MT, Wong ST, Neill GW, Ghali LR, Philpott MP, Quinn AG. FOXM1 is a downstream target of Gli1 in basal cell carcinomas. Cancer Res. 2002;62(16):4773–80.
229. Teh MT, Gemenetzidis E, Chaplin T, Young BD, Philpott MP. Upregulation of FOXM1 induces genomic instability in human epidermal keratinocytes. Mol Cancer . 2010;9:45. Available from: https://www.ncbi.nlm.nih.gov/pmc/articles/PMC2907729/pdf/1476-4598-9-45.pdf
230. Huynh KM, Soh JW, Dash R, Sarkar D, Fisher PB, Kang D. FOXM1 expression mediates growth suppression during terminal differentiation of HO-1 human metastatic melanoma cells. J Cell Physiol. 2011;226(1):194–204.
231. Chan DW, Yu SYM, Chiu PM, Yao KM, Liu VWS, Cheung ANY, et al. Over-expression of FOXM1 transcription factor is associated with cervical cancer progression and pathogenesis. J Pathol. 2008 Jul;215(3):245–52.
232. Cancer Genome Atlas Research N. Integrated genomic analyses of ovarian carcinoma. Nature . 2011;474(7353):609–15. Available from: https://www.ncbi.nlm.nih.gov/pubmed/21720365
233. Gemenetzidis E, Bose A, Riaz AM, Chaplin T, Young BD, Ali M, et al. FOXM1 upregulation is an early event in human squamous cell carcinoma and it is enhanced by nicotine during malignant transformation. PLoS One. 2009;4(3).
234. Nakamura S, Hirano I, Okinaka K, Takemura T, Yokota D, Ono T, et al. The FOXM1 transcriptional factor promotes the proliferation of leukemia cells through modulation of cell cycle progression in acute myeloid leukemia. Carcinogenesis. 2010;31(11):2012–21.
235. Green MR, Aya-Bonilla C, Gandhi MK, Lea RA, Wellwood J, Wood P, et al. Integrative genomic profiling reveals conserved genetic mechanisms for tumorigenesis in common entities of non-Hodgkin's lymphoma. Genes Chromosom Cancer. 2011;50(5):313–26.

236. Hegde NS, Sanders DA, Rodriguez R, Balasubramanian S. The transcription factor FOXM1 is a cellular target of the natural product thiostrepton. Nat Chem . 2011;3(9):725–31. Available from: http://www.nature.com/nchem/journal/v3/n9/pdf/nchem.1114.pdf?origin=publication_detail
237. Gormally M V, Dexheimer TS, Marsico G, Sanders D a, Lowe C, Matak-Vinković D, et al. Suppression of the FOXM1 transcriptional programme via novel small molecule inhibition. Nat Commun . 2014;5:5165. Available from: http://www.pubmedcentral.nih.gov/articlerender.fcgi?artid=4258842&tool=pmcentrez&rendertype=abstract
238. Eskici G, Gur M. Computational design of new Peptide inhibitors for amyloid Beta (abeta) aggregation in Alzheimer's disease: application of a novel methodology. PLoS One. 2013;8(6):e66178.
239. Bulyk ML. Computational prediction of transcription-factor binding site locations. Genome Biol. 2003;5(1):201.
240. Hajjar E, Mihajlovic M, Witko-Sarsat V, Lazaridis T, Reuter N. Computational prediction of the binding site of proteinase 3 to the plasma membrane. Proteins. 2008 Jun;71(4):1655–69.
241. Søndergaard CR, Olsson MHM, Rostkowski M, Jensen JH. Improved treatment of ligands and coupling effects in empirical calculation and rationalization of p K a values. J Chem Theory Comput. 2011;7(7):2284–95.
242. Irwin JJ, Shoichet BK. ZINC - A free database of commercially available compounds for virtual screening. J Chem Inf Model. 2005;45(1):177–82.
243. Jonker HRA, Baumann S, Wolf A, Schoof S, Hiller F, Schulte KW, et al. NMR structures of thiostrepton derivatives for characterization of the ribosomal binding site. Angew Chem Int Ed Engl. 2011 Mar;50(14):3308–12.
244. Pettersen EF, Goddard TD, Huang CC, Couch GS, Greenblatt DM, Meng EC, et al. UCSF Chimera - A visualization system for exploratory research and analysis. J Comput Chem. 2004;25(13):1605–12.
245. Trott O, Olson AJ. Software News and UpdateAutoDock Vina: Improving the Speed and Accuracy ofDocking with a New Scoring Function, EfficientOptimization, and Multithreading. J Comput Chem. 2010;31(16):455–61.
246. Abraham MJ. Gromacs: High performance molecular simulations through multi-level parallelism from laptops to supercomputers. SoftwareX. 2015;1–2:19–25.
247. Harris R, Olson AJ, Goodsell DS. Automated prediction of ligand-binding sites in proteins. Proteins Struct Funct Bioinforma . 2008;70(4):1506–17. Available from: http://dx.doi.org/10.1002/prot.21645
248. Morris GM, Huey R, Lindstrom W, Sanner MF, Belew RK, Goodsell DS, et al. AutoDock4 and AutoDockTools4: Automated Docking with Selective Receptor Flexibility. J Comput Chem . 2009;30(16):2785–91. Available from: http://onlinelibrary.wiley.com/store/10.1002/jcc.21256/asset/21256_ftp.pdf?v=1&t=j0lp29ea&s=268ba110fc49cea5cc905ab2f9352be3cd88ea6e
249. Sousa da Silva AW, Vranken WF. ACPYPE - AnteChamber PYthon Parser interfacE. BMC Res Notes . 2012;5(1):367. Available from: http://www.biomedcentral.com/1756-0500/5/367
250. Kumari R, Kumar R, Lynn A. g_mmpbsa—A GROMACS Tool for High-Throughput MM-PBSA Calculations. J Chem Inf Model . 2014 Jul 28;54(7):1951–

62. Available from: http://dx.doi.org/10.1021/ci500020m
251. Tran N, Van T, Nguyen H, Le L. Identification of novel compounds against an R294K substitution of influenza A (H7N9) virus using ensemble based drug virtual screening. Int J Med Sci. 2015;12(2):163–76.
252. Wooodbury CP. Introduction to Macromolecular Binding Equilibria. Floria: Taylor & Francis Group; 2007. 33 p.
253. Reddy CK, Das a, Jayaram B. Do water molecules mediate protein-DNA recognition? J Mol Biol. 2001;314(3):619–32.
254. Kwok JM-M, Myatt SS, Marson CM, Coombes RC, Constantinidou D, Lam EW-F. Thiostrepton selectively targets breast cancer cells through inhibition of forkhead box M1 expression. Mol Cancer Ther. 2008 Jul;7(7):2022–32.
255. Bond CS, Shaw MP, Alphey MS, Hunter WN. Structure of the macrocycle thiostrepton solved using the anomalous dispersion contribution of sulfur. Acta Crystallogr Sect D . 2001 May;57(5):755–8. Available from: http://dx.doi.org/10.1107/S0907444901003134
256. Tauer TP, Derrick ME, Sherrill CD. Estimates of the ab initio limit for sulfur-pi interactions: the H2S-benzene dimer. J Phys Chem A. 2005;109(1):191–6.
257. Morgan RS, Tatsch CE, Gushard RH, McAdon J, Warme PK. Chains of alternating sulfur and pi-bonded atoms in eight small proteins. Int J Pept Protein Res . 1978;11(3):209–17. Available from: http://www.ncbi.nlm.nih.gov/pubmed/206519
258. Yan S, Lee SJ, Kang S, Choi KH, Rhee SK, Lee JY. Attractive sulfur-pi interaction between fluorinated dimethyl sulfur (FDMS) and benzene. Bull Korean Chem Soc. 2007;28(6):959–64.
259. Viguera AR, Serrano L. Side-chain interactions between sulfur-containing amino acids and phenylalanine in alpha-helices. Biochemistry. 1995 Jul;34(27):8771–9.
260. Tabatabaei Dakhili SA, Pérez DJ, Gopal K, Tabatabaei Dakhili SY, Ussher JR, Velázquez-Martínez CA. A structure-activity relationship study of Forkhead Domain Inhibitors (FDI): The importance of halogen binding interactions. Bioorg Chem . 2019;93:103269. Available from: http://www.sciencedirect.com/science/article/pii/S0045206819304006
261. Korver W, Roose J, Wilson A, Clevers H. The Winged-Helix Transcription Factor Trident is Expressed in Actively Dividing Lymphocytes. Immunobiology . 1997;198(1):157–61. Available from: http://www.sciencedirect.com/science/article/pii/S0171298597800368
262. Chen H, Zou Y, Yang H, Wang J, Pan H. Downregulation of FoxM1 inhibits proliferation, invasion and angiogenesis of HeLa cells in vitro and in vivo. International Journal of Oncology. Int J Oncol. 2014;45:2355–64.
263. Zhang Y, Zhang N, Dai B, Liu M, Sawaya R, Xie K, et al. FoxM1B Transcriptionally Regulates Vascular Endothelial Growth Factor Expression and Promotes the Angiogenesis and Growth of Glioma Cells. Cancer Res . 2008;68(21):8733–42. Available from: http://cancerres.aacrjournals.org/content/canres/68/21/8733.full.pdf
264. Bergamaschi A, Madak-Erdogan Z, Kim YJ, Choi Y-L, Lu H, Katzenellenbogen BS. The forkhead transcription factor FOXM1 promotes endocrine resistance and invasiveness in estrogen receptor-positive breast cancer by expansion of stem-like cancer cells. Breast Cancer Res . 2014;16(5):436. Available from:

http://dx.doi.org/10.1186/s13058-014-0436-4
265. Song X, Fiati Kenston SS, Zhao J, Yang D, Gu Y. Roles of FoxM1 in cell regulation and breast cancer targeting therapy. Med Oncol . 2017 Feb;34(3):41. Available from: https://doi.org/10.1007/s12032-017-0888-3
266. Littler DR, Alvarez-Fernandez M, Stein A, Hibbert RG, Heidebrecht T, Aloy P, et al. Structure of the FoxM1 DNA-recognition domain bound to a promoter sequence. Nucleic Acids Res . 2010;38(13):4527–38. Available from: https://www.ncbi.nlm.nih.gov/pmc/articles/PMC2910063/pdf/gkq194.pdf
267. Fontaine F, Overman J, François M. Pharmacological manipulation of transcription factor protein-protein interactions: opportunities and obstacles. Cell Regen . 2015;4(1):4:2. Available from: http://www.sciencedirect.com/science/article/pii/S2045976917300056
268. Gartel AL. Thiostrepton, proteasome inhibitors and FOXM1. Cell Cycle . 2011;10(24):4341–2. Available from: http://dx.doi.org/10.4161/cc.10.24.18544
269. Abdel-Monem MI, Mohamed OS, Bakhite EA. Fluorine-containing heterocycles: Synthesis and some reactions of new 3-amino-2-functionalized-6-(2′-thienyl)-4-trifluoromethylthieno [2,3-b]pyridines. Pharmazie. 2001;56:41–4.
270. Matulenko MA, Hakeem AA, Kolasa T, Nakane M, Terranova MA, Uchic ME, et al. Synthesis and functional activity of (2-aryl-1-piperazinyl)-N-(3-methylphenyl)acetamides: selective dopamine D4 receptor agonists. Bioorg Med Chem . 2004;12(13):3471–83. Available from: http://www.sciencedirect.com/science/article/pii/S0968089604003372
271. Patel R V, Patel PK, Kumari P, Rajani DP, Chikhalia KH. Synthesis of benzimidazolyl-1,3,4-oxadiazol-2ylthio-N-phenyl (benzothiazolyl) acetamides as antibacterial, antifungal and antituberculosis agents. Eur J Med Chem . 2012;53:41–51. Available from: http://www.sciencedirect.com/science/article/pii/S022352341200195X
272. Zhang W, Ai J, Shi D, Peng X, Ji Y, Liu J, et al. Discovery of novel type II c-Met inhibitors based on BMS-777607. Eur J Med Chem . 2014;80:254–66. Available from: http://www.sciencedirect.com/science/article/pii/S0223523414003778
273. Ma L, Xie C, Ma Y, Liu J, Xiang M, Ye X, et al. Synthesis and biological evaluation of novel 5-benzylidenethiazolidine-2,4-dione derivatives for the treatment of inflammatory diseases. J Med Chem. 2011 Apr;54(7):2060–8.
274. Zhang, S.L; Liu, Y. j; Zhao, Y.F; Guo, Q. T; Gong P. Synthesis and antitumor activities of novel 1,4-substituted phthalazine derivatives. Chinese Chem Lett. 2010;21(9):1071–4.
275. Nikolovska-Coleska Z, Wang R, Fang X, Pan H, Tomita Y, Li P, et al. Development and optimization of a binding assay for the XIAP BIR3 domain using fluorescence polarization. Anal Biochem . 2004;332(2):261–73. Available from: http://www.sciencedirect.com/science/article/pii/S0003269704004944
276. Schrödinger, LLC. The {PyMOL} Molecular Graphics System, Version~1.8. 2015 Nov.
277. Pettersen EF, Goddard TD, Huang CC, Couch GS, Greenblatt DM, Meng EC, et al. UCSF Chimera--a visualization system for exploratory research and analysis. J Comput Chem . 2004;25(13):1605–12. Available from: https://www.ncbi.nlm.nih.gov/pubmed/15264254
278. Berendsen HJC, van der Spoel D, van Drunen R. GROMACS: A message-passing

parallel molecular dynamics implementation. Comput Phys Commun. 1995;91(1–3):43–56.
279. Systèmes D. BIOVIA Discovery Studio Modeling Environment. 2015.
280. Patani GA, LaVoie EJ. Bioisosterism: A Rational Approach in Drug Design. Chem Rev . 1996;96(8):3147–76. Available from: https://doi.org/10.1021/cr950066q
281. Gartel AL. Targeting FOXM1 auto-regulation in cancer. Cancer Biol Ther . 2015;16(2):185–6. Available from: http://dx.doi.org/10.4161/15384047.2014.987566
282. Morgan RS, Tatsch CE, Gushard RH, McAdon J, Warme PK. Chains of alternating sulfur and pi-bonded atoms in eight small proteins. Int J Pept Protein Res . 1978;11(3):209–17. Available from: https://www.ncbi.nlm.nih.gov/pubmed/206519
283. Reid KSC, Lindley PF, Thornton JM. Sulphur-aromatic interactions in proteins. FEBS Lett . 1985 Oct 14;190(2):209–13. Available from: https://doi.org/10.1016/0014-5793(85)81285-0
284. Cheney BV, Schulz MW, Cheney J. Complexes of benzene with formamide and methanethiol as models for interactions of protein substructures. Biochim Biophys Acta - Protein Struct Mol Enzymol . 1989;996(1):116–24. Available from: http://www.sciencedirect.com/science/article/pii/0167483889901039
285. Zauhar RJ, Colbert CL, Morgan RS, Welsh WJ. Evidence for a strong sulfur-aromatic interaction derived from crystallographic data. Biopolymers. 2000 Mar;53(3):233–48.
286. Wang N-Y, Zuo W-Q, Xu Y, Gao C, Zeng X-X, Zhang L-D, et al. Discovery and structure–activity relationships study of novel thieno[2,3-b]pyridine analogues as hepatitis C virus inhibitors. Bioorg Med Chem Lett . 2014;24(6):1581–8. Available from: http://www.sciencedirect.com/science/article/pii/S0960894X1400105X
287. Synthesis and antimicrobial activity of 4-trifluoromethylpyridine nucleosides . Vol. 23, Heterocyclic Communications . 2017. p. 197. Available from: https://www.degruyter.com/view/j/hc.2017.23.issue-3/hc-2017-0019/hc-2017-0019.xml
288. Ma F, Liu J, Zhou T, Lei M, Chen J, Wang X, et al. Discovery and structure-activity relationships study of thieno[2,3-b]pyridine analogues as hepatic gluconeogenesis inhibitors. Eur J Med Chem. 2018 May;152:307–17.
289. Liberato MV, Nascimento AS, Ayers SD, Lin JZ, Cvoro A, Silveira RL, et al. Medium chain fatty acids are selective peroxisome proliferator activated receptor (PPAR) gamma activators and pan-PPAR partial agonists. PLoS One. 2012;7(5):e36297.
290. Lee MA, Tan L, Yang H, Im Y-G, Im YJ. Structures of PPARgamma complexed with lobeglitazone and pioglitazone reveal key determinants for the recognition of antidiabetic drugs. Sci Rep. 2017 Dec;7(1):16837.
291. Nandi D, Cheema PS, Jaiswal N, Nag A. FoxM1: Repurposing an oncogene as a biomarker. Semin Cancer Biol . 2017 Aug 30 [cited 2018 Jun 26]; Available from: https://www.sciencedirect.com/science/article/pii/S1044579X17300615
292. Kelleher FC, O'Sullivan H. FOXM1 in sarcoma: role in cell cycle, pluripotency genes and stem cell pathways. Oncotarget . 2016;7(27):42792–804. Available from:

http://www.ncbi.nlm.nih.gov/pubmed/27074562%0Ahttp://www.pubmedcentral.nih.gov/articlerender.fcgi?artid=PMC5173172
293. Chai N, Xie H hong, Yin J peng, Sa K di, Guo Y, Wang M, et al. FOXM1 promotes proliferation in human hepatocellular carcinoma cells by transcriptional activation of CCNB1. Biochem Biophys Res Commun. 2018;500(4):924–9.
294. Halasi M, Gartel AL. Targeting FOXM1 in cancer. Biochem Pharmacol . 2013;85(5):644–52. Available from: http://dx.doi.org/10.1016/j.bcp.2012.10.013
295. Janus JR, Laborde RR, Greenberg AJ, Wang VW, Wei W, Trier A, et al. Linking expression of FOXM1, CEP55 and HELLS to tumorigenesis in oropharyngeal squamous cell carcinoma. Laryngoscope. 2011;121(12):2598–603.
296. Huang C, Du J, Xie K. FOXM1 and its oncogenic signaling in pancreatic cancer pathogenesis. Biochim Biophys Acta - Rev Cancer . 2014;1845(2):104–16. Available from: http://dx.doi.org/10.1016/j.bbcan.2014.01.002
297. Bhattarai BR, Kafle B, Hwang J-S, Khadka D, Lee S-M, Kang J-S, et al. Thiazolidinedione derivatives as PTP1B inhibitors with antihyperglycemic and antiobesity effects. Bioorg Med Chem Lett. 2009 Nov;19(21):6161–5.
298. Kafle B, Aher NG, Khadka D, Park H, Cho H. Isoxazol-5(4H)one Derivatives as PTP1B Inhibitors Showing an Anti-Obesity Effect. Chem – An Asian J . 2011;6(8):2073–9. Available from: https://onlinelibrary.wiley.com/doi/abs/10.1002/asia.201100154
299. Carrasco-Gomez R, Keppner-Witter S, Hieke M, Lange L, Schneider G, Schubert-Zsilavecz M, et al. Vanillin-derived antiproliferative compounds influence Plk1 activity. Bioorg Med Chem Lett. 2014 Nov;24(21):5063–9.
300. Hrast M, Rozman K, Jukic M, Patin D, Gobec S, Sova M. Synthesis and structure-activity relationship study of novel quinazolinone-based inhibitors of MurA. Bioorg Med Chem Lett. 2017 Aug;27(15):3529–33.
301. Imoto H, Imamiya E, Momose Y, Sugiyama Y, Kimura H, Sohda T. Studies on non-thiazolidinedione antidiabetic agents. 1. Discovery of novel oxyiminoacetic acid derivatives. Chem Pharm Bull (Tokyo). 2002 Oct;50(10):1349–57.
302. Momose Y, Meguro K, Ikeda H, Hatanaka C, Oi S, Sohda T. Studies on antidiabetic agents. X. Synthesis and biological activities of pioglitazone and related compounds. Chem Pharm Bull (Tokyo). 1991 Jun;39(6):1440–5.
303. Brackman G, Al Quntar AAA, Enk CD, Karalic I, Nelis HJ, Van Calenbergh S, et al. Synthesis and evaluation of thiazolidinedione and dioxazaborocane analogues as inhibitors of AI-2 quorum sensing in Vibrio harveyi. Bioorg Med Chem . 2013;21(3):660–7. Available from: http://www.sciencedirect.com/science/article/pii/S0968089612009509
304. Kong X, Li L, Li Z, Le X, Huang C, Jia Z, et al. Dysregulated expression of FOXM1 isoforms drives progression of pancreatic cancer. Cancer Res. 2013 Jul;73(13):3987–96.
305. Schmitt E, Boutros R, Froment C, Monsarrat B, Ducommun B, Dozier C. CHK1 phosphorylates CDC25B during the cell cycle in the absence of DNA damage. J Cell Sci . 2006;119(20):4269–75. Available from: https://jcs.biologists.org/content/119/20/4269
306. Dakhili SAT, Perez DJ, Gopal K, Ussher JR, Martínez CAV. FOXM1 Inhibitors: Emergence of a Neglected Binding Force. Proceedings . 2019 Aug 9 [cited 2019 Oct 30];22(1):58. Available from: https://www.mdpi.com/2504-3900/22/1/58

307. Hannenhalli S, Kaestner KH. The evolution of Fox genes and their role in development and disease. Nat Rev Genet. 2009 Apr;10(4):233–40.
308. Zou P, Liu L, Zheng L, Liu L, Stoneman RE, Cho A, et al. Targeting FoxO1 with AS1842856 suppresses adipogenesis. Cell Cycle. 2014;13(23):3759–67.
309. Liu L, Zheng LD, Zou P, Brooke J, Smith C, Long YC, et al. FoxO1 antagonist suppresses autophagy and lipid droplet growth in adipocytes. Cell Cycle. 2016 Aug;15(15):2033–41.
310. Tan P, Guan H, Xie L, Mi B, Fang Z, Li J, et al. FOXO1 inhibits osteoclastogenesis partially by antagnozing MYC. Sci Rep. 2015 Nov;5:16835.
311. Nagashima T, Shigematsu N, Maruki R, Urano Y, Tanaka H, Shimaya A, et al. Discovery of novel forkhead box O1 inhibitors for treating type 2 diabetes: improvement of fasting glycemia in diabetic db/db mice. Mol Pharmacol. 2010 Nov;78(5):961–70.
312. Nakae J, Kitamura T, Kitamura Y, Biggs WH 3rd, Arden KC, Accili D. The forkhead transcription factor Foxo1 regulates adipocyte differentiation. Dev Cell. 2003 Jan;4(1):119–29.
313. Schmoll D, Walker KS, Alessi DR, Grempler R, Burchell A, Guo S, et al. Regulation of Glucose-6-phosphatase Gene Expression by Protein Kinase Bα and the Forkhead Transcription Factor FKHR: EVIDENCE FOR INSULIN RESPONSE UNIT-DEPENDENT AND -INDEPENDENT EFFECTS OF INSULIN ON PROMOTER ACTIVITY . J Biol Chem . 2000 Nov;275(46):36324–33.
314. Kim H-J, Kobayashi M, Sasaki T, Kikuchi O, Amano K, Kitazumi T, et al. Overexpression of FoxO1 in the hypothalamus and pancreas causes obesity and glucose intolerance. Endocrinology. 2012 Feb;153(2):659–71.
315. Gross DN, van den Heuvel APJ, Birnbaum MJ. The role of FoxO in the regulation of metabolism. Oncogene. 2008 Apr;27(16):2320–36.
316. Wang F, Demir S, Gehringer F, Osswald CD, Seyfried F, Enzenmüller S, et al. Tight regulation of FOXO1 is essential for maintenance of B-cell precursor acute lymphoblastic leukemia. Blood. 2018 Jun;131(26):2929–42.
317. Lin S, Zhang J, Mulloy JC. Tumor Suppressor FOXO1 Serves As a Critical Oncogenic Mediator in AML1-ETO Leukemia. Blood. 2014 Dec;124(21):264.
318. Barger CJ, Zhang W, Hillman J, Stablewski AB, Higgins MJ, Vanderhyden BC, et al. Genetic determinants of FOXM1 overexpression in epithelial ovarian cancer and functional contribution to cell cycle progression. Oncotarget . 2015 Sep 29;6(29):27613–27. Available from: https://www.ncbi.nlm.nih.gov/pubmed/26243836
319. Barger JC, Branick C, Chee L, Karpf RA. Pan-Cancer Analyses Reveal Genomic Features of FOXM1 Overexpression in Cancer. Vol. 11, Cancers . 2019.
320. Haque M, Li J, Huang Y-H, Almowaled M, Barger JC, Karpf RA, et al. NPM-ALK Is a Key Regulator of the Oncoprotein FOXM1 in ALK-Positive Anaplastic Large Cell Lymphoma. Vol. 11, Cancers. 2019.
321. Zhang X, Gan L, Pan H, Guo S, He X, Olson ST, et al. Phosphorylation of serine 256 suppresses transactivation by FKHR (FOXO1) by multiple mechanisms. Direct and indirect effects on nuclear/cytoplasmic shuttling and DNA binding. J Biol Chem. 2002 Nov;277(47):45276–84.
322. Radhakrishnan SK, Gartel AL. FOXM1: the Achilles' heel of cancer? Vol. 8,

Nature reviews. Cancer. England; 2008. p. c1; author reply c2.
323. Kim I-M, Ackerson T, Ramakrishna S, Tretiakova M, Wang I-C, Kalin T V., et al. The Forkhead Box m1 Transcription Factor Stimulates the Proliferation of Tumor Cells during Development of Lung Cancer. Cancer Res . 2006;66(4):2153–61. Available from: http://cancerres.aacrjournals.org/lookup/doi/10.1158/0008-5472.CAN-05-3003
324. Ko YS, Cho SJ, Park J, Kim Y, Choi YJ, Pyo J-S, et al. Loss of FOXO1 promotes gastric tumour growth and metastasis through upregulation of human epidermal growth factor receptor 2/neu expression. Br J Cancer. 2015 Oct;113(8):1186–96.

Appendices

A.1 NMR Spectroscopy Data

A1.1 ^{1}H-NMR 600 MHz, 7a

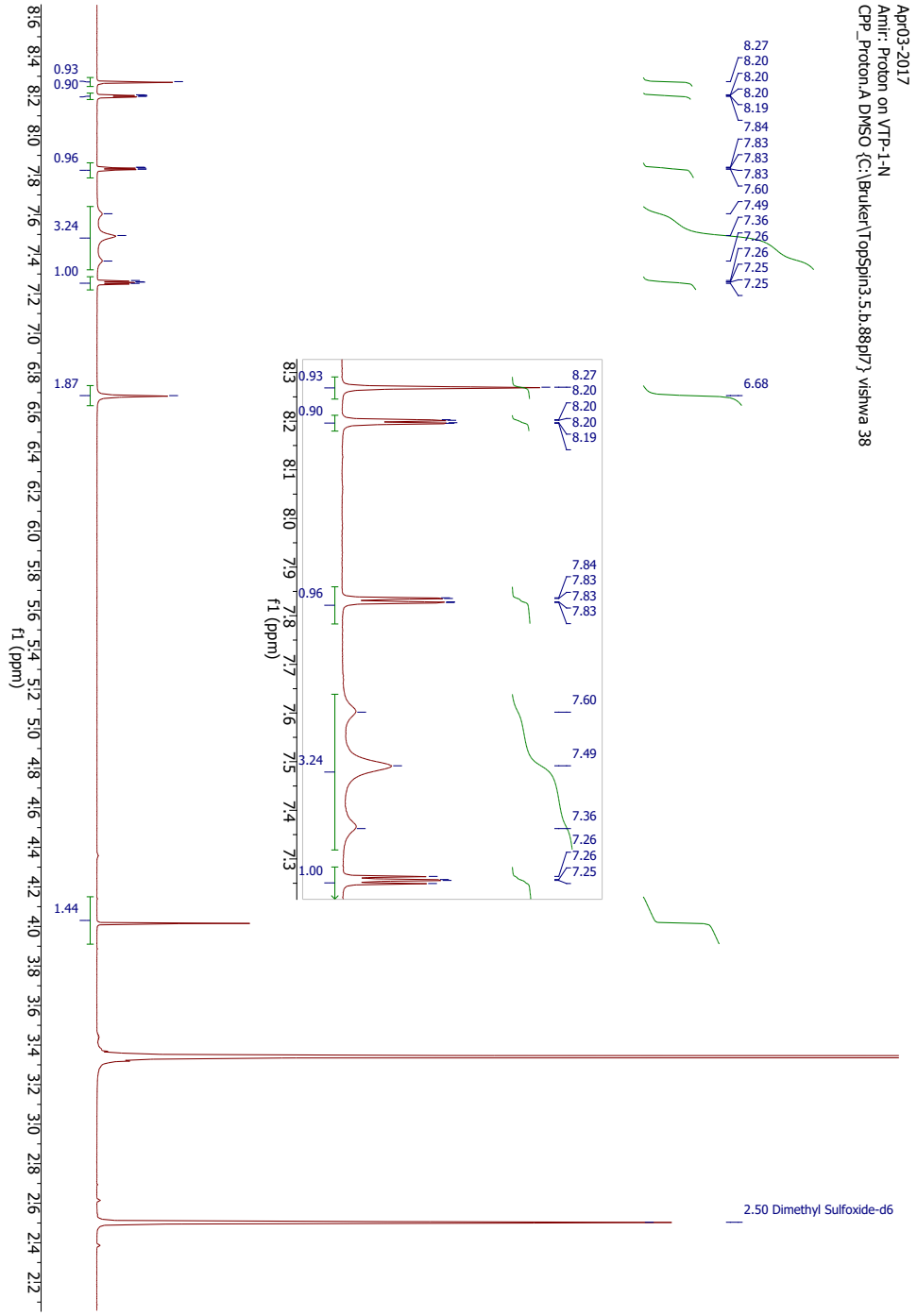

A1.2 ^{13}C-NMR (DEPTQ) 150 MHz, 7a

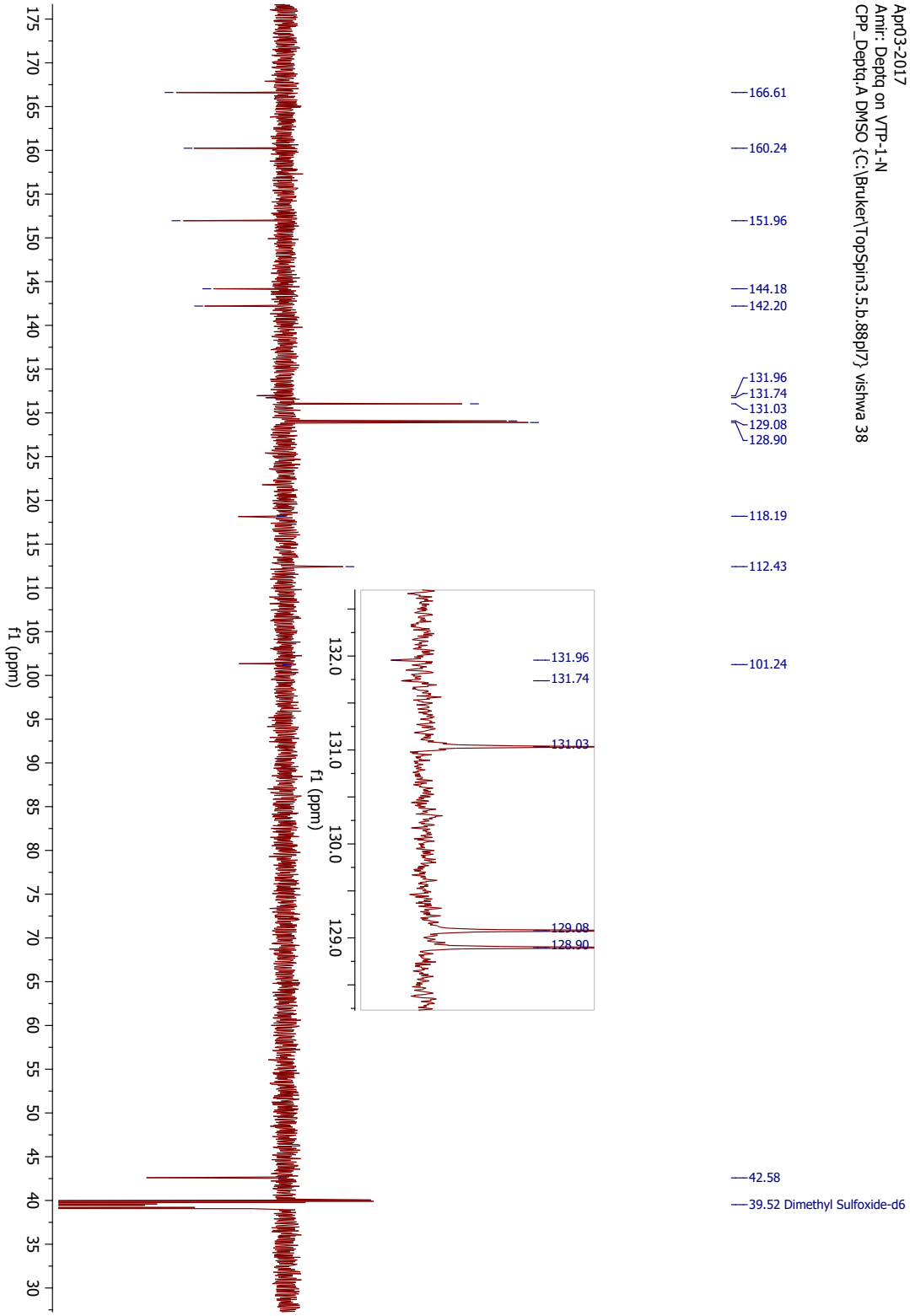

A1.3 ^{1}H-NMR 600 MHz, 7b

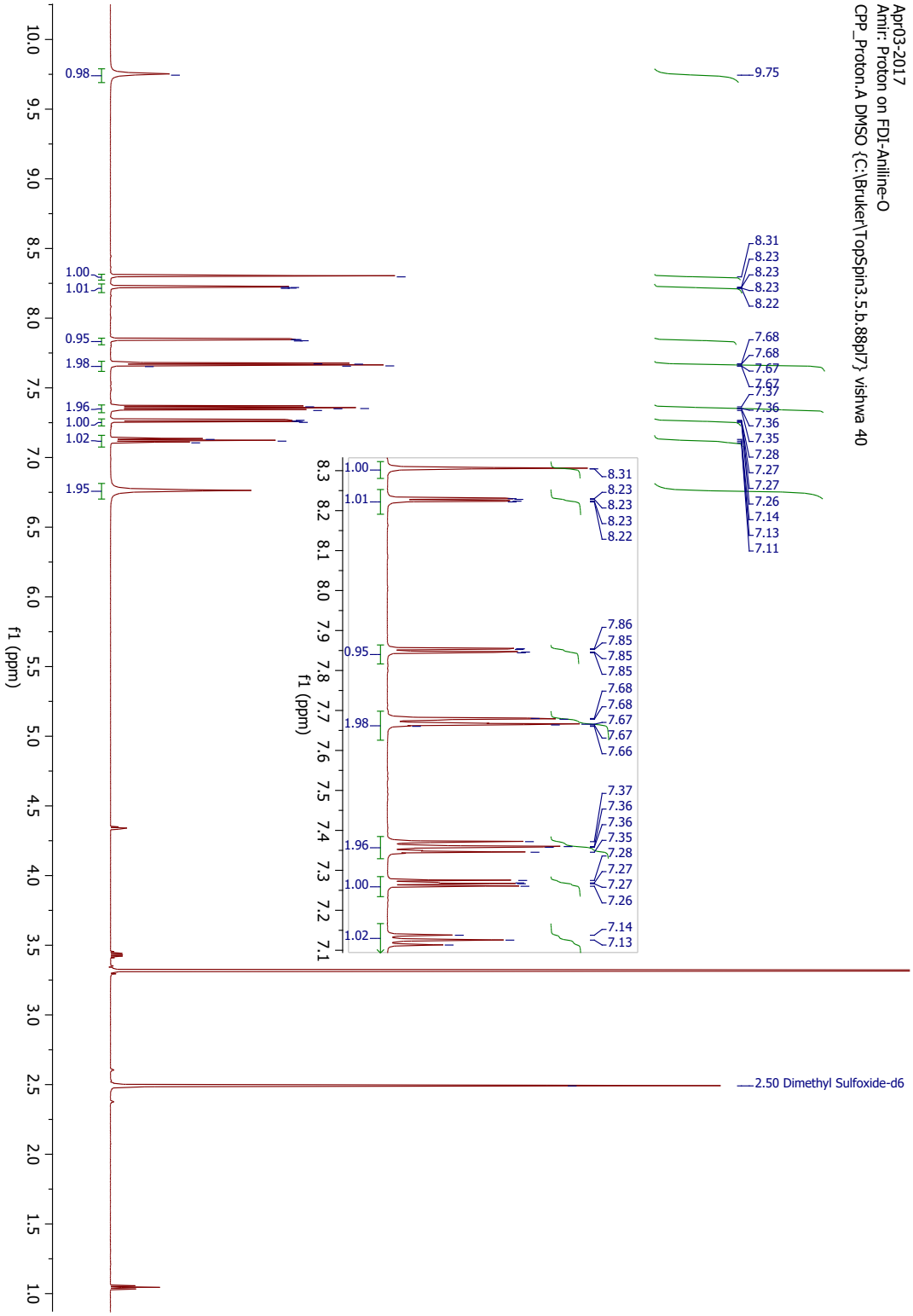

A1.4 ^{13}C-NMR (DEPTQ) 150 MHz, 7b

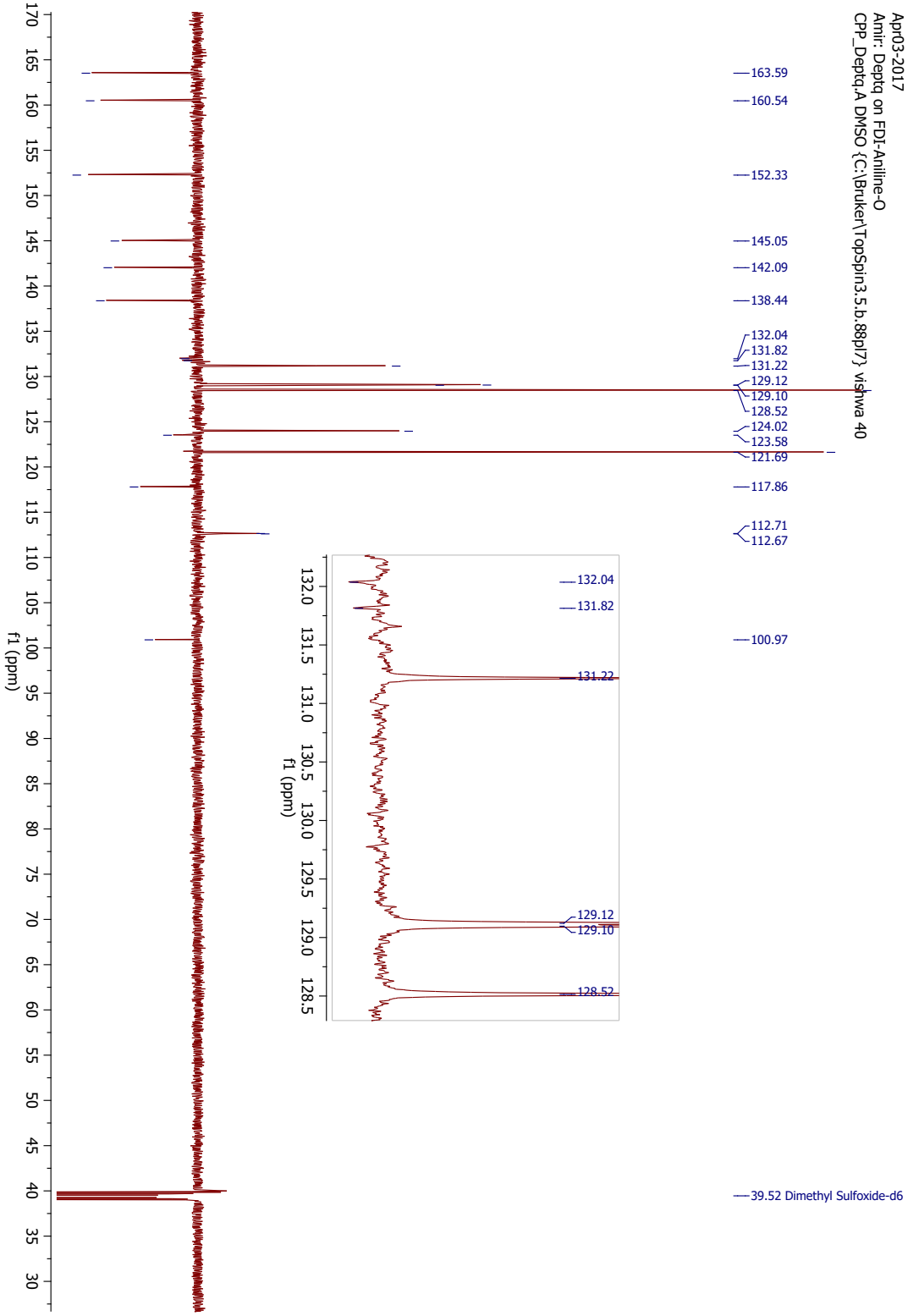

A1.5 ^{1}H-NMR 600 MHz, 7c

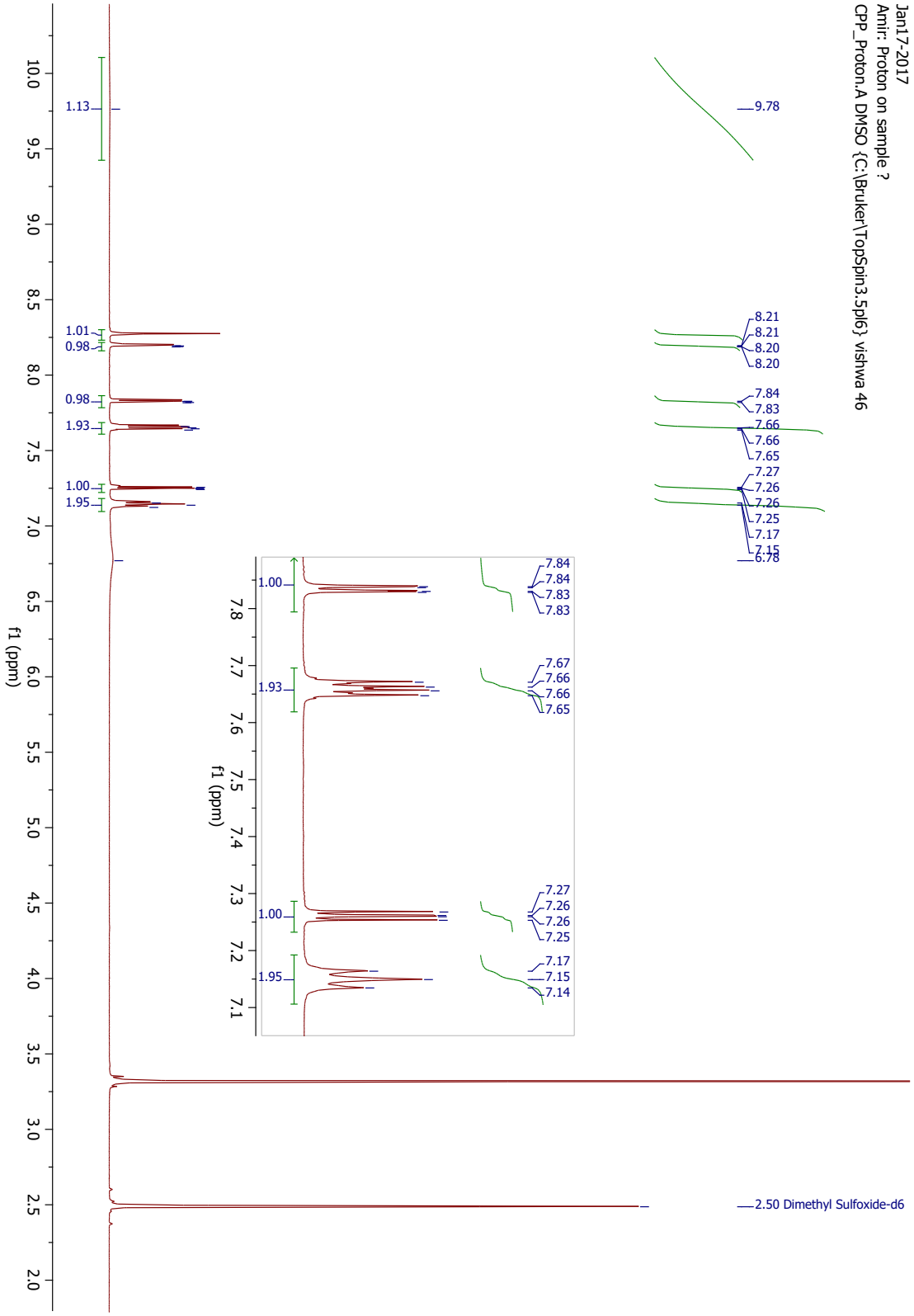

A1.6 ^{13}C-NMR (DEPTQ) 150 MHz, 7c

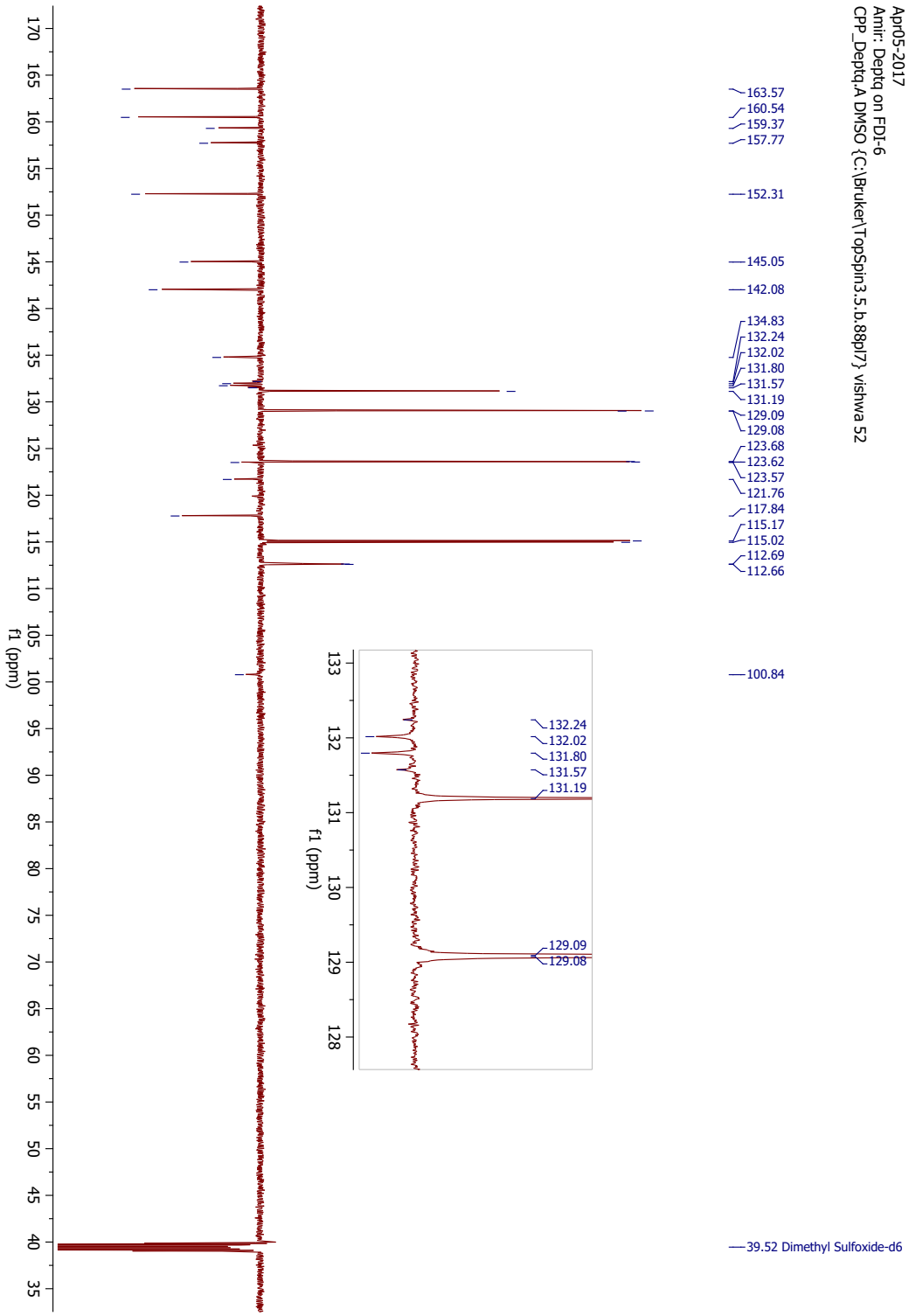

A1.7 ^{1}H-NMR 600 MHz, 7d

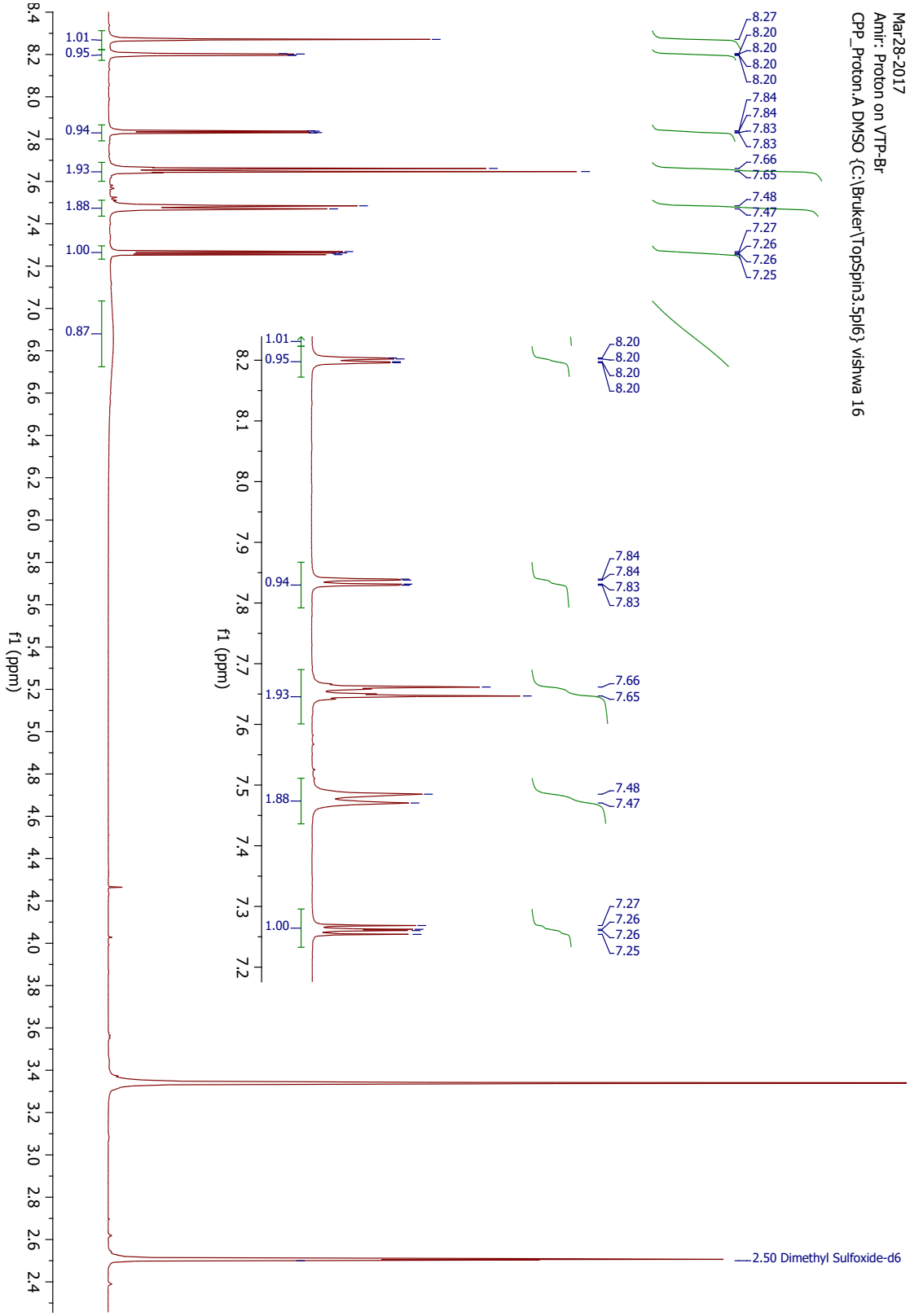

A1.8 ^{13}C-NMR (DEPTQ) 150 MHz, 7d

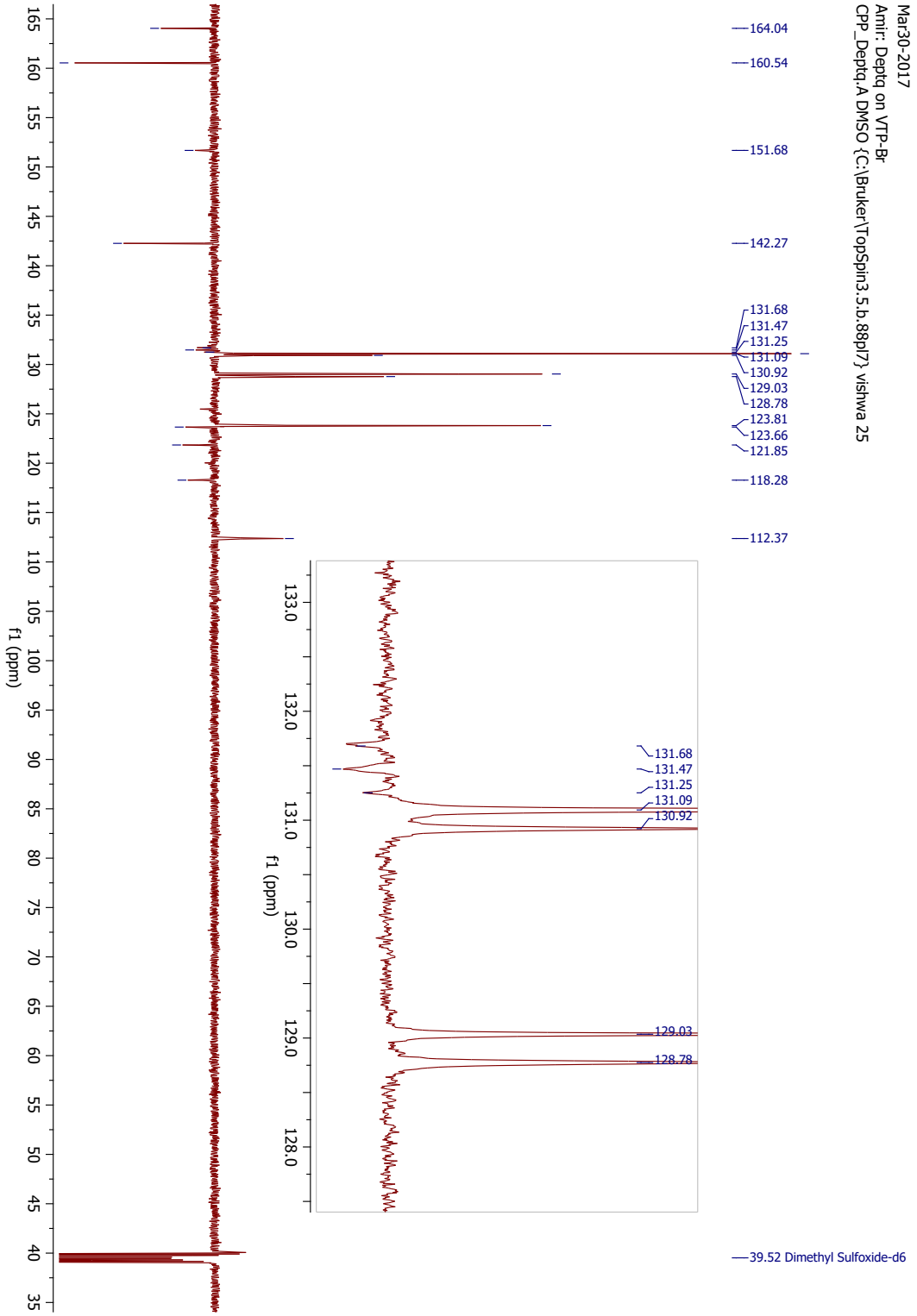

A1.9 ^{1}H-NMR 600 MHz, 7e

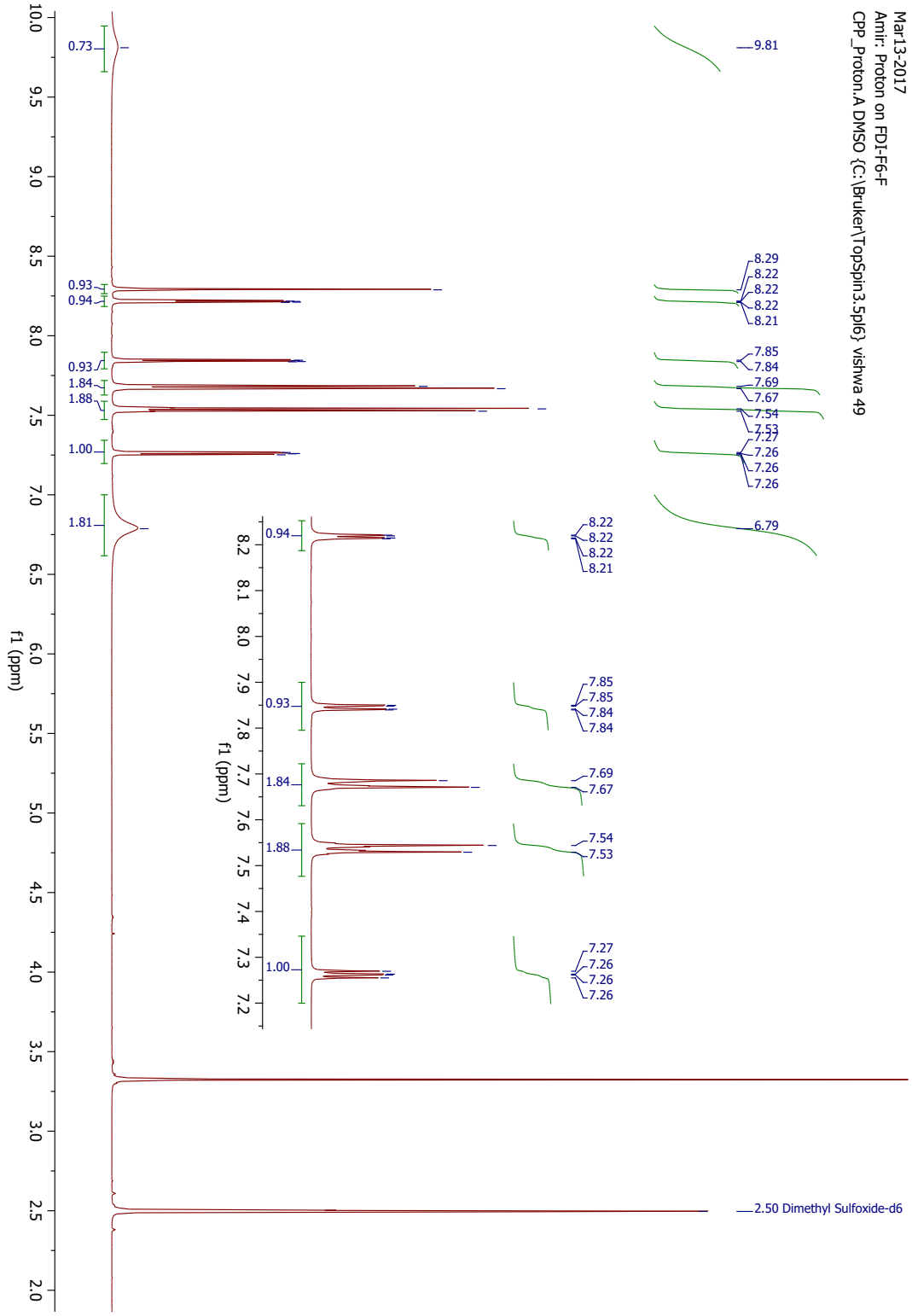

A1.10 ^{13}C-NMR (DEPTQ) 150 MHz, 7e

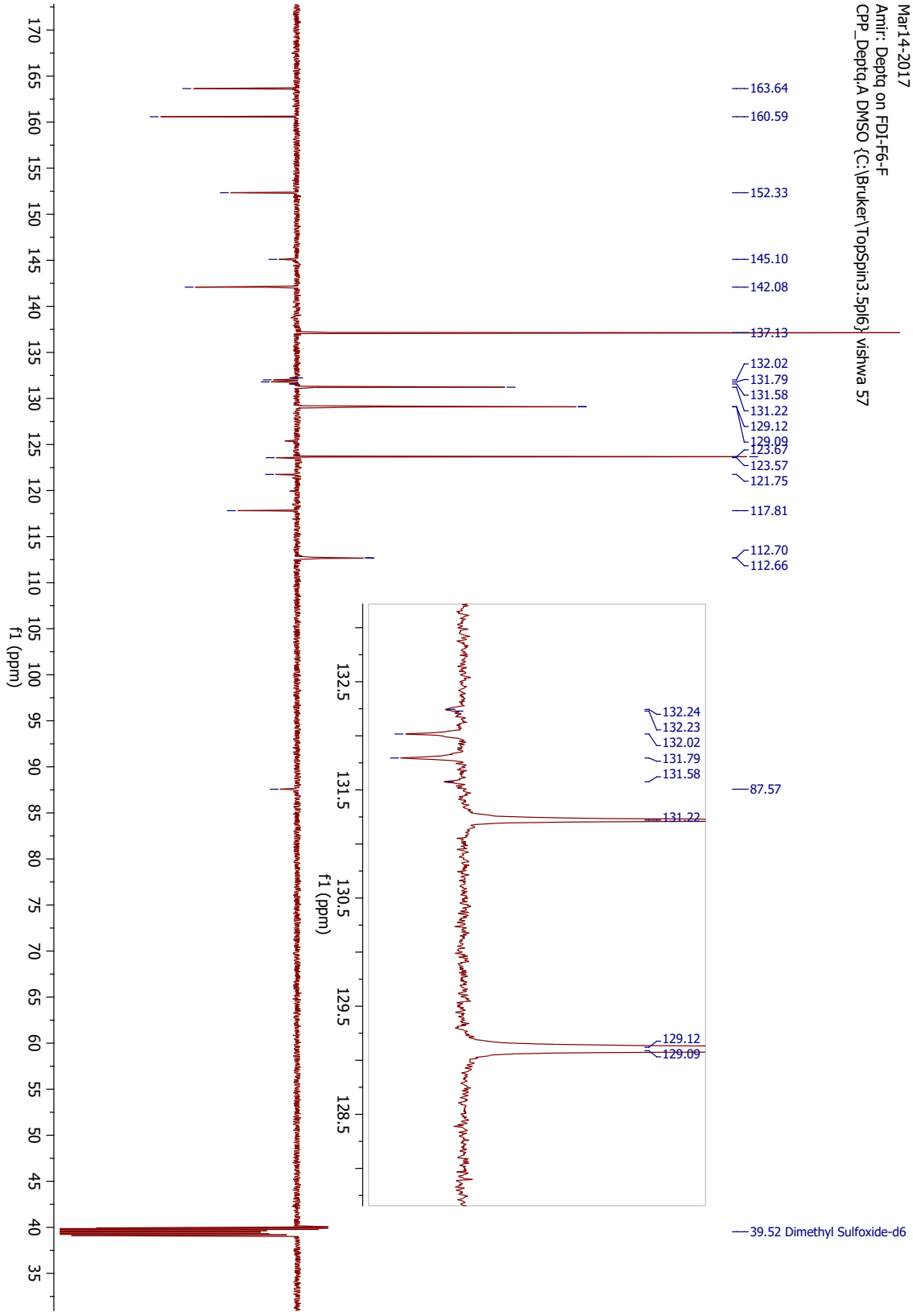

A1.11 ^{1}H-NMR 600 MHz, 7f

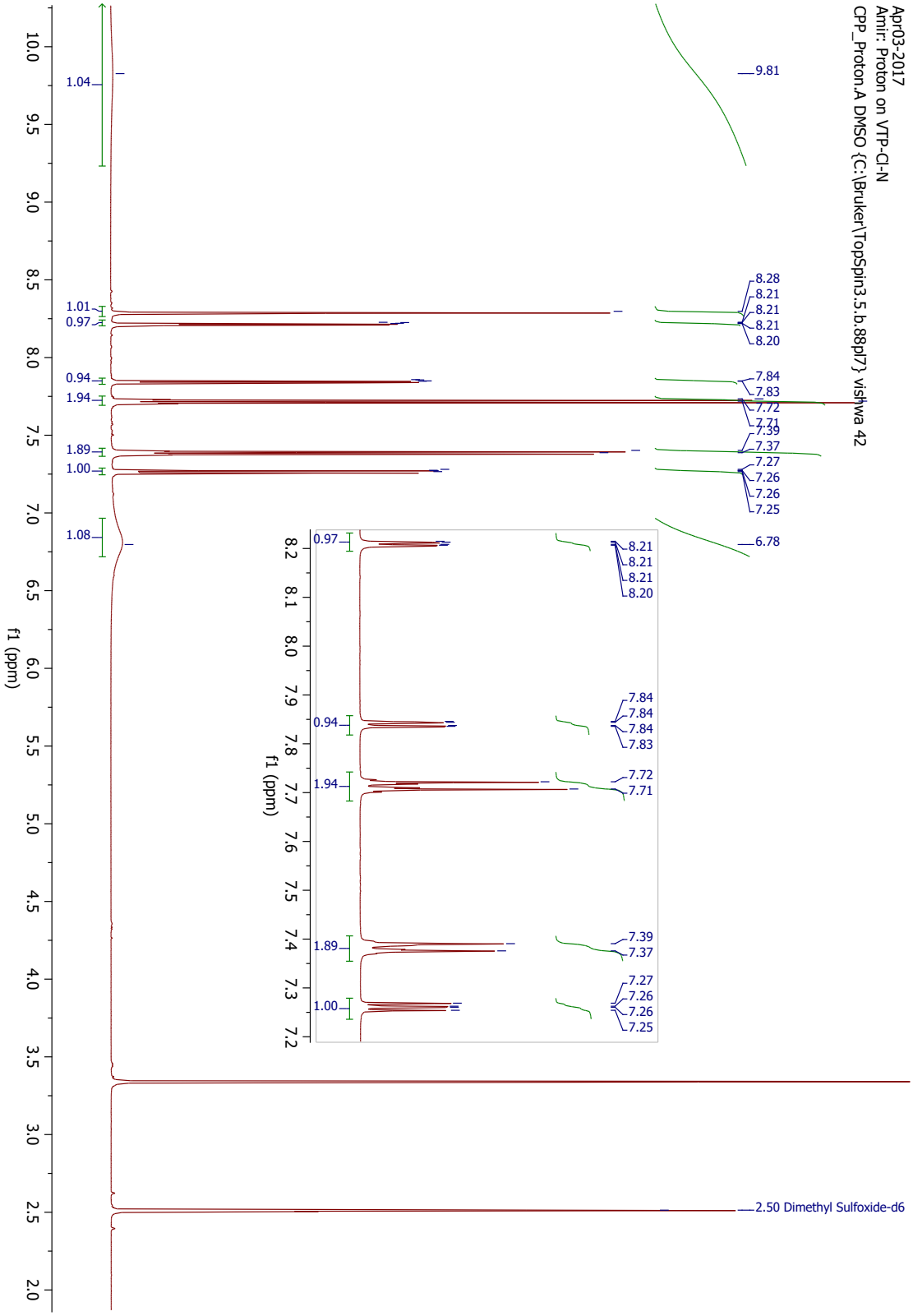

A1.12 ^{13}C-NMR (DEPTQ) 150 MHz, 7f

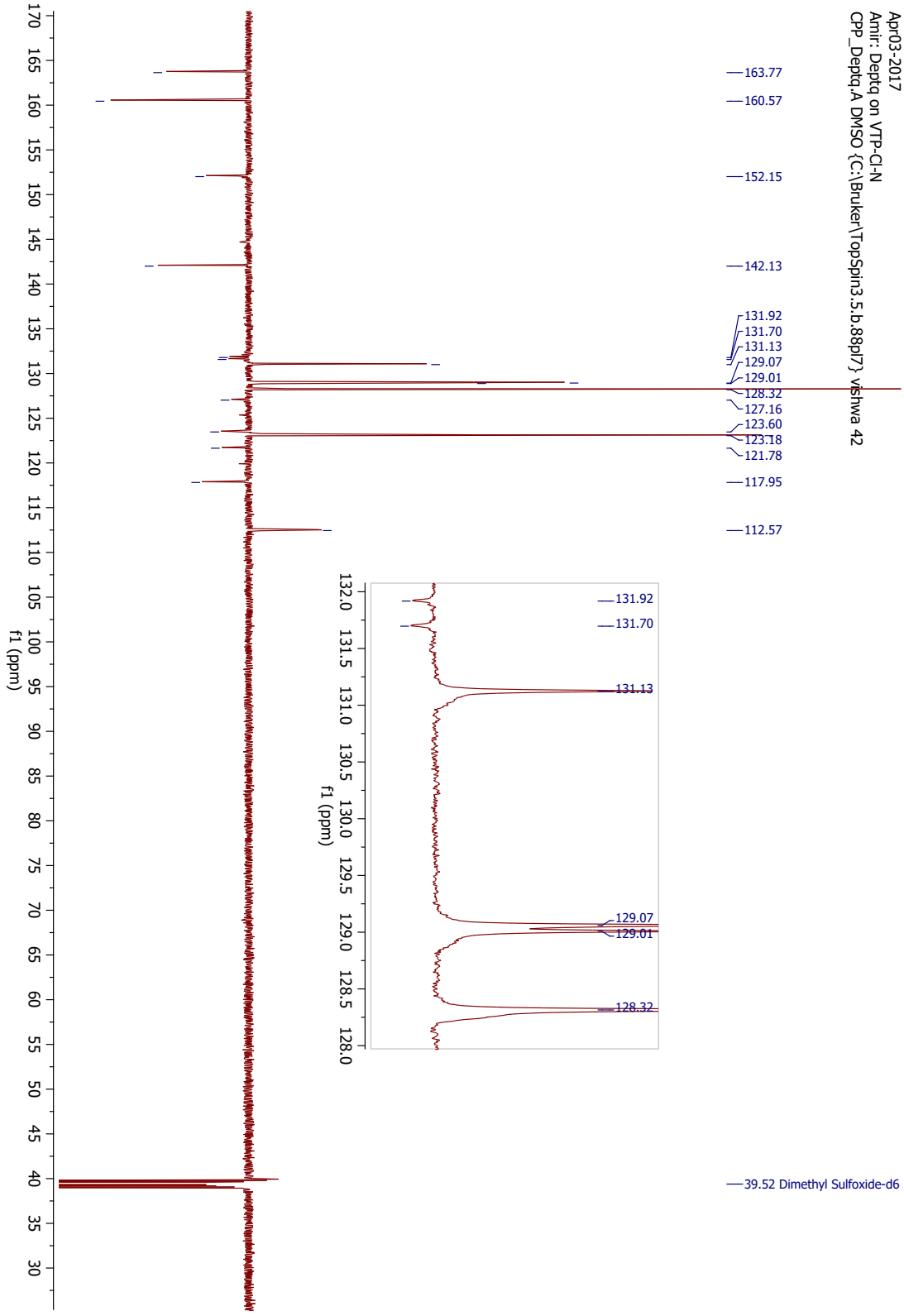

A1.13 ^{1}H-NMR 600 MHz, 7g

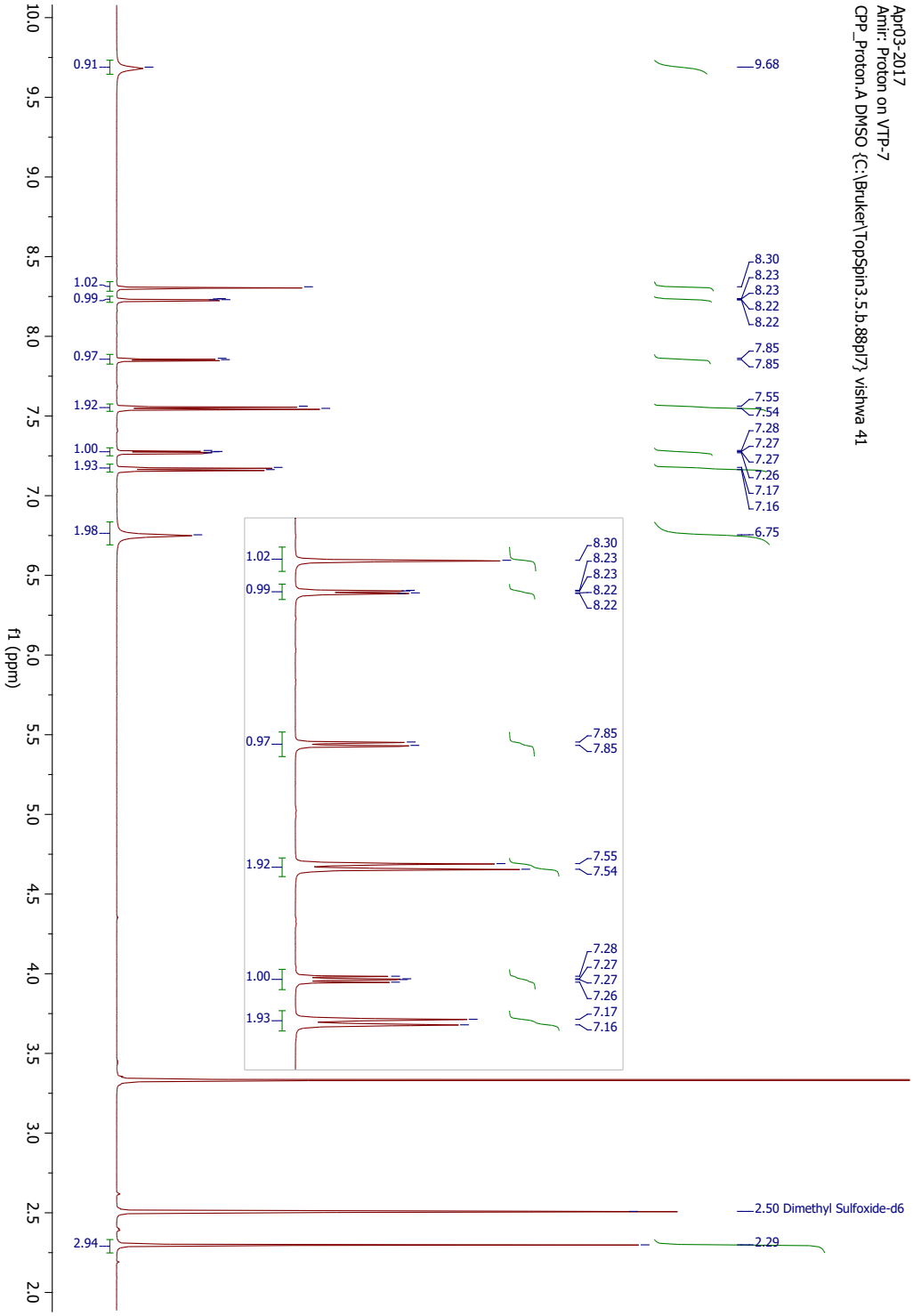

A1.14 ^{13}C-NMR (DEPTQ) 150 MHz, 7g

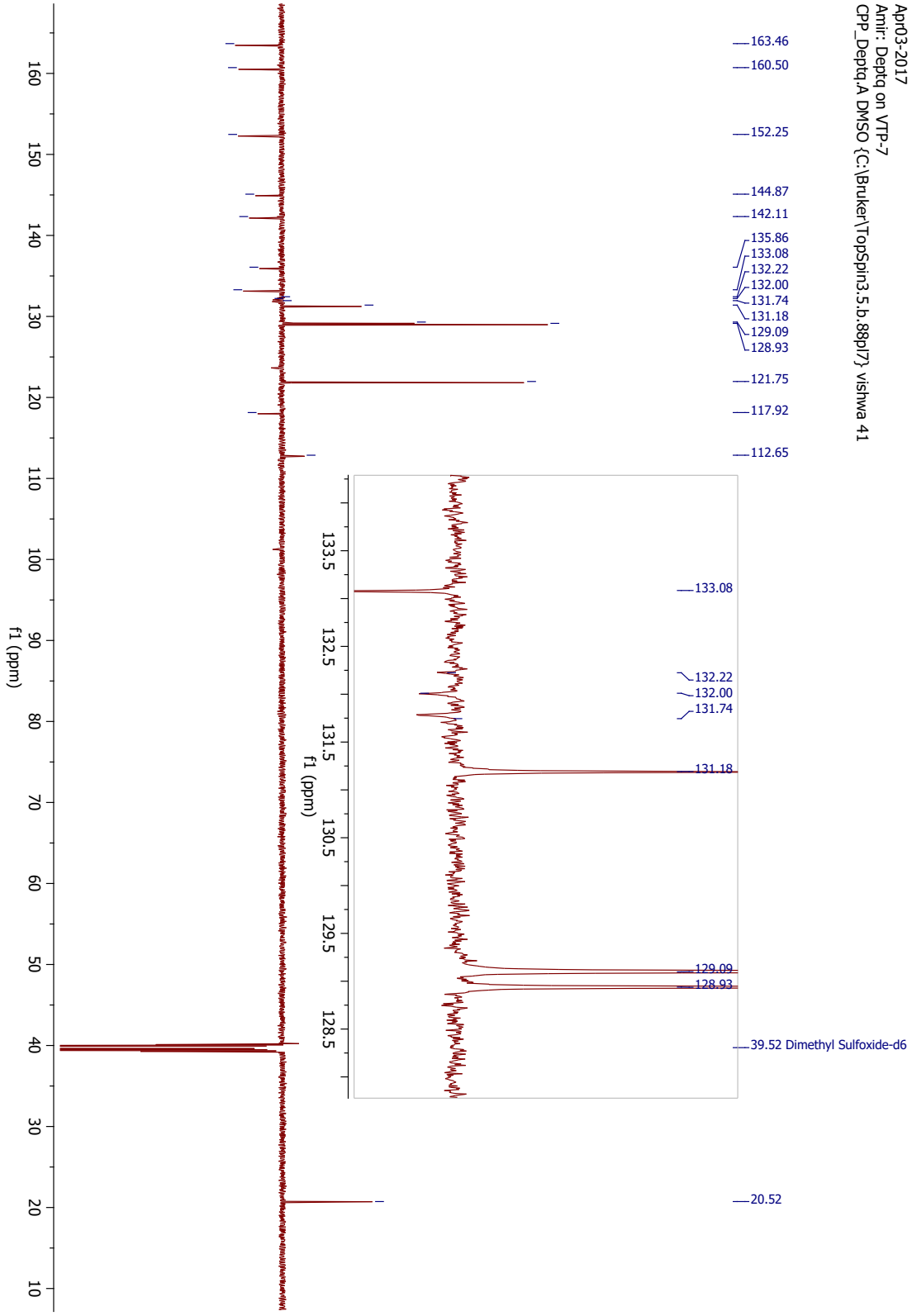

A1.15 ^{1}H-NMR 600 MHz, 7h

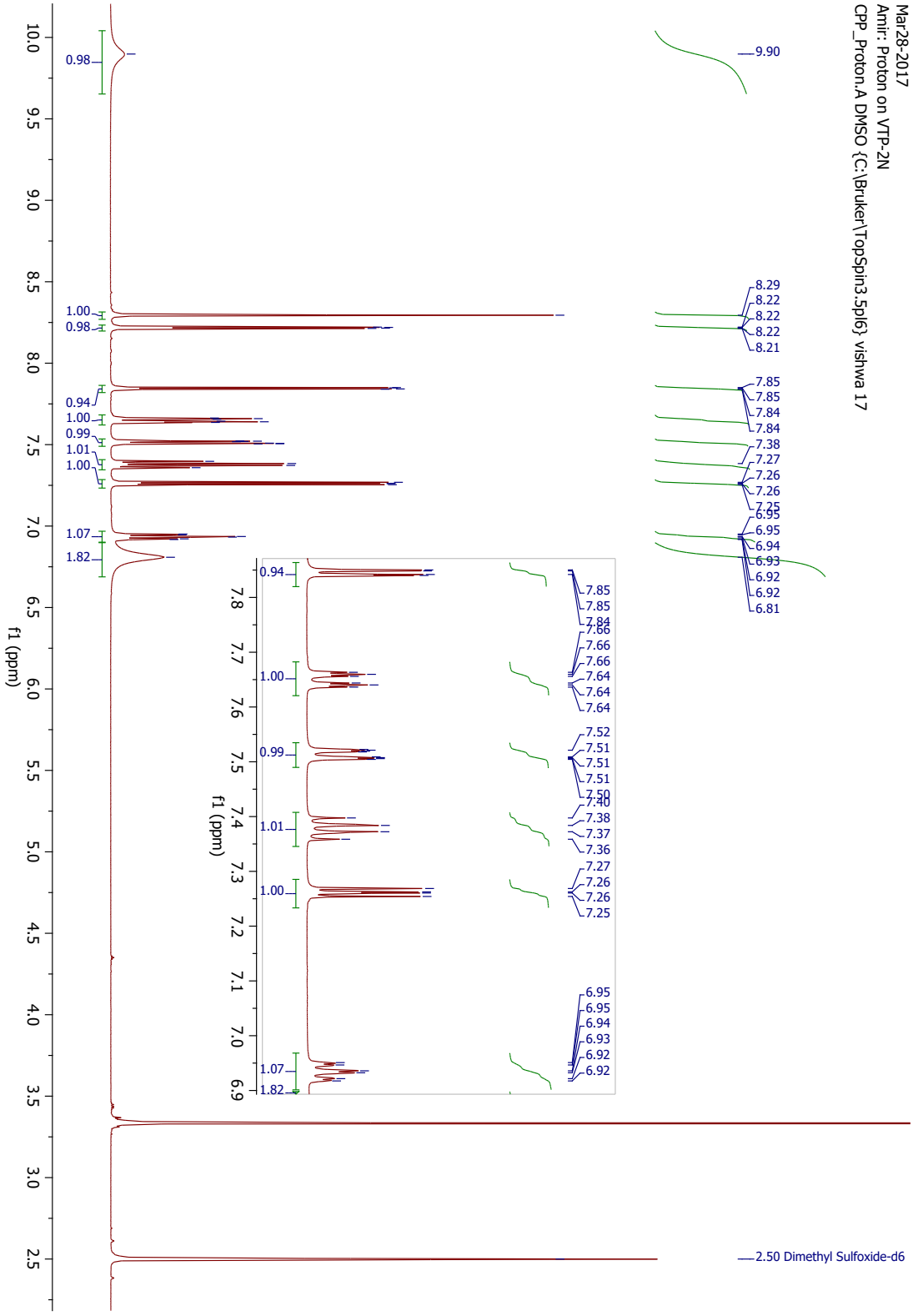

A1.16 ^{13}C-NMR (DEPTQ) 150 MHz, 7h

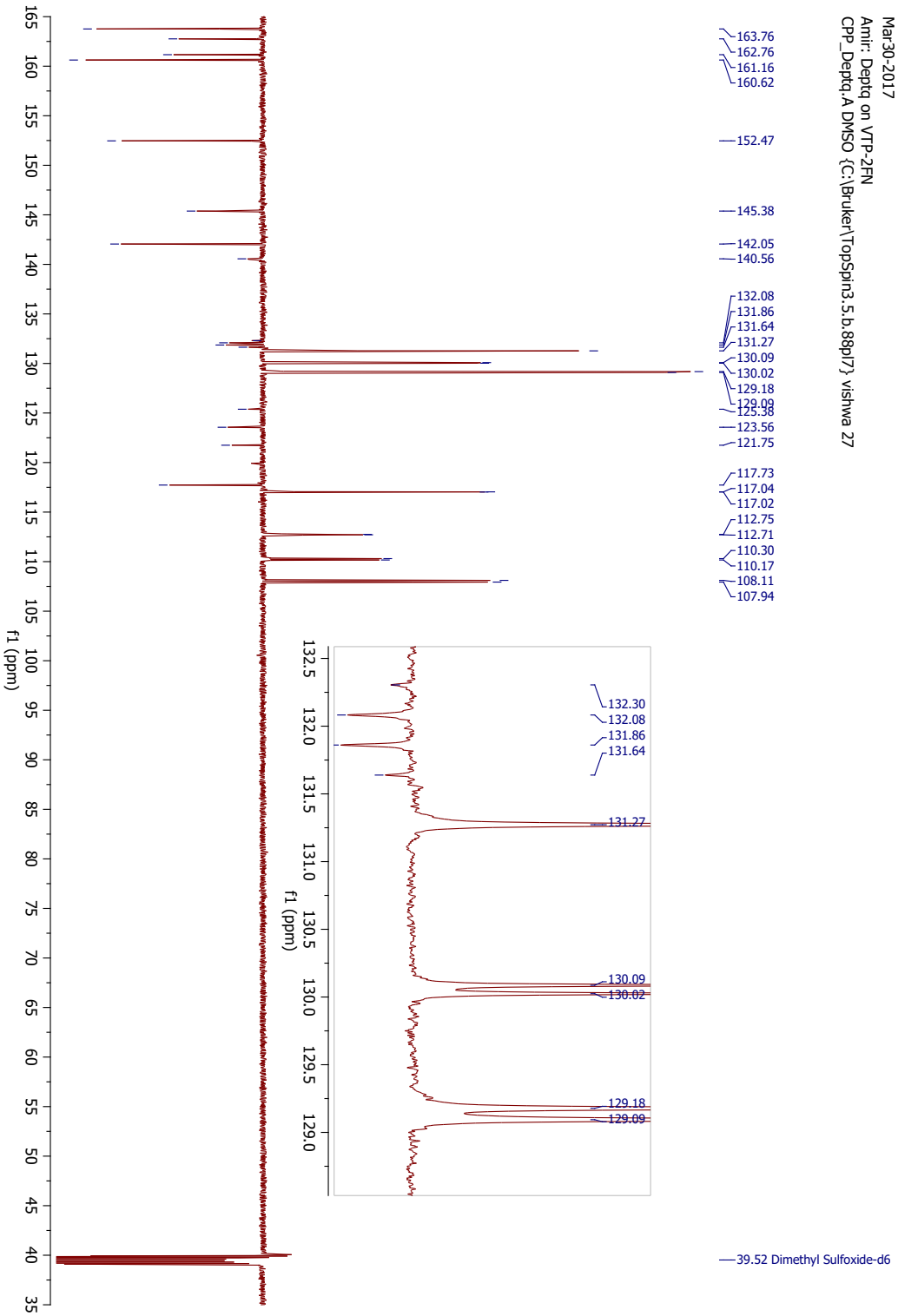

A1.17 ^{1}H-NMR 600 MHz, 7i

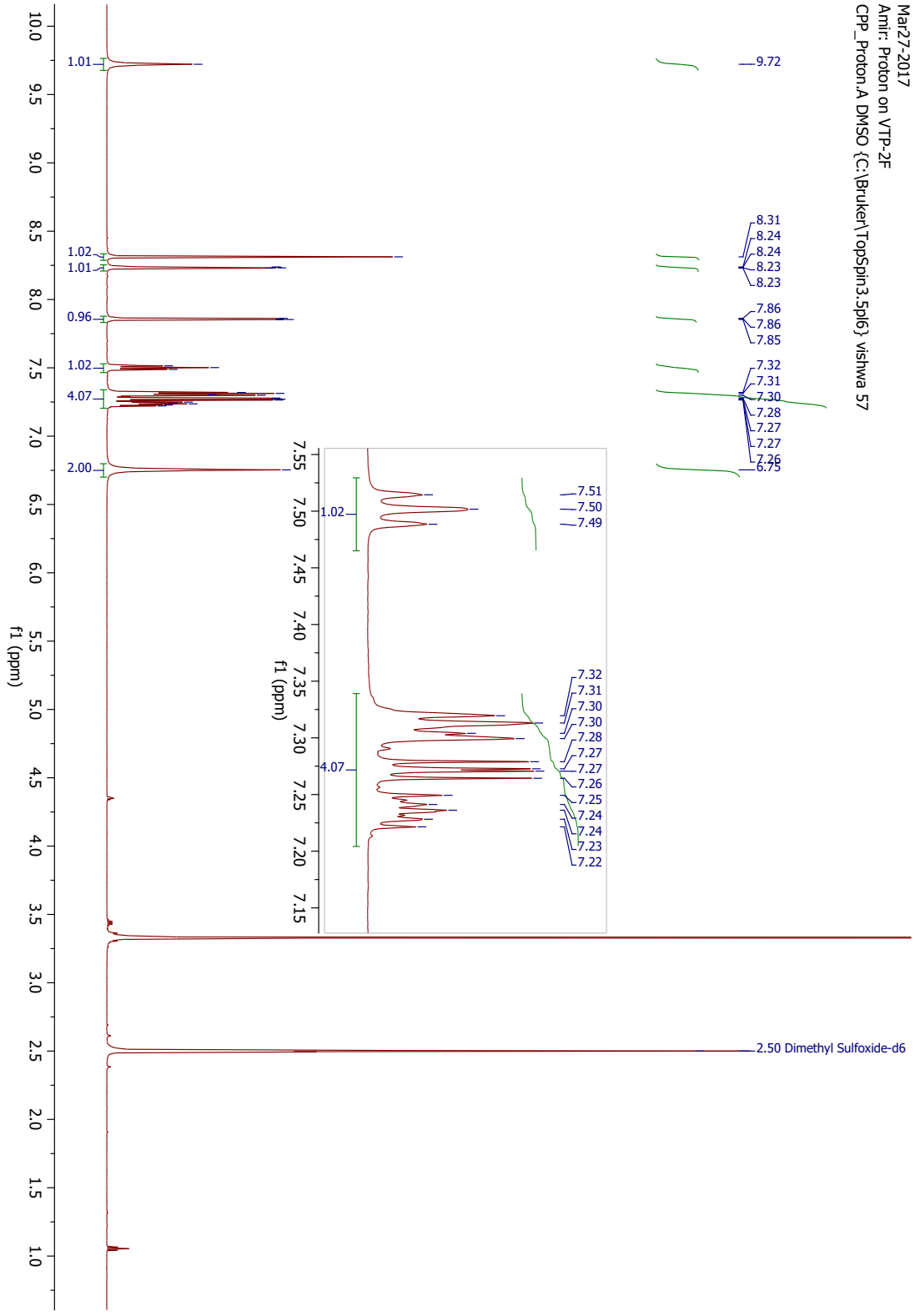

A1.18 ^{13}C-NMR (DEPTQ) 150 MHz, 7i

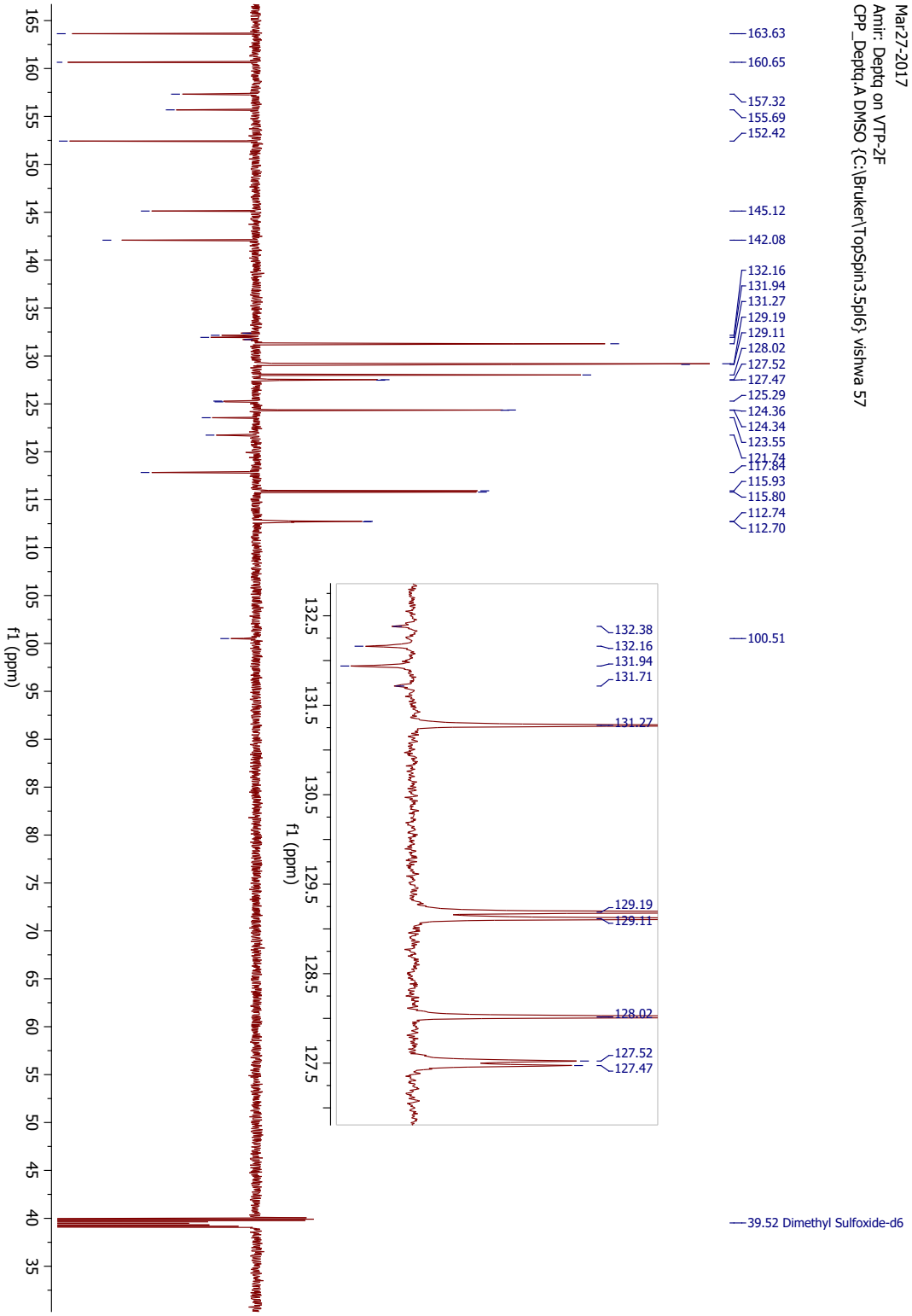

A1.19 ^{1}H-NMR 600 MHz, 7j

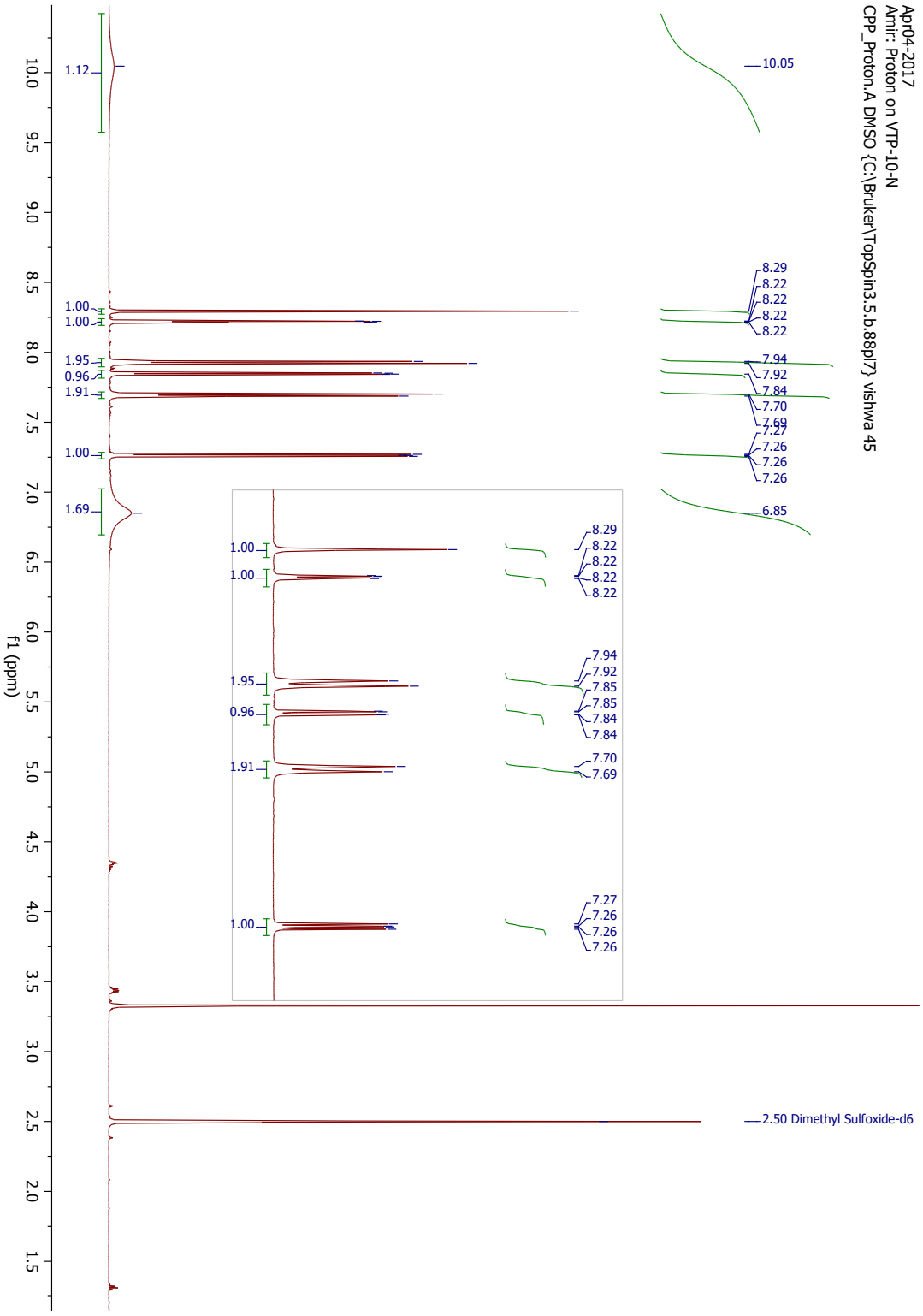

A1.20 ^{13}C-NMR (DEPTQ) 150 MHz, 7j

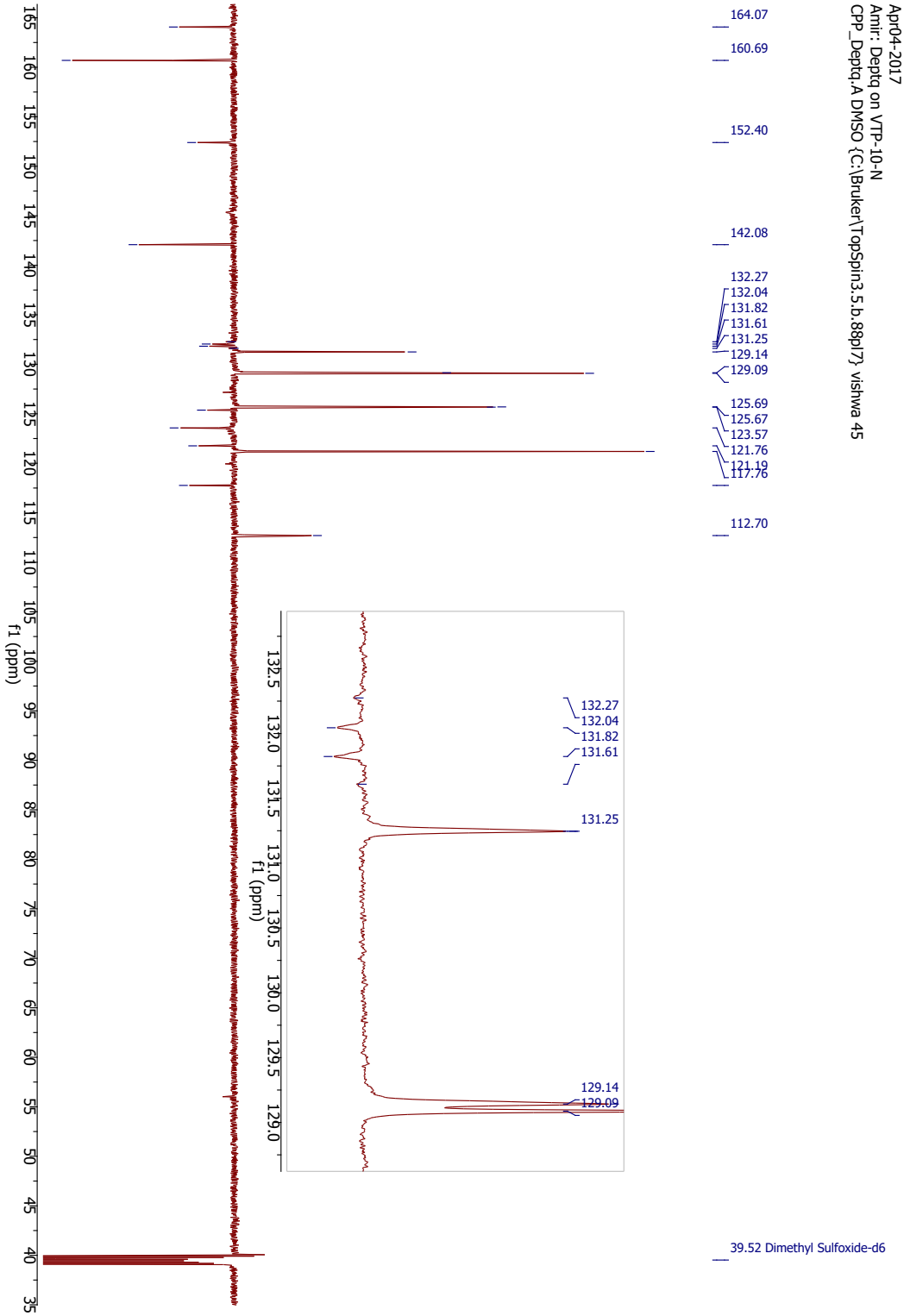

A1.21 ^{1}H-NMR 600 MHz, 7K

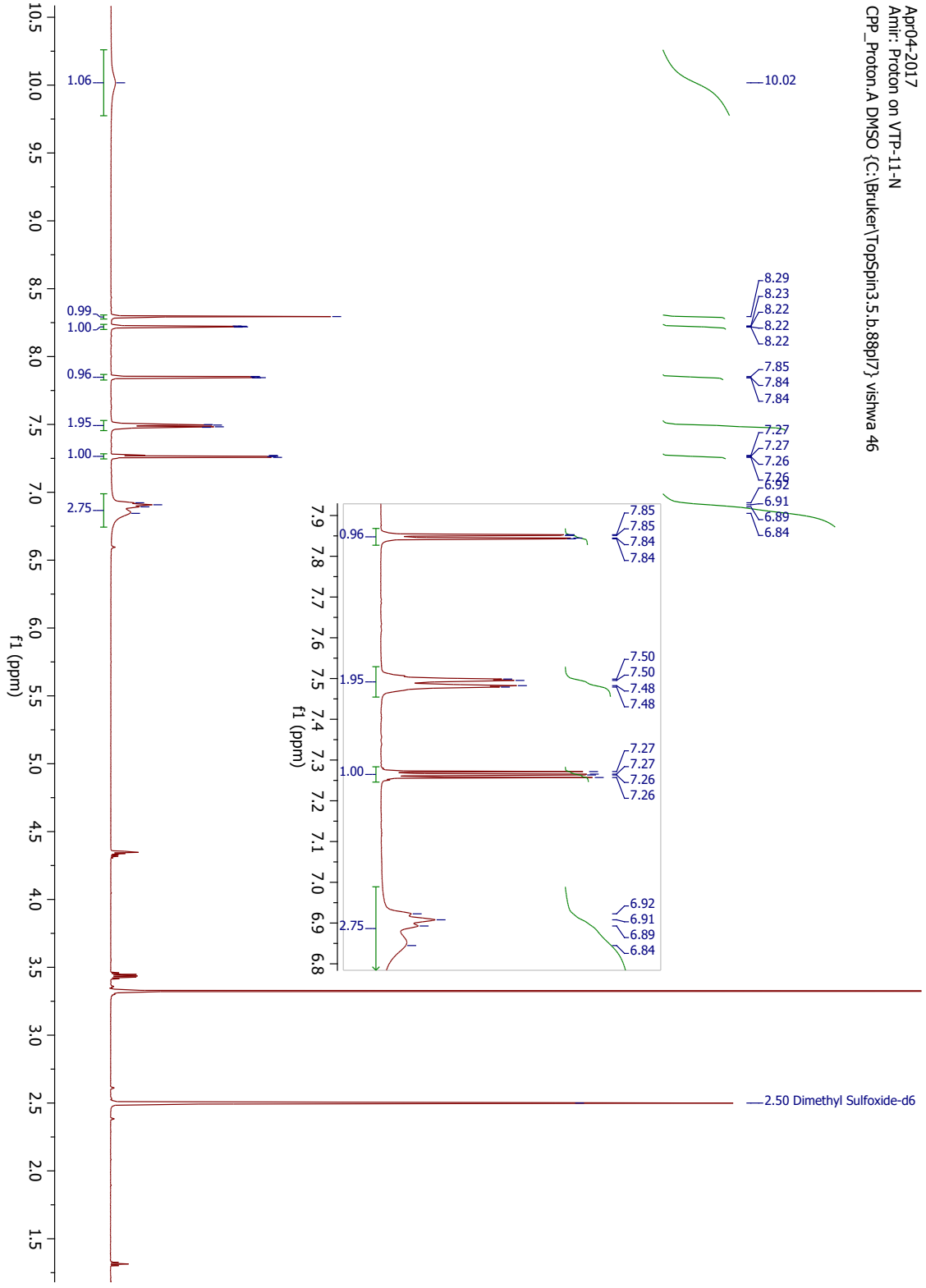

A1.22 ^{13}C-NMR (DEPTQ) 150 MHz, 7k

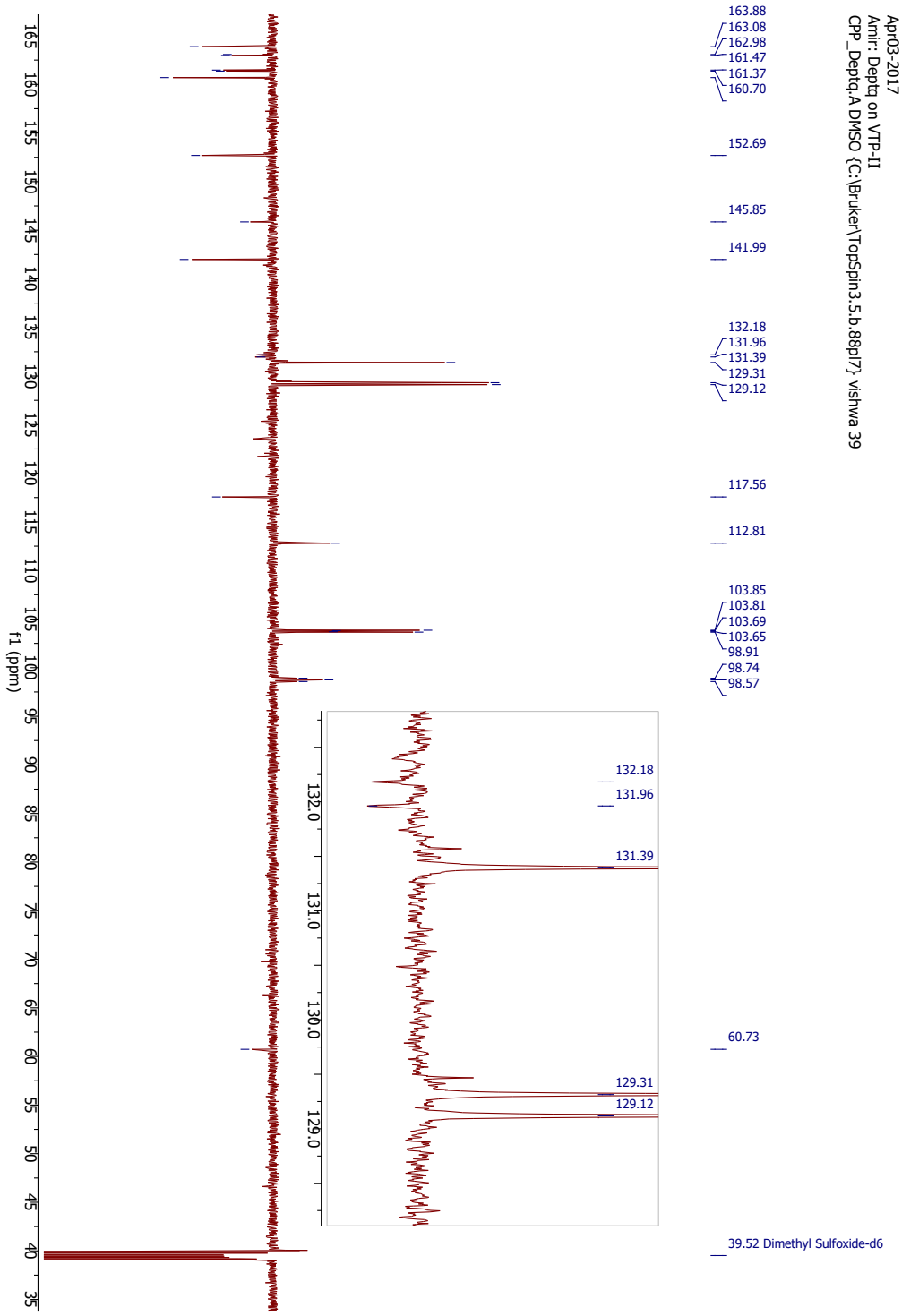

A1.23 ^{1}H-NMR 600 MHz, F2

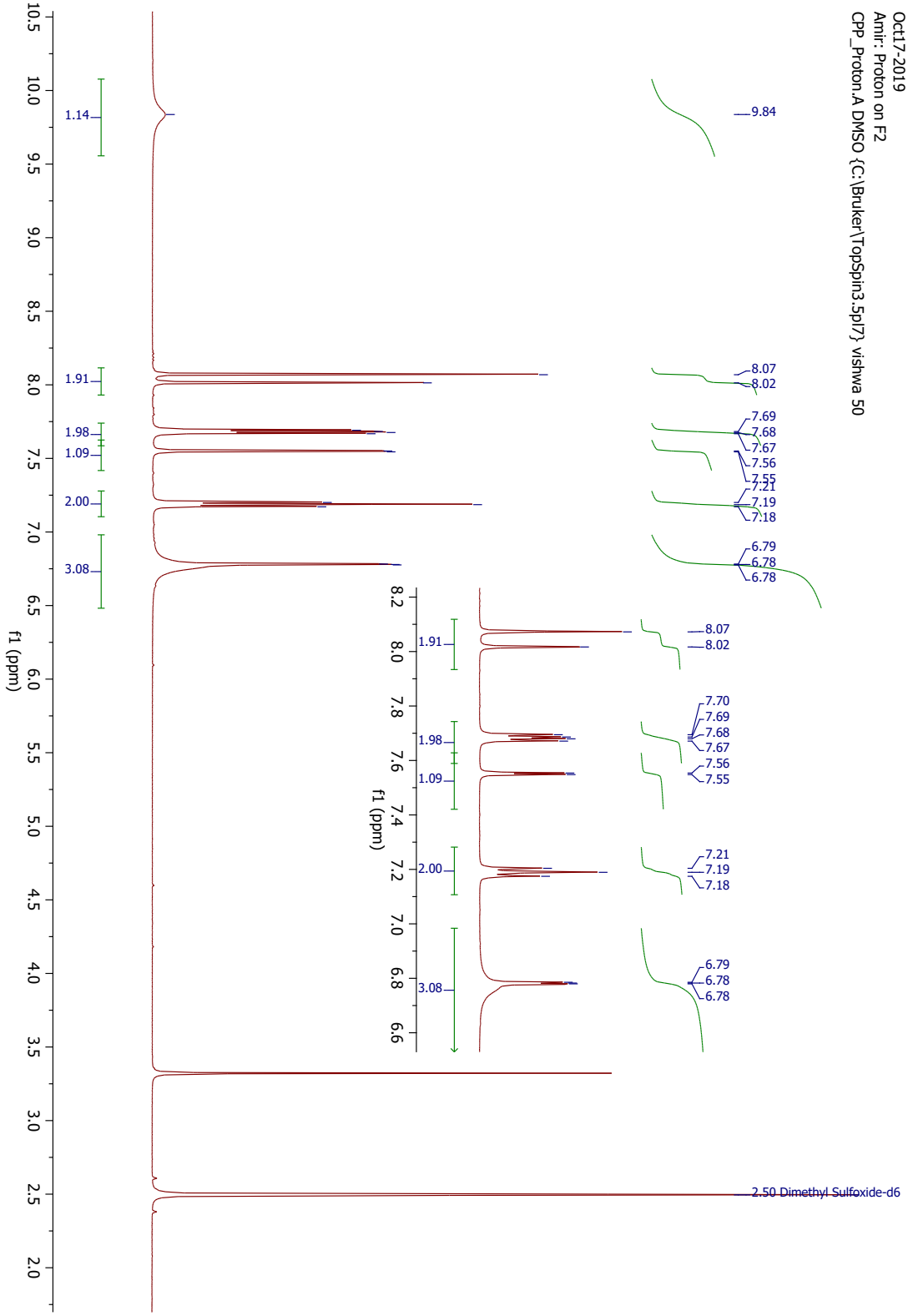

A1.24 ^{13}C-NMR (DEPTQ) 150 MHz, F2

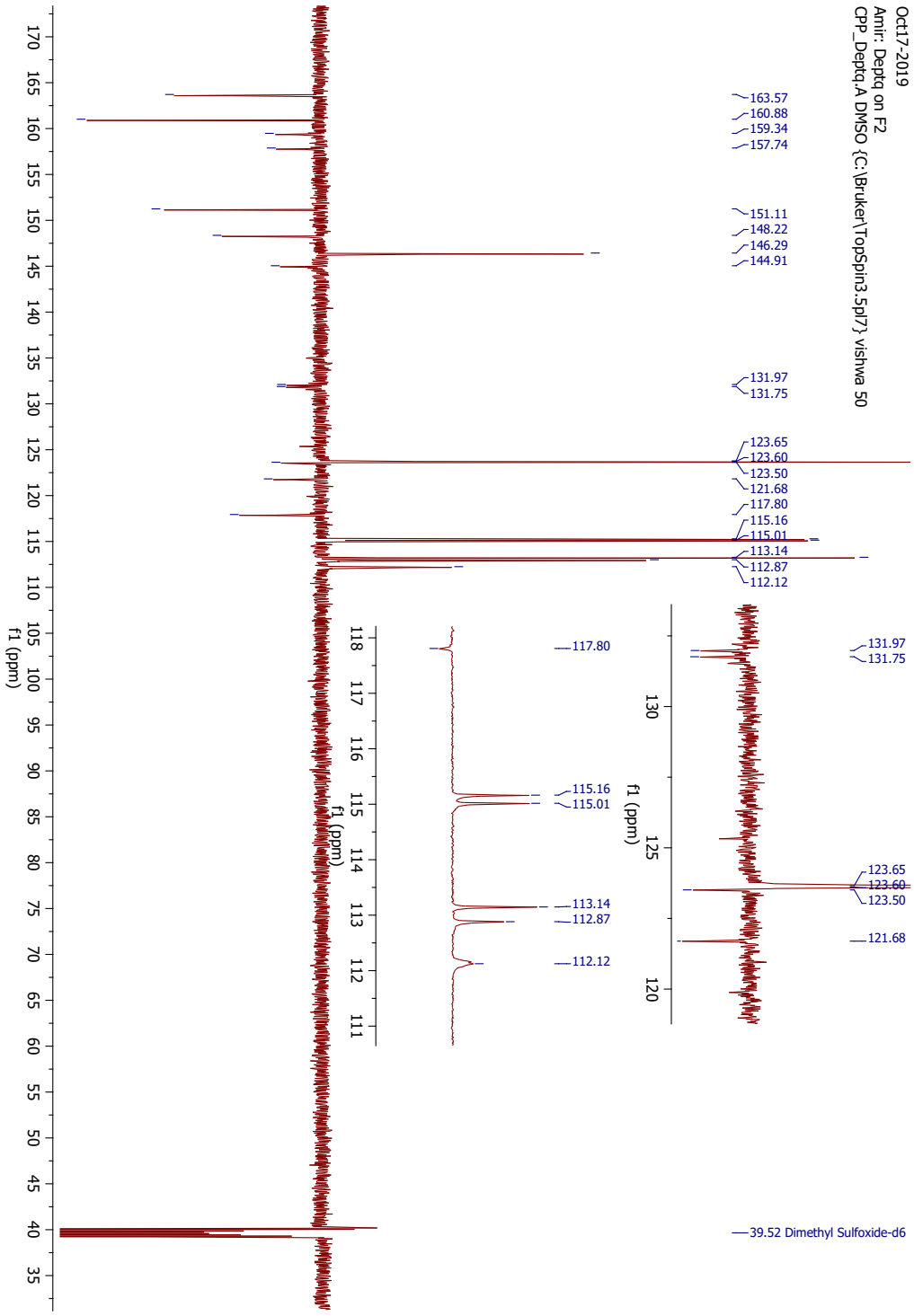

A1.25 ^{1}H-NMR 600 MHz, F3

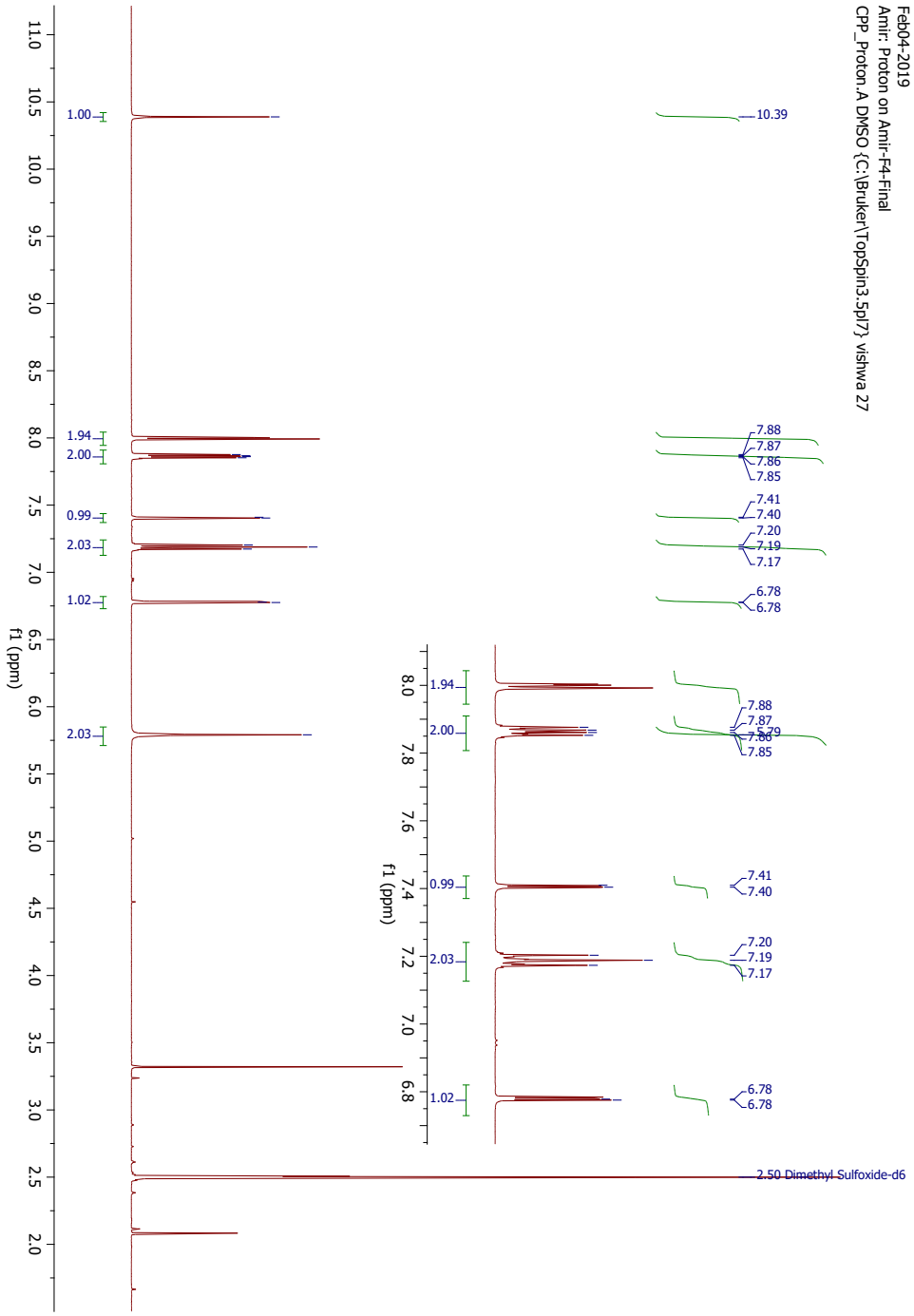

A1.26 ^{13}C-NMR (DEPTQ) 150 MHz, F3

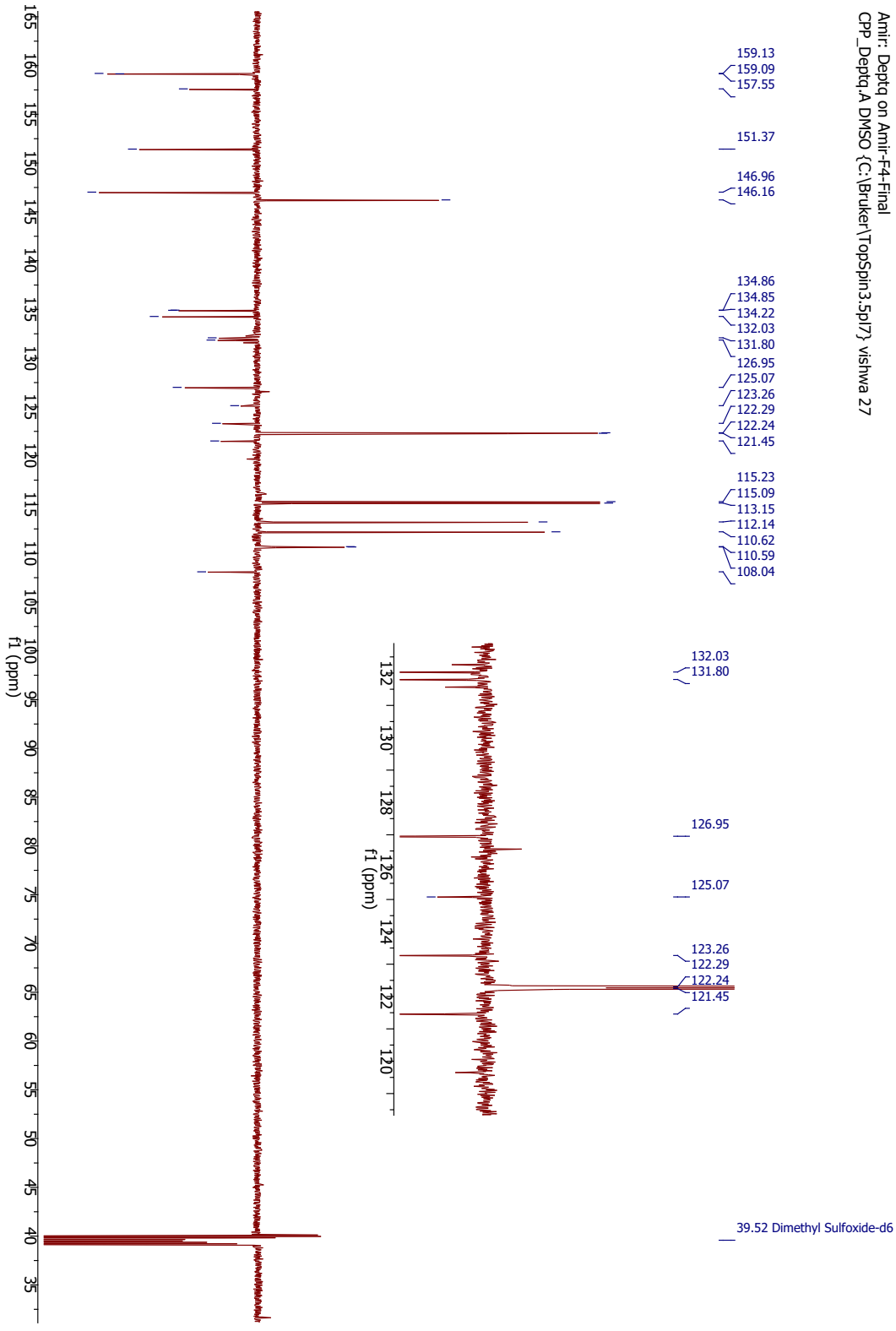

A1.27 ^{1}H-NMR 600 MHz, F4

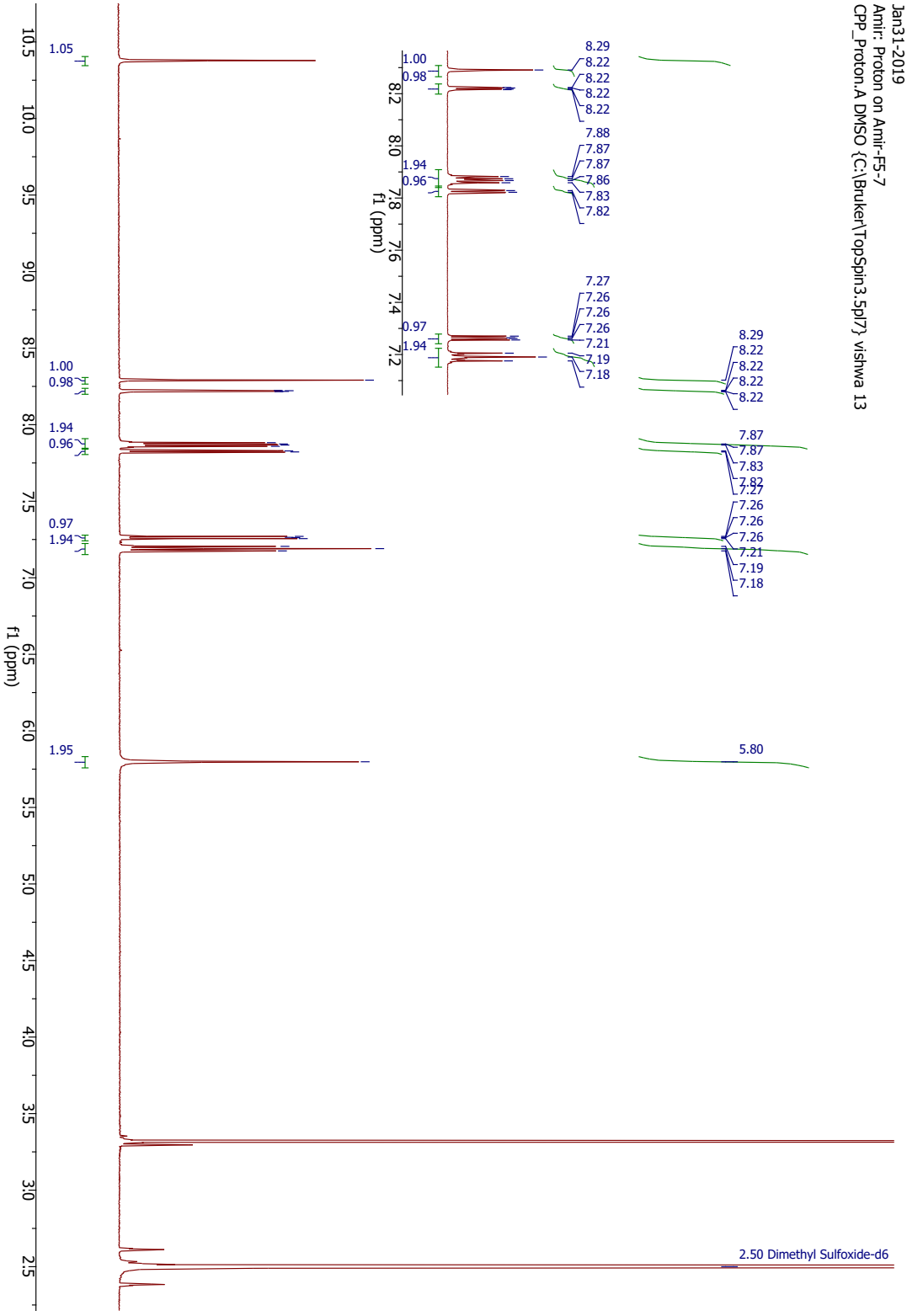

A1.28 ^{13}C-NMR (DEPTQ) 150 MHz, F4

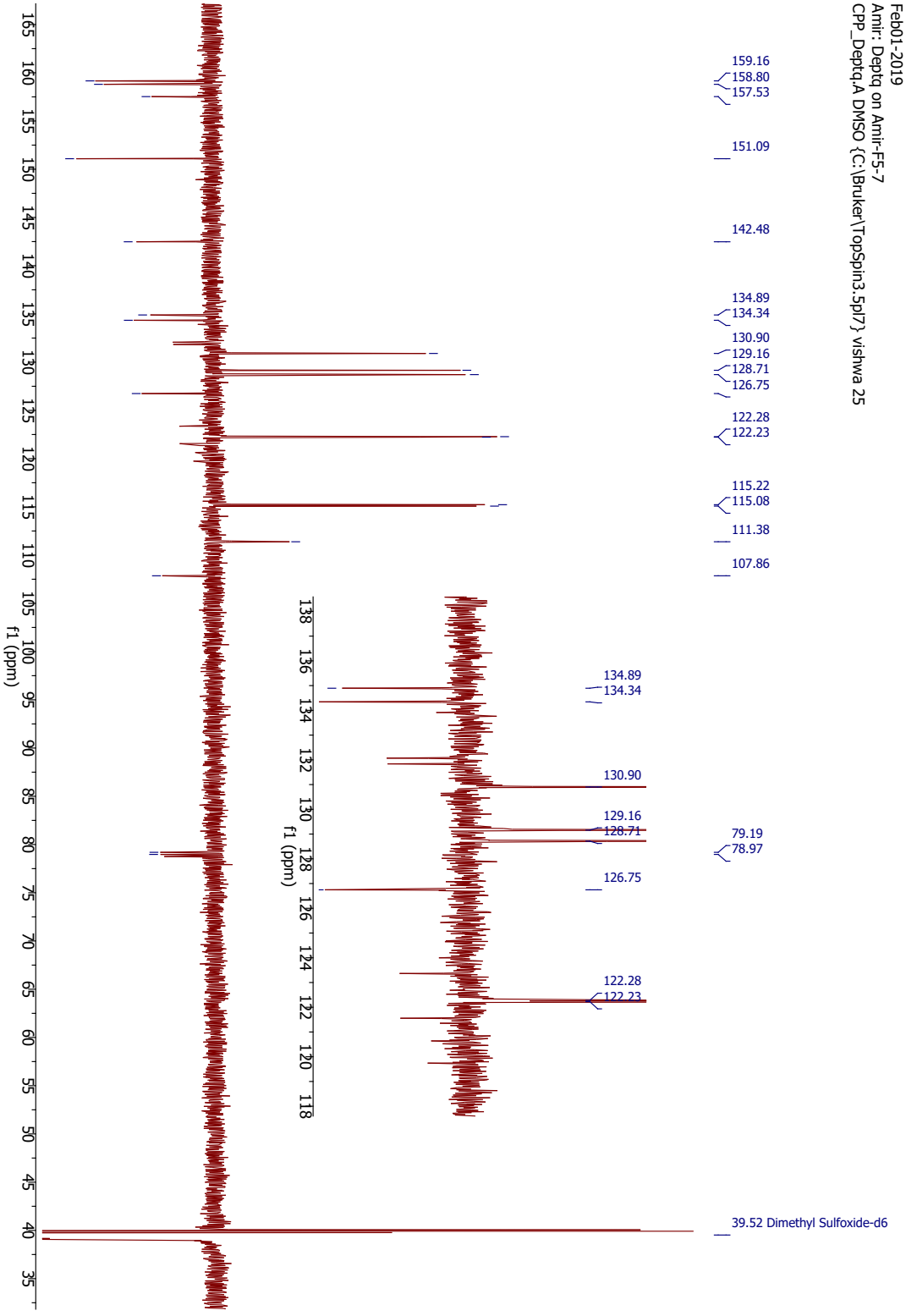

A1.29 ^{1}H-NMR 600 MHz, F5

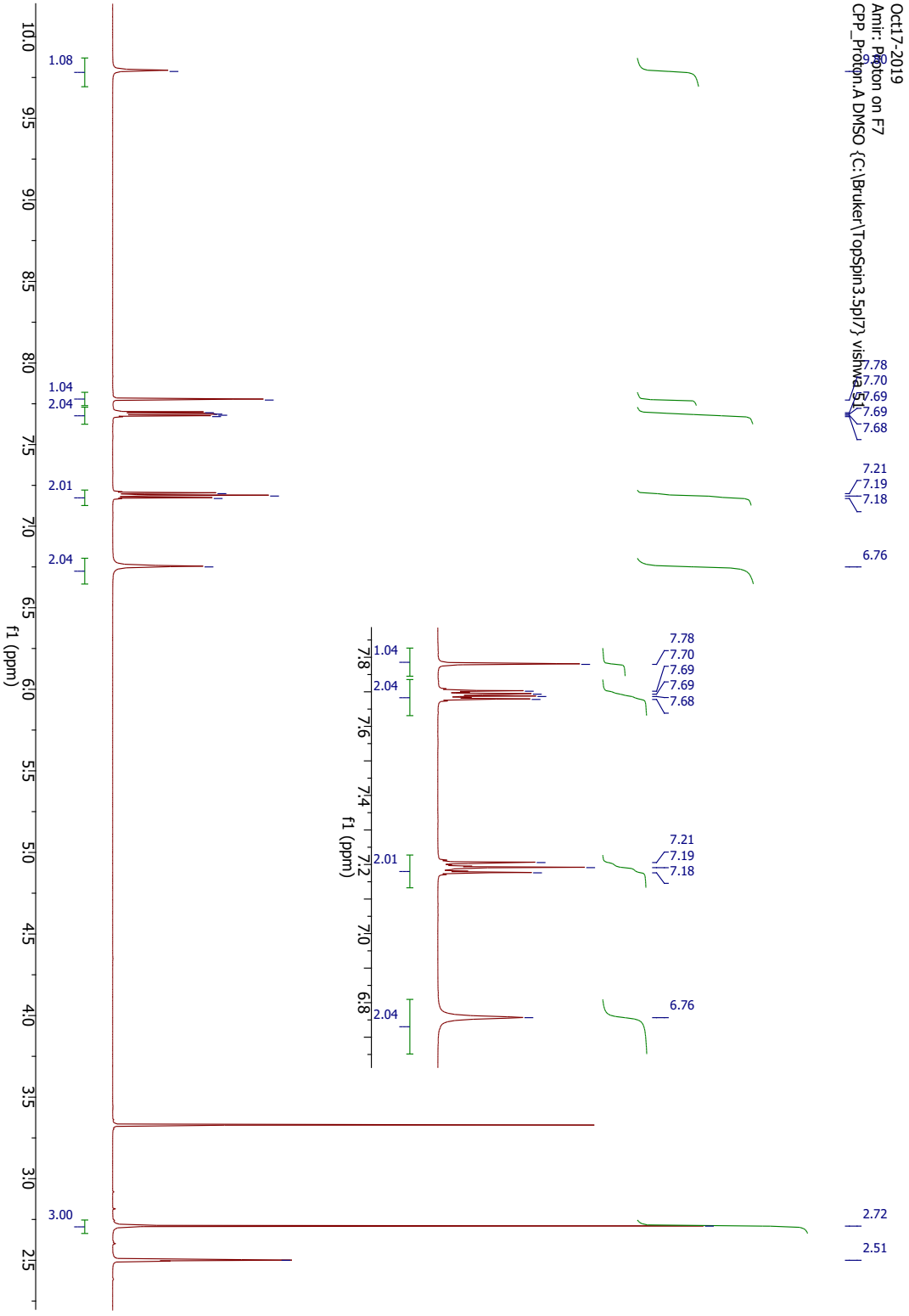

A1.30 ^{13}C-NMR (DEPTQ) 150 MHz, F5

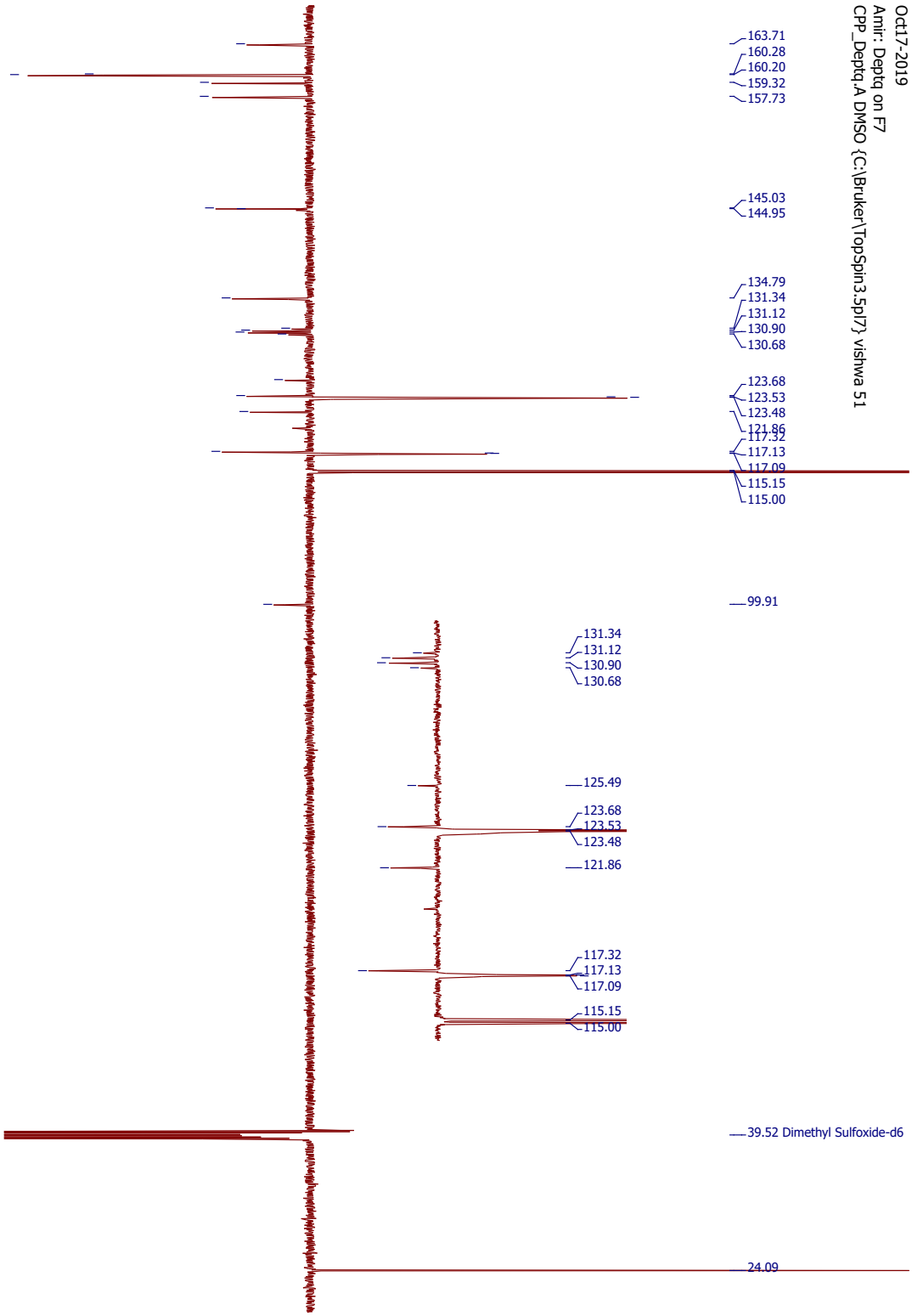

A1.31 ^{1}H-NMR 600 MHz, F6

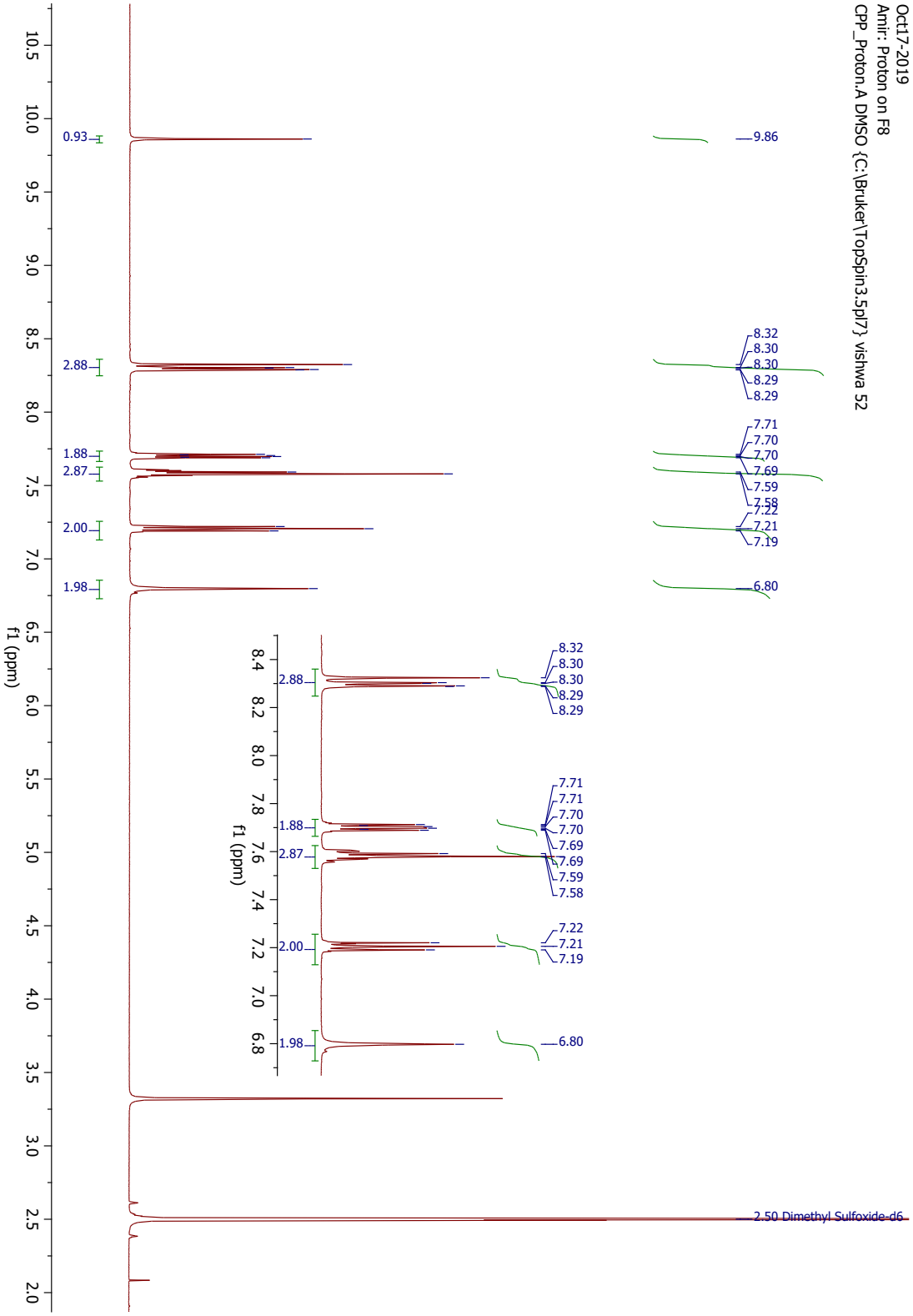

A1.32 ^{13}C-NMR (DEPTQ) 150 MHz, F6

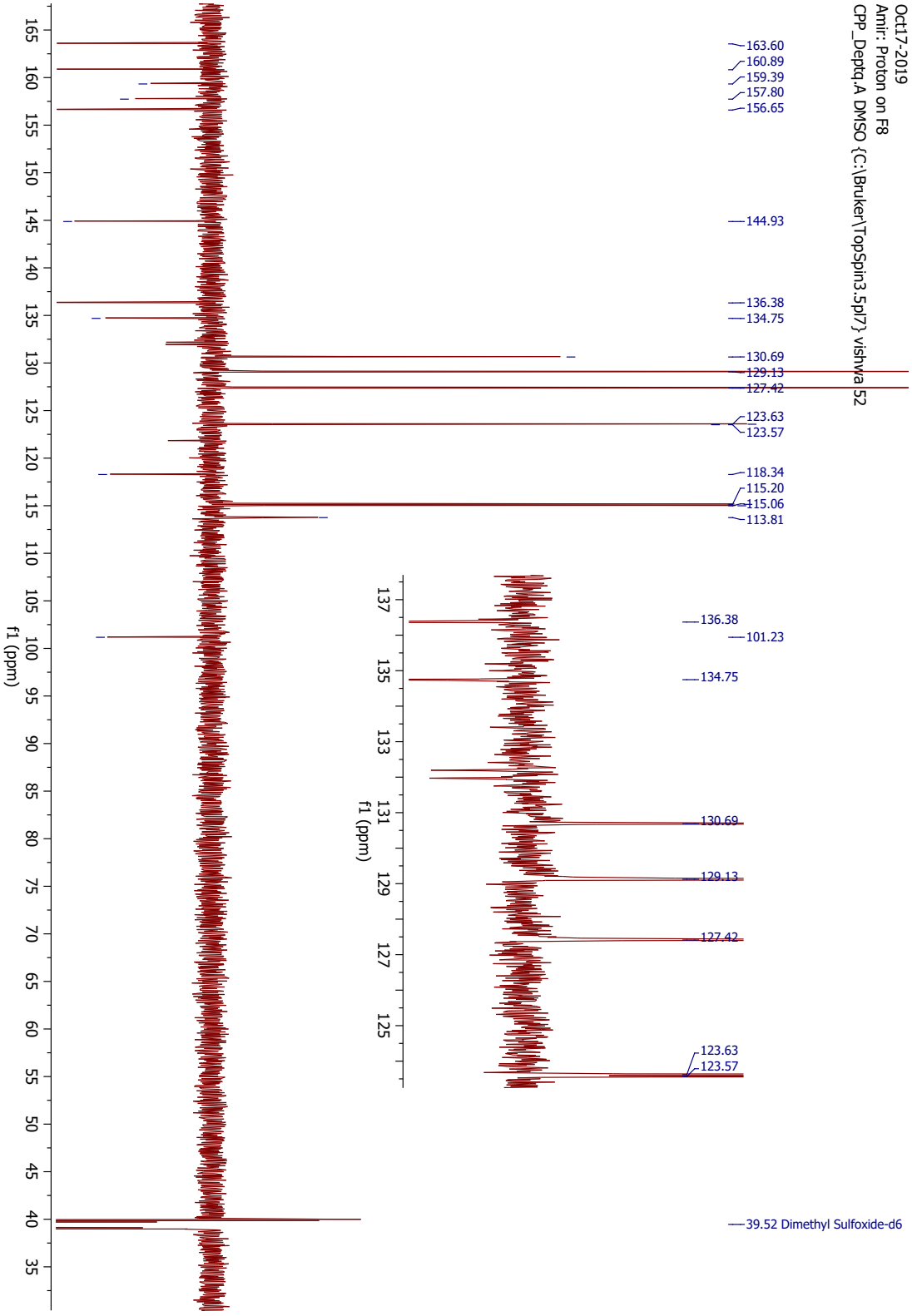

A1.33 ^{1}H-NMR 600 MHz, TFI-4INT

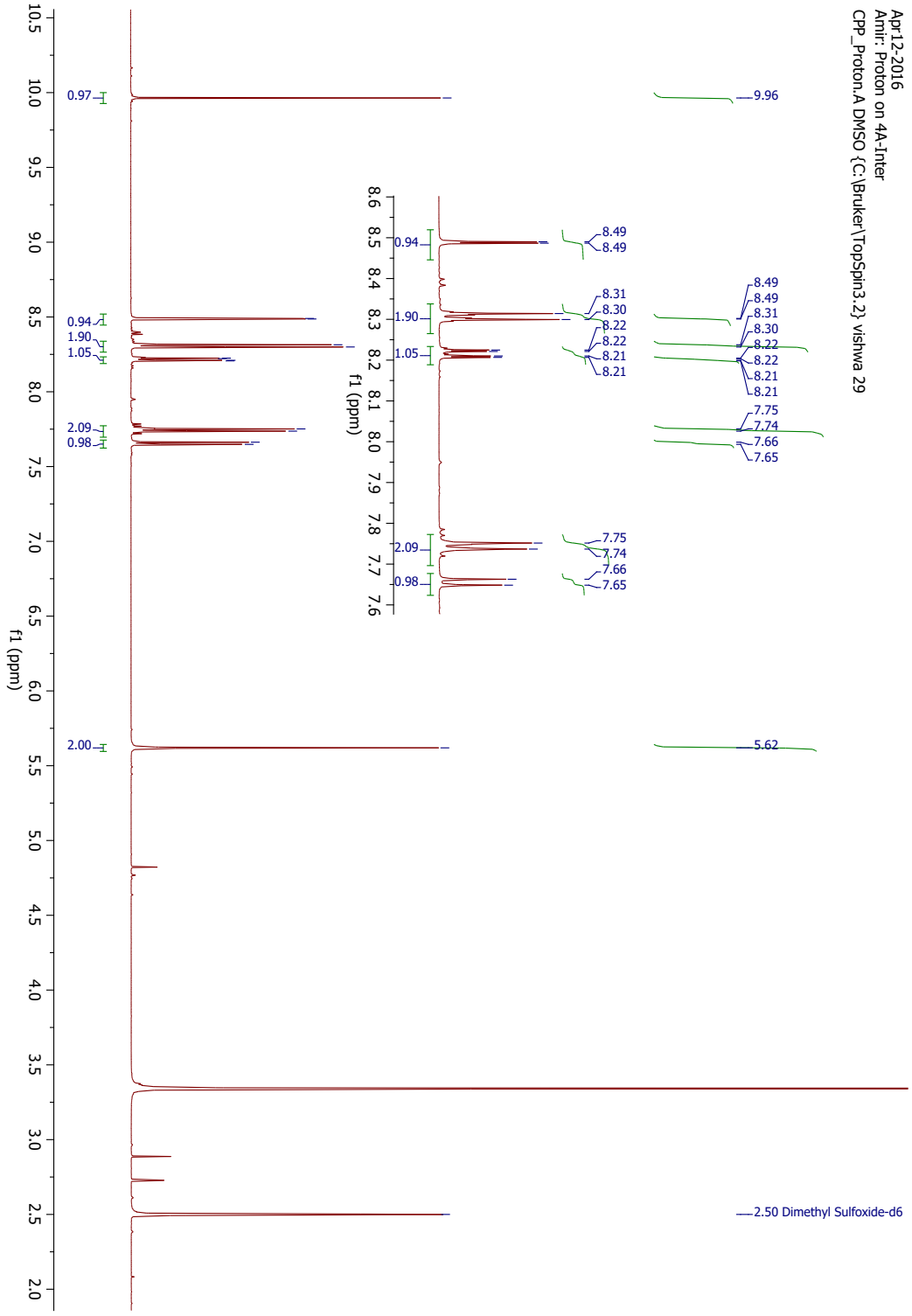

A1.34 ^{13}C-NMR (DEPTQ) 150 MHz, TFI-4INT

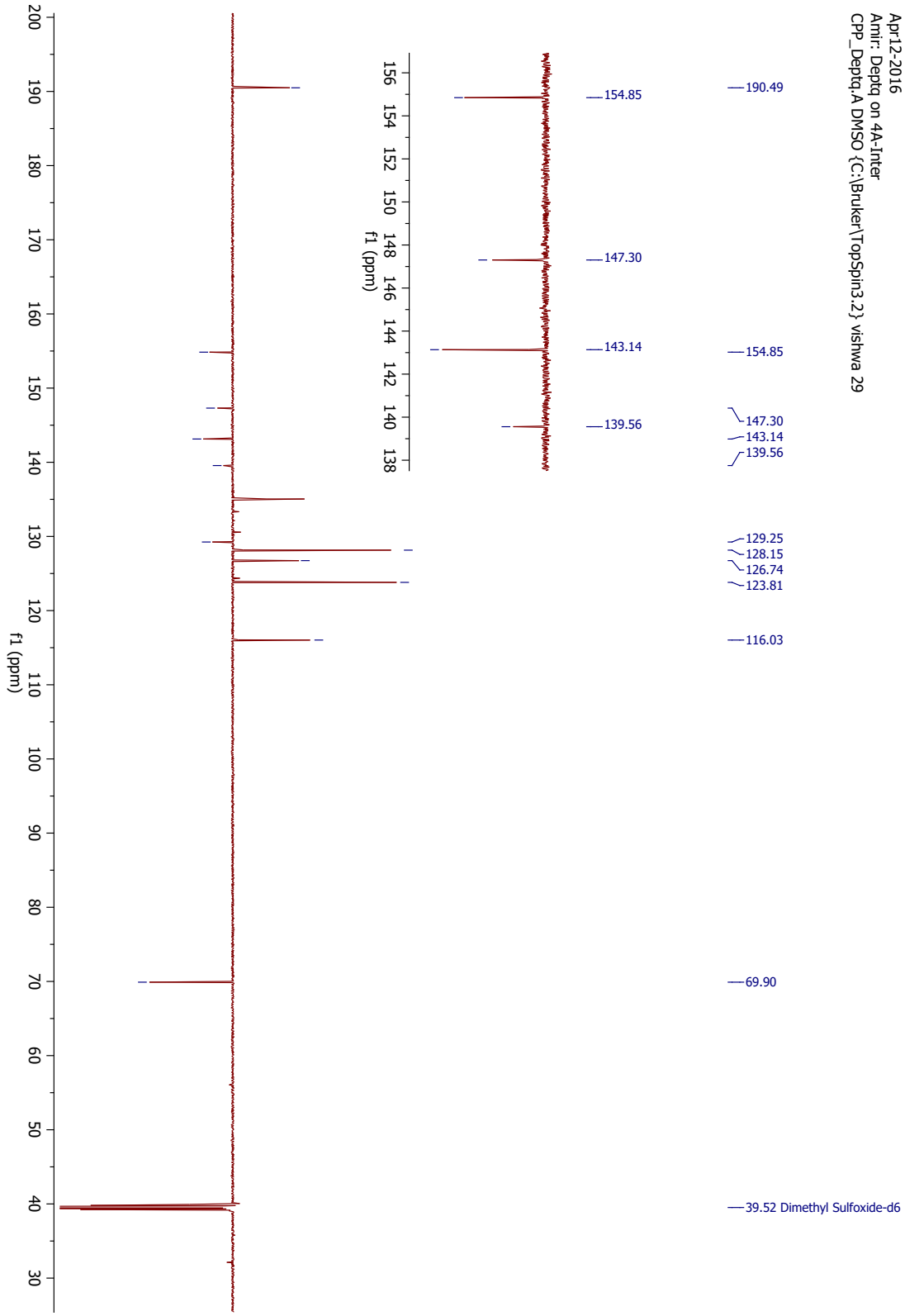

A1.35 ^{1}H-NMR 600 MHz, TFI-5INT

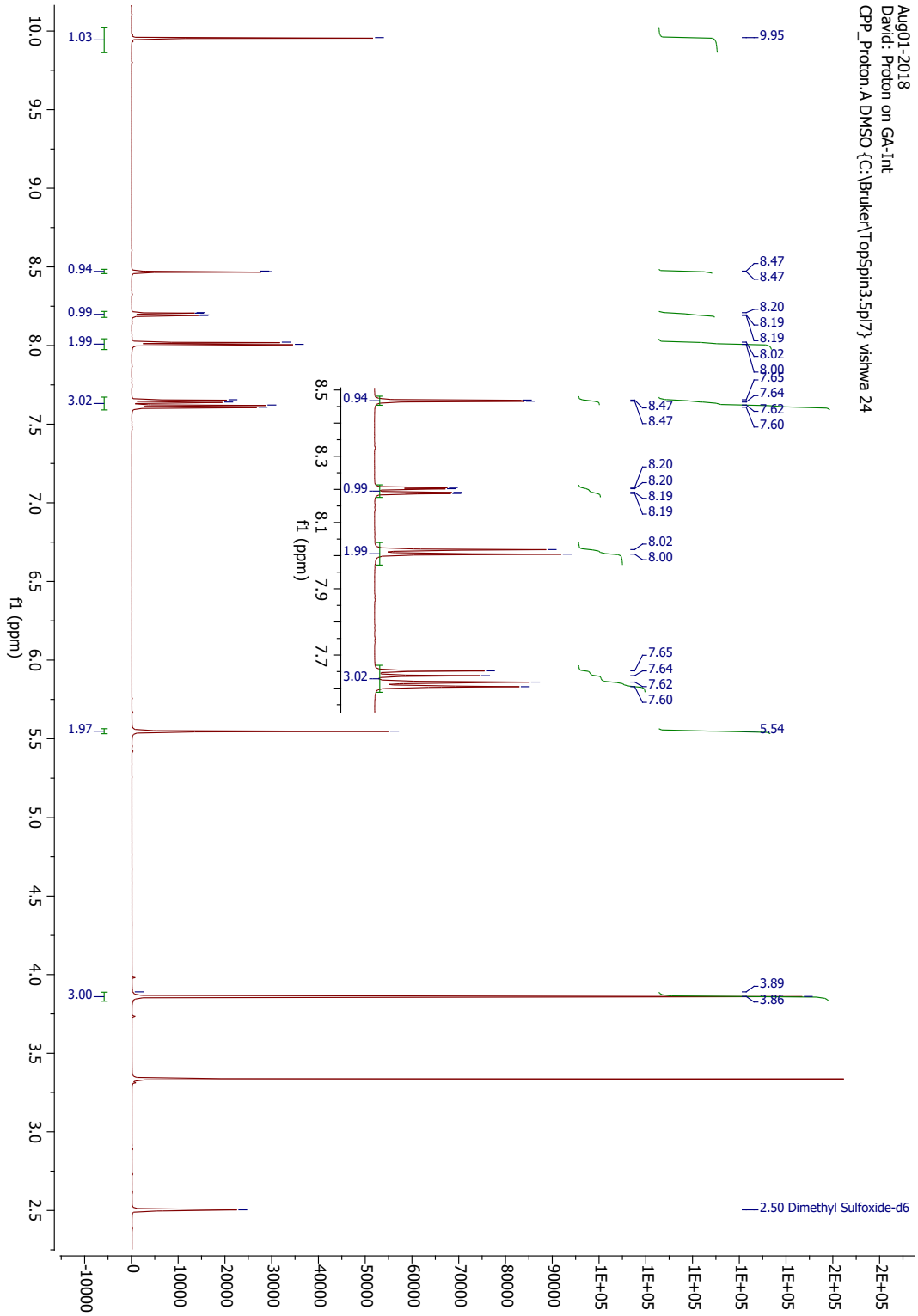

A1.36 ^{13}C-NMR (DEPTQ) 150 MHz, TFI-5INT

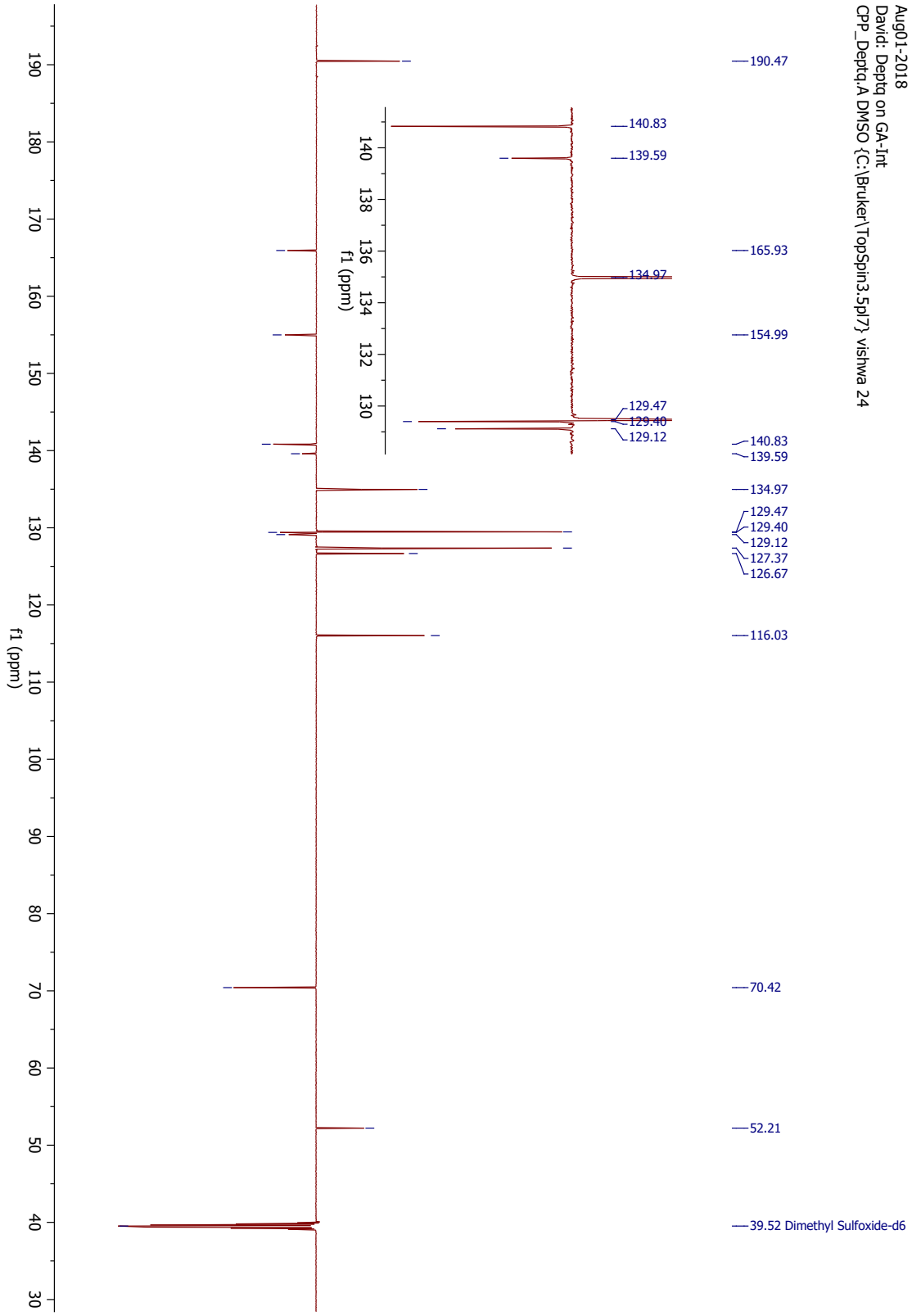

A1.37 ^{1}H-NMR 600 MHz, TFI-6INT

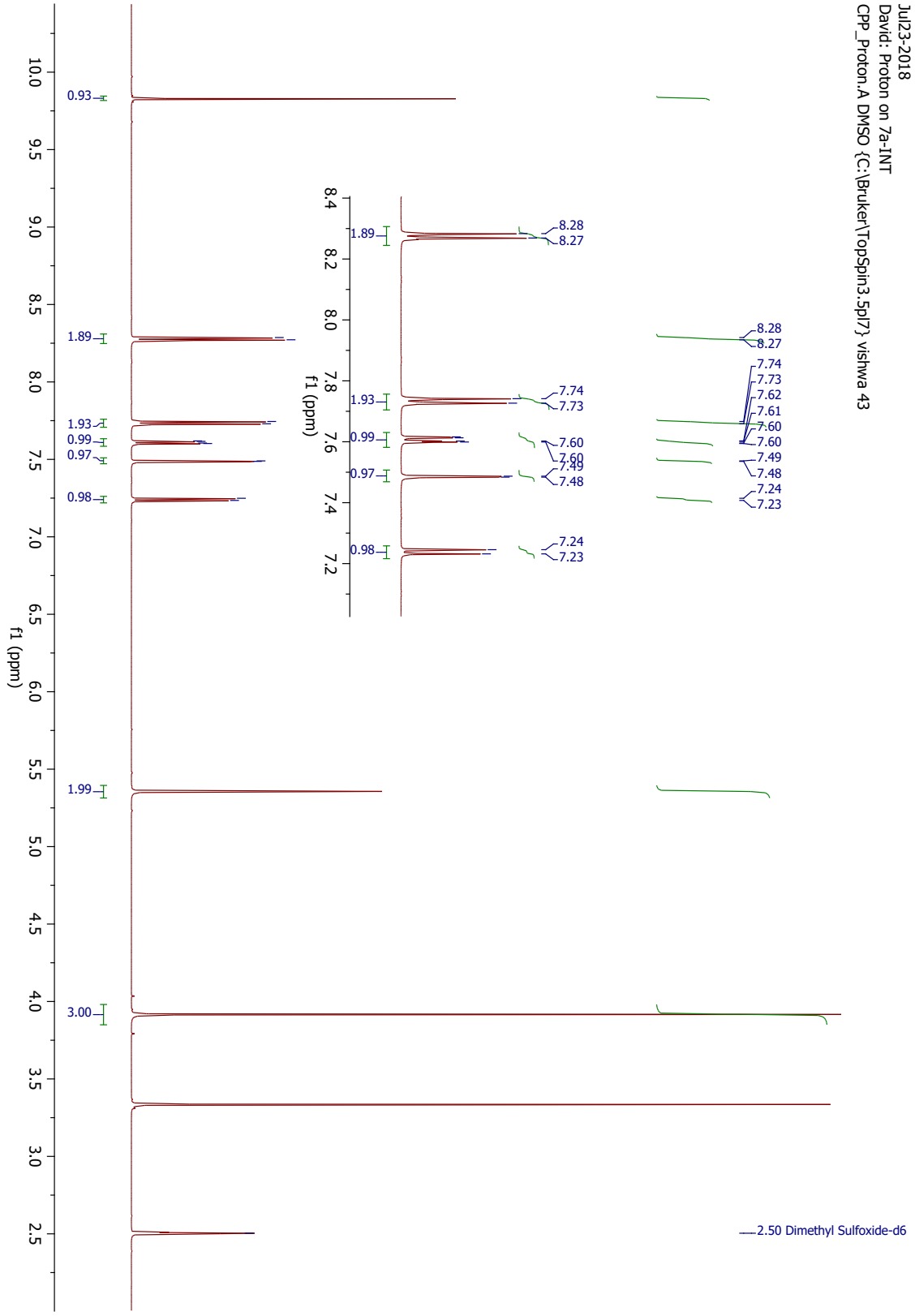

A1.38 ^{13}C-NMR (DEPTQ) 150 MHz, TFI-6INT

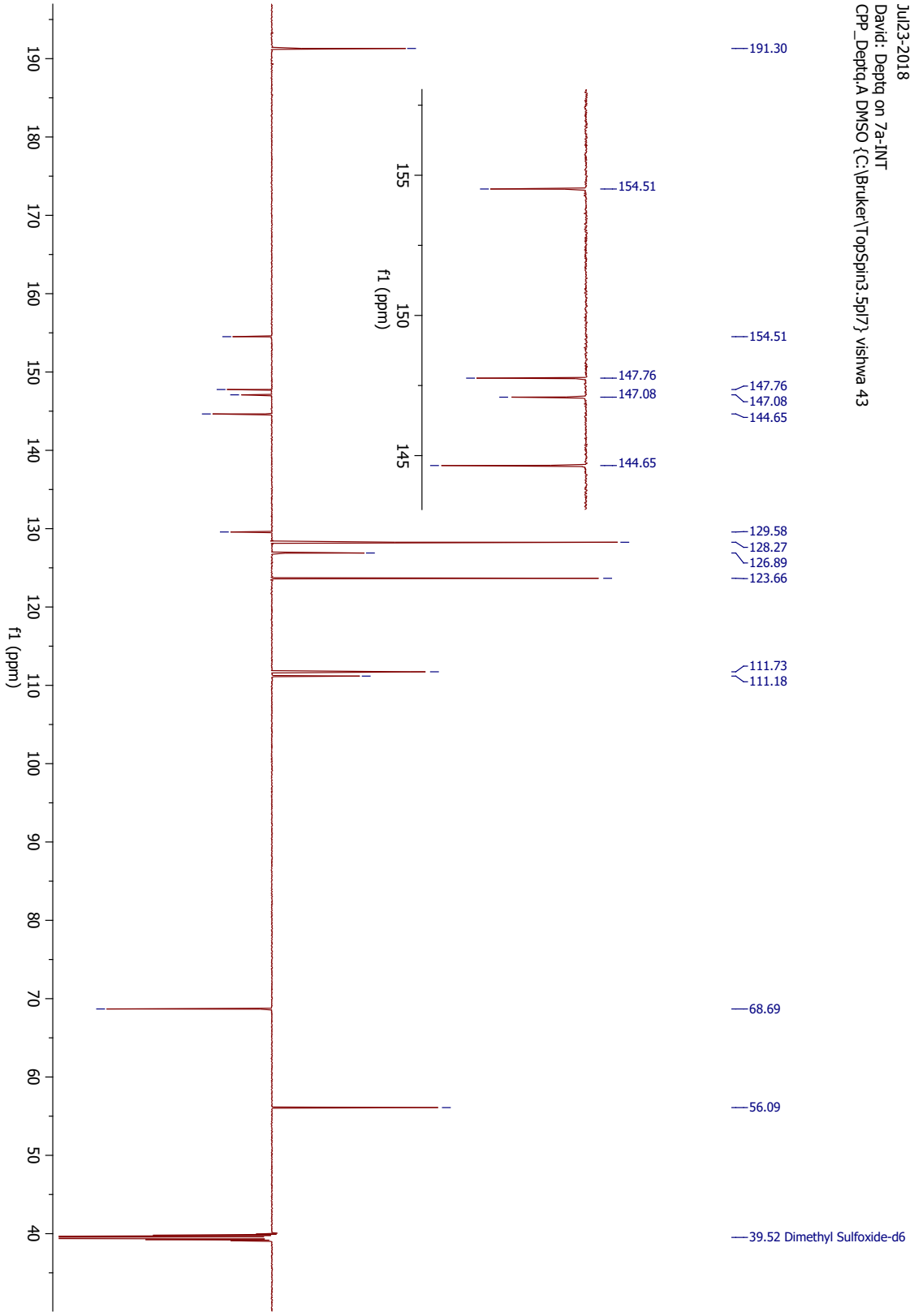

A1.39 ^{1}H-NMR 600 MHz, TFI-7INT

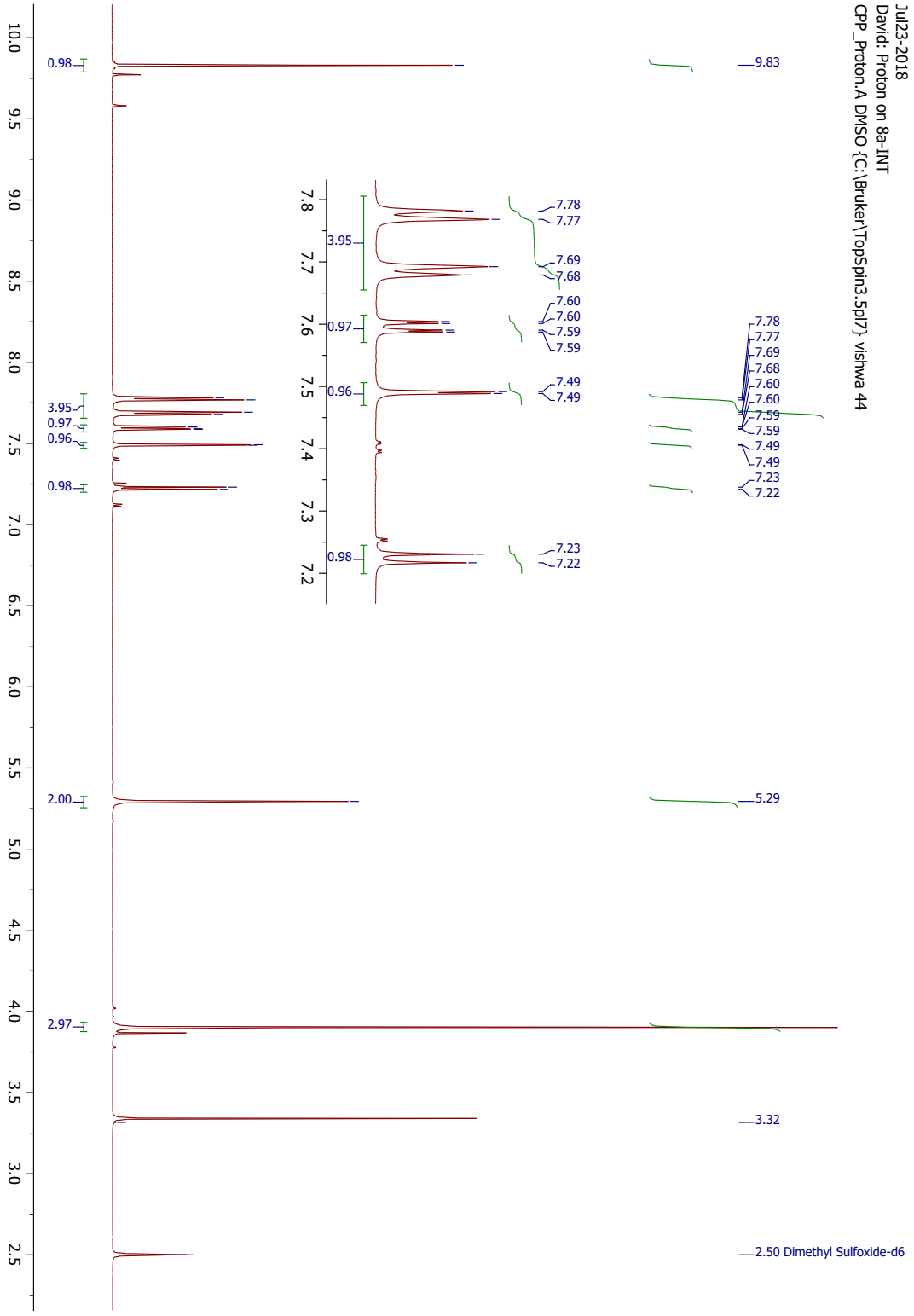

A1.40 ^{13}C-NMR (DEPTQ) 150 MHz, TFI-7INT

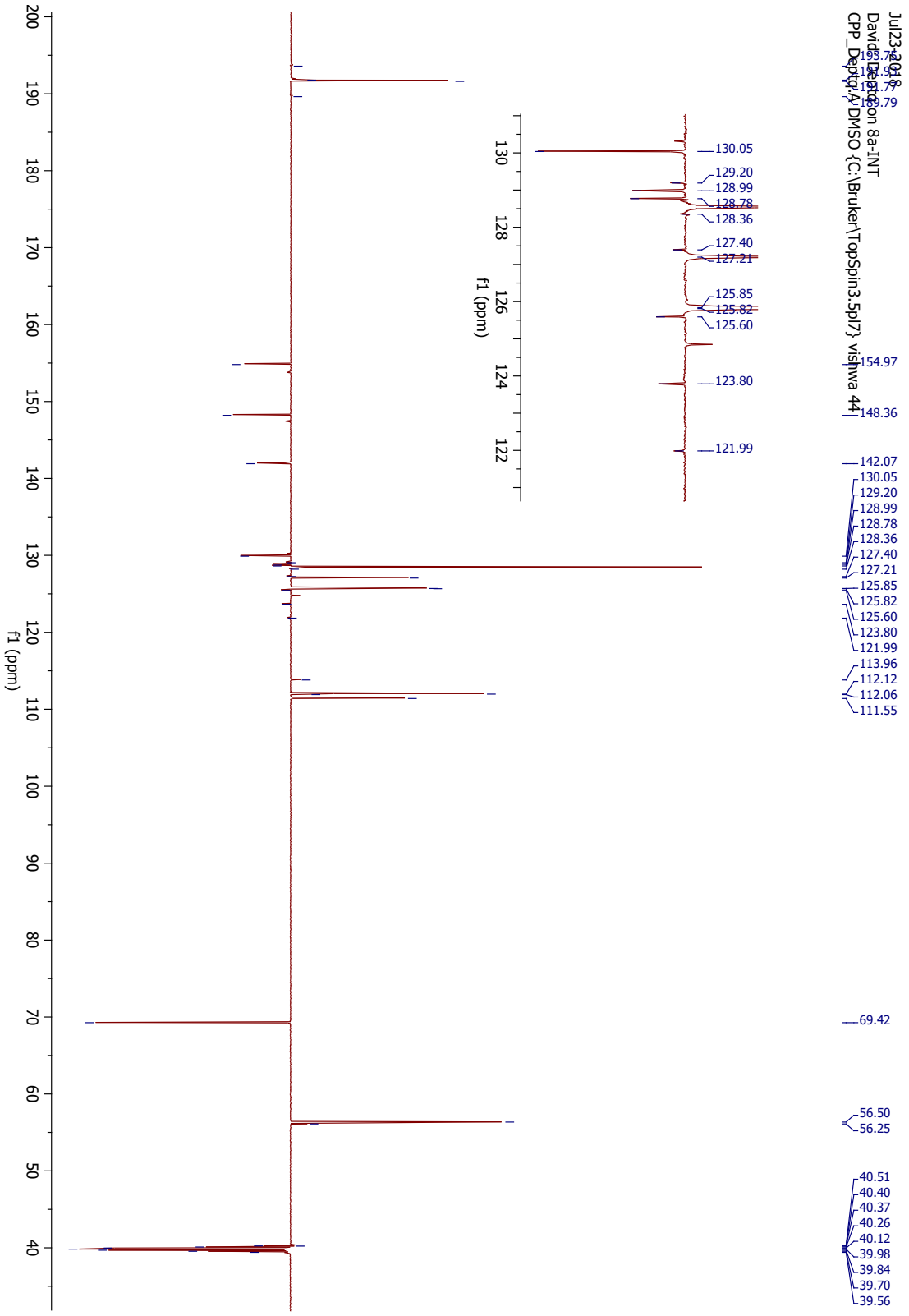

A1.41 ^{19}F NMR 565 MHz, TFI-7INT

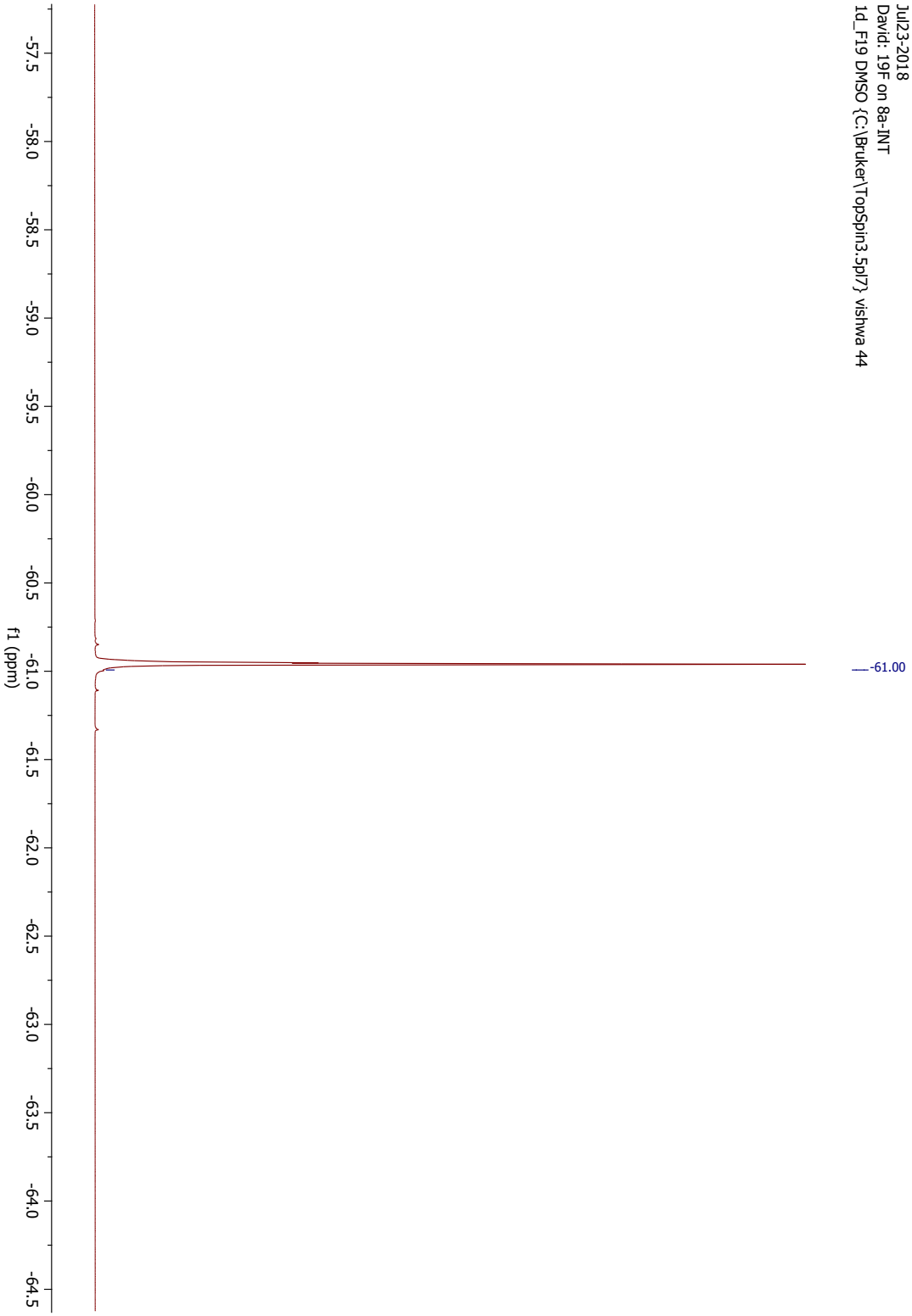

A1.42 ^{1}H-NMR 600 MHz, TFI-8INT

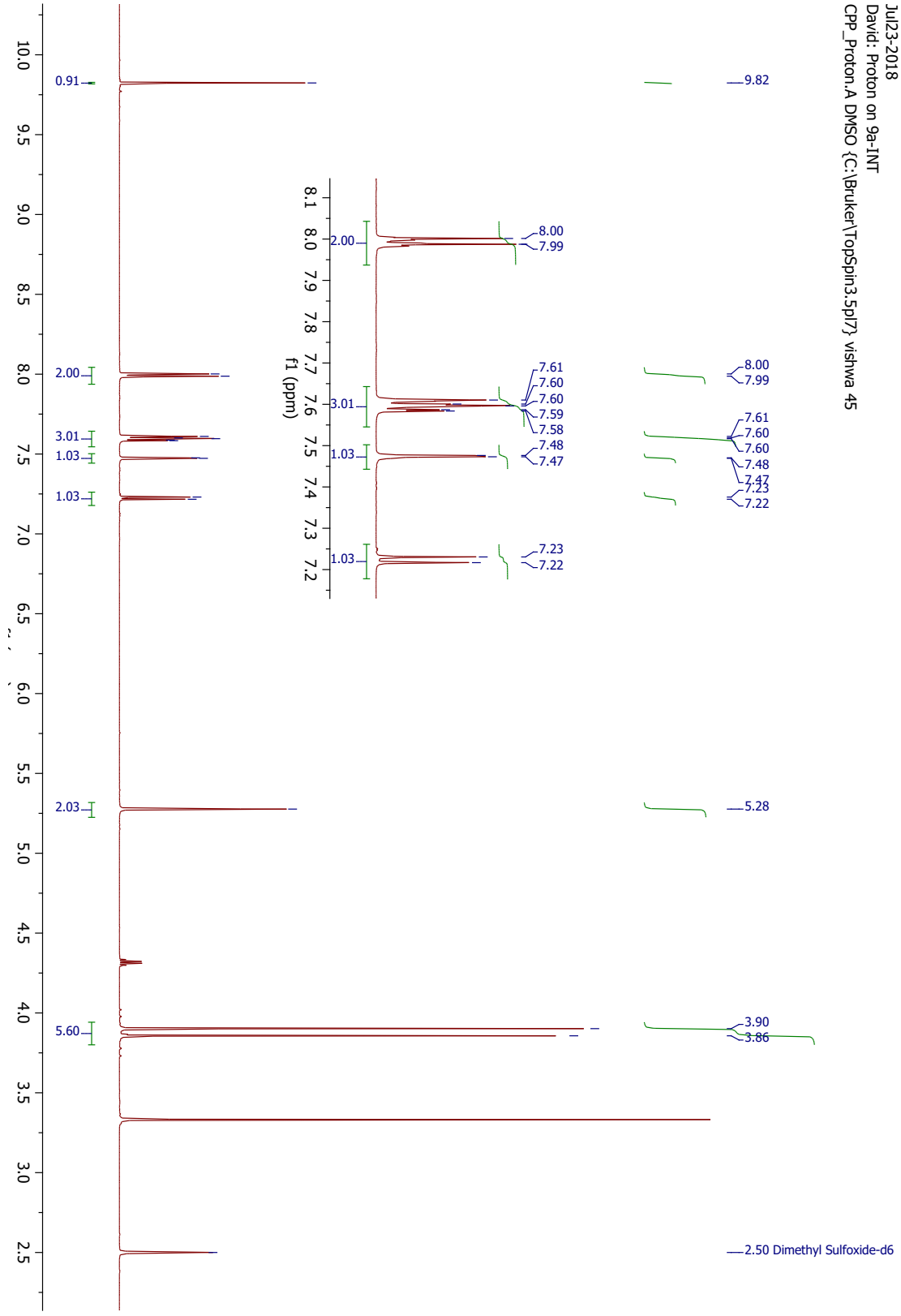

A1.43 ^{13}C-NMR (DEPTQ) 150 MHz, TFI-8INT

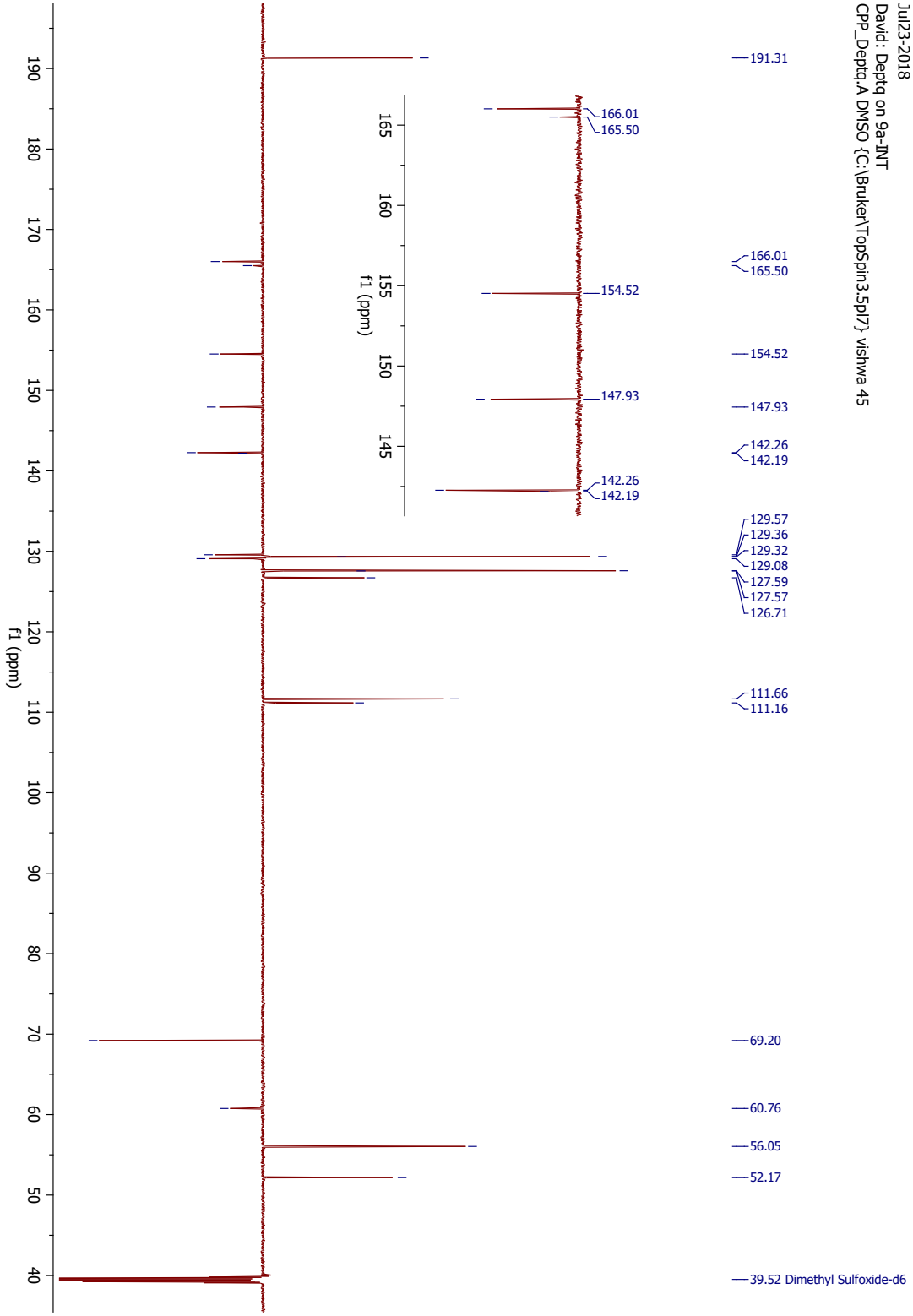

A1.44 ^{1}H-NMR 600 MHz, TFI-9INT

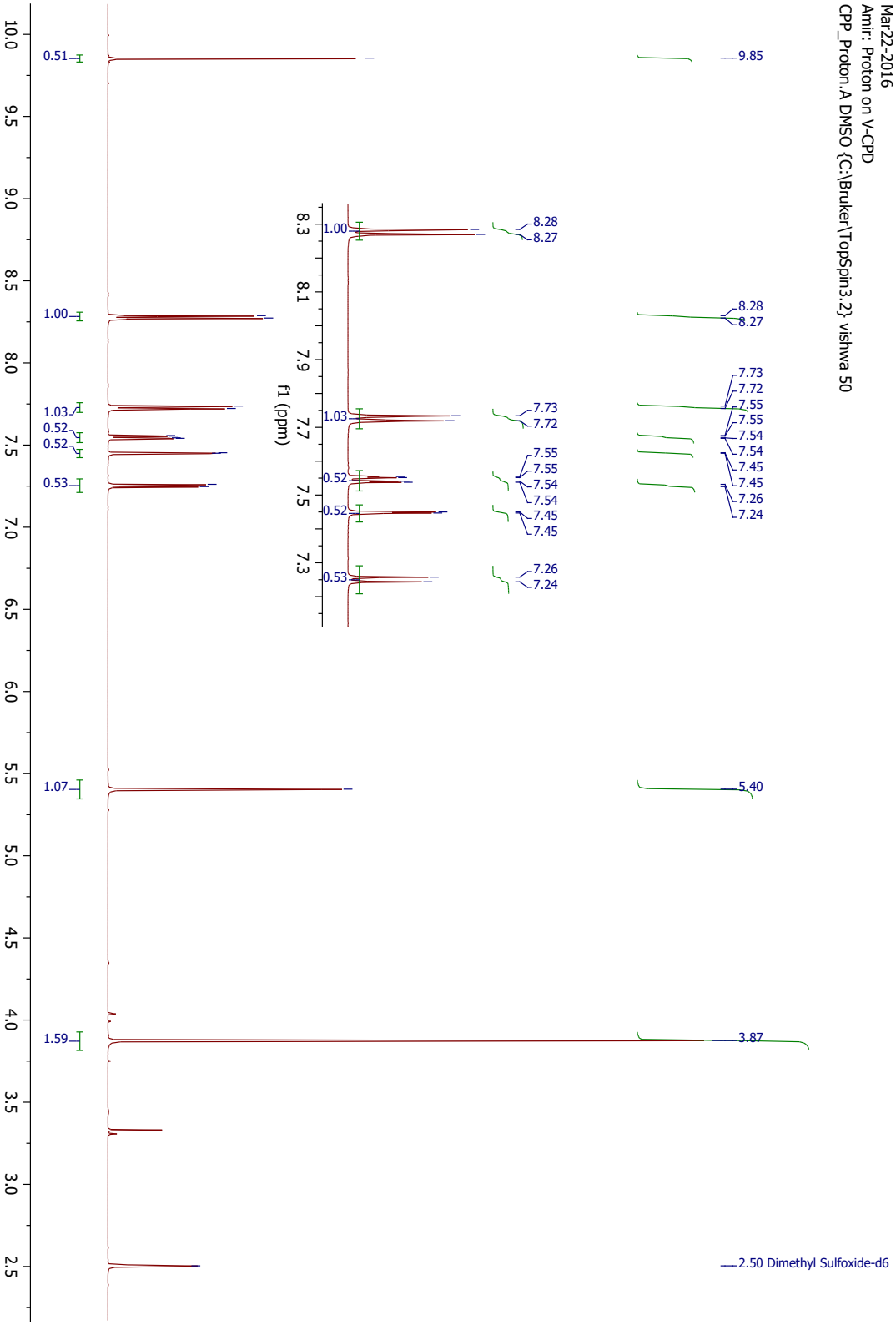

A1.45 ^{13}C-NMR (DEPTQ) 150 MHz, TFI-9INT

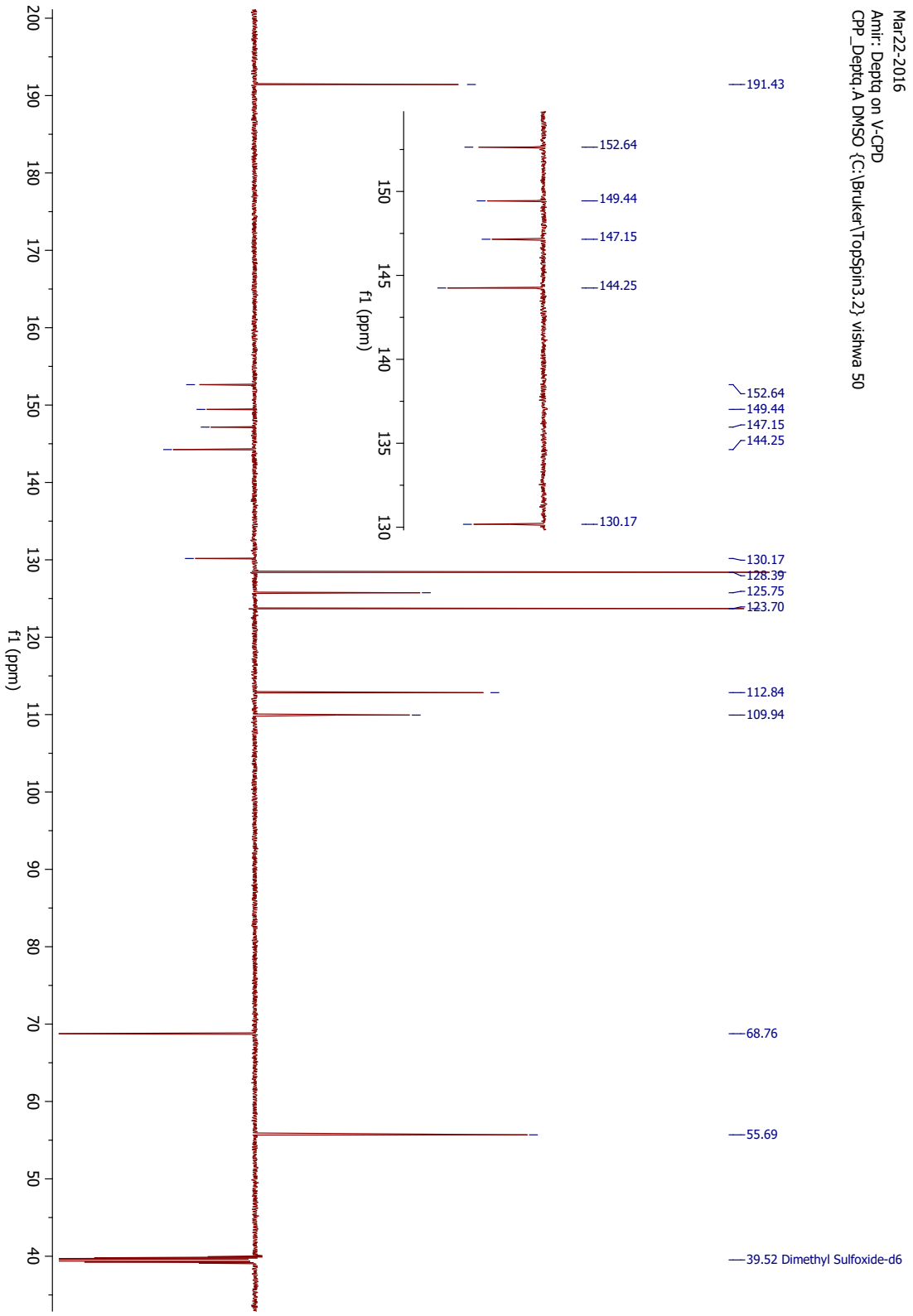

A1.46 ^{1}H-NMR 600 MHz, TFI-11INT

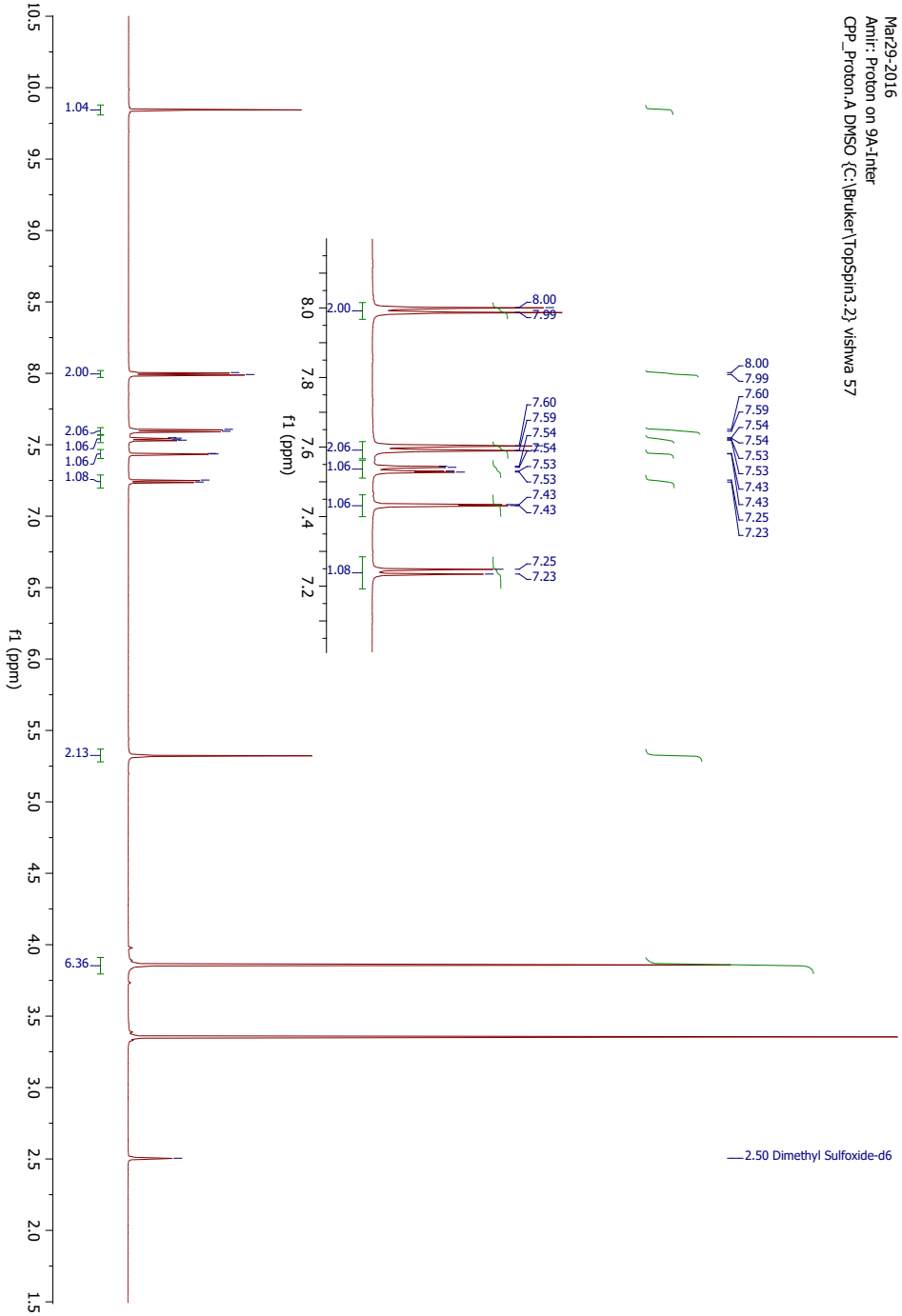

A1.47 ^{13}C-NMR (DEPTQ) 150 MHz, TFI-11INT

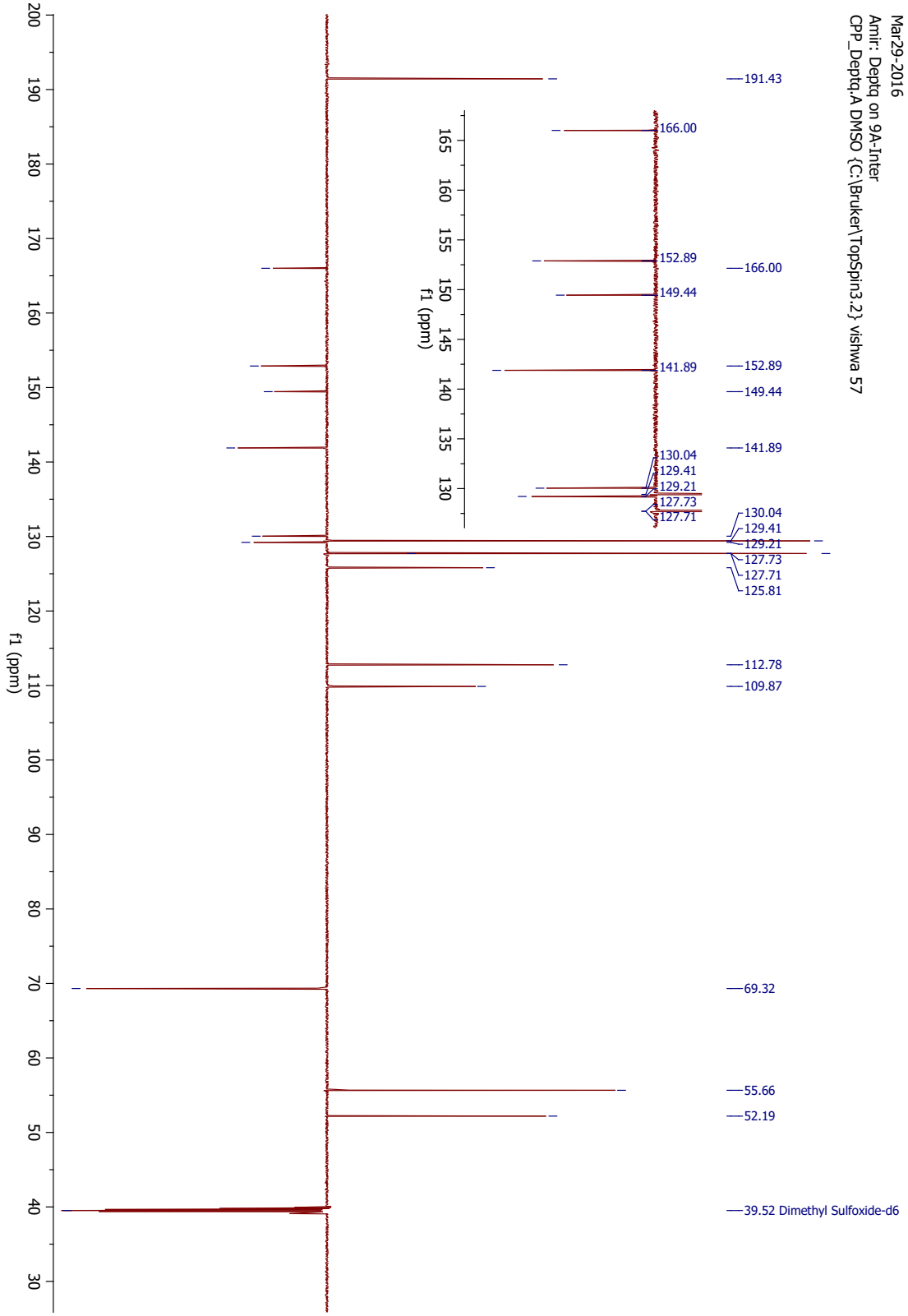

A1.48 ^{1}H-NMR 600 MHz, TFI-1

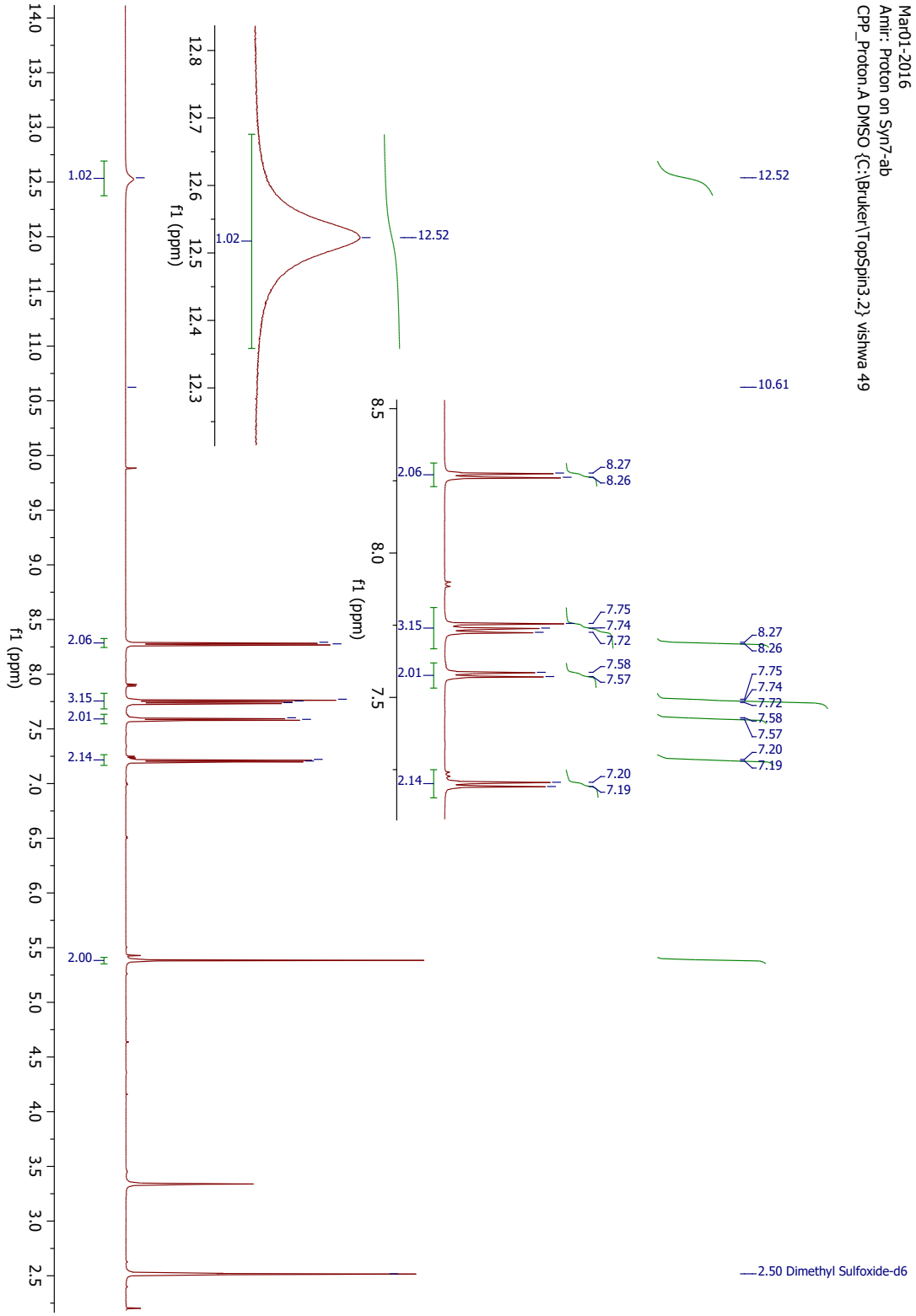

A1.49 ^{13}C-NMR (DEPTQ) 150 MHz, TFI-1

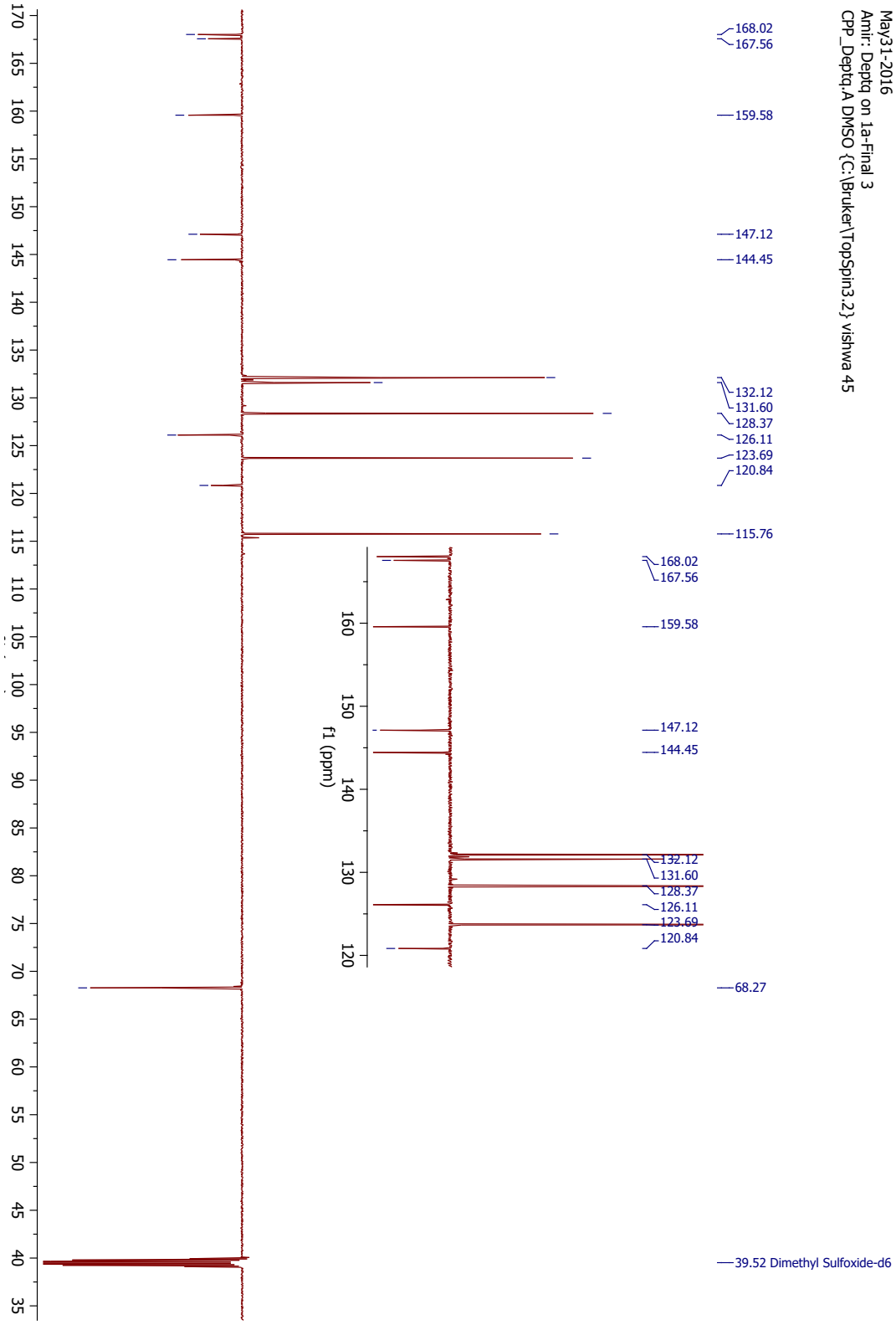

A1.50 ^{1}H-NMR 600 MHz, TFI-2

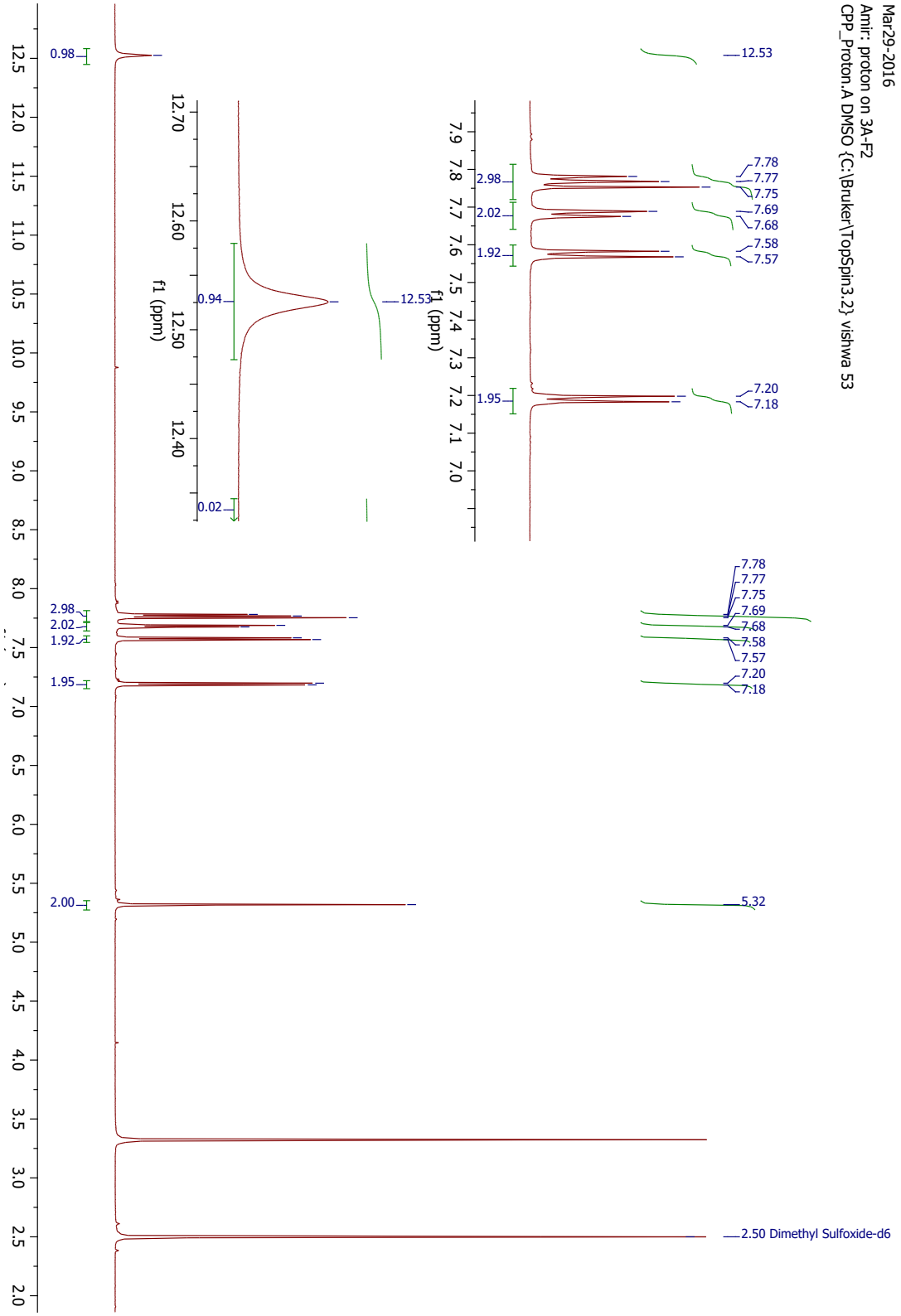

A1.51 ^{13}C-NMR (DEPTQ) 150 MHz, TFI-2

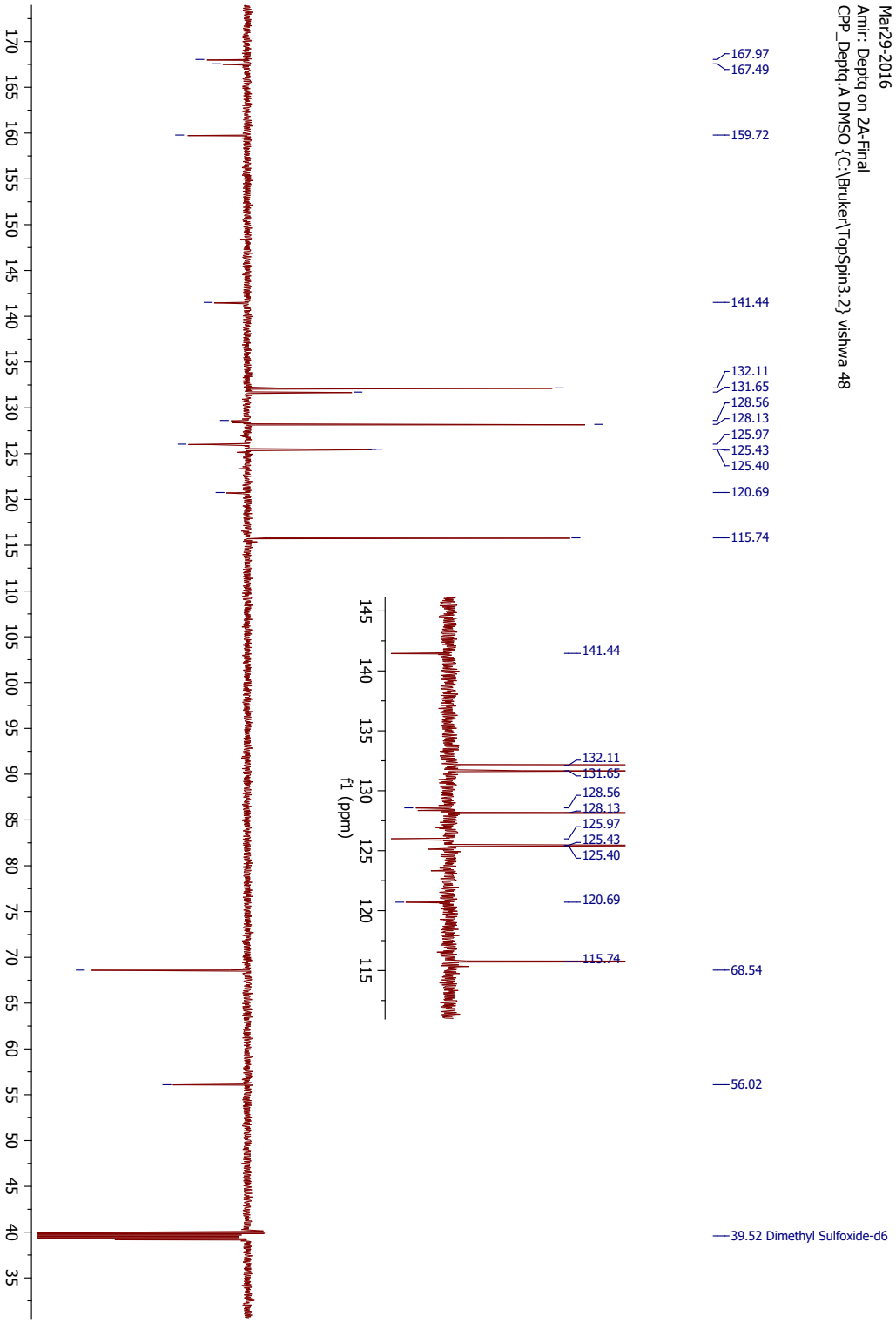

A1.52 ^{1}H-NMR 600 MHz, TFI-3

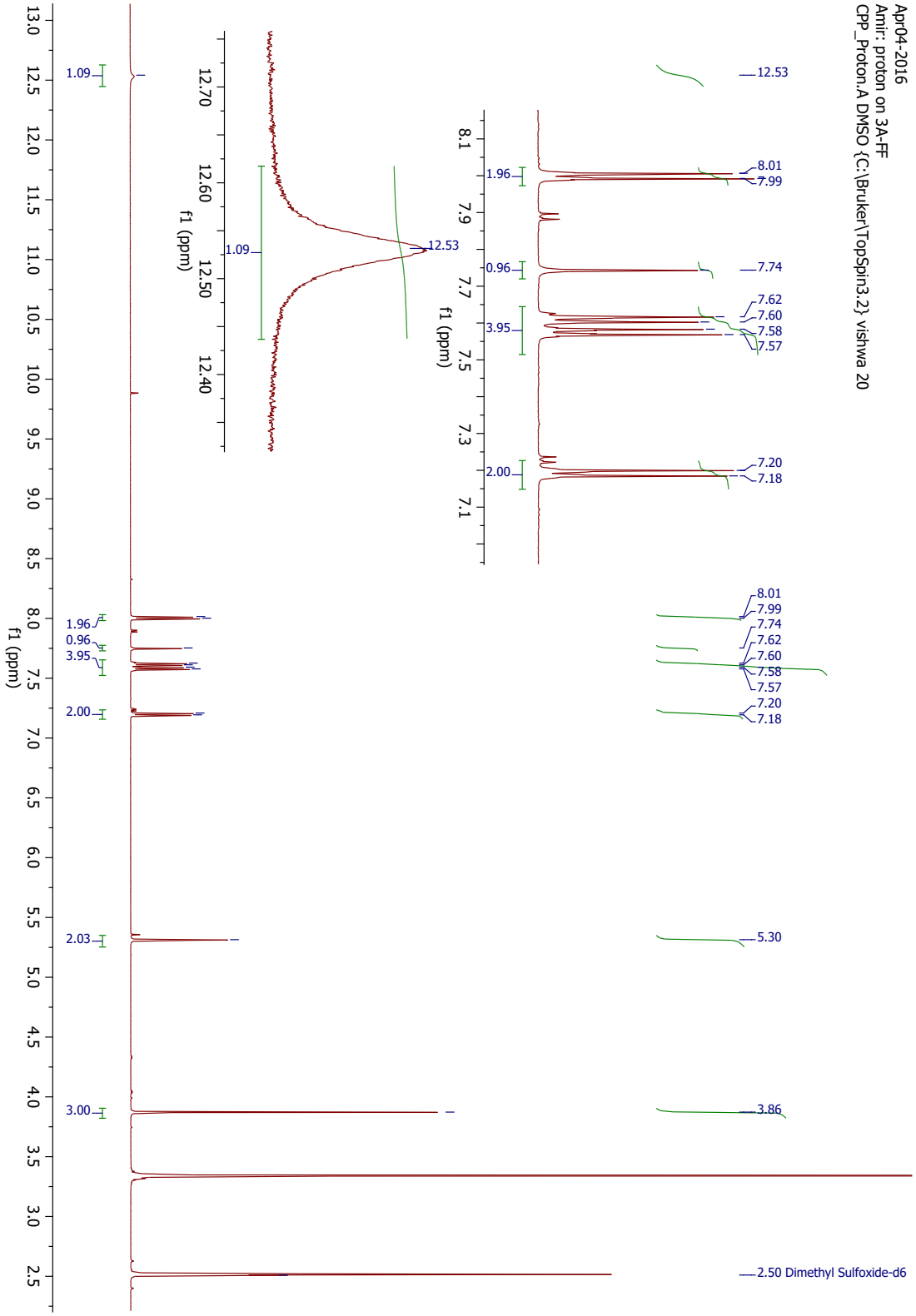

A1.53 ^{13}C-NMR (DEPTQ) 150 MHz, TFI-3

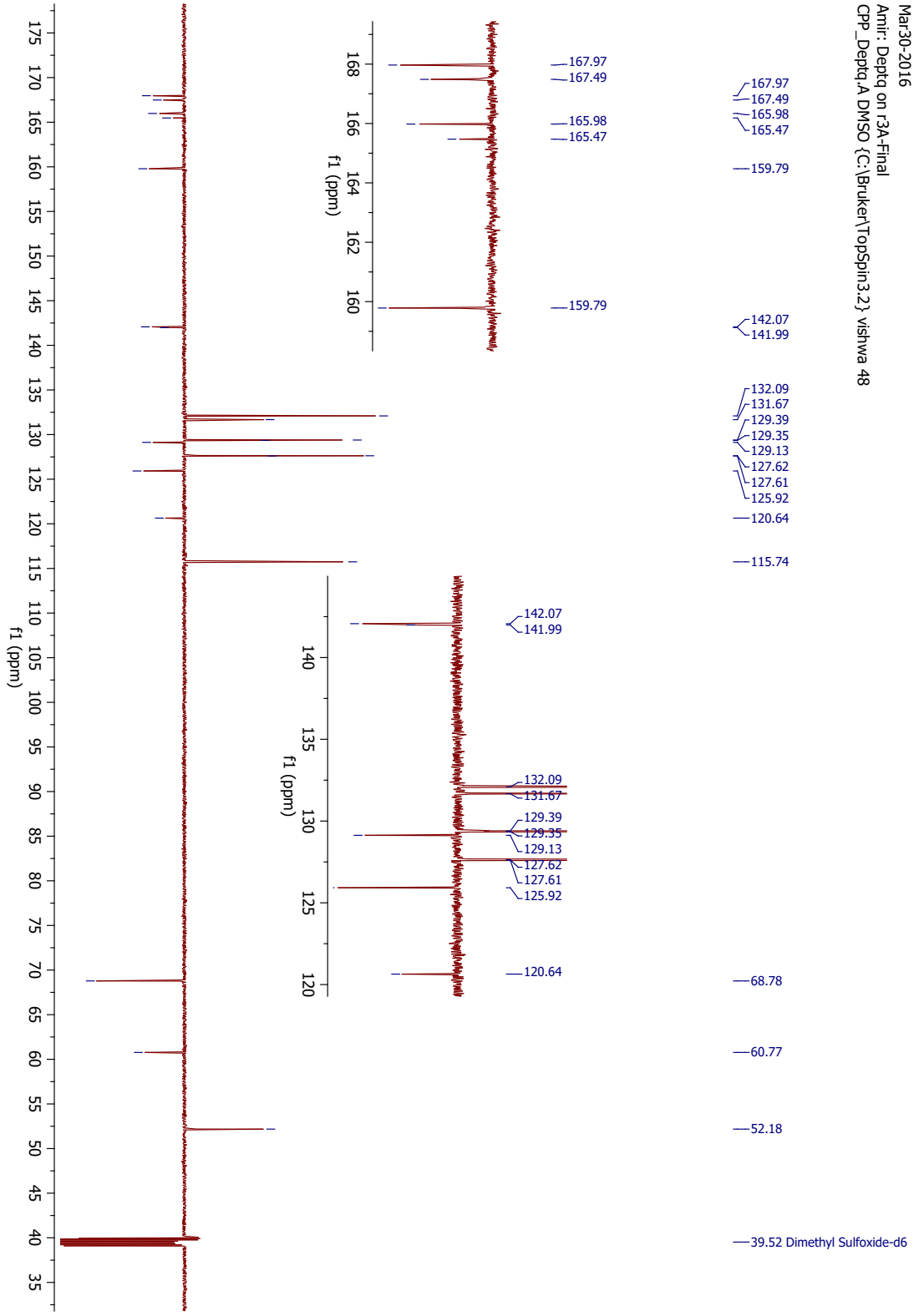

A1.54 ^{1}H-NMR 600 MHz, TFI-4

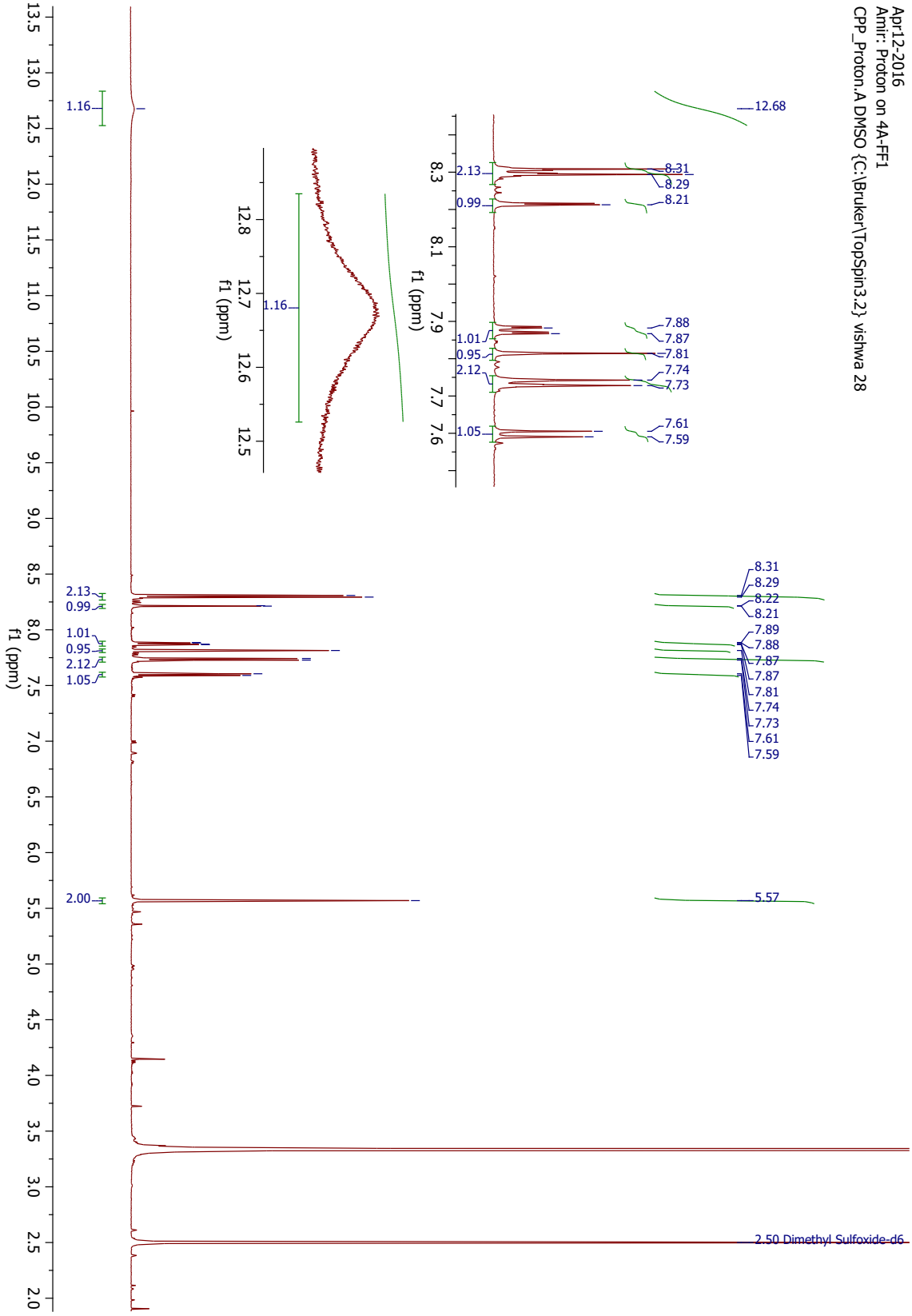

A1.55 ^{13}C-NMR (DEPTQ) 150 MHz, TFI-4

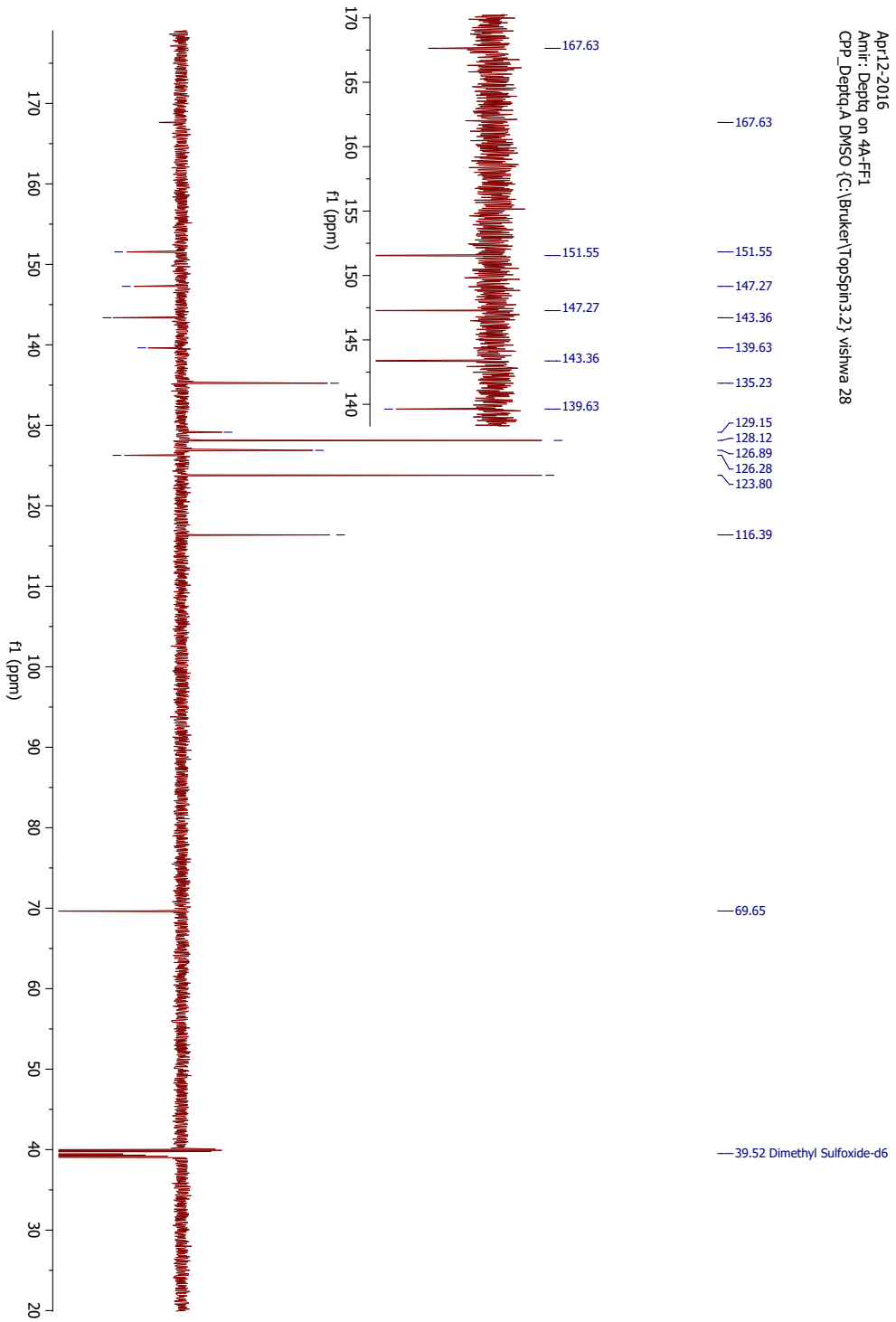

A1.56 ^{1}H-NMR 600 MHz, TFI-5

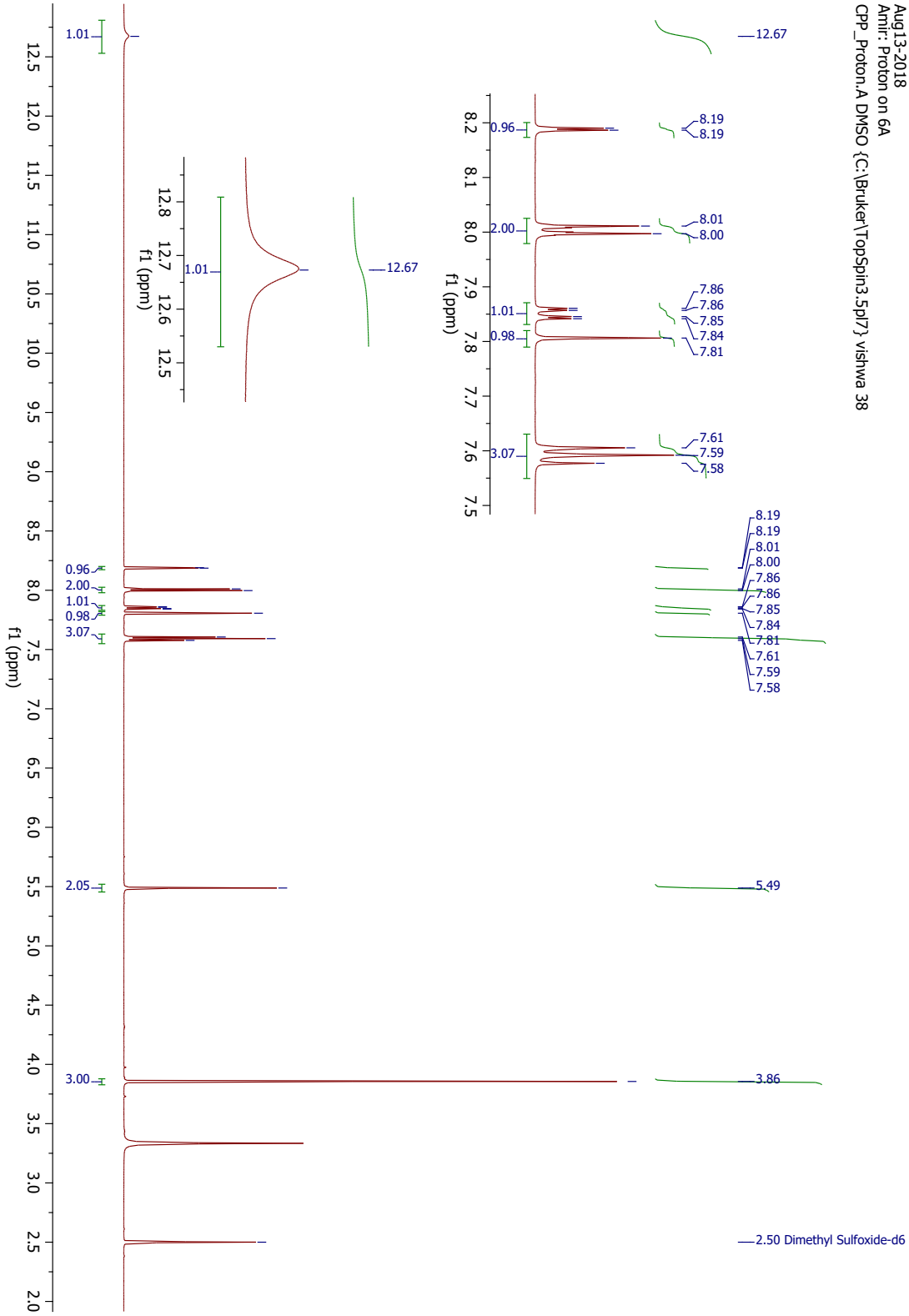

A1.57 ^{13}C-NMR (DEPTQ) 150 MHz, TFI-5

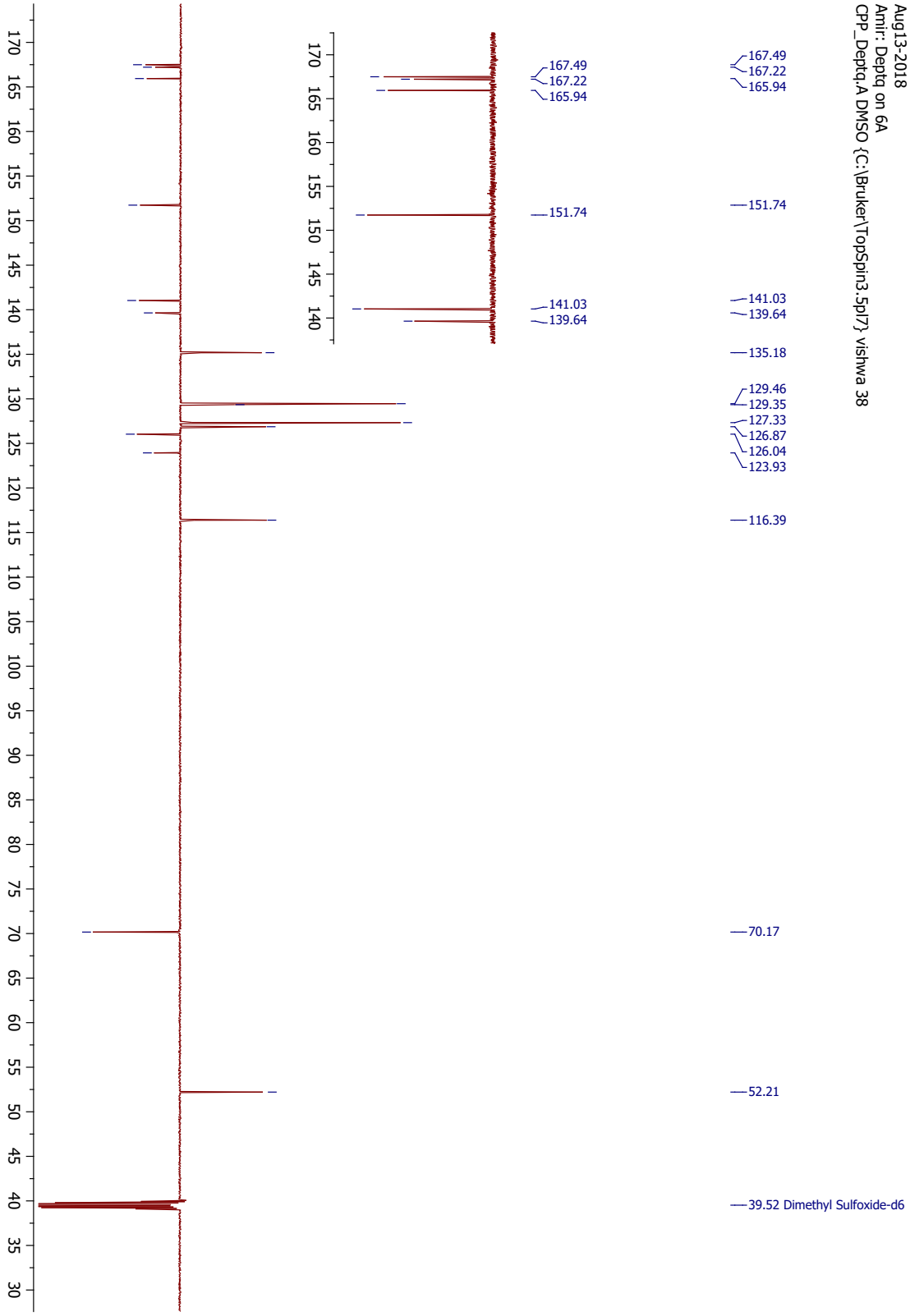

A1.58 ^{1}H-NMR 600 MHz, TFI-6

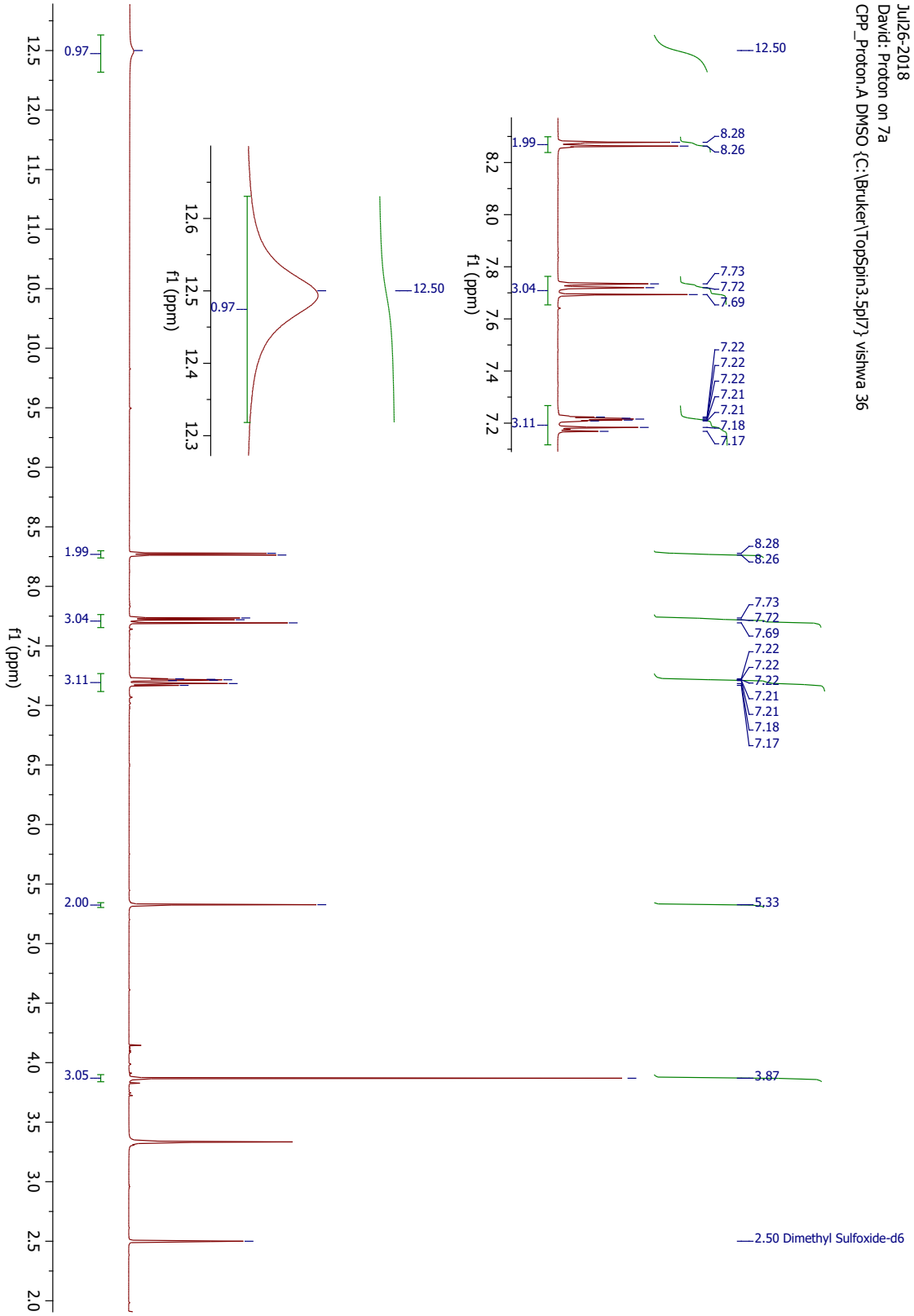

A1.59 ^{13}C-NMR (DEPTQ) 150 MHz, TFI-6

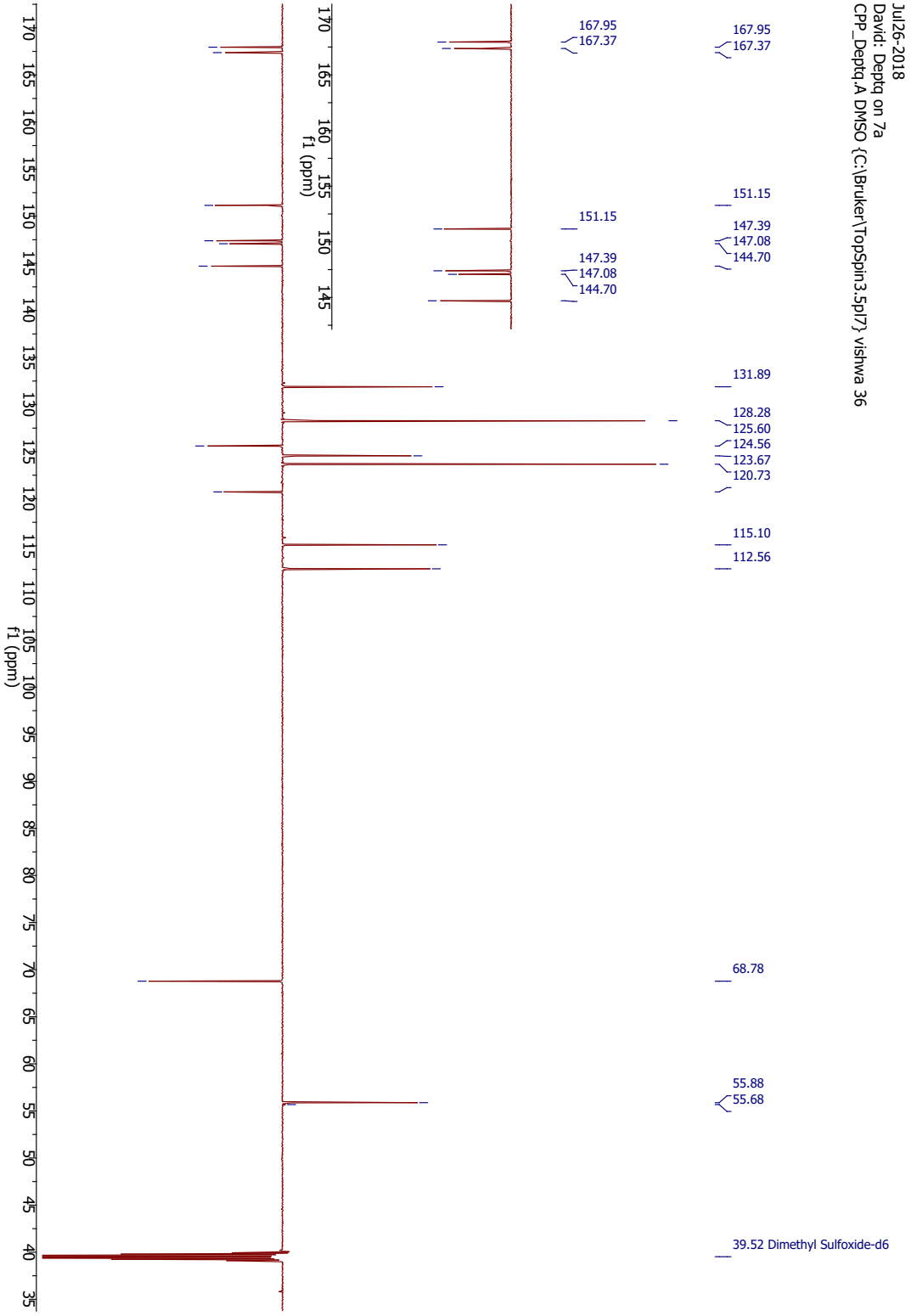

A1.60 ^{1}H-NMR 600 MHz, TFI-7

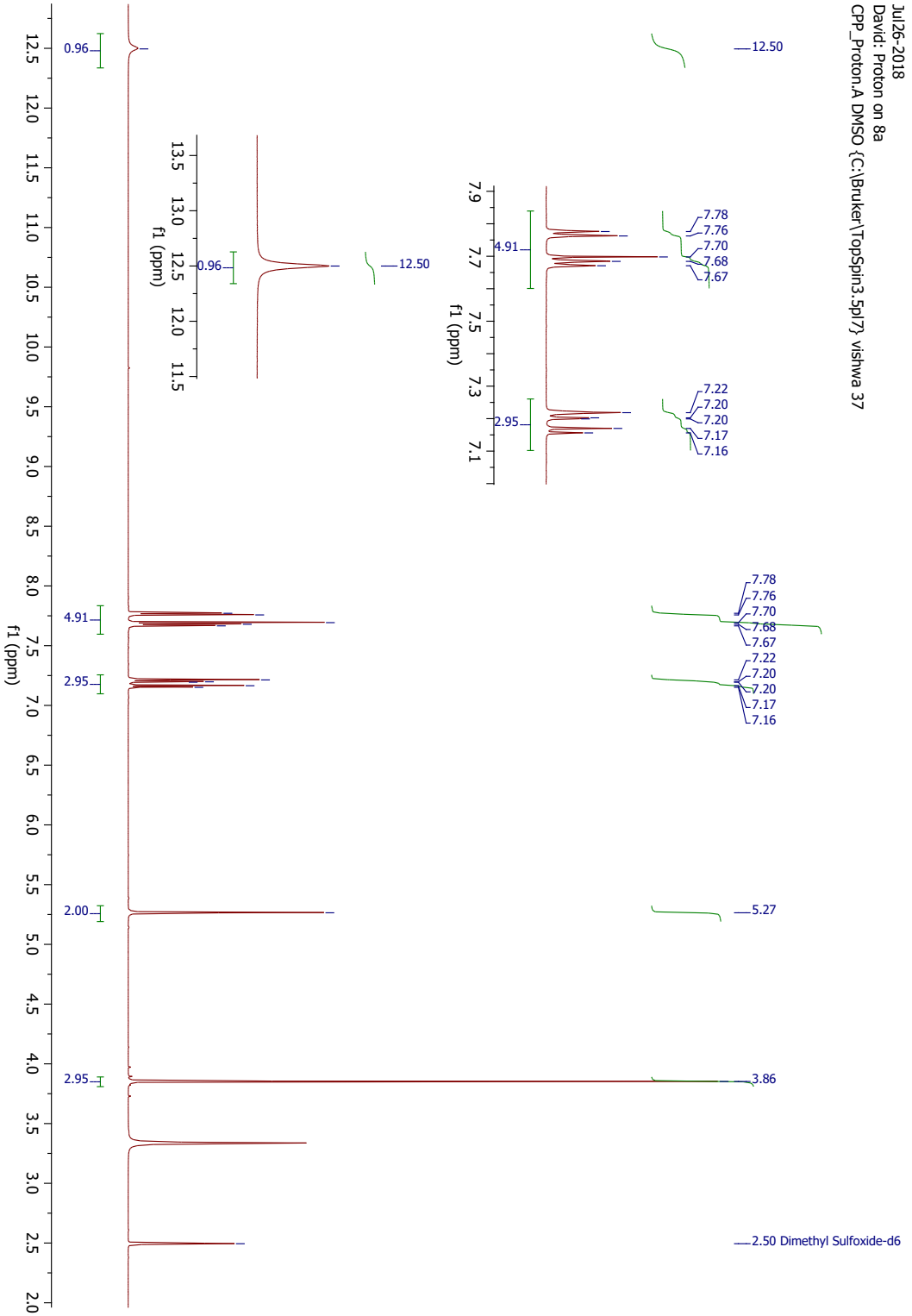

A1.61 ^{13}C-NMR (DEPTQ) 150 MHz, TFI-7

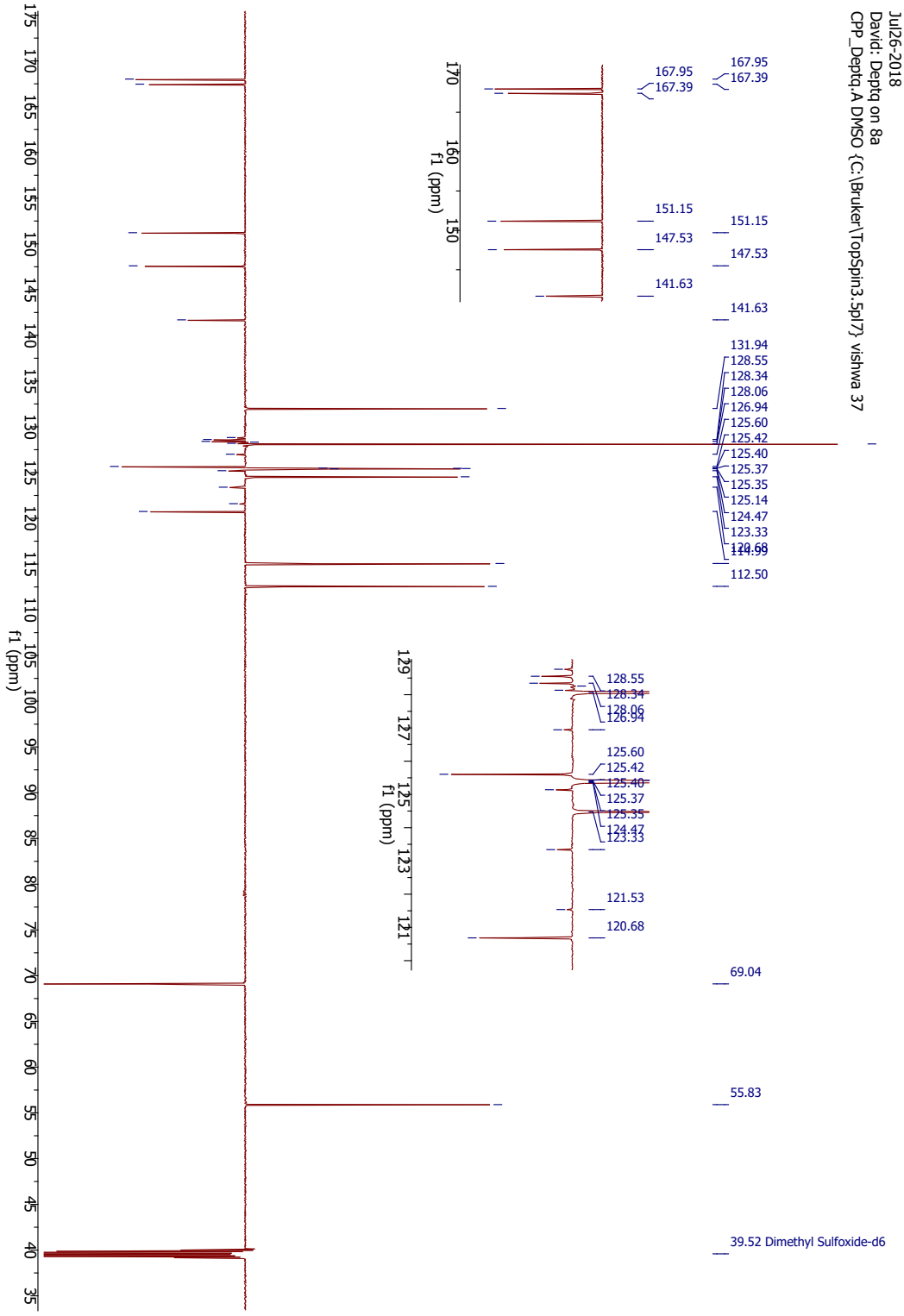

A1.62 ^{19}F NMR 565 MHz, TFI-7

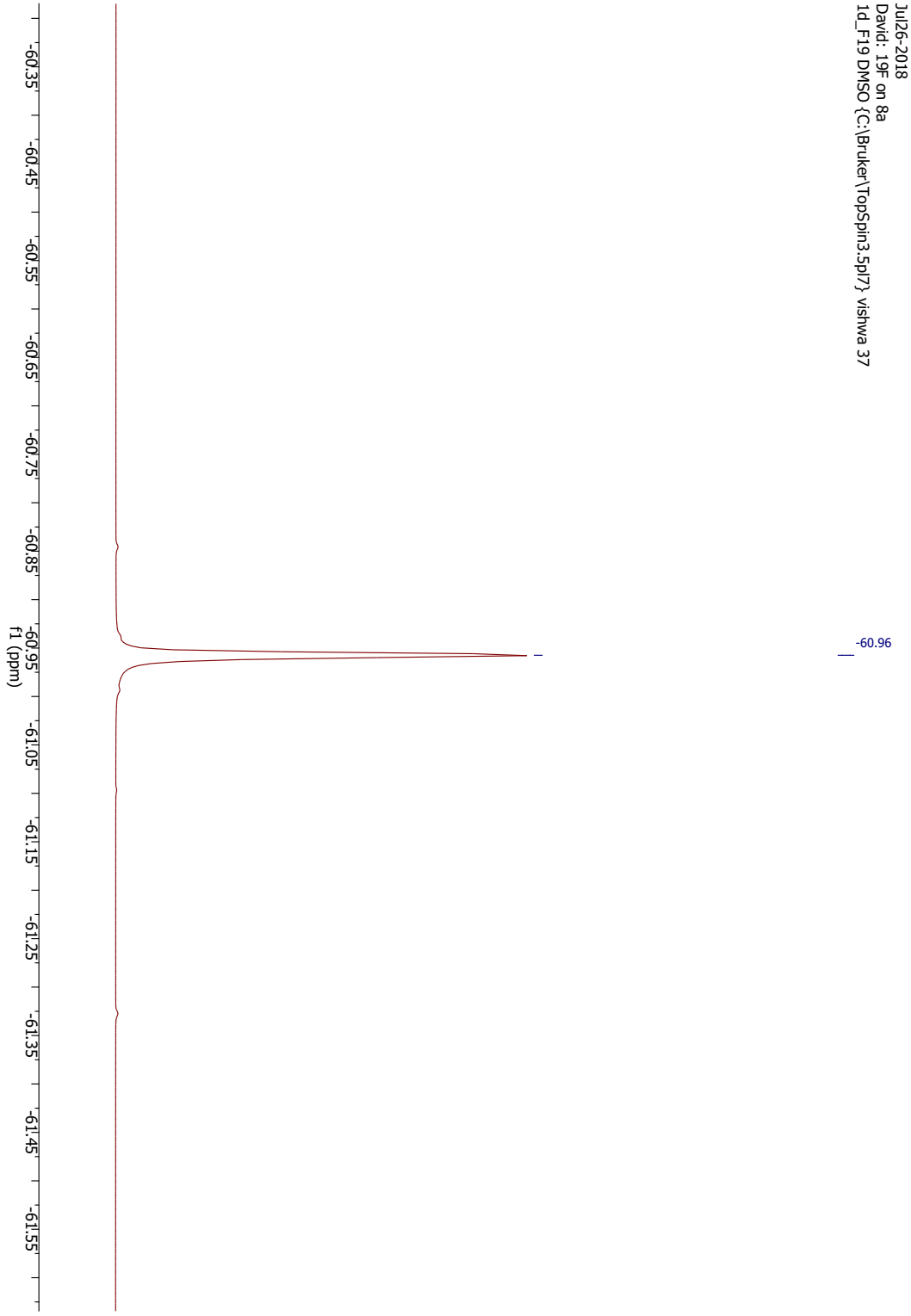

A1.63 ^{1}H-NMR 600 MHz, TFI-8

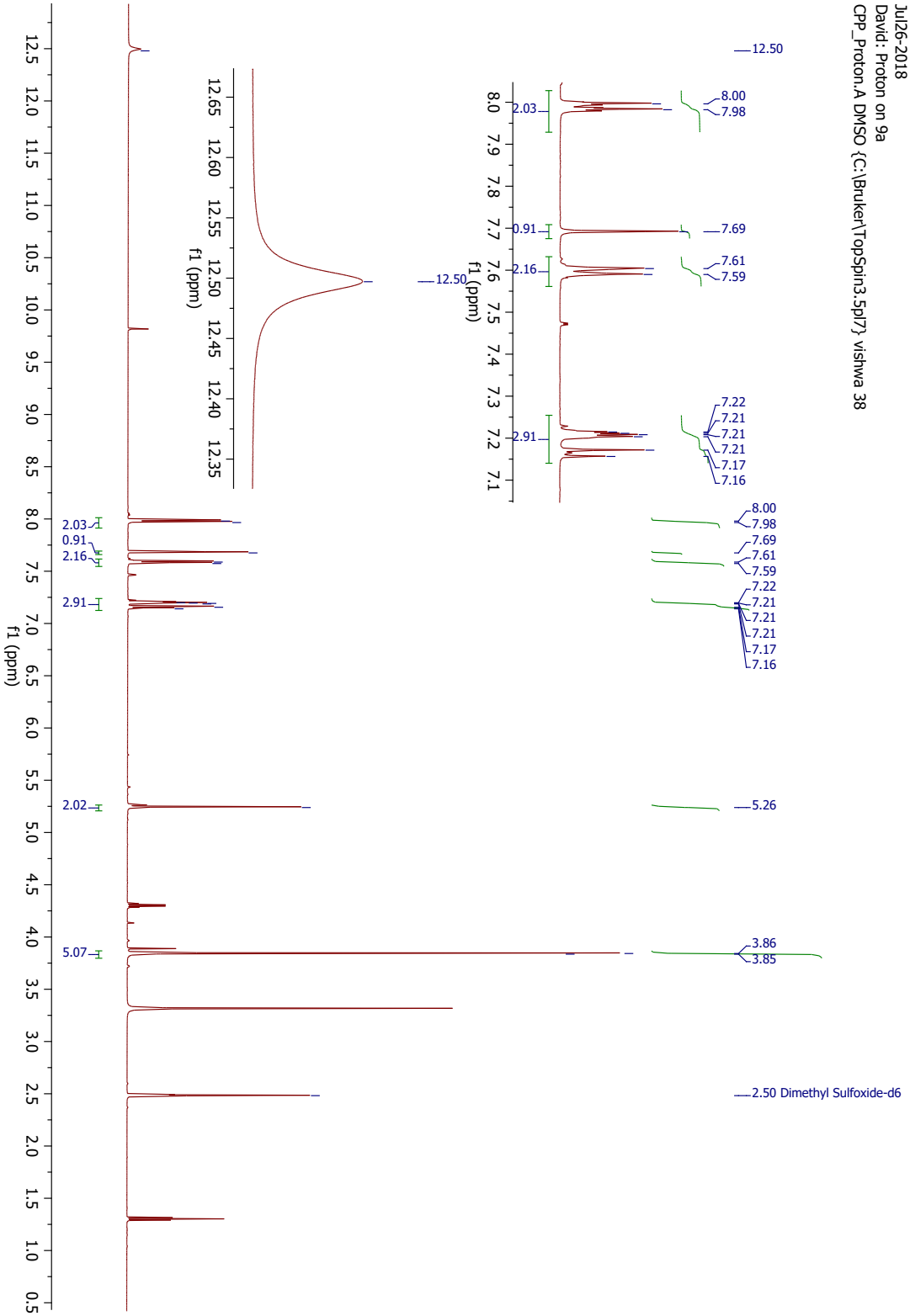

A1.64 ^{13}C-NMR (DEPTQ) 150 MHz, TFI-8

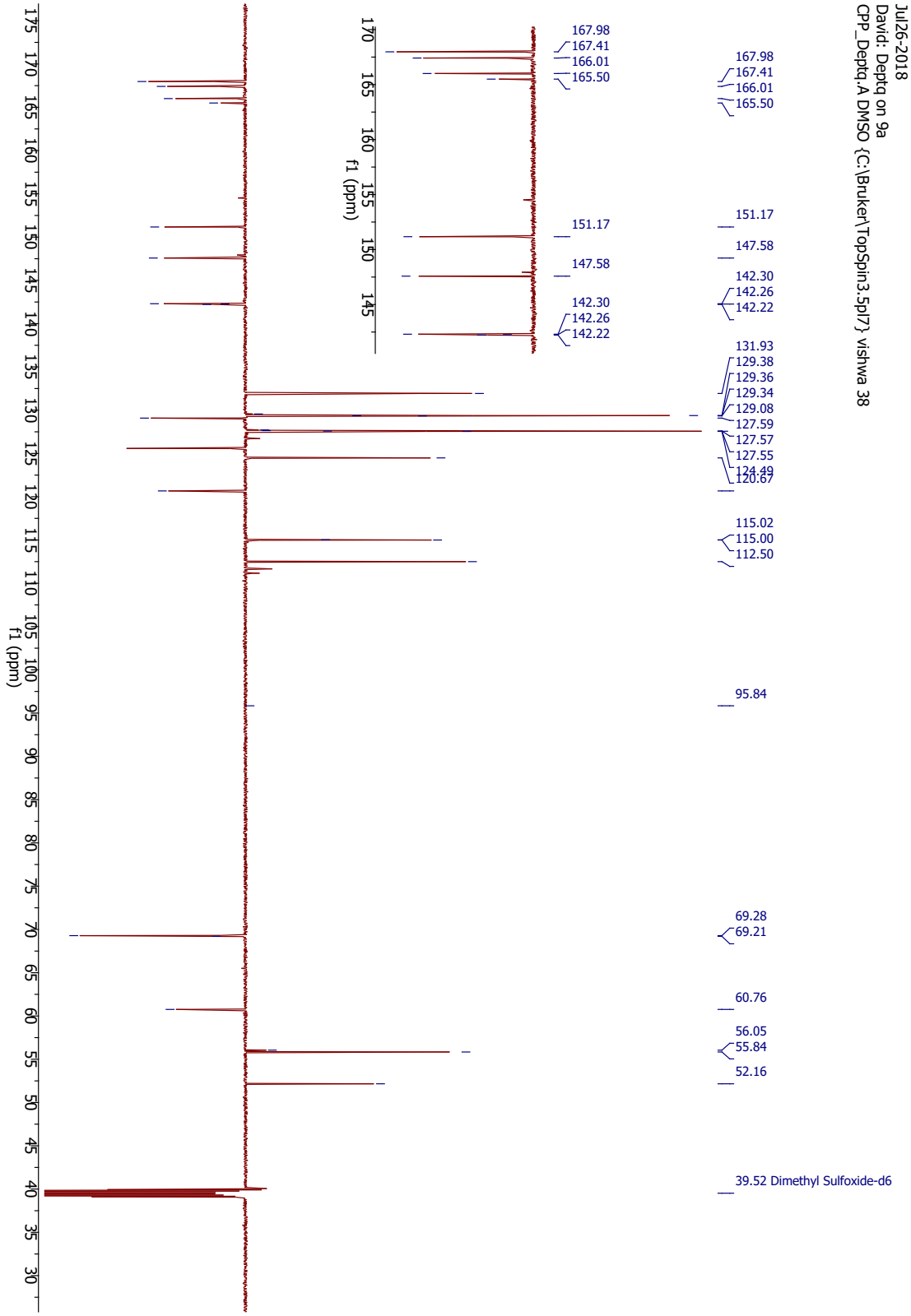

A1.65 ^{1}H-NMR 600 MHz, TFI-9

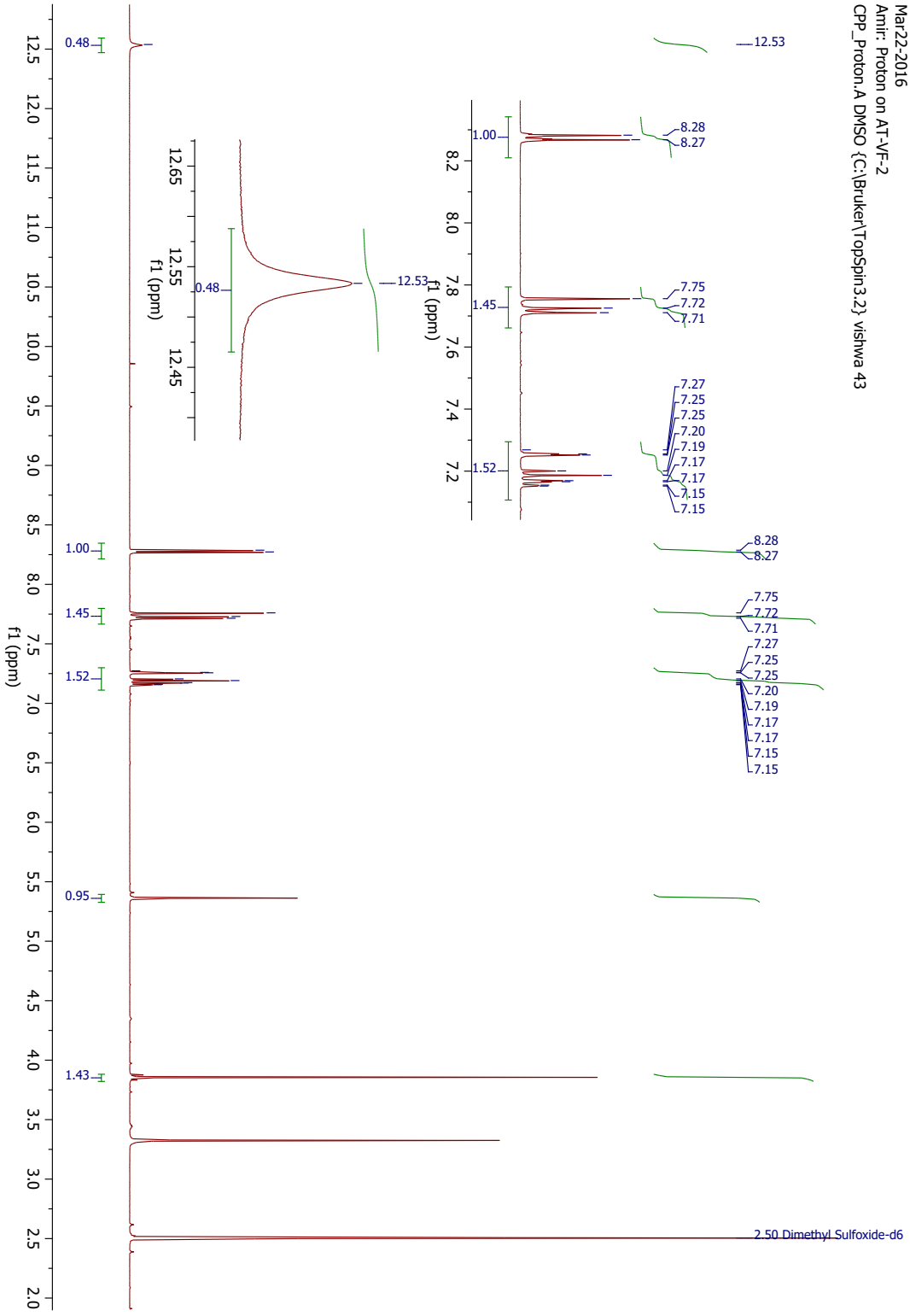

A1.66 ^{13}C-NMR (DEPTQ) 150 MHz, TFI-9

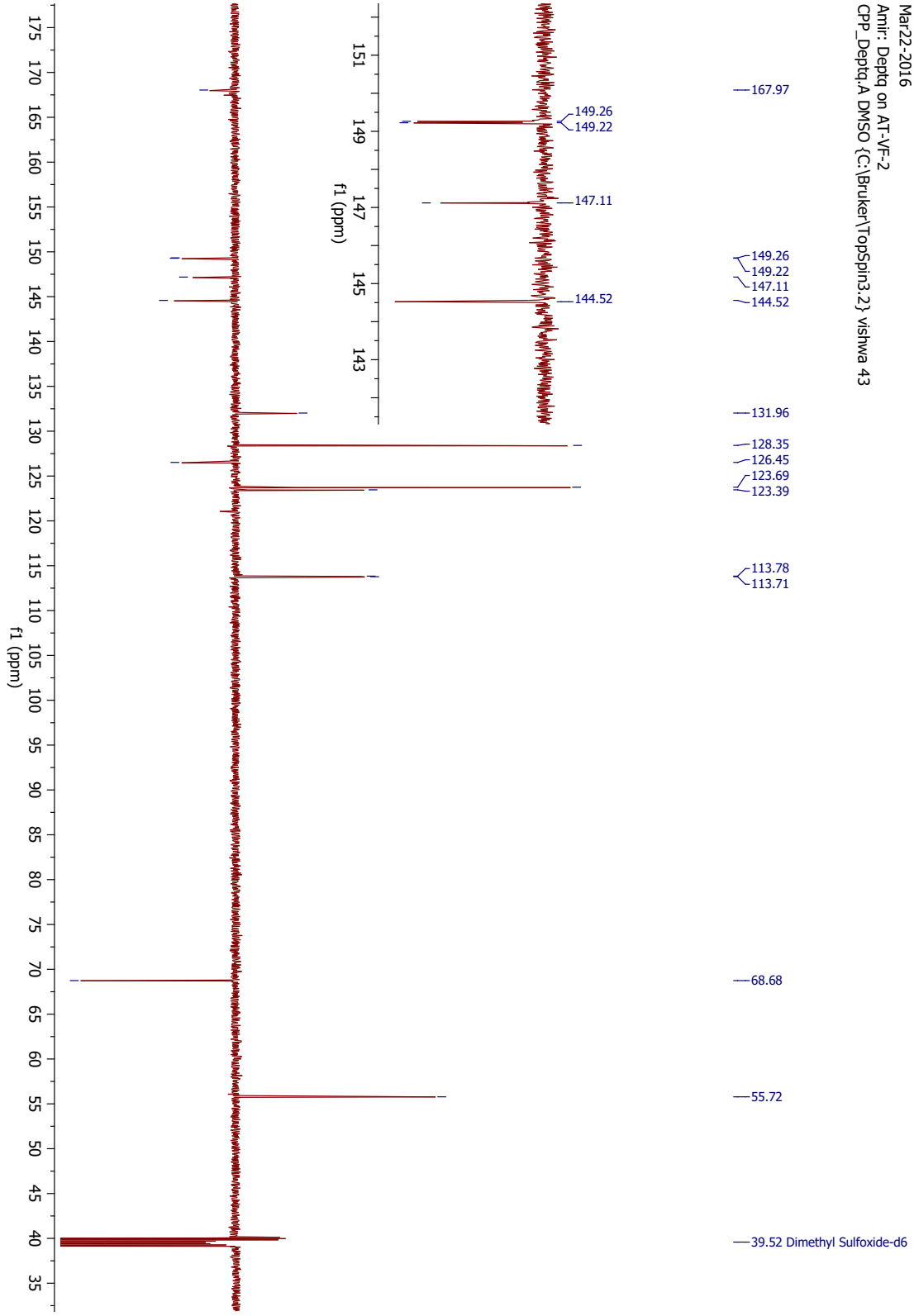

A1.67 ^{1}H-NMR 600 MHz, TFI-10

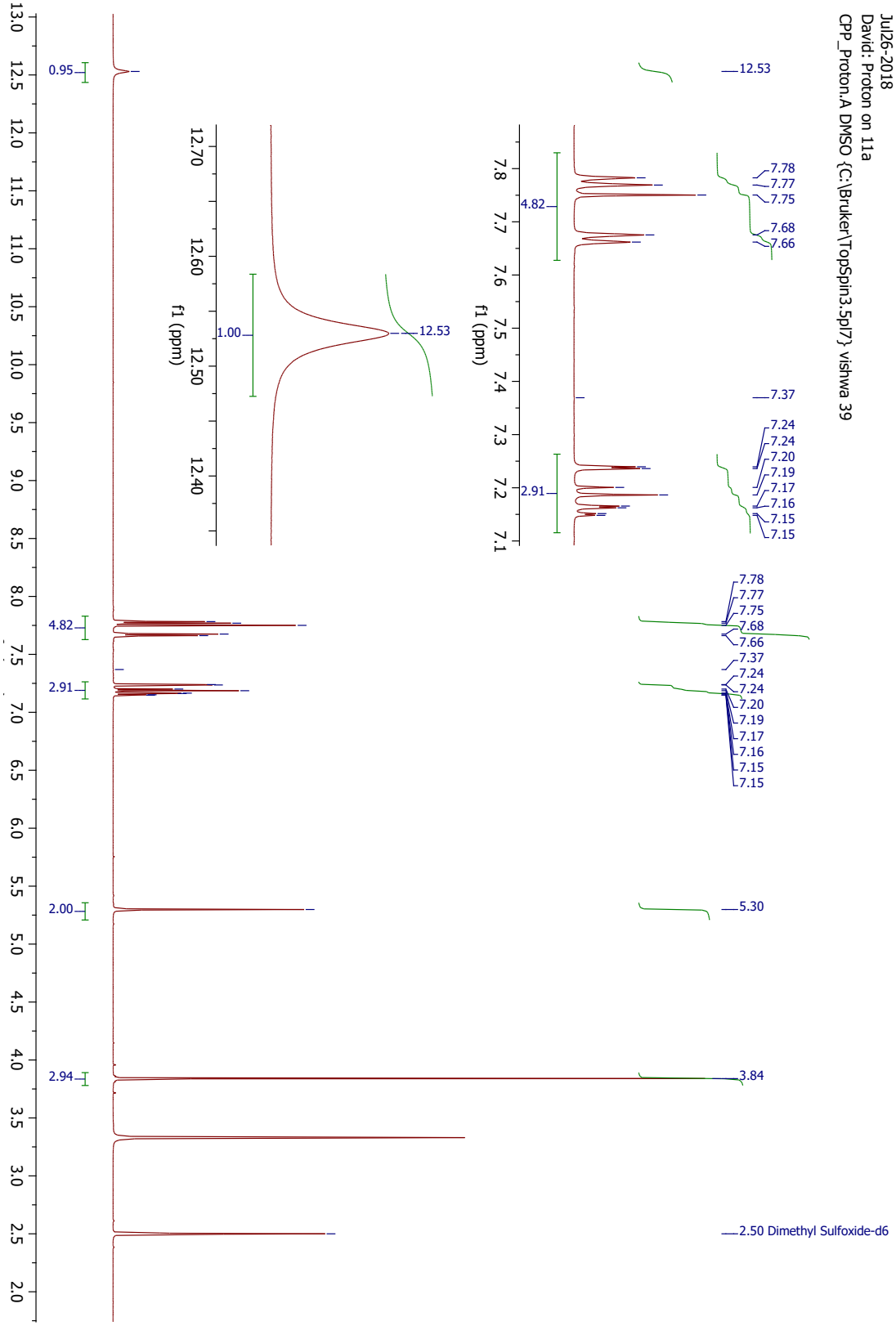

A1.68 ^{13}C-NMR (DEPTQ) 150 MHz, TFI-10

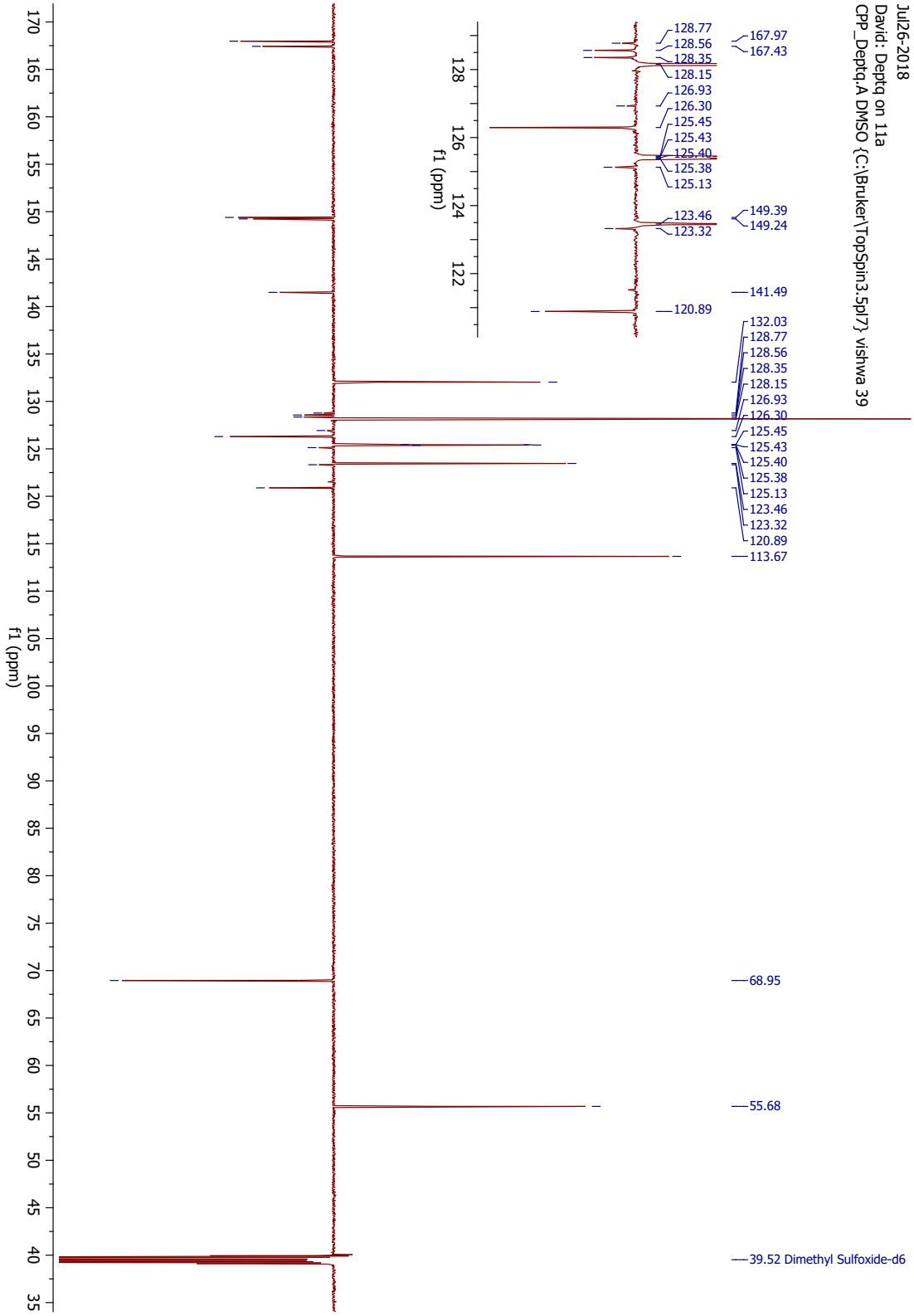

A1.69 ^{19}F NMR 565 MHz, TFI-10

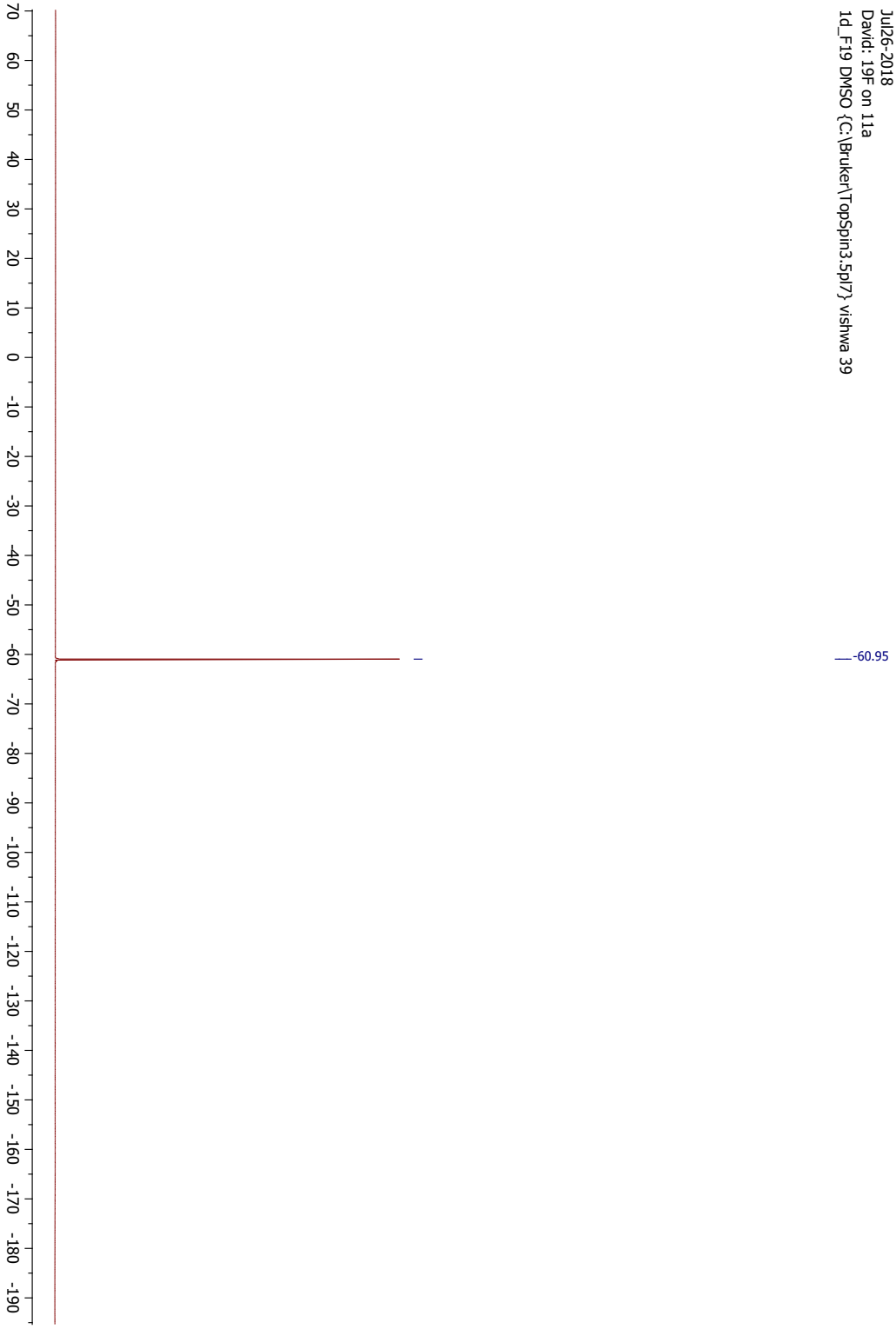

A1.70 ^{1}H-NMR 600 MHz, TFI-11

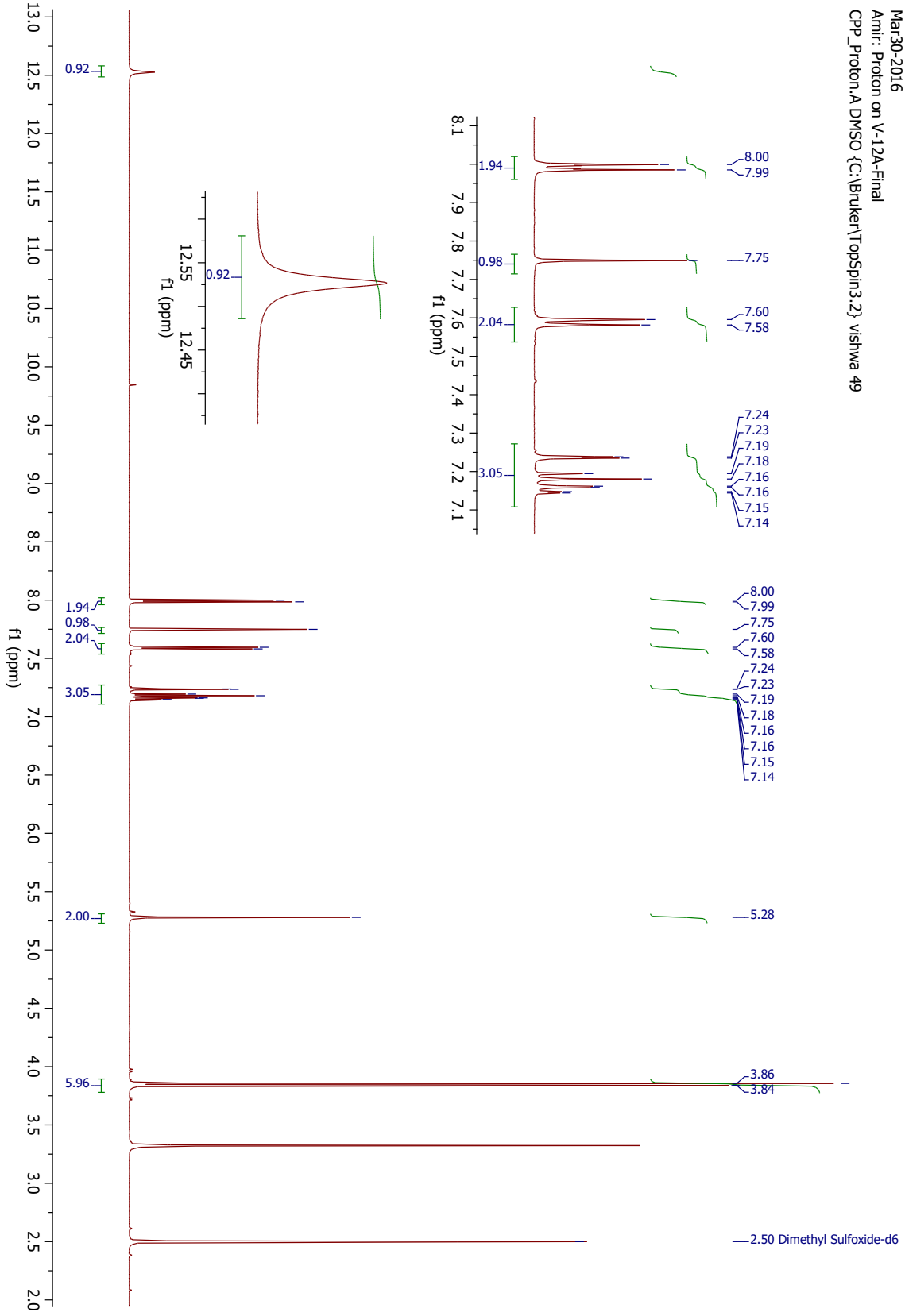

A1.71 ^{13}C-NMR (DEPTQ) 150 MHz, TFI-11

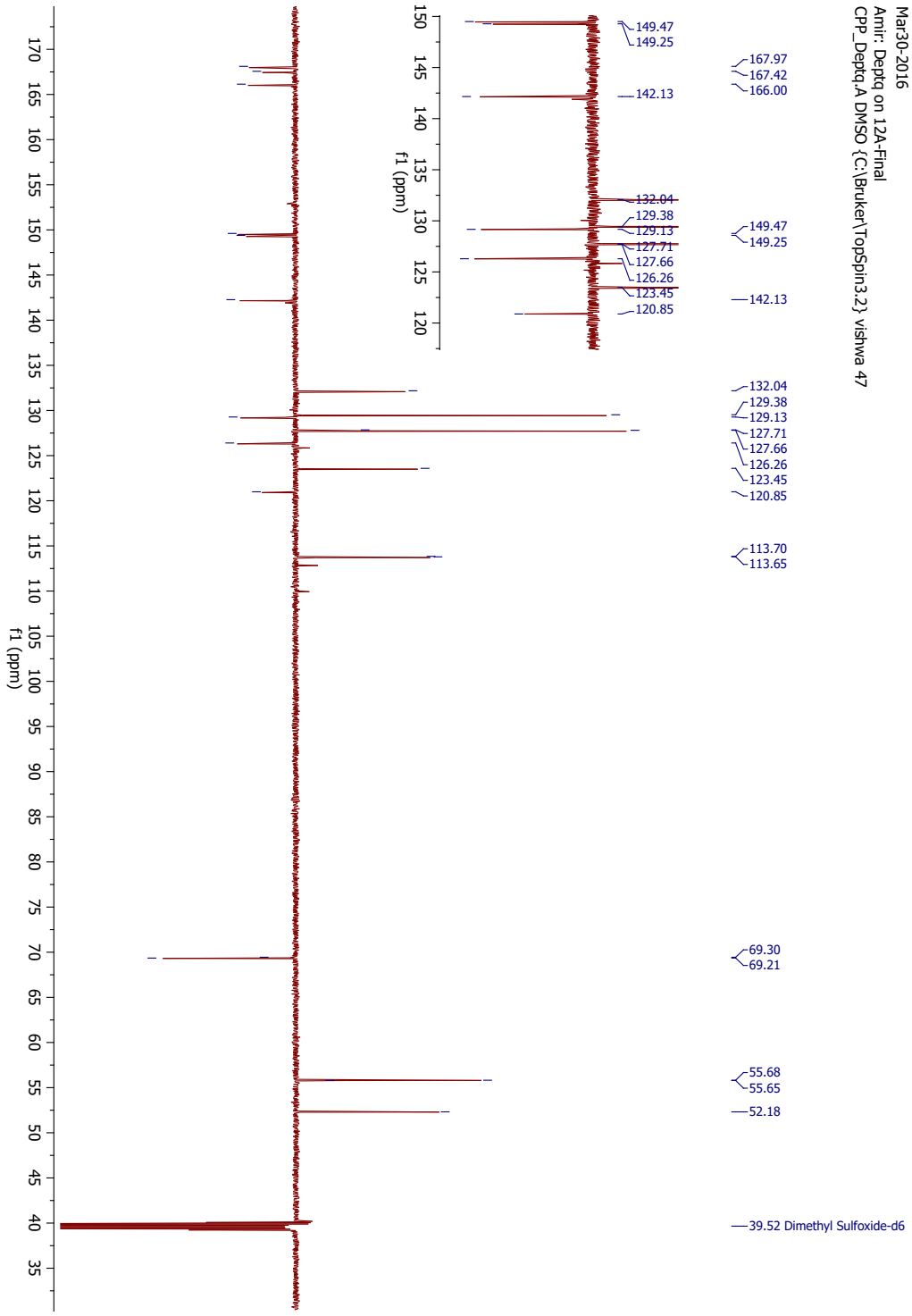

A1.72 ^{1}H-NMR 600 MHz, TFI-10-RHO

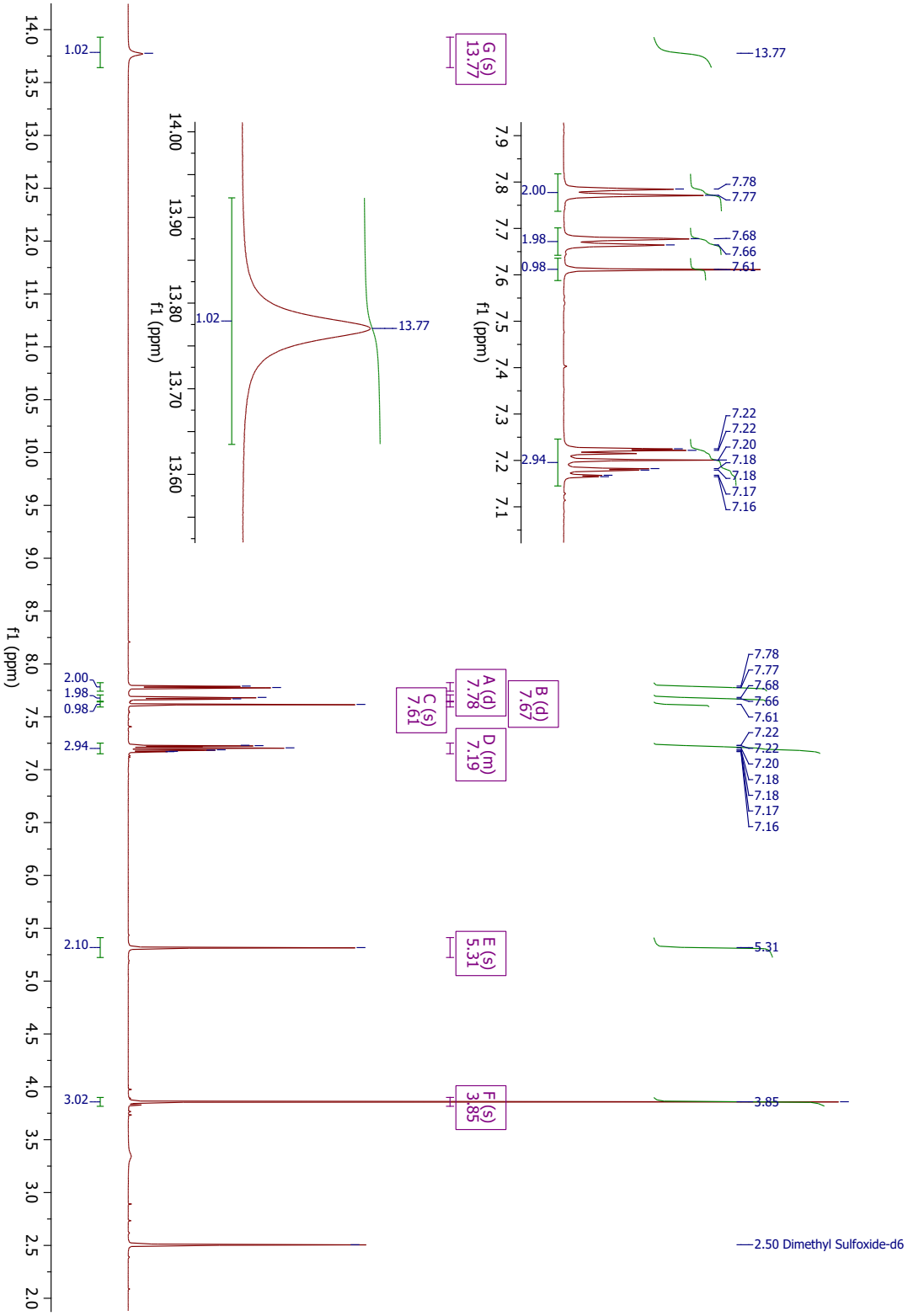

A1.73 ^{13}C-NMR (DEPTQ) 150 MHz, TFI-10-RHO

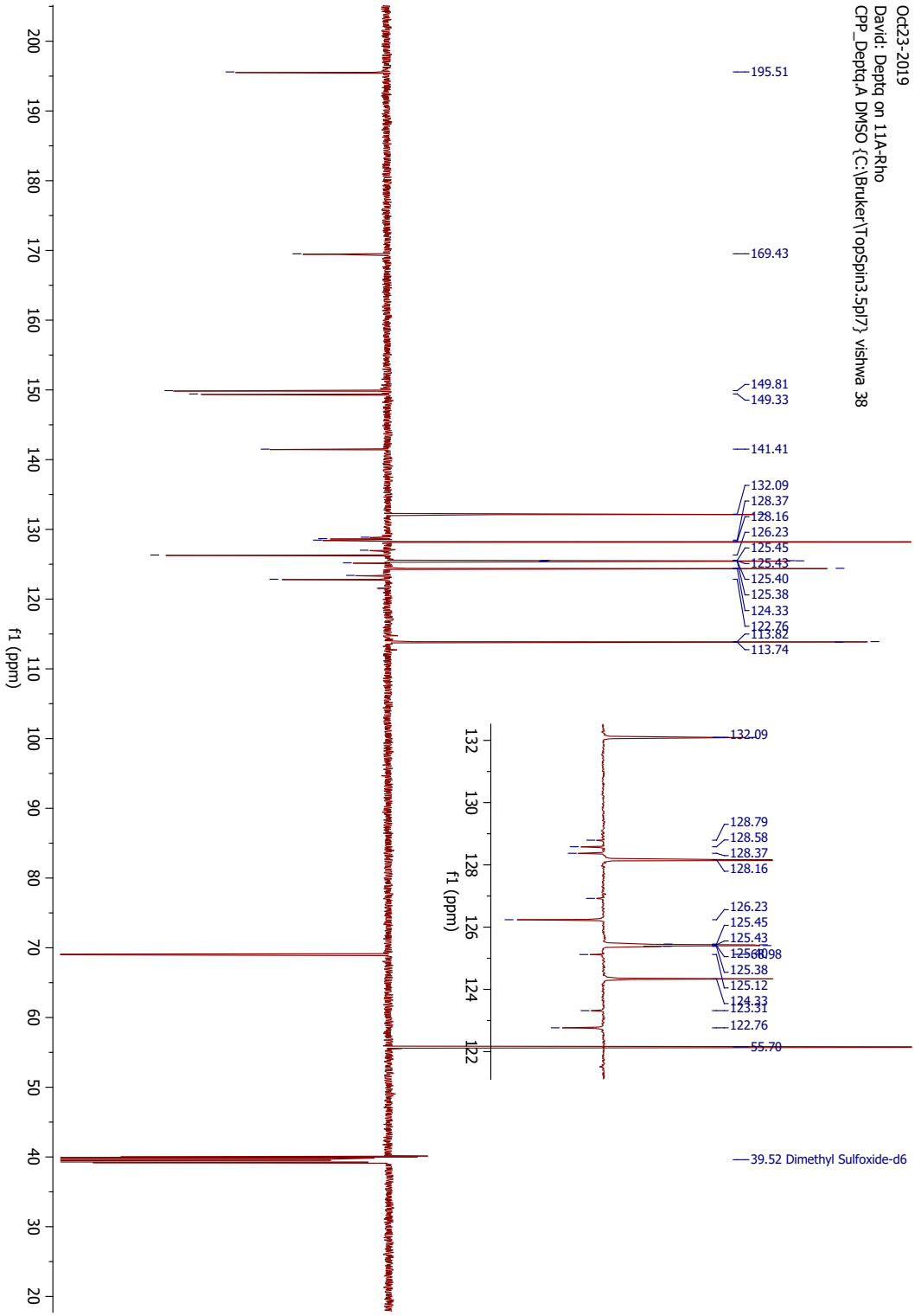

A1.74 1H-NMR 600 MHz, P11

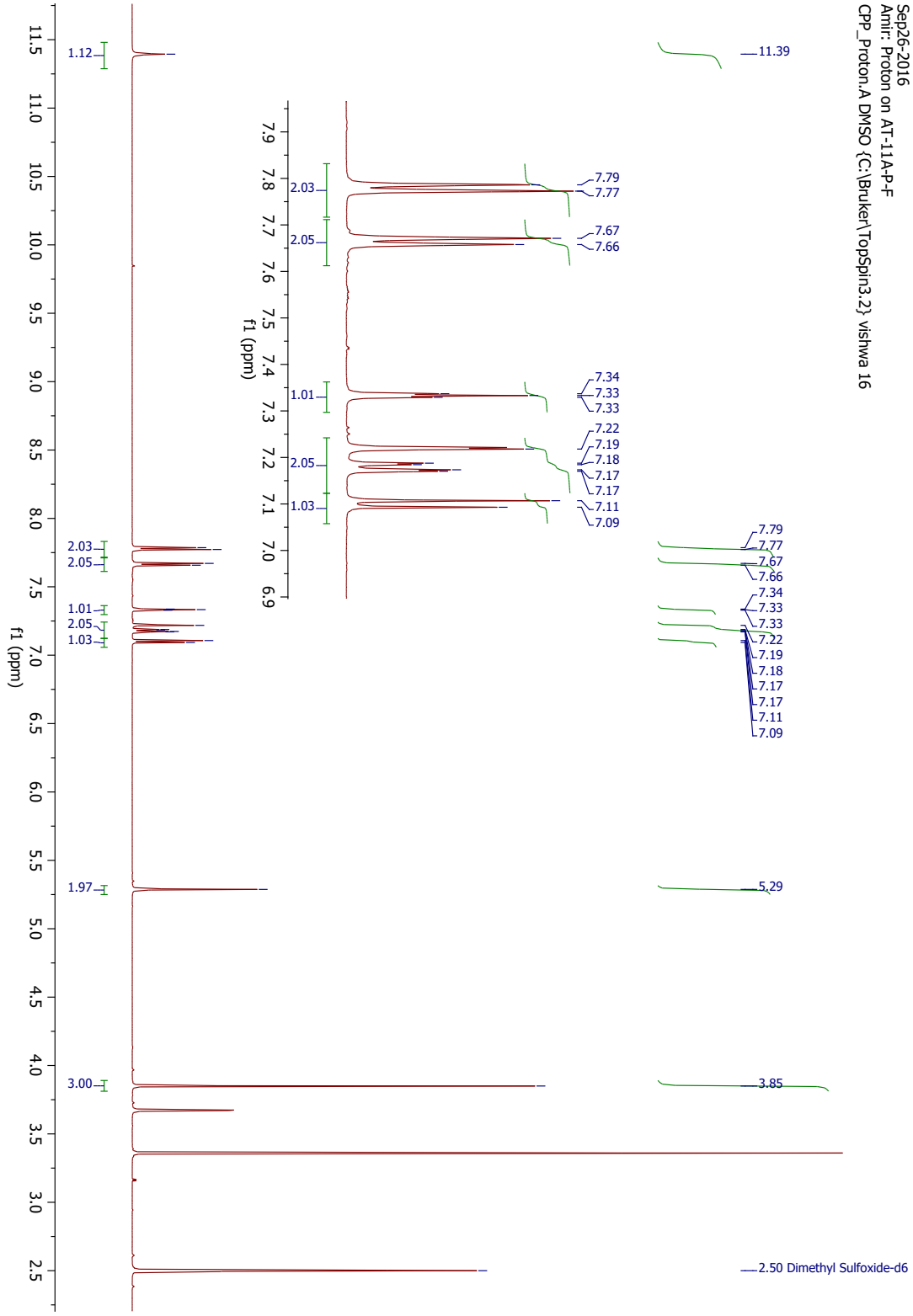

A.2 Images of Purified Protein Gel

A.2.1 GST-FOXM1-DBD (Wild type) Purified Protein

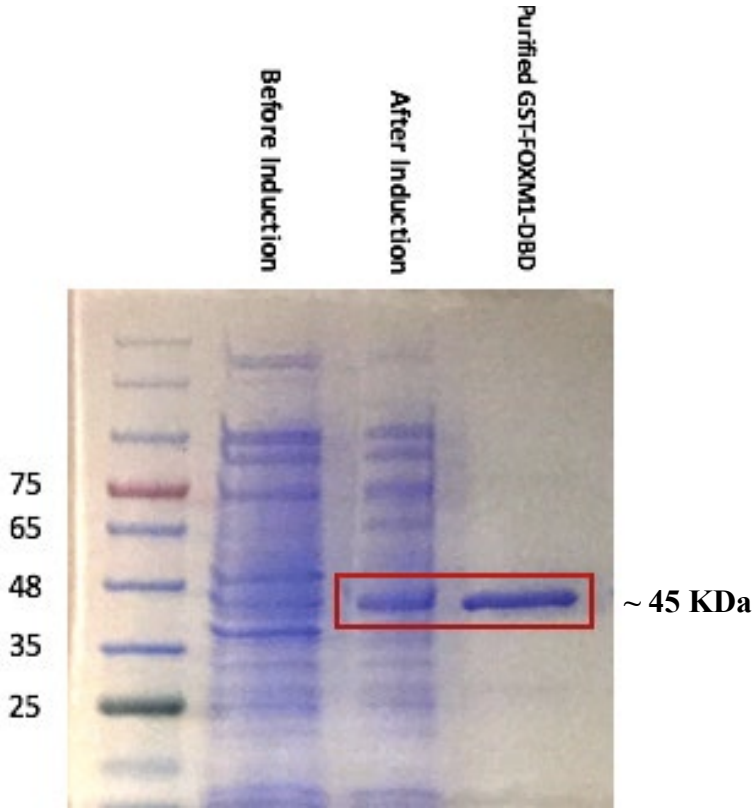

A.2.2 GST-FOXM1-DBD (His287:Ala) Purified Protein

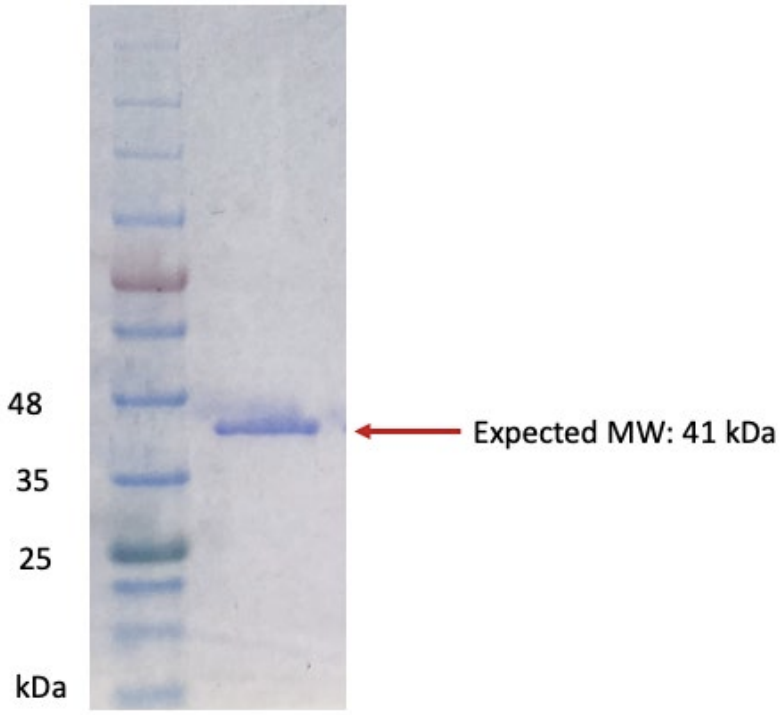

A.2.3 GST-FOXM1-DBD (His287:Phe) purified protein

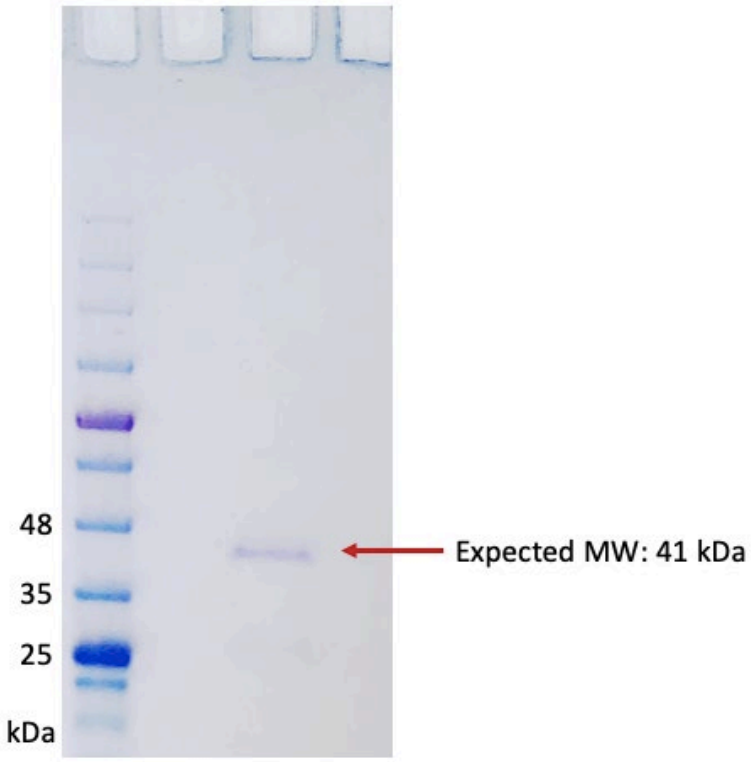

A.3 Validation of Mutation by Sanger Sequencing

A.3.1 GST-FOXM1-DBD (His287:Ala)

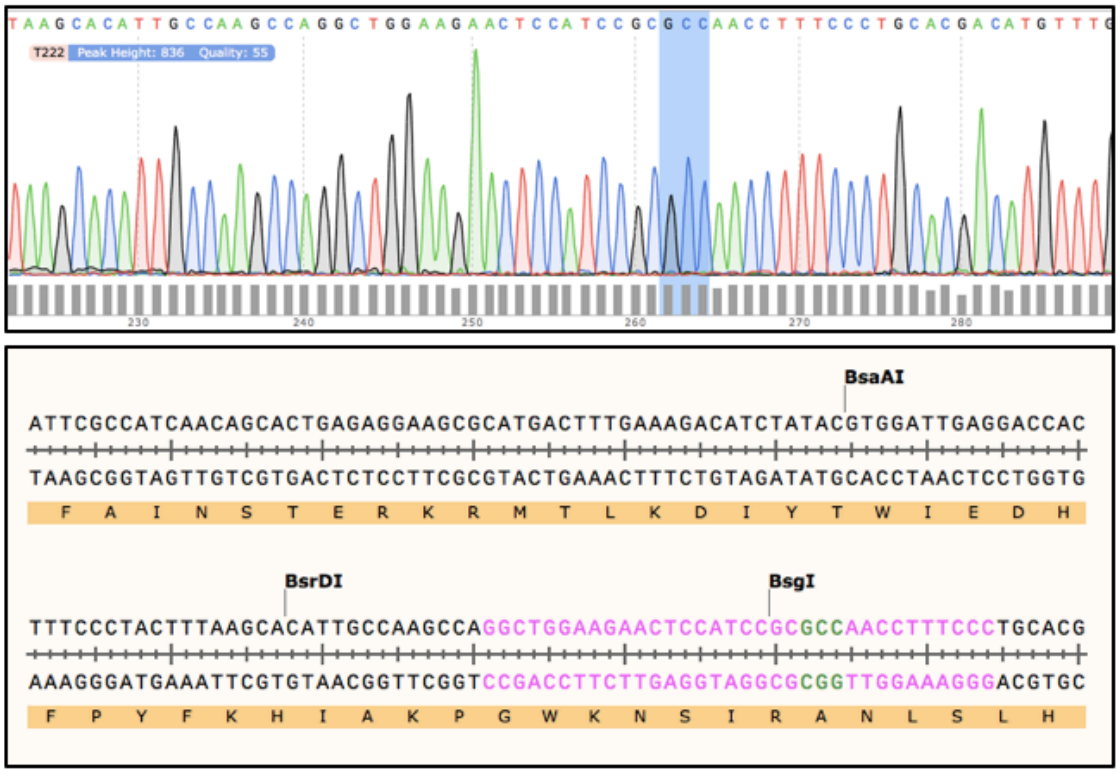

A.3.1 GST-FOXM1-DBD (His287:Phe)